PROGRAMMING MOLECULAR ASSOCIATION AND VISCOELASTIC BEHAVIOR IN PROTEIN HYDROGELS

Thesis by

Lawrence Joseph Dooling

In Partial Fulfillment of the Requirements for

the degree of

Doctor of Philosophy

CALIFORNIA INSTITUTE OF TECHNOLOGY

Pasadena, California

2016

(Defended May 25, 2016)

Lawrence Joseph Dooling
ORCID ID 0000-0002-1688-2066

ACKNOWLEDGEMENTS

I am deeply grateful to my adviser, Professor David Tirrell, for his guidance, patience, and continued support. I could not have asked for a better research adviser and mentor. Dave brings a level of scientific rigor and integrity to research that I will continue to aspire to throughout my career. These qualities are matched by his humility, kindness, and sense of humor. Thank you Dave for everything.

I would also like to thank the current and former members of the Tirrell group with whom I have had the privilege to work over the past several years. I have learned a tremendous amount from all of them and have appreciated their support and friendship.

My thesis committee – Professor Julia Kornfield, Professor Zhen-Gang Wang, and Professor Guruswami Ravichandran – provided me with helpful advice and guidance in completing my thesis, for which I am very grateful. In particular, I would like to thank Professor Kornfield and her group for generous access to the rheometer in her laboratory and advice on measurements.

Finally, I would like to express my gratitude to my family for their continued support in my graduate school years and throughout my entire life. Any success I may have, I owe to them.

ABSTRACT

Recombinant artificial proteins contain genetically encoded information that specifies their assembly into higher order structures by physical or chemical cross-linking as well as elastic behavior and biological or chemical function. This thesis describes the use of artificial proteins to construct molecular networks containing covalent cross-links involving the thiol side chain of cysteine residues and physical cross-links involving the association of helical domains as coiled coils. The goal of this work was to demonstrate how the viscoelastic properties of protein hydrogels could be encoded within an artificial protein sequence.

Using genetic engineering methods, a telechelic protein denoted ERE was designed from elastin- and fibronectin-derived repeating units and expressed in *Escherichia coli*. ERE was end-linked by the reaction of terminal cysteine residues with tetrakis-vinyl sulfone-functionalized 4-arm star PEG to form hydrogel networks. The effects of varying the precursor concentration and cross-linker stoichiometry on the swelling ratio and mechanical properties of the hydrogels were studied in detail in Chapter 2. The capacity for ERE hydrogels to serve as an artificial extracellular matrix was also assessed by the encapsulation of mouse fibroblasts, which survived the cross-linking reaction and exhibited a spread morphology within the gel.

Chapter 3 describes a set of recombinant artificial proteins that can be cross-linked by covalent bonds, by association of helical domains, or by both mechanisms. These proteins were used to construct chemical, physical, and chemical-physical hydrogel networks in which the mechanism of cross-linking determines whether the material response to mechanical deformation is elastic or viscoelastic. In viscoelastic networks, stress relaxation and energy dissipation could be tuned by controlling the ratio of physical cross-linking to chemical cross-linking, and the physical cross-links could be disrupted either by protein denaturation or by mutation of the primary sequence.

Network dynamics control the viscoelasticity and erosion rate of materials and influence biological processes at multiple length scales. In Chapter 4, variation of the protein sequence was explored as a strategy to tune the characteristic relaxation timescale of protein networks. Single point mutations to coiled-coil physical cross-linking domains in chemical-physical hydrogels altered the characteristic relaxation time over five orders of magnitude. Using a pair of orthogonal coiled-coil physical cross-linking domains, networks with two distinct relaxation timescales were also engineered.

The dynamic properties of protein hydrogels can also be controlled by interactions between protein domains and small molecule ligands. In Chapter 5, the viscoelastic behavior of chemical-physical protein gels was tuned by swelling the gels with small hydrophobic molecules including vitamin D3 and fatty acids. The proposed mechanism for this effect involves binding of the ligands within the hydrophobic pore or channel created by a coiled-coil physical cross-link. Exploiting natural and designed protein-ligand interactions represents a new approach to developing hydrogel "formulations" in which the viscoelastic properties of the material can be engineered to meet specific design criteria.

In addition to exhibiting interesting dynamic properties, polymeric hydrogels containing permanent covalent cross-links and reversible physical cross-links often display enhanced toughness and extensibility. Protein hydrogels cross-linked by covalent thioether bonds and physical coiled coils could be extended further than control covalent hydrogels and exhibited a greater work of extension, which is considered a measure of material toughness. These results demonstrate progress toward engineering tougher, more extensible protein-based materials by the incorporation of coiled-coil physical cross-links within a covalent hydrogel network.

PUBLISHED CONTENT AND CONTRIBUTIONS

L.J. Dooling, M.E. Buck, W.-B. Zhang, and D.A. Tirrell. “Programming molecular association and viscoelastic behavior in protein networks.” *Advanced Materials*. doi:10.1002/adma.201506216

Author contributions: L.J.D. conceived the project (with W.-B.Z., and D.A.T.), performed research (M.E.B. contributed to Fig. 4), analyzed data (with D.A.T.), and wrote the paper (with D.A.T.).

TABLE OF CONTENTS

LIST OF FIGURES, SCHEMES, AND TABLES

Chapter I

CHEMICAL AND PHYSICAL CROSS-LINKING OF ARTIFICIAL PROTEIN HYDROGELS

1. Abstract

Recombinant artificial proteins contain genetically encoded information specifying their assembly into higher order structures, elastic behavior, and biological or chemical function. The goal of this introductory chapter is to describe the some of the common sequences used to design artificial proteins and how materials are fabricated from these proteins by the formation of physical or covalent interactions between protein chains. The focus of this chapter is cross-linking approaches for artificial protein hydrogels, although some of the interactions described can also be used to prepare films, fibrous materials, and particulate systems. Finally, challenges and future directions are discussed with a focus on the specific areas addressed in this thesis.

2. Introduction

Hydrogels are polymeric or supramolecular networks that absorb large amounts of water without dissolving in the aqueous medium or precipitating into the solid phase. As such, hydrogels require a balance between the forces promoting solvation of the polymer chains and the forces driving their association. While the materials and methods for engineering hydrogels vary widely, their high water content and favorable mechanical properties have attracted significant attention for applications in biomedical engineering as well as consumer products [1, 2].

Two central questions arise in the design and application of hydrogels. The first question concerns the source of the polymers (or other macromolecules) that will be used to construct the hydrogel network. Most polymeric hydrogels can be classified as being prepared from either synthetic or natural polymers. Synthetic polymers for hydrogels are typically carbon-based, although silicone polymers are an important exception. Examples include poly(ethylene glycol) (PEG), poly(vinyl alcohol) (PVA), and poly(acrylic acid) (PAA) and its derivatives [3]. Natural polymers for hydrogels include proteins such as collagen and fibrin and polysaccharides such as agarose and alginate [3]. Recombinant artificial proteins, which are the subject of this chapter, combine many of the desirable features of synthetic and naturally-derived polymers [4, 5]. These features include the ability to engineer chemically-defined polymers with precise sequences and the ability to incorporate biological and chemical activity. Other advantages and disadvantages of artificial proteins are discussed in the next section.

The second question in the design and application of hydrogels concerns how these polymers will be assembled into an extended network. Polymers can be cross-linked by covalent bonds between chains, by noncovalent association of chains through hydrogen bonding, hydrophobic interactions, and ionic bonds, or by the entanglement of long chains in a concentrated

solution. Artificial protein hydrogels are well-suited to chemical and physical cross-linking. Strategies for both methods are discussed in detail in this chapter and throughout this thesis.

3. Artificial Proteins and Protein-Based Materials

3.1 Artificial Proteins

Biosynthesis of artificial proteins offers numerous advantages when compared to synthetic routes to polymers. While synthetic polymers exhibit at least some degree of polydispersity, or variation in chain length, proteins synthesized by the ribosome are monodisperse and have a precise chain length that can vary from tens of monomers in small proteins to over 10,000 monomers in the giant muscle protein titin. Proteins are also stereospecific polymers, composed entirely of L-amino acids. This has important consequences for the higher order structures formed in proteins. Most importantly, however, is that like the chain length and stereochemistry, the sequence of amino acid monomers in proteins is also precisely controlled. The sequence of amino acids determines the folded structure of a protein, which in turn determines protein function. While proteins have evolved to perform an enormous number of tasks in living organisms, they have three primary functions:

(1) catalysis by enzymes
(2) maintaining the (dynamic) structures of cells, tissues, and natural protein-based materials
(3) molecular recognition including interactions with other proteins and biomolecules and binding of organic and inorganic ligands

When designing artificial proteins for materials applications, sequences can be adapted from proteins that occur in nature or they can be designed *de novo*. Currently, there are more than

500,000 protein sequences in the UnitProtKB/Swiss-Prot database [6] and over 120,000 protein structures in the Worldwide Protein Databank [7]. This provides an enormous library of sequences for the design of artificial proteins. Many artificial proteins are inspired by sequences found in natural protein-based materials including silk fibers spun by silkworms and spiders, mussel byssus thread, mineralized shells, and the extracellular matrices of various tissues. Other protein designs incorporate domains with useful properties like extreme thermal stability or responsiveness to specific environmental stimuli. When necessary, protein engineering approaches including directed evolution and rational and computational design can be used to improve artificial protein sequences toward a desired specification. Finally, artificial proteins are a green alternative to synthetic polymers, which is likely to become important as the petroleum-based feedstocks that are the current source of monomers for synthetic polymerization reactions are replaced by renewable, biobased feedstocks.

The disadvantages of artificial proteins must be considered along with the advantages described above. Ribosomal synthesis of proteins is limited to 20 amino acid monomers, although a number of strategies have been developed to engineer organisms that are capable of incorporating noncanonical amino acids during protein synthesis [8, 9]. Biosynthesis of proteins is also restricted in terms of the backbone polymer chemistry and the polymer topology; ribosomes produce exclusively linear polypeptide chains. Again, however, several engineering efforts have made some progress in both areas [10, 11]. In addition to the inherent limitations of the cellular protein synthesis machinery, several technical challenges to producing artificial proteins also exist. Each new polymer sequence requires a new template in the form of a gene encoding the artificial protein. Fortunately, recent advances in gene synthesis as well as advanced cloning techniques have made the generation of genetic templates for artificial proteins easier than ever. Other potential

challenges that are specific to each artificial protein include poor yields and difficulties purifying the target protein from the complex mixture of host proteins and other host macromolecules. Artificial proteins may exhibit poor stability under certain conditions and may be susceptible to degradation by proteases. Finally, the immunological properties of artificial proteins have not been well studied, which may pose challenges as well as opportunities for biomedical applications.

3.2 Design of Artificial Proteins for Protein-Based Materials

The sequences of artificial proteins for protein-based materials are composed of three types of domains (Figure I-1): (1) cross-linking or assembly domains, (2) unstructured elastomeric domains, and (3) biologically or chemically functional domains. Examples of these types of domains are given in Table I-1.

Cross-linking or assembly domains mediate interactions between chains in protein-based materials, giving rise to a polymeric or supramolecular network. They are typically folded and possess higher order (secondary, tertiary, and quaternary) structure that is related to their function. Examples discussed in Section 4 include helical domains that form coiled coils or triple helices, β-motifs including extended β-sheets, β-rolls and WW domains, and multimeric globular proteins. Several types of physical protein hydrogels can be obtained depending on how the cross-linking or assembly domains associate. Cross-linking domains can associate to form well-defined aggregates separated by a hydrophilic spacer (Figure I-2 a). Alternatively, cross-linking domains can assemble in less well ordered micellar phases that are also separated by hydrophilic spacers (Figure I-2 b). Finally, proteins can assemble into extended supramolecular fibers to produce nanofibrous hydrogels (Figure I-2 c).

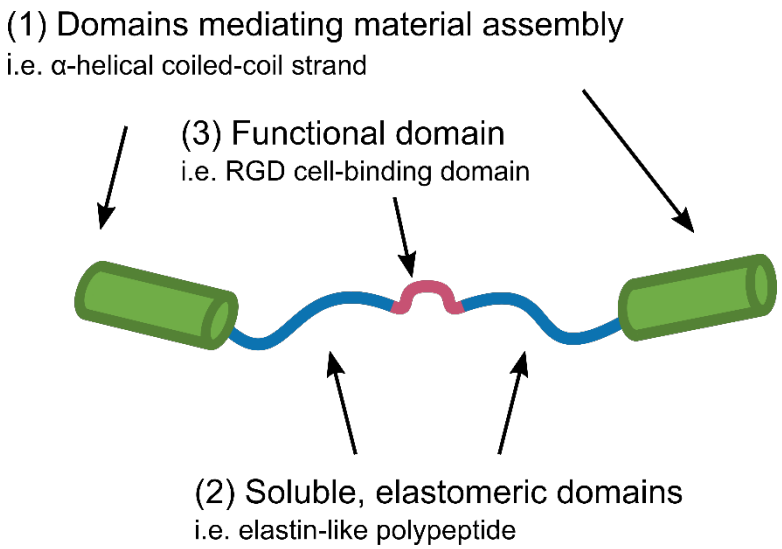

Figure I-1. Design of artificial proteins for protein-based materials. Artificial proteins can include (1) domains mediating the cross-linking or assembly of protein chains by the mechanisms described in Figure I-2, (2) soluble elastomeric domains, and (3) domains encoding biological or chemical function.

The second type of sequence in artificial protein materials includes domains that are unstructured or contain relatively simple structures such as β-turns. In many hydrogel designs, these sequences are required as soluble spacer or linker regions between cross-linking domains in order to prevent the network from precipitating (Figure I-2 a and b). Alternatively, chemical hydrogel networks may be formed by covalent cross-linking of proteins containing these soluble domains, as described in Section 5 (Figure I-2 d). Elastomeric polypeptide domains commonly found in protein hydrogels include elastin-like polypeptides [12, 13], resilin-like polypeptides [13, 14], gelatin-like polypeptides [15], and the alanylglycl-rich nonapeptide repeat, $[AGAGAG(PEG)]_n$ [16].

The final type of sequence in artificial proteins encodes biological or chemical function. This type of sequence includes relatively short cell-binding domains and protease-sensitive

Cross-linking or Assembly Domains	Elastomeric Domains	Functional Domains
Coiled coils and helical bundles	Elastin-like polypeptides	Cell-binding domains
Collagen-like polypeptides	(hydrophilic)	e.g. RGD, REDV, IKVAV
Elastin-like polypeptides (hydrophobic)	Gelatin-like polypeptides	Proteolytic degradation sequences
Silk-like polypeptides	Resilin-like polypeptides	e.g. GPQGIAGQ
WW/Proline-rich domains	Alanylglycl polypeptides	Heparin binding
β-roll domains		Fluorescent proteins
Low complexity sequences		Enzymes
SpyTag/SpyCatcher		Cytokines
Multimeric globular proteins		
e.g. CutA, fluorescent proteins, enzymes		
Calmodulin/CaM binding peptide		

Table I-1. Design of artificial proteins for protein-based materials. Examples of the three types of domains in artificial proteins.

domains as well as much larger domains that can possess enzymatic activity, fluorescence, or growth factor activity. Peptide sequences that promote cell adhesion are included in most artificial protein designs for cellular and tissue engineering applications. The most common cell-binding sequence is the RGD (Arg-Gly-Asp) tripeptide, which is found in a large number of natural proteins including fibronectin, fibrinogen, collagen, vitronectin, and many others [17, 18]. Other cell-adhesion peptides that have been incorporated into artificial proteins include the fibronectin-derived tetrapeptide, REDV (Arg-Glu-Asp-Val) [19], and the laminin-derived pentapeptide, IKVAV (Ile-Lys-Val-Ala-Val) [20]. In addition to promoting cell adhesion, artificial proteins designed for tissue engineering and cell culture applications often include peptide sequences that allow for cell-mediated degradation by secreted or membrane-bound proteases. Degradable peptide sequences incorporated into artificial proteins allow chains to be cleaved by plasmin [21], tissue or urokinase plasminogen activator (tPA, uPA) [22], and matrix metalloproteinases [23].

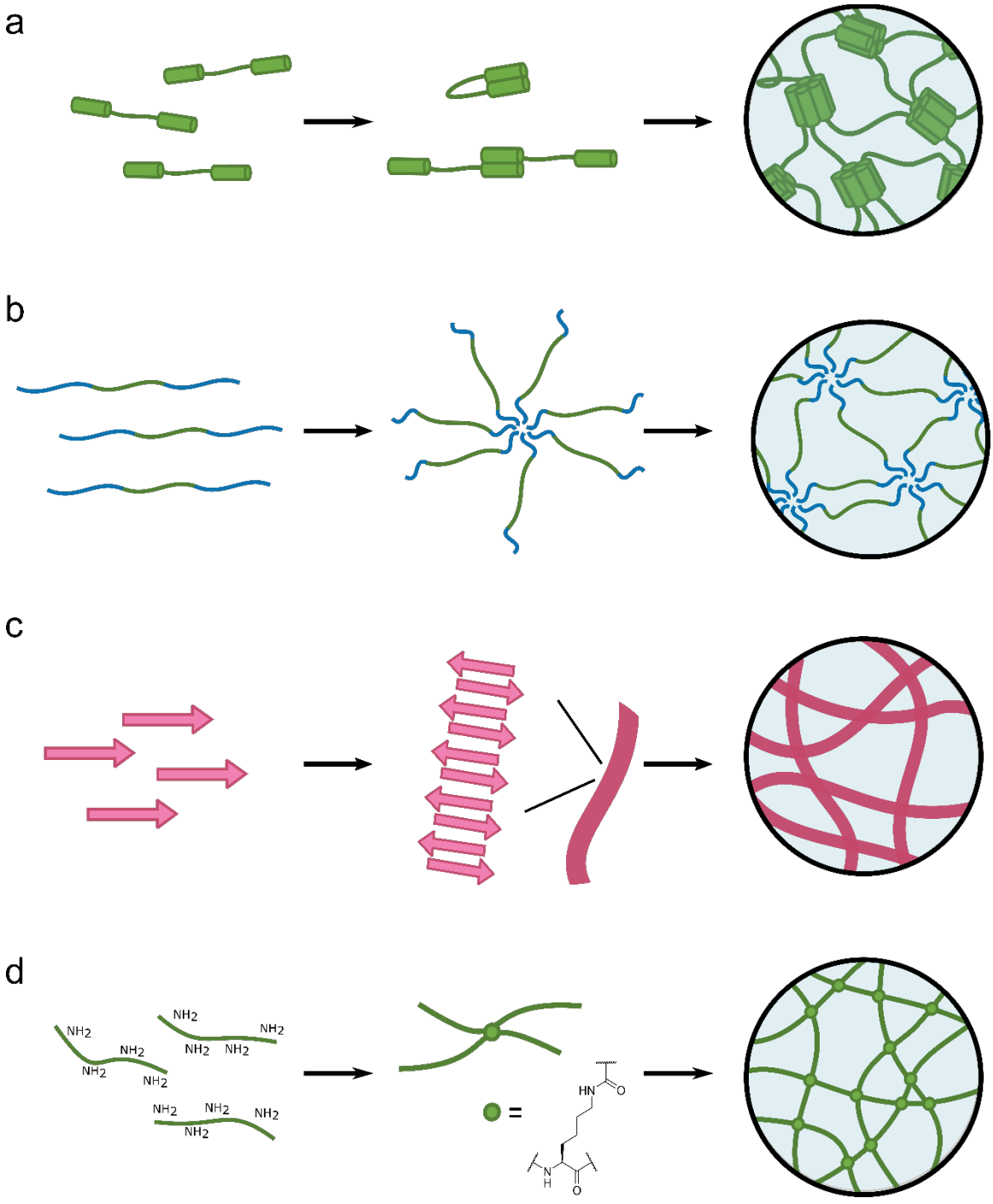

Figure I-2. Cross-linking of protein hydrogels. (**a**) Controlled aggregation of associative domains separated by a soluble elastomeric domain. (**b**) Aggregation of colloidal or micellar domains separated by a soluble elastomeric domain. (**c**) Assembly of proteins into nanofibers that can associate or become entangled to form hydrogels. (**d**) Covalent cross-linking of artificial proteins by reaction of amino acid side chains, such as the ε-amine of lysine.

Recent artificial protein designs have also included heparin-binding domains such as KAAKRPKAAKDKQTK [21, 24]. This sequence contains a high number of positively charged lysine and arginine residues that binding to negatively charged heparin polymers, which in turn sequester a number of different growth factors.

While these three categories are useful for describing artificial protein materials, it is important to note that overlap is both possible and common. By design, many structural cross-linking domains are stimuli responsive and exhibit reversible folding and unfolding based on temperature, pH, and ligand binding. Therefore, domains mediating the cross-linking or assembly of materials under certain conditions may be unstructured or unfolded under other conditions. Similarly, sequences that are primarily characterized as functional domains, such as enzymes encoded within the protein hydrogel backbone, can also contribute to material cross-linking through multimerization of domains on different chains.

4. Physical Cross-linking of Protein Hydrogels

Proteins are especially well-suited for preparing physical hydrogel networks. Nature has evolved folded structural motifs that form highly specific noncovalent interactions to mediate the assembly of protein complexes in biological mixtures. Some of these structural motifs have been adopted in the design of cross-linking domains in artificial proteins. Under the appropriate conditions, the cross-linking domains associate with one another to form the junction points that connect an extended polymer network. In order for the network to swell or absorb water rather than precipitate, soluble spacer or linker domains are also required.

The noncovalent interactions between physical cross-linking domains include hydrogen bonding, ionic bonds, hydrophobic interactions, and others. The reversibility of these interactions imparts important properties to physical protein hydrogels. Changes in the pH, temperature, or ionic strength that alter the folding or association of cross-linking domains can trigger a gel-sol transition in protein hydrogels. In this way, it is possible to program the assembly and disassembly of a network in response to environmental stimuli. Reversible cross-linking in protein hydrogels also has implications for the how the material responds when deformed. Physical protein hydrogels are viscoelastic fluids. When stress is applied over a short duration relative to the lifetime of the cross-links, the gel is deformed elastically and recovers its original shape when the stress is removed. When stress is applied over a long time, however, the material flows like a liquid and can be molded into a new shape. Because the protein-protein interactions that are responsible for cross-linking are specified by sequence of amino acids, artificial protein hydrogels offer the exciting prospect of encoding macroscopic material properties such as self-assembly and viscoelasticity at the molecular level.

4.1 Cross-linking based on the Association of Helical Domains

An important example of physical cross-linking in protein hydrogels is the controlled aggregation or multimerization of coiled-coil domains (Figure I-3 a). Coiled coils are composed of two to seven helical strands wrapped around one another to form a supercoil [25]. Self-assembling hydrogels have been prepared from artificial proteins containing coiled-coil domains that serve as physical cross-linkers. Telechelic artificial proteins with coiled-coil endblocks flanking a water-soluble midblock can form hydrogels when one of the endblocks has an

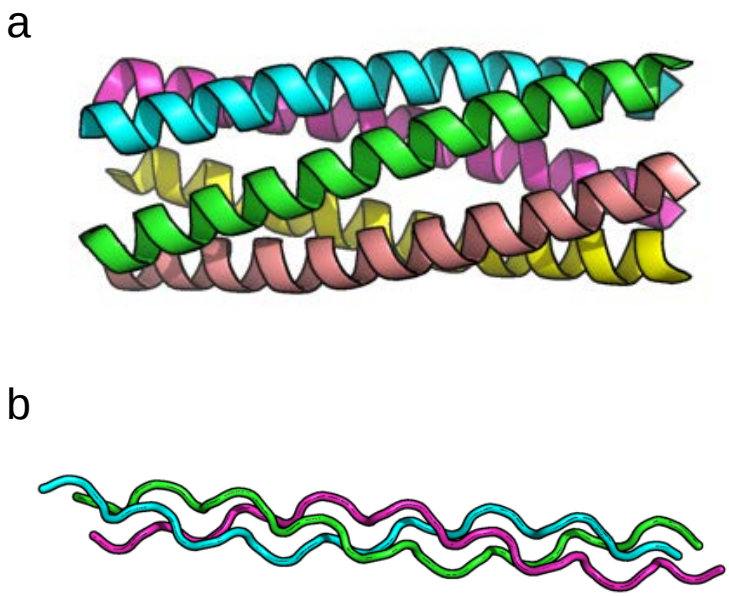

Figure I-3. Physical cross-linking domains based on helical motifs. (**a**) Pentameric coiled coil. (**b**) Collagen-mimetic triple helix. Structures were rendered in PyMol from PDB 1VDF (ref. [123]) and PDB (ref. [124]).

aggregation number greater than or equal to three. The first example of this type of self-assembling protein, denoted ACA, featured designed coiled-coil endblocks A flanking a polyelectrolyte random coil C [26]. The A domain assembles into tetramers under the appropriate conditions, but can be reversibly unfolded by increasing the temperature or the pH. The design of self-assembling protein hydrogels crosslinked by coiled-coil domains has been elaborated in many ways to tune the stability and viscoelastic behavior of coiled-coil gels. Other coiled-coil cross-linking domains have been introduced [27-29] as well as four-helix bundles that do not form a supercoil [30]. Conjugating coiled-coil peptides to synthetic polymers such as pHEMA or PEG results in a hybrid hydrogel where the peptide domains act as cross-linkers and the synthetic polymers act as water-soluble linkers [31, 32].

Physical protein hydrogels have also been designed with cross-linking that is based on the triple helical structure of collagen (Figure I-3 b). Collagen-like cross-linking domains have been incorporated into telechelic, triblock artificial proteins in a design that is analogous to the self-assembling coiled-coiled proteins described above [33, 34]. The collagen-like blocks, denoted T (for triple helix), consist of repeats of the tripeptide sequence (Pro-Gly-Pro) and flank a random coil midblock R (for random coil). The resulting TRT proteins form viscoelastic hydrogels below the melting temperature of the helical blocks. Above the melting temperature, TRT behaves as a viscous liquid. An important feature of the collagen-like block is its well-defined aggregation number of three. This feature enabled the development of a thermodynamic model that accurately predicts the number of network junctions, dangling ends, and looped chains as a function of temperature and protein concentration [33]. Sequence engineering of the endblock triple helical domains has been used to tune hydrogel properties including the gel melting temperature and the network relaxation time [35].

4.2 Cross-linking based on β-motifs

Numerous physical protein hydrogels have been developed with cross-linking domains based on *β*-motifs. Silk-like sequences containing repeats of the hexapeptide GAGAGS were among the earliest recombinant artificial proteins [36]. When combined with elastin-like sequences to form silk-elastin-like proteins (SELPs), the silk domains can aggregate irreversibly to form physical cross-links that are separated by the elastin-like domains, which remain solvated [37]. Nanofibrous hydrogels have also been formed from multiblock artificial proteins containing repeats of the silk-like octapeptide $(AGAGAGEG)_n$ and random coil gelatin-like blocks [38]. Significant efforts have been undertaken to produce recombinant spider silk proteins in a variety

of host organisms. In addition to spinning these recombinant silks into strong fibers, strategies for cross-linking them into hydrogels have also been described [39, 40].

The aggregation of elastin-like polypeptides (ELPs) into a coacervate phase at temperatures above their lower critical solution temperature (LCST) has been exploited in several physical protein hydrogel designs. For example, a triblock elastin-like artificial protein with hydrophobic ELP endblocks flanking a hydrophilic ELP midblock domain exhibits a transition from liquid sol to a hydrogel as the temperature is increased above the LCST of the endblock sequence [41]. Gelation is driven by the phase separation of the hydrophobic ELPs into coacervates that are linked together by the hydrophilic ELP midblock, which by design exhibits a much higher LCST than the endblocks. Physical hydrogels have also been prepared by coacervation of ELPs above their LCST, which causes phase separation into a protein-rich phase that exhibits gel-like properties [42]. More recently, hydrogels were formed by heating concentrated solutions of ELPs composed of repeats of the pentapeptide sequence XPAVG, where X is occupied by Val and Ile at a 4:1 ratio [43]. Hydrogel formation was attributed to an arrested phase transition of the ELPs to create a nanostructured network rather than coacervation.

Other physical cross-linking domains in protein hydrogel designs include β-roll domains [44, 45], WW and proline-rich domains [46, 47], and low complexity sequences [48, 49]. All three of these physical cross-linkers form β-sheet structures. The β-roll cross-linking domain consists of two β-sheets formed by alternating β-strands separated by turns [44, 45]. The folded structure is a flattened helix with a β-sheet on each face of the helix (Figure I-4 a). Folding of this domain from a disordered peptide into a β-roll requires calcium (Ca^{2+}) binding to conserved aspartic acid

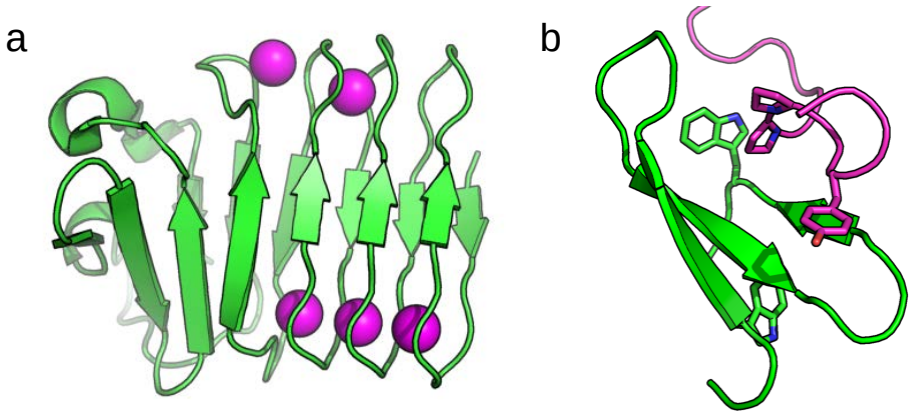

Figure I-4. Physical cross-linking domains based on *β*-motifs. (**a**) *β*-roll domain with Ca^{2+} (magenta spheres). (**b**) WW domain (green) interacting with a proline-rich domain (magenta). The Trp side chains of the WW domain and the Pro and Tyr side chains of the proline-rich domain are shown. Structures were rendered in PyMol from PDB 2Z8X (ref. [125]) and 1I5H (ref. [126]).

residues in the turns. Several solvent-exposed residues on the *β*-sheets were mutated to leucine under the hypothesis that this would increase the hydrophobicity of the exposed surface and lead to the association of the hydrophobic surfaces to form physical cross-links.

Some applications of protein hydrogels, particularly the encapsulation of sensitive cells and biomolecules, would benefit from mild gelation conditions that do not require abrupt changes in temperature, pH, or ionic strength. The simplest hydrogel design that addresses this need consists of two protein solutions that gel upon mixing. This design is accomplished with physical cross-links formed by two different protein domains encoded on separate chains [46, 47]. The first component of the hydrogel is an artificial protein containing WW domains derived from both designed and natural proteins. WW domains consist of approximately 40 amino acids (including two conserved tryptophan residues from which their name is derived) and form antiparallel *β*-sheets (Figure I-4 b). Several artificial proteins were created with 3-8 repeats of the WW domain

separated by soluble polyelectrolyte linkers. The second component is an artificial protein with a sequence consisting of repeats of 3-9 repeats of a proline-rich domain PPxY also separated by soluble linkers. Mixtures of two components with high functionality (7 repeats of the WW domain and 9 repeats of the PPxY domain) formed soft elastic gels (9-50 Pa) through physical cross-linking between WW and PPxY domains (Figure I-4 b).

The β-motif has been exploited widely in fibrous hydrogels consisting of short oligopeptides that form extended β-sheet fibers [50, 51]. Recently, proteins isolated from RNA- and protein-rich subcellular structures known as RNA granules were also observed to form similar fibrous hydrogels [48, 49]. Subsequent analysis showed that many of these proteins contained low complexity (LC) domains that are necessary and sufficient for gelation. Sequencing of an LC domain derived from the RNA-binding protein fused in sarcoma (FUS) revealed repeats of the tripeptide (Gly/Ser)-Tyr-(Gly/Ser), where (Gly/Ser) stands for either glycine or serine. Fusion of green fluorescent protein (GFP) or mCherry fluorescent protein to the LC domain of FUS resulted in fluorescent hydrogels capable of trapping other LC domain proteins with varying affinity. The primary application of hydrogels prepared from LC domains has been *in vitro* experiments to identify how RNA and RNA-regulatory proteins might localize to RNA granules as well as other cellular processes involving LC domains [52-54]. Interestingly, these experiments also revealed the importance of phosphorylation of Ser residues in the LC domain in regulating localization dynamics, offering a potential mechanism for hydrogel assembly and disassembly. Further applications of LC domain hydrogels have not been explored but could be similar to other β-sheet peptide hydrogels.

4.3 Globular Protein Cross-linkers

Well-folded globular protein domains have been incorporated into protein hydrogels to impart chemical or biological activity. Examples include fluorescent proteins to study gel structure and dynamics, enzymes to catalyze desired chemical reactions, and signaling proteins to respond to environmental stimuli. Many globular proteins assemble into multimers or require an interaction with a binding partner to fulfill their function. Therefore, it is possible that globular proteins can also contribute to the cross-linking of networks in addition to their intended function. For example, a chimeric protein was designed in which the A helical domain, which forms coiled coils, was fused to the fluorescent protein dsRed [55]. This artificial protein can assemble into a hydrogel network that contains two types of physical cross-linking. The first is the aggregation of coiled coils and the second is the formation of dsRed tetramers. Similar network formation is possible with a chimera of the A domain fused to an oxidase or a hydrolase enzyme that forms dimers [56, 57].

The calcium-responsive signaling molecule calmodulin (CaM) is another example of a globular protein that has been incorporated into protein hydrogels and protein-polymer hybrid gels [58]. A chimeric protein consisting of the A domain fused to CaM is capable of forming a network in the presence of calcium ions by binding to a bifunctional cross-linker containing two CaM binding peptides (CBP). When Ca^{2+} is removed by chelation, the network is disassembled. Globular domains have the potential to greatly expand the scope of physical cross-linking in protein hydrogels beyond the comparatively simple structural domains such as coiled coils or triple helices. Other globular proteins used in protein and protein-polymer hybrid hydrogels include enzymes and antibody fragments [59, 60].

The CutA protein from the thermophilic archaeon *Pyrococcus horikoshii* forms highly thermostable trimers (Figure I-5) that have been used as physical cross-linkers in protein hydrogels [61-63]. An innovative approach was demonstrated to obtain a two-component system from a single physical cross-linking domain. Two chimeric proteins were designed in which the CutA protein was fused to either the N- or C-terminal fragment of the DnaE split intein from *Nostoc punctiforme*. In solutions of the isolated proteins, trimers form due to the association of the CutA domains but network formation is not possible. Upon mixing of the two proteins, the split intein domains from each protein assemble and undergo trans-splicing to form a new peptide bond. This links the CutA trimers together in a physical hydrogel network. The hydrogel is highly stable to surface erosion, a property that is attributed to the stability of the trimeric cross-linkers. However, the gel is also significantly softer than expected, indicating that most of the cross-links are not elastically effective.

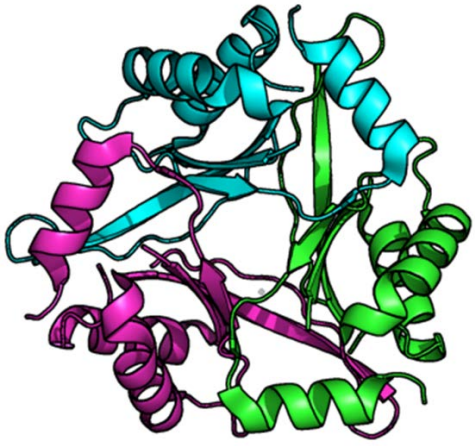

Figure I-5. CutA trimer. The three chains of the CutA trimer are shown in green, blue, and magenta. The structure was rendered in PyMol from PDB 1UMJ (ref. [127]).

5. Chemical Cross-linking of Protein Hydrogels

Protein networks can be prepared by covalent or chemical cross-linking of protein chains. This typically involves reactions linking together amino acid side chains but in principal can also include reactions of the protein backbone or termini. In contrast to the transient and often weak noncovalent association of physical network junctions, chemical cross-links are strong and usually permanent. The chemical reactions employed for protein cross-linking into hydrogel networks closely resembles the vast set of bioconjuagation reactions developed to label proteins with fluorescent dyes and affinity probes and to form intramolecular and intermolecular cross-links for protein structural studies [64]. A key advantage of artificial proteins is that the density and location of these cross-linking residues can be controlled through the design of the protein sequence. Cross-linking is often accomplished by small molecules with two or more functional groups capable of reacting with the artificial proteins. Due to concerns over the toxicity and poor solubility of some small molecule cross-linkers, alternative cross-linking strategies have been developed including photo-chemical cross-linking, bioorthogonal cross-linking, enzymatic cross-linking, and cross-linking by macromolecules such as end-functionalized poly(ethylene glycol).

5.1 Cross-linking Reactions Involving Lysine

The ε-amine of lysine is mildly nucleophilic with a typical pK_a of 9-10 and is a common target for bioconjugation reactions. The bifunctional cross-linkers disuccinimidyl suberate (DSS) and bis(sulfosuccinimidyl) suberate (BS3) [65, 66] and the trifunctional cross-linker tris-succinimidyl aminotriacetate (TSAT) [67] contain either two or three succinimidyl esters that are capable of reacting with amines to form amide bonds (Scheme I-1). Reaction of the ester groups

on DSS, BS3, and TSAT with lysine residues on different protein chains creates a covalent cross-link. More recently, hydroxymethyl phosphine and phosphonium (HMP) compounds (Scheme I-2) have emerged as popular cross-linking reagents for artificial protein hydrogels due to their high solubility in aqueous buffer, rapid gelation kinetics, and commercial availability. Examples of these reagents include β-[tris(hydroxymethyl)phosphino] propionic acid (THPP) [68, 69], tris(hydroxymethyl) phosphine (THP) [70], and tetrakis(hydroxymethyl) phosphoninium chloride (THPC) [71]. Other cross-linking reagents targeting primarily lysine residues include diisocyantates [72], glutaraldehyde [73-75], and the natural product genipin [76]. Elastin-like artificial proteins and resilin-like artificial proteins containing lysine residues have been cross-linked with these reagents.

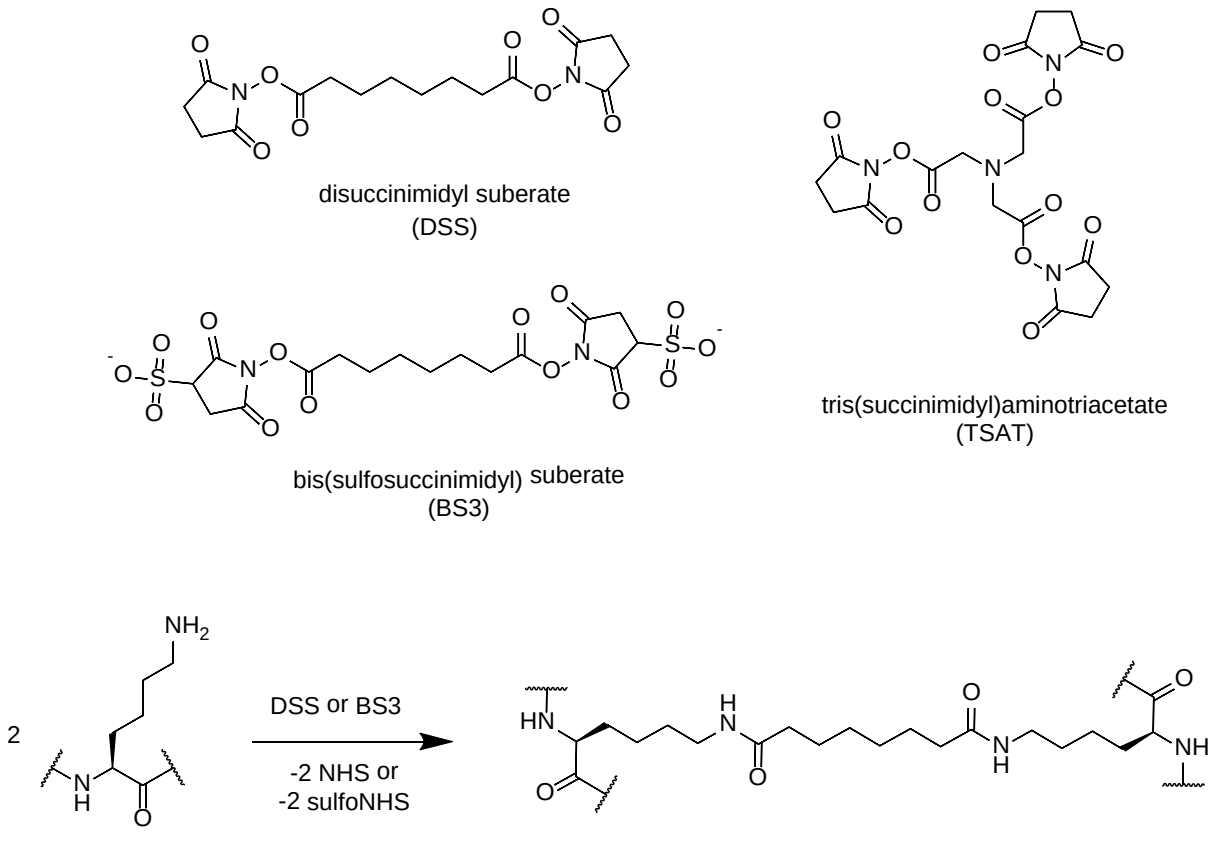

Scheme I-1: Cross-linking of Lys with succinimidyl ester compounds.

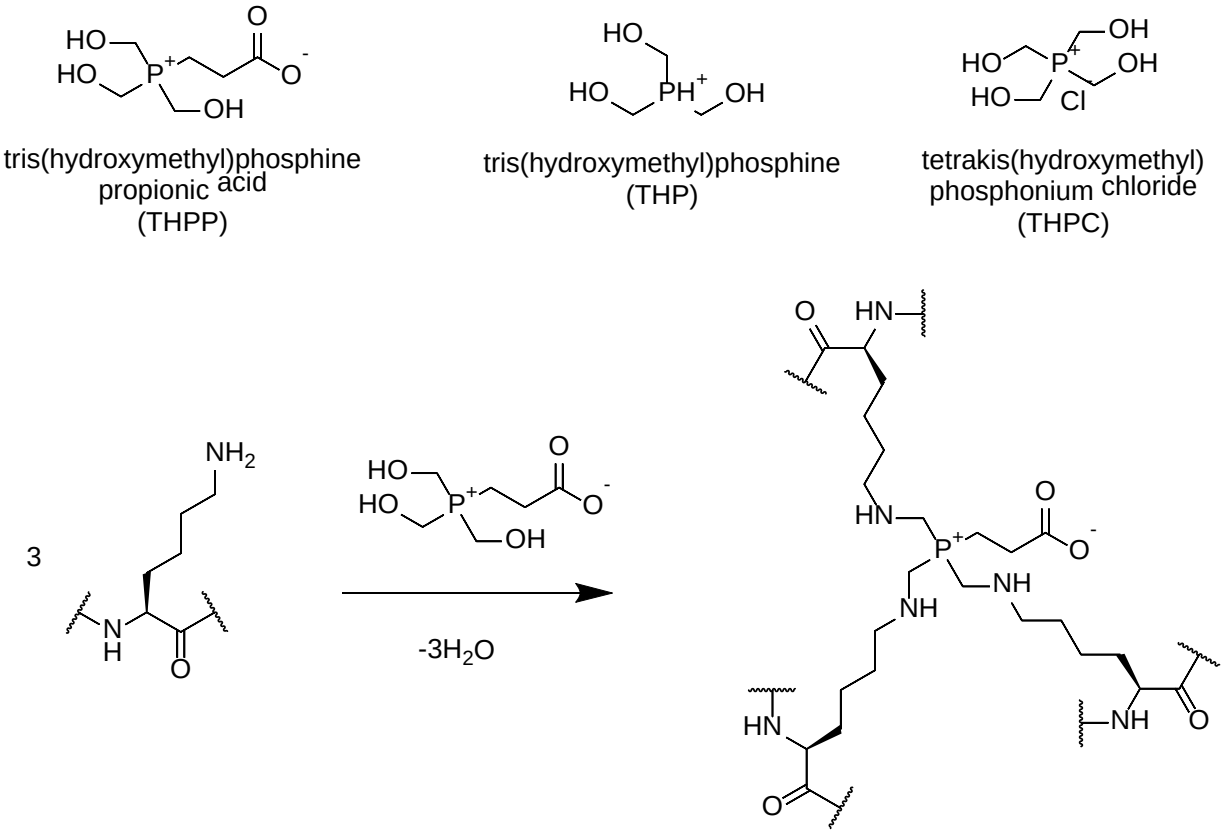

Scheme I-2. Cross-linking of Lys with hydroxymethyl phosphine compounds.

5.2 Cross-linking Reactions Involving Cysteine

Cysteine is an attractive target for cross-linking artificial proteins. Its thiol side chain is nucleophilic with a typical pK_a of 8-9 and can undergo Michael-type conjugate addition to electrophiles including maleimides, vinyl sulfones, and acrylates or displacement reactions with haloacetyls and benzyl halides. This set of reactions is used widely for both bioconjugation and protein cross-linking. Hydrogels have been formed from artificial proteins by cross-linking cysteine residues by Michael-type conjugate addition reactions. These reactions are frequently performed with macromolecular cross-linkers such as PEG-divinyl sulfone and 4-arm PEG tetra

vinyl sulfone (Scheme I-3). Examples include hydrogels prepared from artificial proteins based on fibrinogen- and collagen-like sequences [23, 77], elastin-like artificial proteins (Chapter 2 in this thesis), and resilin-like artificial proteins [78].

An alternative approach to cross-linking artificial protein hydrogels takes advantage of the oxidation of cysteine to form cystine disulfide cross-links between protein chains. Elastin-like artificial proteins with the guest residue occupied periodically by cysteine were oxidized by the addition of hydrogen peroxide, forming a covalent protein network [79]. Disulfide bonds were also used to stabilize physical protein gels cross-linked by leucine zipper coiled coils [80]. In these materials, an oxidant was not required because the reacting cysteine residues were brought into proximity at the coiled-coil interface. The placement of the cysteine residues also favored the antiparallel orientation of coiled coils, preventing loop formation and stabilizing the hydrogels against surface erosion.

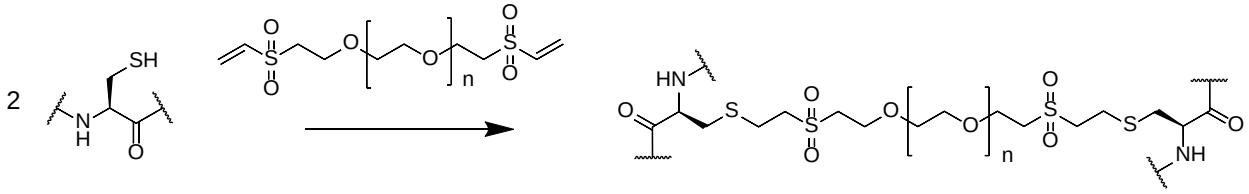

Scheme I-3. Michael-type conjugate addition of Cys and PEG-divinyl sulfone.

5.3 Photo Cross-linking

Cross-linking of polymeric materials including protein hydrogels by irradiation with visible or ultraviolet (UV) light is a powerful method for spatial and temporal control over network formation. One of the earliest methods for cross-linking recombinant elastin-like artificial proteins was the use of γ-irradiation [81-84]. The dose of irradiation could be used to control the cross-

linking density in ELP networks and tune their mechanical properties and swelling behavior. For UV and visible light photo cross-linking, artificial proteins have been modified at lysine and cysteine residues with photo-reactive functional groups including acrylates [21, 85], norbornenes [86], and diazirines [87].

Aromatic amino acid side chains are also potential targets for photo cross-linking. Several artificial proteins including recombinant resilin [88], resilin-like proteins [89-92], and silk-like proteins [40, 93, 94] have been cross-linked by dityrosine formation after irradiation with visible light in the presence of tris(bipyridine)ruthenium(II), $[Ru(bpy)_3]^{2+}$ and ammonium persulfate (Scheme I-4). Elastin-like artificial proteins with phenylalanine guest residues replaced by a noncanonical Phe analog, 4-azidophenylalanine, were cross-linked into films by UV irradiation [95-97]. The mechanical properties of the films could be tuned by controlling the level of Phe replacement during protein expression. A similar strategy would likely be possible using other photoreactive noncanoncial amino acids such as the diazirine analogs of methionine, leucine, and lysine [98, 99].

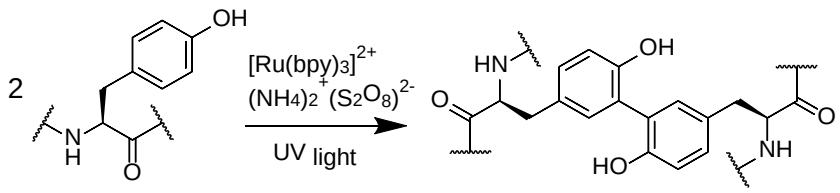

Scheme I-4. Photo cross-linking of Tyr to dityrosine.

5.4 Bioorthogonal Cross-linking

Applications that require the encapsulation of cells or biomolecules or the incorporation of functional protein domains within the hydrogel backbone impose significant limitations on the use of chemical cross-linking methods. The hydrogel protein and cargo proteins are composed of the same 20 amino acids, leading to inevitable side reactions between the cross-linker and the cargo. In the case of cell encapsulation, these side reactions may prove toxic to the cells. Likewise, side reactions with encapsulated biomolecules may interfere with their performance by inhibiting diffusion or by irreversibly binding to an active site. These challenges may potentially be met by advances in the field of bioorthogonal chemistry [100] as well as efforts to expand the genetic code beyond the 20 proteinogenic amino acids. Recently, the copper-catalyzed azide-alkyne cycloaddition (CuAAC), strain-promoted azide-alkyne cycloaddition (SPAAC) (Scheme I-5), and hydrazone formation (Scheme I-6) reactions have been used to cross-link artificial protein hydrogels [101-103]. In each example, the bioorthogonal functional groups were installed on recombinant elastin-like artificial proteins after purification by modification of Lys or Glu residues. Rather than functionalize artificial proteins post-translationally, bioorthogonal groups could instead be introduced into proteins during translation using various methods for the residue-specific [8] or site-specific [9] incorporation of an appropriate noncanonical amino acid.

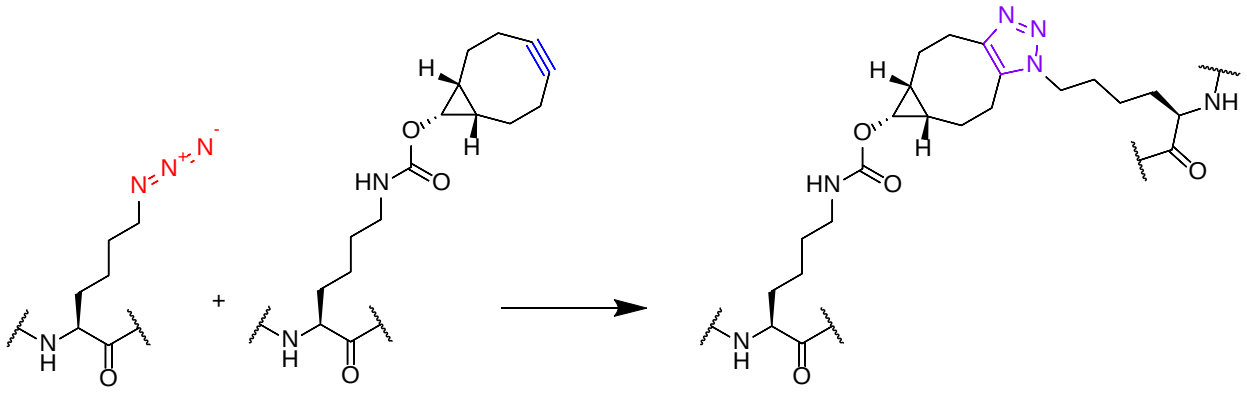

Scheme I-5: Strain-promoted azide-alkyne cycloaddition.

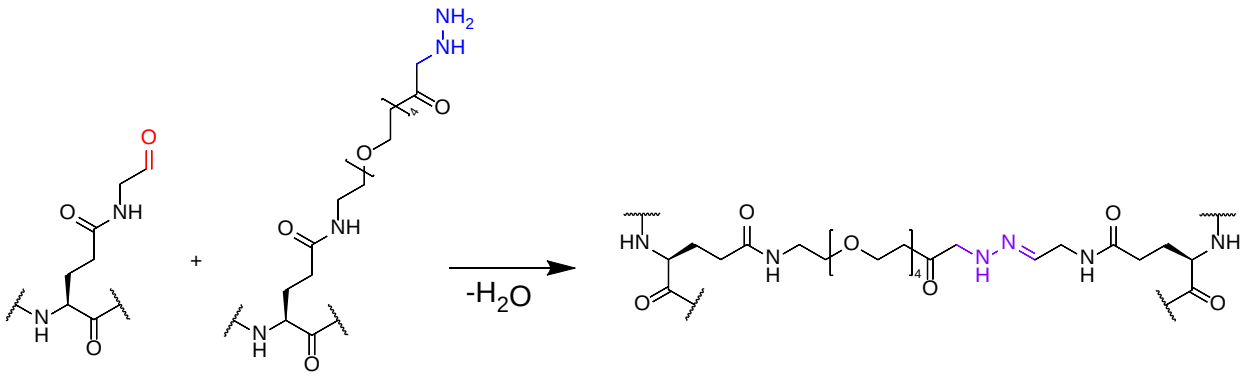

Scheme I-6: Hydrazone formation.

5.5 Enzymatic Cross-linking

Enzymes are also used catalyze the formation of covalent cross-links between artificial proteins to form hydrogel networks. In particular, tissue transglutaminase (tTG) has been used to form intermolecular isopeptide bonds between glutamine and lysine residues on different protein

chains. Artificial proteins cross-linked by this method include elastin-like proteins with guest residues occupied by Gln or Lys [104], recombinant tropoelastin [105], and a pair of designed artificial proteins containing repeat domains rich in Lys and Gln [106]. A highly specific "enzymatic" cross-linking strategy has recently been developed using isopeptide bond formation between the split protein domains SpyTag and SpyCatcher derived from the FbaB protein of *Streptococcus pyogenes* (Figure I-6) [107]. Using this reaction, networks were formed between a pair of elastin-like artificial proteins containing either three repeats of the SpyTag domain or two repeats of the SpyCatcher domain [108]. The highly specific nature of the SpyTag-SpyCatcher covalent bond enabled the formation of networks from multiblock ELP sequences containing a functional LIF (leukemia inhibitory factor) cytokine for the encapsulation of mouse embryonic stem cells.

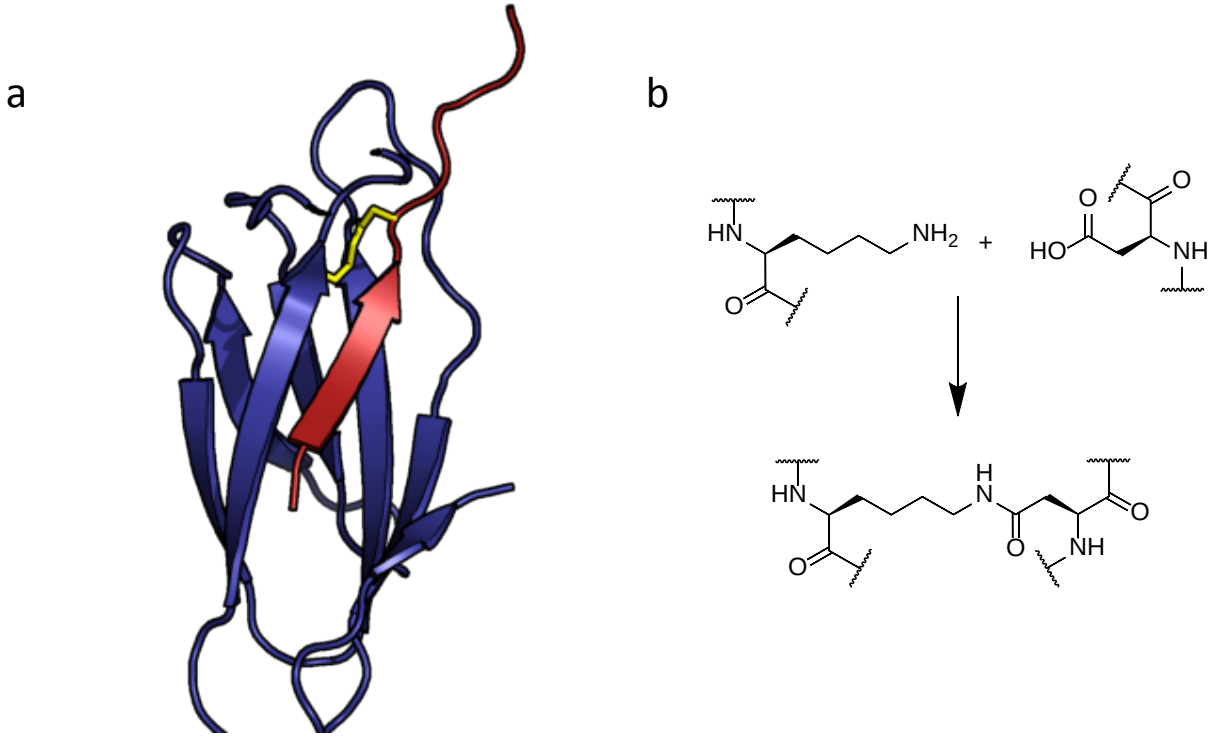

Figure I-6. SpyTag-SpyCatcher cross-linking. (**a**) Reconstitution of the split SpyTag (red) and SpyCatcher (blue) protein domains results in a spontaneous isopeptide bond (yellow) between Lys31 and Asp117 (**b**). The structure was rendered in PyMol from PDB 4MLI (ref. [128]).

6. Current Challenges Addressed by New Cross-linking Strategies

6.1 Dynamic, Viscoelastic Hydrogels

A major advancement in cell and tissue engineering was the recognition that the physical environment in which a cell resides greatly influences cellular behaviors such as proliferation and apoptosis, spreading and migration, and differentiation [109]. This has had a profound effect on the design of hydrogels and other biomaterials, with significant attention now given to engineering materials with the appropriate compliance or stiffness for a particular application. More recently, investigators have begun to develop a similar appreciation for the role of the viscoelastic or time-dependent mechanical properties of the cellular environment [110-112]. For example, fibroblast cells cultured on alginate hydrogels capable of stress relaxation exhibited enhanced spreading when compared to cells cultured on purely elastic substrates [111]. Similarly, stress-relaxing hydrogels can also influence the differentiation of encapsulated mesenchymal stem cells into adipose and osteogenic lineages [110, 112]. The behavior of cells and tissues in viscoelastic environments is particularly relevant for physical protein hydrogels containing transient network junctions. Epithelial cells cultured within a physical protein hydrogel cross-linked by coiled coils were capable of forming multicellular acinar structures [32]. This behavior was attributed to the migration of individual cells through the transiently cross-linked matrix. In contrast, when the same gel was formed and then covalently cross-linked, formation of acinar structures did not occur. Beyond this study, however, the relationship between the dynamic properties of protein hydrogels and cellular behavior has not been investigated. Further progress in this area will require new strategies to engineer the dynamic properties of materials in the same way that the modulus or stiffness is currently controlled.

Protein hydrogels cross-linked by the association of coiled-coil domains are an attractive platform for engineering dynamic materials. Viscoelastic behavior in coiled-coil gels arises from the transient association of the physical cross-links. Shen *et al*. established the relationship between the network relaxation time of coiled-coils gels, as measured by creep rheology experiments, and the rate of exchange of helical strands between coiled coils, as measured by a fluorescence dequenching assay [113]. Coiled coils derived from natural proteins or designed *de novo* exhibit characteristic strand exchange times ranging from approximately 1 second [114] to more than 10,000 seconds [115], suggesting that this dynamic range might also be accessible to engineer the relaxation timescales in viscoelastic hydrogels cross-linked by coiled coils.

In this thesis, the dynamic properties of protein networks containing chemical cross-links and physical cross-links are investigated in detail. Chapter 3 describes the time-dependent mechanical responses of artificial protein hydrogels cross-linked by covalent thioether bonds, by physical association of coiled coils, and by both interactions. These materials can be described as elastic solids, viscoelastic liquids, and viscoelastic solids, respectively. In Chapter 4, variation of the protein sequence is explored as a strategy to engineer the characteristic timescale of stress relaxation in chemical-physical protein networks. It is shown that single point mutations within the physical cross-linking domain can be used to tune the relaxation timescale over five orders of magnitude. In Chapter 5, the relaxation dynamics of chemical-physical protein hydrogels are tuned by addition of external stimuli, specifically small hydrophobic ligands including vitamin D3 and fatty acids that bind within the coiled-coil physical cross-links. By selection of different ligands, it is possible to increase the network relaxation time by 10- to 1000-fold.

6.2 Enhanced Mechanical Properties: Toughness, Strength, and Extensibility

The high water content and elasticity that make hydrogels attractive materials for biomedical engineering applications also result in potentially weak and brittle gels. Several strategies have been proposed for developing tougher hydrogels that can withstand higher strains and stress prior to fracture [116, 117]. Three of these strategies that are well-suited to protein hydrogels are discussed here.

One strategy is to prepare more homogenous hydrogel networks by cross-linking macromolecalar precursors with highly efficient reactions. For example, hydrogels prepared from azide and alkyne end-functionalized poly(ethylene glycol) (PEG) polymers cross-linked by the CuAAC reaction could be extended up to 15 times their original length and sustain a maximum true stress of more than 2 MPa prior to breaking [118]. In comparison, hydrogels formed by photochemical polymerization of PEG-diacrylate, which is known to generate heterogeneous network structures consisting of densely cross-linked regions connected by long chains, fractured at extensions of less than 2 times their original length and sustained maximum stresses of less than 0.2 MPa. Similarly, step-growth PEG networks cross-linked by the Michael-type addition of 4-arm PEG thiol star polymers and PEG-diacrylate were tougher and more extensible than chain-growth networks [119]. The monodispersity of artificial proteins makes them well-suited to this approach, assuming that efficient cross-linking strategies can be developed and that the gelation process results in a homogeneous network structure. Chapter 2 of this thesis describes the formation of a step-growth hydrogel network consisting of a telechelic artificial protein, ERE, and a 4-arm PEG star polymer functionalized with vinyl sulfone on each arm (PEG-4VS) (Figure I-7 a). Tensile experiments with ERE networks are discussed in Chapter 6.

Other emerging strategies for toughening hydrogels rely on various energy-dissipating mechanisms to prevent the stress concentrated near network defects or fracture zones from propagating and resulting in material failure [117, 120, 121]. Hydrogels cross-linked by a combination of permanent covalent cross-links and reversible physical cross-links have been proposed for this purpose. The covalent cross-links maintain the shape and elasticity of the network while the sacrificial physical cross-links can be broken prior to the rupture of polymer chains. As will be described in Chapter 3, hydrogels prepared by end-linking the telechelic artificial protein EPE with PEG-4VS contain both covalent thioether cross-links and physical coiled-coil cross-links (Figure I-7 b). The transient coiled-coil cross-links are expected to dissociate by either thermal or mechanical forces. Tensile experiments with EPE networks, including a comparison to covalent ERE networks, are discussed in Chapter 6.

A final mechanism for hydrogel toughening that is also applicable to protein networks is termed domain transformation [117]. In this strategy, a compact folded domain is stretched and unfolded, dissipating energy and increasing the chain contour length in the process. Protein hydrogels have been prepared with folded structures including the GB1 immunoglobulin-binding domain of streptococcal protein G [89], and FL, a *de novo* designed protein domain with ferrodoxin-like structure [90]. The GB1 domain is mechanically strong, with unfolding forces of 200 pN as measured by single molecule force spectroscopy. As a result, it is difficult to unfold within a hydrogel. In contrast, the FL domain unfolds easily at forces of approximately 10 pN. When cross-linked in a covalent hydrogel network, a fraction of the FL domains appear to unfold easily under forces generated as chains stretch during swelling. While not discussed in this thesis, a variant of the ERE protein containing the full-length tenth type III domain of fibronectin (^{10}FnIII) has also been synthesized and cross-linked with PEG-4VS (Figure I-7 c). These networks may

display enhanced mechanical properties based on the unfolding of ^{10}FnIII, which exhibits moderate unfolding forces of 75-100 pN in single molecule experiments [122].

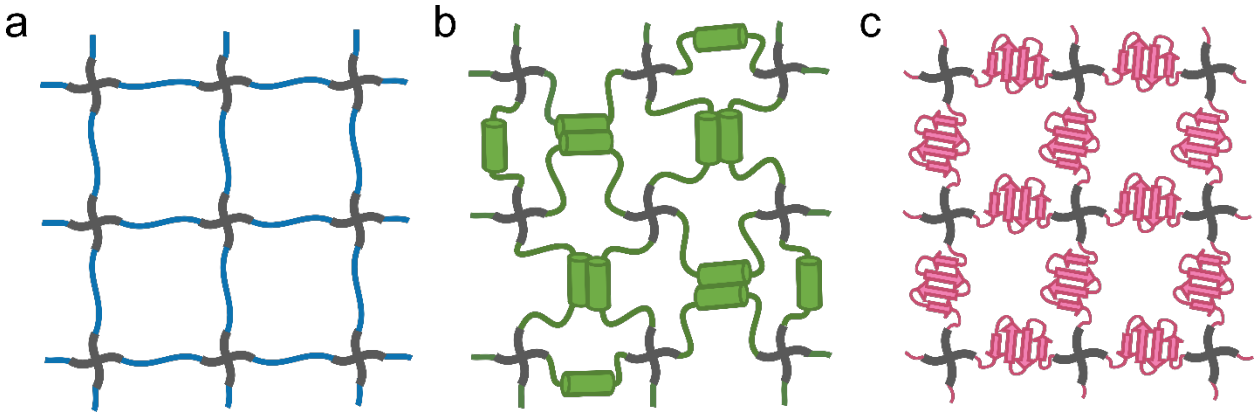

Figure I-7. Hydrogel toughening strategies. (**a**) Network prepared from macromer precursors ERE and PEG-4VS. (**b**) Network containing thioether covalent cross-links between EPE and PEG-4VS and physical cross-links between the midblock domains of EPE. (**c**) Network containing a folded protein domain that can potentially be unfolded by mechanical force.

7. Conclusions

The sequences of artificial proteins contain domains specifying physical or chemical cross-linking, elastic behavior, and biological or chemical function. Physical cross-links are formed by the association of helical domains, β-motif domains, and globular protein domains. Chemical cross-links are formed by the reaction of side chain functional groups with small molecule or macromolecular cross-linkers, by photochemical reactions, and by enzymatic reactions. New approaches to chemical and physical cross-linking of protein hydrogels have the potential to address current challenges in materials design, including engineering dynamic materials and enhancing hydrogel toughness.

8. References

[1] B.V. Slaughter, S.S. Khurshid, O.Z. Fisher, A. Khademhosseini, and N.A. Peppas *Adv. Mater.* **2009** *21*, 3307-3329.

[2] M.W. Tibbitt, K.S. Anseth *Biotech. Bioeng.* **2009** *103*, 655-663.

[3] J.L. Drury, D.J. Mooney *Biomaterials* **2003** *24*, 4337-4351.

[4] S.A. Maskarinec, D.A. Tirrell *Curr. Opin. Biotechnol.* **2005** *16*, 422-426.

[5] J.C.M. van Hest, D.A. Tirrell *Chem. Commun.* **2001** 1897-1904.

[6] UniProtKB/Swiss-Prot Protein Knowledgebase Release 2016_04 Statistics. http://web.expasy.org/docs/relnotes/relstat.html. (accessed 2016 April 29).

[7] Worldwide Protein Databank Deposition Statistics. http://www.wwpdb.org/stats/deposition. (accessed 2016 April 29).

[8] J.A. Johnson, Y.Y. Lu, J.A. Van Deventer, D.A. Tirrell *Curr. Opin. Chem. Biol.* **2010** *14*, 774-780.

[9] C.C. Liu, P.G. Schultz *Ann. Rev. Biochem.* **2010** *79*, 413-444.

[10] A. Ohta, H. Murakami, E. Higashimura, H. Suga *Chem. Biol.* **2007** *14*, 1315-1322.

[11] W.-B. Zhang, F. Sun, D.A. Tirrell, F.H. Arnold *J. Am. Chem. Soc.* **2013** *135*, 13988-13997.

[12] D.W. Urry, T. Hugel, M. Seitz, H.E. Gaub, L. Sheiba, J. Dea, J. Xu, and T. Parker *Phil. Trans. R. Soc. B* **2002** *357*, 169-184.

[13] M.B. van Eldijk, C.L. McGann, K.L. Kiick, J.C.M. van Hest, in *Peptide-Based Materials*, T. Deming, Ed., Springer Berlin Heidelberg, Berlin, Heidelberg **2012**.

[14] R.S.C. Su, Y. Kim, J.C. Liu *Acta Biomater.* **2014** *10*, 1601-1611.

[15] M.W.T. Werten, W.H. Wisselink, T.J. Jansen-van den Bosch, E.C. de Bruin, and F.A. de Wolf *Protein Eng.* **2001** *14*, 447-454.

[16] K.P. McGrath, M.J. Fournier, T.L. Mason, D.A. Tirrell *J. Am. Chem. Soc.* **1992** *114*, 727-733.

[17] M.D. Pierschbacher, E. Ruoslahti *Nature* **1984** *309*, 30-33.

[18] E. Ruoslahti, M.D. Pierschbacher *Cell* **1986** *44*, 517-518.

[19] M.J. Humphries, S.K. Akiyama, A. Komoriya, K. Olden, and K.M. Yamada *J. Cell Biol.* **1986** *103*, 2637-2647.

[20] K. Tashiro, G.C. Sephel, B. Weeks, M. Sasaki, G.R. Martin, H.K. Kleinman, and Y. Yamada *J. Biol. Chem.* **1989** *264*, 16174-16182.

[21] S. Halstenberg, A. Panitch, S. Rizzi, H. Hall, and J.A. Hubbell *Biomacromolecules* **2002** *3*, 710-723.

[22] K.S. Straley, S.C. Heilshorn *Adv. Mater.* **2009** *21*, 4148-4152.

[23] S.C. Rizzi, J.A. Hubbell *Biomacromolecules* **2005** *6*, 1226-1238.

[24] M.B. Charati, J.L. Ifkovits, J.A. Burdick, J.G. Linhardt, and K.L. Kiick *Soft Matter* **2009** *5*, 3412-3416.

[25] J.M. Mason, K.M. Arndt *ChemBioChem* **2004** *5*, 170-176.

[26] W.A. Petka, J.L. Harden, K.P. McGrath, D. Wirtz, and D.A. Tirrell *Science* **1998** *281*, 389-392.

[27] B.D. Olsen, J.A. Kornfield, D.A. Tirrell *Macromolecules* **2010** *43*, 9094-9099.

[28] W. Shen, K. Zhang, J.A. Kornfield, D.A. Tirrell *Nat. Mater.* **2006** *5*, 153-158.

[29] C. Xu, V. Breedveld, J. Kopeček *Biomacromolecules* **2005** *6*, 1739-1749.

[30] A.F. Mehl, S.P. Feer, J.S. Cusimano *Biomacromolecules* **2012** *13*, 1244-1249.

[31] C. Wang, R.J. Stewart, J. Kopeček *Nature* **1999** *397*, 417-420.

[32] Y. Liu, B. Liu, J.J. Riesberg, W. Shen *Macromol. Biosci.* **2011** *11*, 1325-1330.

[33] P.J. Skrzeszewska, F.A. de Wolf, M.W.T. Werten, A.P.H.A. Moers, M.A. Cohen Stuart, and J. van der Gucht *Soft Matter* **2009** *5*, 2057-2062.

[34] M.W.T. Werten, H. Teles, A.P.H.A. Moers, E.J.H. Wolbert, J. Sprakel, G. Eggink, and F.A. de Wolf *Biomacromolecules* **2009** *10*, 1106-1113.

[35] C.I.F. Silva, P.J. Skrzeszewska, M.D. Golinska, M.W.T. Werten, G. Eggink, and F.A. de Wolf *Biomacromolecules* **2012** *13*, 1250-1258.

[36] J. Cappello, J. Crissman, M. Dorman, M. Mikolajczak, G. Textor, M. Marquet, and F. Ferrari *Biotechnol. Prog.* **1990** *6*, 198-202.

[37] J. Cappello, J.W. Crissman, M. Crissman, F.A. Ferrari, G. Textor, O. Wallis, J.R. Whitledge, X. Zhou, D. Burman, L. Aukerman, and E.R. Stedronsky *J. Control. Release* **1998** *53*, 105-117.

[38] A.A. Martens, G. Portale, M.W.T. Werten, R.J. de Vries, G. Eggink, M.A. Cohen Stuart, and F.A. de Wolf *Macromolecules* **2009** *42*, 1002-1009.

[39] S. Rammensee, D. Huemmerich, K.D. Hermanson, T. Scheibel, and A.R. Bausch *Appl. Phys. A* **2005** *82*, 261-264.

[40] K. Schacht, T. Scheibel *Biomacromolecules* **2011** *12*, 2488-2495.

[41] E.R. Wright, R.A. McMillan, A. Cooper, R.P. Apkarian, and V.P. Conticello *Adv. Funct. Mater.* **2002** *12*, 149-154.

[42] H. Betre, L.A. Setton, D.E. Meyer, A. Chilkoti *Biomacromolecules* **2002** *3*, 910-916.

[43] M.J. Glassman, B.D. Olsen *Biomacromolecules* **2015** *16*, 3762-3773.

[44] K. Dooley, B. Bulutoglu, S. Banta *Biomacromolecules* **2014** *15*, 3617-3624.

[45] K. Dooley, Y.H. Kim, H.D. Lu, R. Tu, and S. Banta *Biomacromolecules* **2012** *13*, 1758-1764.

[46] C.T.S. Wong Po Foo, J.S. Lee, W. Mulyasasmita, A. Parisi-Amon, and S.C. Heilshorn *Proc. Natl. Acad. Sci. USA* **2009** *106*, 22067-22072.

[47] W. Mulyasasmita, J.S. Lee, S.C. Heilshorn *Biomacromolecules* **2011** *12*, 3406-3411.

[48] M. Kato, Tina W. Han, S. Xie, K. Shi, X. Du, Leeju C. Wu, H. Mirzaei, Elizabeth J. Goldsmith, J. Longgood, J. Pei, Nick V. Grishin, Douglas E. Frantz, Jay W. Schneider, S. Chen, L. Li, Michael R. Sawaya, D. Eisenberg, R. Tycko, and Steven L. McKnight *Cell* **2012** *149*, 753-767.

[49] S. Xiang, M. Kato, Leeju C. Wu, Y. Lin, M. Ding, Y. Zhang, Y. Yu, and Steven L. McKnight *Cell* **2015** *163*, 829-839.

[50] A. Aggeli, M. Bell, N. Boden, J.N. Keen, P.F. Knowles, T.C.B. McLeish, M. Pitkeathly, and S.E. Radford *Nature* **1997** *386*, 259-262.

[51] S. Zhang, T. Holmes, C. Lockshin, A. Rich *Proc. Natl. Acad. Sci. USA* **1993** *90*, 3334-3338.

[52] Tina W. Han, M. Kato, S. Xie, Leeju C. Wu, H. Mirzaei, J. Pei, M. Chen, Y. Xie, J. Allen, G. Xiao, and Steven L. McKnight *Cell* **2012** *149*, 768-779.

[53] I. Kwon, M. Kato, S. Xiang, L. Wu, P. Theodoropoulos, H. Mirzaei, T. Han, S. Xie, Jeffry L. Corden, and Steven L. McKnight *Cell* **2013** *155*, 1049-1060.

[54] I. Kwon, S. Xiang, M. Kato, L. Wu, P. Theodoropoulos, T. Wang, J. Kim, J. Yun, Y. Xie, and S.L. McKnight *Science* **2014** *345*, 1139-1145.

[55] I.R. Wheeldon, S. Calabrese Barton, S. Banta *Biomacromolecules* **2007** *8*, 2990-2994.

[56] H.D. Lu, I.R. Wheeldon, S. Banta *Protein Eng. Des. Sel.* **2010**.

[57] I.R. Wheeldon, J.W. Gallaway, S.C. Barton, S. Banta *Proc. Natl. Acad. Sci. USA* **2008** *105*, 15275-15280.

[58] S. Topp, V. Prasad, G.C. Cianci, E.R. Weeks, and J.P. Gallivan *J. Am. Chem. Soc.* **2006** *128*, 13994-13995.

[59] T. Miyata, N. Asami, T. Uragami *Nature* **1999** *399*, 766-769.

[60] W. Yuan, J. Yang, P. Kopečková, J. Kopeček *J. Am. Chem. Soc.* **2008** *130*, 15760-15761.

[61] F. Ito, K. Usui, D. Kawahara, A. Suenaga, T. Maki, S. Kidoaki, H. Suzuki, M. Taiji, M. Itoh, Y. Hayashizaki, and T. Matsuda *Biomaterials* **2010** *31*, 58-66.

[62] M. Ramirez, D. Guan, V. Ugaz, Z. Chen *J. Am. Chem. Soc.* **2013** *135*, 5290-5293.

[63] D. Guan, M. Ramirez, L. Shao, D. Jacobsen, I. Barrera, J. Lutkenhaus, and Z. Chen *Biomacromolecules* **2013** *14*, 2909-2916.

[64] G.T. Hermanson, *Bioconjugate Techniques* Elsevier/Academic Press, Amsterdam **2008**.

[65] R.A. McMillan, V.P. Conticello *Macromolecules* **2000** *33*, 4809-4821.

[66] K. Di Zio, D.A. Tirrell *Macromolecules* **2003** *36*, 1553-1558.

[67] K. Trabbic-Carlson, L.A. Setton, A. Chilkoti *Biomacromolecules* **2003** *4*, 572-580.

[68] D.W. Lim, D.L. Nettles, L.A. Setton, A. Chilkoti *Biomacromolecules* **2007** *8*, 1463-1470.

[69] D.W. Lim, D.L. Nettles, L.A. Setton, A. Chilkoti *Biomacromolecules* **2008** *9*, 222-230.

[70] J.N. Renner, K.M. Cherry, R.S.C. Su, J.C. Liu *Biomacromolecules* **2012** *13*, 3678-3685.

[71] C. Chung, K.J. Lampe, S.C. Heilshorn *Biomacromolecules* **2012** *13*, 3912-3916.

[72] P.J. Nowatzki, D.A. Tirrell *Biomaterials* **2004** *25*, 1261-1267.

[73] R.E. Sallach, W. Cui, J. Wen, A. Martinez, V.P. Conticello, and E.L. Chaikof *Biomaterials* **2009** *30*, 409-422.

[74] W. Teng, J. Cappello, X. Wu *Biomacromolecules* **2009** *10*, 3028-3036.

[75] E.R. Welsh, D.A. Tirrell *Biomacromolecules* **2000** *1*, 23-30.

[76] S. Vieth, C.M. Bellingham, F.W. Keeley, S.M. Hodge, and D. Rousseau *Biopolymers* **2007** *85*, 199-206.

[77] S.C. Rizzi, M. Ehrbar, S. Halstenberg, G.P. Raeber, H.G. Schmoekel, H. Hagenmüller, R. Müller, F.E. Weber, and J.A. Hubbell *Biomacromolecules* **2006** *7*, 3019-3029.

[78] C.L. McGann, R.E. Akins, K.L. Kiick *Biomacromolecules* **2016** *17*, 128-140.

[79] D. Xu, D. Asai, A. Chilkoti, S.L. Craig *Biomacromolecules* **2012** *13*, 2315-2321.

[80] W. Shen, R.G.H. Lammertink, J.K. Sakata, J.A. Kornfield, and D.A. Tirrell *Macromolecules* **2005** *38*, 3909-3916.

[81] J. Lee, C.W. Macosko, D.W. Urry *Macromolecules* **2001** *34*, 4114-4123.

[82] J. Lee, C.W. Macosko, D.W. Urry *Macromolecules* **2001** *34*, 5968-5974.

[83] J. Lee, C.W. Macosko, D.W. Urry *Biomacromolecules* **2001** *2*, 170-179.

[84] J. Lee, C.W. MacOsko, D.W. Urry *J. Biomater. Sci. Polym. Ed.* **2001** *12*, 229-242.

[85] K. Nagapudi, W.T. Brinkman, J.E. Leisen, L. Huang, R.A. McMillan, R.P. Apkarian, V.P. Conticello, and E.L. Chaikof *Macromolecules* **2002** *35*, 1730-1737.

[86] C.L. McGann, R.E. Dumm, A.K. Jurusik, I. Sidhu, and K.L. Kiick *Macromol. Biosci.* **2016** *16*, 129-138.

[87] J. Raphel, A. Parisi-Amon, S.C. Heilshorn *J. Mater. Chem.* **2012** *22*, 19429-19437.

[88] C.M. Elvin, A.G. Carr, M.G. Huson, J.M. Maxwell, R.D. Pearson, T. Vuocolo, N.E. Liyou, D.C.C. Wong, D.J. Merritt, and N.E. Dixon *Nature* **2005** *437*, 999-1002.

[89] S. Lv, D.M. Dudek, Y. Cao, M.M. Balamurali, J. Gosline, and H. Li *Nature* **2010** *465*, 69-73.

[90] J. Fang, A. Mehlich, N. Koga, J. Huang, R. Koga, X. Gao, C. Hu, C. Jin, M. Rief, J. Kast, D. Baker, and H. Li *Nat. Commun.* **2013** *4*.

[91] S. Lv, T. Bu, J. Kayser, A. Bausch, and H. Li *Acta Biomater.* **2013** *9*, 6481-6491.

[92] E. Degtyar, B. Mlynarczyk, P. Fratzl, M.J. Harrington *Polymer* **2015** *69*, 255-263.

[93] S. Rammensee, D. Huemmerich, K.D. Hermanson, T. Scheibel, and A.R. Bausch *Applied Physics A* **2005** *82*, 261-264.

[94] Y.J. Yang, C.S. Kim, B.-H. Choi, H.J. Cha *Biomacromolecules* **2015** *16*, 3819-3826.

[95] I.S. Carrico, S.A. Maskarinec, S.C. Heilshorn, M.L. Mock, J.C. Liu, P.J. Nowatzki, C. Franck, G. Ravichandran, and D.A. Tirrell *J. Am. Chem. Soc.* **2007** *129*, 4874-4875.

[96] P.J. Nowatzki, C. Franck, S.A. Maskarinec, G. Ravichandran, and D.A. Tirrell *Macromolecules* **2008** *41*, 1839-1845.

[97] H. Wang, L. Cai, A. Paul, A. Enejder, and S.C. Heilshorn *Biomacromolecules* **2014** *15*, 3421-3428.

[98] M. Suchanek, A. Radzikowska, C. Thiele *Nat. Methods* **2005** *2*, 261-268.

[99] T. Yang, X.-M. Li, X. Bao, Y.M.E. Fung, and X.D. Li *Nat. Chem. Biol.* **2016** *12*, 70-72.

[100] E.M. Sletten, C.R. Bertozzi *Angew. Chem. Int. Ed. Engl.* **2009** *48*, 6974-6998.

[101] I. González de Torre, M. Santos, L. Quintanilla, A. Testera, M. Alonso, and J.C. Rodríguez Cabello *Acta Biomater.* **2014** *10*, 2495-2505.

[102] A.M. Testera, A. Girotti, I.G. Torre, L. Quintanilla, M. Santos, M. Alonso, and J.C. Rodríguez-Cabello *J. Mater. Sci. Mater. Med.* **2015** *26*, 1-13.

[103] U.M. Krishna, A.W. Martinez, J.M. Caves, E.L. Chaikof *Acta Biomater.* **2012** *8*, 988-997.

[104] M.K. McHale, L.A. Setton, A. Chilkoti *Tissue Eng.* **2005** *11*, 1768-79.

[105] S. Bozzini, L. Giuliano, L. Altomare, P. Petrini, A. Bandiera, M.T. Conconi, S. Farè, and M.C. Tanzi *J. Mater. Sci. Mater. Med.* **2011** *22*, 2641-2650.

[106] N.E. Davis, S. Ding, R.E. Forster, D.M. Pinkas, and A.E. Barron *Biomaterials* **2010** *31*, 7288-7297.

[107] B. Zakeri, J.O. Fierer, E. Celik, E.C. Chittock, U. Schwarz-Linek, V.T. Moy, and M. Howarth *Proc. Natl. Acad. Sci. USA* **2012** *109*, E690-E697.

[108] F. Sun, W.-B. Zhang, A. Mahdavi, F.H. Arnold, and D.A. Tirrell *Proceedings of the National Academy of Sciences* **2014** *111*, 11269-11274.

[109] D.E. Discher, P. Janmey, Y.-l. Wang *Science* **2005** *310*, 1139-1143.

[110] A.R. Cameron, J.E. Frith, J.J. Cooper-White *Biomaterials* **2011** *32*, 5979-5993.

[111] O. Chaudhuri, L. Gu, M. Darnell, D. Klumpers, S.A. Bencherif, J.C. Weaver, N. Huebsch, and D.J. Mooney *Nat. Commun.* **2015** *6*.

[112] O. Chaudhuri, L. Gu, D. Klumpers, M. Darnell, S.A. Bencherif, J.C. Weaver, N. Huebsch, H.-p. Lee, E. Lippens, G.N. Duda, and D.J. Mooney *Nat. Mater.* **2016** *15*, 326-334.

[113] W. Shen, J.A. Kornfield, D.A. Tirrell *Macromolecules* **2007** *40*, 689-692.

[114] H. Wendt, C. Berger, A. Baici, R.M. Thomas, and H.R. Bosshard *Biochemistry* **1995** *34*, 4097-4107.

[115] S. Ozeki, T. Kato, M.E. Holtzer, A. Holtzer *Biopolymers* **1991** *31*, 957-966.

[116] S. Naficy, H.R. Brown, J.M. Razal, G.M. Spinks, and P.G. Whitten *Aust. J. Chem.* **2011** *64*, 1007-1025.

[117] X. Zhao *Soft Matter* **2014** *10*, 672-687.

[118] M. Malkoch, R. Vestberg, N. Gupta, L. Mespouille, P. Dubois, A.F. Mason, J.L. Hedrick, Q. Liao, C.W. Frank, K. Kingsbury, and C.J. Hawker *Chem. Commun.* **2006** 2774-2776.

[119] M.W. Tibbitt, A.M. Kloxin, L.A. Sawicki, K.S. Anseth *Macromolecules* **2013** *46*, 2785-2792.

[120] J.-Y. Sun, X. Zhao, W.R.K. Illeperuma, O. Chaudhuri, K.H. Oh, D.J. Mooney, J.J. Vlassak, and Z. Suo *Nature* **2012** *489*, 133-136.

[121] T.L. Sun, T. Kurokawa, S. Kuroda, A.B. Ihsan, T. Akasaki, K. Sato, M.A. Haque, T. Nakajima, and J.P. Gong *Nat Mater.* **2013** *12*, 932-937.

[122] A.F. Oberhauser, C. Badilla-Fernandez, M. Carrion-Vazquez, J.M. Fernandez *J. Mol. Biol.* **2002** *319*, 433-447.

[123] V.N. Malashkevich, R.A. Kammerer, V.P. Efimov, T. Schulthess, and J. Engel *Science* **1996** *274*, 761-765.

[124] K. Okuyama, K. Miyama, K. Mizuno, H.P. Bächinger *Biopolymers* **2012** *97*, 607-616.

[125] C. Angkawidjaja, D.-j. You, H. Matsumura, K. Kuwahara, Y. Koga, K. Takano, and S. Kanaya *FEBS Lett.* **2007** *581*, 5060-5064.

[126] V. Kanelis, D. Rotin, J.D. Forman-Kay *Nat. Struct. Mol. Biol.* **2001** *8*, 407-412.

[127] Y. Tanaka, K. Tsumoto, M. Umetsu, T. Nakanishi, Y. Yasutake, N. Sakai, M. Yao, I. Tanaka, T. Arakawa, and I. Kumagai *Biochem. Biophys. Res. Commun.* **2004** *323*, 185-191.

[128] L. Li, J.O. Fierer, T.A. Rapoport, M. Howarth *J. Mol. Biol.* **2014** *426*, 309-317.

Chapter II

HYDROGEL NETWORKS FROM END-LINKED ELASTIN-LIKE ARTIFICIAL PROTEINS

1. Abstract

Recombinant proteins can be used to prepare artificial extracellular matrices for tissue engineering and other biomedical applications. Using genetic engineering methods, a telechelic protein bearing terminal thiols was designed from elastin- and fibronectin-derived repeating units and expressed in *Escherichia coli*. The recombinant protein, denoted ERE, was purified by inverse thermal cycling and obtained in good yield (100 mg per L of culture) with a free thiol content of approximately 90%. ERE was end-linked with tetrakis-vinyl sulfone-functionalized 4-arm star PEG to form hydrogel networks. The effects of varying the precursor concentration and cross-linker stoichiometry on the swelling ratio and mechanical properties of the hydrogels were studied in detail. The capacity for ERE hydrogels to serve as an artificial extracellular matrix was assessed by the encapsulation of mouse fibroblasts, which can survive the cross-linking reaction and exhibit a spread morphology within the gel.

2. Introduction

Hydrogels are cross-linked polymer networks that absorb a large amount of water. Due to their tissue-like elasticity and high water content, they have attracted significant attention as biomaterials that recapitulate essential features of cellular microenvironments for both tissue regeneration and fundamental biological studies. Hydrogels have been prepared from biomacromolecules such as proteins and polysaccharides, as well as from synthetic polymers such as poly(ethylene glycol) (PEG), poly(hydroxyethylmethacrylate) (pHEMA), and poly(lactic-*co*-glycolic) acid (PLGA) [1]. While biomacromolecular gels derived from natural proteins such collagen and fibrinogen can promote cell adhesion and are subject to proteolytic degradation, there are limited opportunities to engineer their physical and chemical properties. In contrast, synthetic polymers lack the instructive biological cues present in biomacromolecules but are versatile with respect to their molecular weight, topology, and chemical composition. Recombinant artificial proteins combine many of the advantages of naturally-derived biomacromolecules and synthetic polymers. A unique feature of recombinant proteins is the capacity to genetically encode and biologically synthesize a polypeptide chain with a precisely controlled sequence and molecular weight, and more importantly, with folded structures that specify function. An important example of recombinant artificial proteins for biomaterials applications are the artificial extracellular matrix (aECM) proteins [2]. These proteins combine structural elastin-like polypeptide (ELP) domains with cell-instructive amino acid sequences that promote cell adhesion or degradation by specific proteases. aECM proteins have been absorbed onto surfaces to promote cell-adhesion, cross-linked in films and hydrogels, and electrospun into fibers.

Hydrogel networks can be cross-linked by covalent bonds between artificial protein chains. The ε-amine of lysine is by far the most common target for cross-linking reagents, which include

bi- and trifunctional succinimidyl esters [3-5], hydroxymethyl phosphines [6-8], glutaraldehyde [9], diisocyanates [10], and others. However, as artificial protein designs become more complex in order to encode more advanced functionalities, the use of these established cross-linking chemistries may become limited by off target effects. For example, artificial proteins have been designed with enzymatic activity and well-folded three-dimensional structures that might be compromised or inactivated by lysine-specific cross-linkers, requiring either redesign of the protein sequence to remove Lys [11] or alternative cross-linking strategies. The same concerns are also relevant for the encapsulation of cells and biomolecules within hydrogels. Several approaches have been devised to overcome these issues including enzyme-mediated cross-linking [12, 13], bioorthogonal cross-linking reactions such as the strain-promoted azide-alkyne cycloaddition [14, 15], and genetically encoded SpyTag-SpyCatcher chemistry [16]. Still, these methods are somewhat limited by the efficiency of the cross-linking reactions or the ease with which they can be implemented.

Cysteine is perhaps the most promising of the 20 canonical amino acids for performing cross-linking of artificial proteins in the presence of cells or biomolecules, or for cross-linking artificial proteins with more complex structures and functions that could be affected by off-target effects. Cysteine occurs in proteins at an estimated frequency of 1.9% [17]. In contrast, lysine, which has been used extensively to modify and cross-link artificial proteins, occurs at a frequency of 5.9% [17]. Furthermore, cysteine often forms disulfide bonds in native proteins, which would render the thiol side chains of encapsulated cells or protein cargo inaccessible and inert to the cross-linking reaction. This is especially true in the extracellular space, which is regarded as an oxidizing environment.

The thiol side chain of cysteine is readily modified by molecules containing an activated alkene such as vinyl sulfones or maleimides to form stable thioether linkages. These reactions occur near physiological temperature and pH, making them broadly useful for bioconjugation and for applications in biomaterials. The latter has been demonstrated by Hubbell and coworkers, who have described two different examples of PEG-*co*-peptide hydrogels formed by cross-linking reactions between cysteine and vinyl sulfone. In the first example, short oligopeptides with terminal cysteine residues were reacted with 4-arm poly(ethylene glycol) vinyl sulfone to form a step growth network [18]. More recently, this approach has also been demonstrated with 4-arm PEG maleimide and 4-arm PEG acrylate [19]. In the second example, Hubbell and coworkers designed recombinant artificial proteins with sequences derived from fibrinogen and collagen [20]. The proteins contained 3-5 cysteines per chain and were cross-linked into hydrogel networks with PEG-divinyl sulfone. A similar approach was used by Kiick and coworkers to cross-link resilin-like artificial proteins with 4-arm PEG vinyl sulfone [21]. To date, the only example of ELP cross-linking through cysteines was described by Craig and coworkers, who designed an artificial protein containing repeats of the pentapeptide VPGCG and formed disulfide cross-links between the cysteine guest residues by oxidation with hydrogen peroxide [22].

This chapter describes the design and synthesis of a telechelic artificial protein ERE. Recombinant expression and non-chromatographic purification resulted in high yields of ERE with terminal cysteine residues in the reduced state. Hydrogel networks were formed by end-linking ERE with 4-arm PEG vinyl sulfone. The modulus and swelling behavior of ERE hydrogels could be tuned by varying the polymer concentration and functional group stoichiometry during cross-linking. Preliminary experiments indicate that ERE hydrogels can be formed in the presence of

fibroblast cells, enabling their encapsulation for three-dimensional cell culture and tissue engineering.

3. Materials and Methods

3.1 Plasmid Construction

The gene encoding the ERE protein was synthesized (Genscript, Piscataway, NJ) and subcloned into the pQE-80L expression vector (Qiagen, Valencia, CA) using the DH10B *Escherichia coli* cloning strain. The synthesized gene did not contain the 24 bp fragment encoding the MMP-1 degradable octapeptide near the C-terminus. In order to introduce this small fragment, complimentary oligonucleotide strands containing this sequence were synthesized (IDT, Coralville, IA), annealed by heating to 95 °C for five minutes followed by slow cooling, and phosphorylated with T4 polynucleotide kinase (New England Biolabs, Ipswich, MA). The annealed oligo strands contained overhangs that were used to direct ligation into the pQE-80L ERE plasmid that had been digested with *XhoI* (NEB). The resulting plasmid was used to transform the *Escherichia coli* expression strain BL21. The ERE gene sequence and amino sequence are given in Appendix A.

3.2 Protein Expression and Purification

Expression of the ERE protein was carried out in 1 L cultures in 2.8 L Fernbach flasks. A single colony of BL21/pQE-80L ERE was used to inoculate 5 mL of Luria broth (LB) supplemented with 100 μg mL^{-1} of ampicillin (BioPioneer, San Diego, CA). This culture was grown at 37 °C for 8 hr and then used to inoculate 25 mL of 2xYT containing 100 μg mL^{-1} of

ampicillin at a dilution of 1:100. This culture was grown overnight (approximately 12 hr) at 37 °C and then used to inoculate 1 L of Terrific broth containing 100 μg mL^{-1} of ampicillin at a dilution of 1:50. The culture was grown at 37 °C until the optical density at 600 nm (OD_{600}) reached approximately 0.9-1, at which point protein expression was induced by the addition of 1 mM isopropyl β-D-1-thiogalactopyranoside (IPTG) (BioPioneer). Expression proceeded for 5 hr and the cells were harvested by centrifugation at 6000 *g*, 4 °C for 8 min. The cell pellets (approximately 9 g per L of culture) were resuspended in 25 mL of TEN buffer (10 mM Tris, 1 mM EDTA, 100 mM NaCl) supplemented with 5% (v/v) glycerol, 0.1% (w/v) sodium deoxycholate (Sigma), 0.1% (v/v) TritonX-100 (Sigma) and frozen at -20 °C.

The cell resuspension was thawed and treated with 10 μg mL^{-1} DNase I (Sigma, St. Louis, MO), 10 μg mL^{-1} RNase A (Sigma), 1 mM pheynlmethylsulfonyl fluoride (Gold Biotechnology, Olivette, MO), and 5 mM $MgCl_2$ at 37 ^oC for 30 min with agitation. The cells were lysed by sonication with a probe sonicator (QSonica, Newton, CT), and 1% (v/v) β-mercaptoethanol (β-ME) (Sigma) was added to the lysate to reduce disulfide bonds for 1 hr on ice. Purification of the ERE protein from the *E. coli* lysate was accomplished by inverse temperature cycling [23]. The lysate was centrifuged at 39,000 *g*, 4 °C for 1 hr to remove insoluble cell debris. Crystalline NaCl was added to the supernatant to a final concentration of 2 M, and the solution was agitated at 37 °C for 1 hr. The coacervate phase containing ERE was collected by centrifugation at 39,000 *g*, 37 °C for 1 hr. ERE was extracted from the resulting pellet with TEN buffer containing 1% (v/v) β-ME overnight at 4 °C. This procedure was repeated twice with 30 min centrifugation steps. After the third and final cycle, the pelleted protein was resuspended in TEN buffer containing 5 mM tris(hydroxypropyl)phosphine (THP) (Santa Cruz Biotechnology, Dallas, TX) rather than β-ME. After reduction for 2 hr at 4 °C, the buffer and THP were removed by desalting using Zeba 7 kDa

MWCO columns equilibrated with degassed water (LCMS grade, Sigma). The eluted ERE protein was frozen immediately, lyophilized for 72 hr, and stored at -80 °C under argon. Typical yields were 100 mg of lyophilized ERE per L of culture.

The ERE protein could also be obtained from 10 L cultures in a BioFlo 3000 fermentor (New Brunswick, Edison, NJ). Typical yields from fermentation were greater than 300 mg per L. However, due to the limited throughput of the desalting step and concerns about eventual oxidation of the cysteine residues in ERE during storage, smaller batches of proteins were preferred.

3.3 Protein Characterization

The purity and molecular weight of ERE were assessed by sodium dodecyl sulfate polyacrylamide gel electrophoresis (SDS-PAGE), Western blotting, and intact liquid chromatography-mass spectrometry (LCMS) with electrospray ionization (ESI). For SDS-PAGE, lyophilized ERE was dissolved at 5 mg mL^{-1} in 100 mM sodium phosphate, 1 mM EDTA, pH 8. This solution was diluted 1:10 into SDS loading buffer, and 5 μL was loaded on a 10-well NuPage Novex 4-12% Bis-Tris gel (Thermo Fisher Scientific, Waltham, MA). Protein electrophoresis was performed in MES-SDS running buffer (Boston BioProducts, Ashland, MA) at 180 V for 45 min. The proteins were visualized with InstantBlue protein stain (Expedion, San Diego, CA).

The fraction of free cysteines in the purified ERE protein was measured by Ellman's assay. Lyophilized ERE protein was dissolved in reaction buffer (100 mM sodium phosphate, 1 mM EDTA, pH 8) at a concentration of 5 mg mL^{-1}. A stock solution of Ellman's reagent, (5,5'-dithio-bis-[2-nitrobenzoic acid]), (Sigma) was also prepared at 5 mg mL^{-1}. In a cuvette, 250 μL of protein solution and 50 μL of Ellman's stock solution were added to 2.5 mL of reaction buffer. The reaction was incubated at ambient temperature for 15 min and the absorbance at 412 nm was

measured on a Cary 50 spectrophotometer. The extinction coefficient of the reaction product, 2-nitro-5-thiobenzoate (14,150 M^{-1} cm^{-1}) [24], was used to determine the concentration of free thiols.

3.4 Hydrogel Cross-linking

Cross-linking with PEG-4VS was performed under denaturing conditions in 0.1 M sodium phosphate, 6 M guanidinium chloride, 0.4 M triethanolamine (TEOA) (Sigma) at pH 7.4. To prepare 15 wt% gels (initial concentration of total polymer), lyophilzed ERE protein (150 mg) was dissolved in 1 mL of degassed cross-linking buffer. PEG-4VS (Jenkem USA, Plano, TX) was dissolved at the same concentration in degassed 0.4 M TEOA, pH 7.4. The solutions were sonicated for 2 min in an ultrasonic bath and centrifuged for 1 min, 10,000 *g* to remove air bubbles. In a microcentrifuge tube, 271 μL of the cross-linker solution was added to 1 mL of the protein solution. This volumetric ratio gives a nominal 1:1 stoichiometric ratio of vinyl sulfone to thiol functional groups. The actual stoichiometric ratio will vary slightly based on fraction of free thiols in the ERE protein preparation and the functionalization of the PEG-4VS. The mixture was vortexed and droplets (50-70 μL) were pipetted onto glass slides that had been treated with SigmaCote (Sigma) according to the manufacturer's protocol. A second treated glass slide was placed on top, separated by a spacer cut from a sheet of silicone rubber (McMaster-Carr, Santa Fe Springs, CA) (1 mm or 2 mm). The slides were clamped together with binder clamps. The cross-linking reaction was allowed to proceed overnight (>12 hr). Gels were also prepared in this manner with different initial polymer concentrations (7.5, 10, 15, 20, 25 wt%) at a constant 1:1 vinyl sulfone to thiol stoichiometry, and with different functional group stoichiometry (0.6:1, 0.8:1, 1:1, 1.2:1, 1.4:1 vinyl sulfone to thiol) at a constant polymer concentration of 15 wt%.

A second cross-linking protocol that omitted the guanidinium chloride and triethanolamine was also assessed. ERE and PEG-4VS were dissolved at 5, 7.5, and 10 wt% in HEPES buffered saline (25 mM HEPES, 150 mM NaCl, pH 7.4) without triethanolamine. Solutions of ERE and PEG-4VS at equal concentration were mixed at a 1:1 vinyl sulfone to thiol stoichiometry in a microcentrifuge tube, vortexed, and pipetted onto a treated glass slide with 1 mm spacers as described. The gels were cured overnight.

3.5 Equilibrium Swelling and Sol Fraction Determination

Hydrogel disks (50 μL in the as-prepared or unswollen state) were swollen for 48 hours in 1 mL of sterile distilled, deionized (ddH_2O). The amount of unreacted material removed from the gel was estimated by measuring the protein concentration using a bicinchoninic acid assay (BCA, Pierce, Rockford, IL) according to the manufacturer's protocol. A standard curve was generated using ERE solutions of known concentration prepared from lyophilized protein. After removing the ddH_2O, the gels were swollen in phosphate buffered saline (PBS) (1.5 mM KH_2PO_4, 4.3 mM Na_2HPO_4, 137 mM NaCl, 2.7 mM KCl, pH 7.4) for 48 hr and the swollen mass was determined by weighing the gels on an analytical balance (Mettler Toledo, Columbus, OH). The gels were transferred to ddH_2O, which was changed five times over the course of 3 days to remove the salts. The gels were frozen in microcentrifuge tubes and lyophilized so that the dry mass could be measured. The equilibrium swelling ratio, Q_m, was determined by dividing the swollen mass by the dry mass. Six replicates were performed for each gel.

3.6 Rheological Characterization

Rheological measurements were performed on a TA Instruments (New Castle, DE) ARES-RFS strain-controlled rheometer with a parallel-plate geometry (8 mm diameter). Hydrogel disks were cut to this size from larger samples using an 8 mm diameter biopsy punch (Miltex, York, PA) and loaded between the sample plates according to the protocol described by Meyvis *et al* [25]. Briefly, the gap between the upper and lower plates was lowered until a normal force was detected. The storage modulus (*G'*) was then measured at 1% strain amplitude, 5 rad s^{-1}, 25 °C. The gap was then lowered by 20 μm and the measurement of *G'* was repeated. This process was continued until *G'* at 5 rad s^{-1}, 1% strain amplitude reached a constant value. A strain sweep test from 0.1-10% was performed to confirm the linear viscoelastic regime of each sample at 10 rad s^{-1} and 25°C. Following the strain sweep, a frequency sweep was performed at 5% strain amplitude, 25 °C over an angular frequency range of 100 to 0.1 rad s^{-1}. Three replicates were performed for each gel.

3.7 Dynamic Oscillatory Time Sweep

The gelation time was determined by performing a dynamic oscillatory time sweep experiment on the ARES-RFS equipped with a 25 mm parallel plate geometry and Peltier temperature controller set to 37 °C. Solutions of ERE and PEG-4VS were prepared in HEPES buffered saline at 5, 7.5, and 10 wt%, vortexed to mix, and centrifuged briefly to remove bubbles. In a microcentrifuge tube, 54.2 μL of PEG-4VS solution was added to 200 μL of ERE solution giving a 1:1 vinyl sulfone to thiol stoichiometry. The mixture was vortexed briefly before pipetting 200 μL onto the lower plate of the rheometer. The gap height was adjusted incrementally to 200 μm and the edge of the gel was covered with paraffin oil. This process had a typical lag time of approximately 2 minutes from the time at which the two components were mixed until data

collection began. A time sweep experiment was performed at 5% strain amplitude, 10 rad s^{-1}. The gelation time is taken as the time at which *G'* and *G"* intersect. Three replicates were performed for each concentration.

3.8 Encapsulation of Fibroblasts

NIH 3T3 mouse fibroblasts (American Type Culture Collection, Manassas, VA) were maintained at 37 °C with 5% CO_2 in Dulbecco's Modified Eagle Medium (DMEM) (Life Technologies, Carlsbad, CA) with 10% (v/v) bovine serum (Life Technologies), and 1% (v/v) penicillin/streptomycin (Life Technologies). At ≈80% confluence, cells were detached with 2 mL of trypsin (0.05%) – EDTA (0.02%) solution (Life Technologies) for 5 min at ambient temperature followed by addition of 8 mL of complete growth medium to neutralize the trypsin. The cell suspension was centrifuged at 200 *g* for 3 minutes. After removal of the medium, the pelleted cells were washed in 10 mL of HEPES buffered saline (HBS), and centrifuged again. Finally, the cells were resuspended in 1 mL HBS and counted using a hemocytometer.

Cells were encapsulated in 5, 7.5, and 10 wt% ERE hydrogels cross-linked at a 1:1 vinyl sulfone to thiol stoichiometry. ERE and PEG-4VS were dissolved at these concentrations in HBS, pH 7.4 and sterile-filtered using a 0.2 μm centrifugal filter (Corning, Corning, NY). Cells were aliquoted in microcentrifuge tubes and centrifuged to remove the buffer. The pellet was resuspended in the ERE solution at a concentration of 3 x 10^6 cells mL^{-1} and mixed with the PEG-4VS solution by gentle vortexing. A 30 μL droplet was pipetted onto a 35 mm glass bottom dish (MatTek, Ashland, MA). The gelation mixtures were cured at 37 °C in a humidified incubator. Based on the results of the gelation kinetics experiments, 10 wt% gels were cured for 1 hr prior to adding 3 mL DMEM (without phenol red) + 10% bovine serum + 1% penicillin/streptomycin; 7.5

wt% gels were cured for 1.5 hr, and 5 wt% gels were cured for 2 hr. Following the addition of media, the gels were incubated at 37 °C with 5% CO_2. The medium was changed the next day.

The viability of fibroblasts encapsulated in hydrogels was determined using a Live/Dead stain (Invitrogen, Carlsbad, CA) 3 days post-encapsulation. Briefly, after removal of DMEM, the hydrogel was washed with 3 mL of PBS. The Live/Dead staining solution (2.5 mL), which contained 4 μM ethidium homodimer-1 (EthD-1) and 2 μM calcein AM in PBS, was added to the cell-laden hydrogel and incubated for 45 minutes at room temperature. Following incubation, the staining solution was removed and the hydrogels were washed with PBS (3 mL) and covered in cell culture medium (3 mL). Laser scanning confocal microscopy (LSM 510, Zeiss, Irvine, CA) was used to visualize the stained cells. A 20x/0.3 long working distance objective was used for all images. The calcein fluorophore was detected by excitation at 488 nm with an argon laser and a 505 nm LP emission filter. The EthD-1 fluorophore was detected by excitation at 543 nm with a He/Ne laser and a 630 nm LP emission filter. Images were acquired as z-stack sections every 10 μm over a 200 μm thick region of the gel beginning at least 100 μm away from the coverslip. The images were analyzed with ImageJ (NIH, Bethesda, MD) to generate max intensity projections in the z-direction.

4. Results and Discussion

4.1 Protein Design and Synthesis

The multiblock, telechelic protein ERE (Figure II-1 a and b) was designed with an amino acid sequence that encodes the desired biological activity (cell-adhesion and proteolytic degradation) and physical properties (cross-linking sites and elastin-like domains). ERE contains two domains that confer biological activity required for cell encapsulation. The first is a cell-

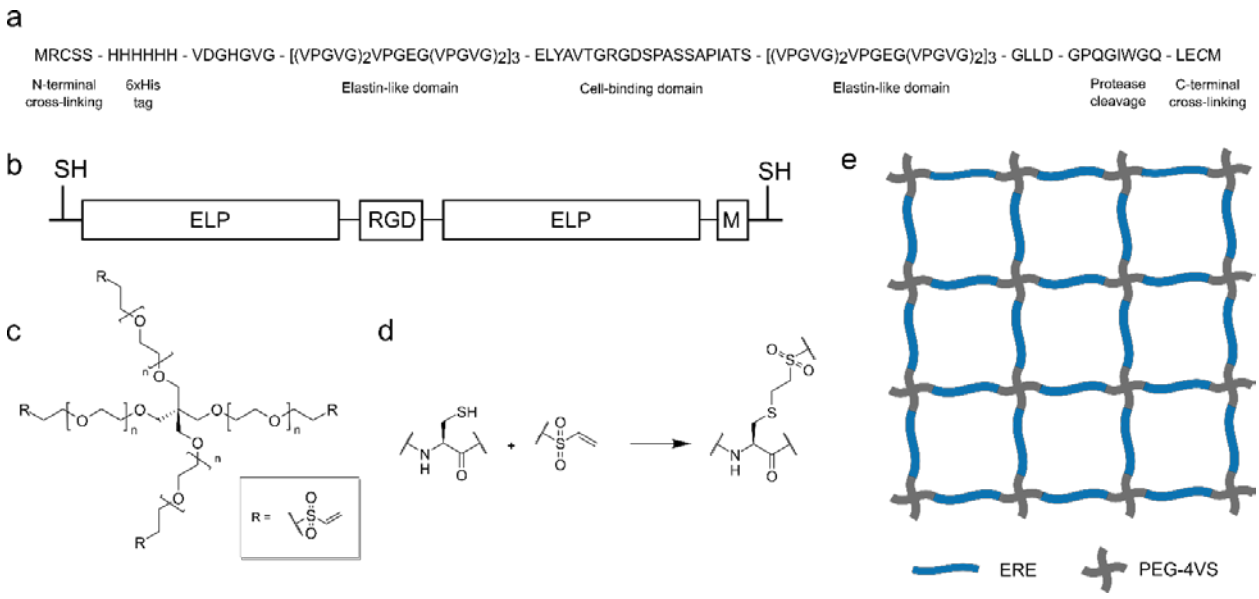

Figure II-1. Sequence of ERE and cross-linking scheme. (**a**) Amino acid sequence and (**b**) multiblock structure of ERE, which is composed of elastin-like polypeptide (ELP) endblocks, a cell-binding domain R, an MMP-1-degradable sequence M, and terminal cysteine residues. (**c**) 4-arm poly(ethylene glycol) tetrakis-vinyl sulfone (PEG-4VS) is used to end-link ERE through a Michael-type conjugate addition of the thiol side chain of cysteine to vinyl sulfone (**d**), resulting in a step-growth network idealized in (**e**).

binding domain, denoted R, that promotes cell adhesion through integrin receptors. The R domain consists of 17 amino acids from a solvent exposed loop in the tenth type III repeat of human fibronectin [26, 27]. This loop contains the RGD (Arg-Gly-Asp) tripeptide that has been widely used in biomaterials prepared from artificial proteins and from synthetic peptides [28]. The second biologically active domain encoded in the ERE protein is the octapeptide sequence GPQGIWGQ that can be digested by several matrix metalloproteinases (MMPs). This peptide sequence is based on degradable sequences in various collagen proteins and was originally designed as one of many substrates to study the sequence specificity of MMPs [29]. It was found to be a good substrate for several MMPs including collagenases (MMP-1 and MMP-8), gelatinases (MMP-2 and MMP-9),

stromelysin (MMP-3), and matrilysin (MMP-7). Several biomaterial designs have incorporated this peptide or similar sequences to create degradable scaffolds that allow encapsulated cells to remodel their local environment in order to spread or migrate [18, 30]. Including this sequence between the cross-linking sites in ERE is expected have a similar effect in this work.

ERE contains unique cysteine residues at the N- and C-termini for end-linking with thiol-reactive cross-linkers. The remainder of the protein is composed primarily of elastin-like repeats (E), meaning that these domains are likely to determine the physical properties of hydrogels prepared from ERE. ELPs have received signification attention as biomaterials for tissue engineering and are well known for their lower critical solution temperature (LCST) transition. At temperatures below their LCST, ELPs are soluble and unstructured. At temperatures above their LCST, ELPs aggregate into a protein-rich coacervate phase. Inverse thermal cycling at temperatures above and below the LCST can be used to separate ELPs from proteins and other contaminants that do not possess this transition behavior as a low-cost alternative to chromatographic purification [23]. However, in many cases, the phase transition of ELPs in biomaterials also results in protein aggregation and heterogeneous network structures at physiological temperature [3, 31]. This can alter the mechanical properties of the material and results in poor optical transparency, obstructing the observation of encapsulated cells by light microscopy. Mixing hydrophilic poly(ethylene glycol) with ELPs that have a low LCST has been reported to improve the transparency, but the effect is limited [31]. To address this problem, the elastin-like domains in ERE are more hydrophilic sequences with guest residues occupied by valine and glutamic acid at a ratio of 4:1. The LCST of an ELP with this composition was reported to be approximately 75 °C at a neutral pH and an ionic strength of 150 mM [32], which are typical physiological conditions. By increasing the ionic strength of the ELP solution, the LCST can be

suppressed significantly. In this way, it was anticipated that the ERE protein could be purified by the inverse thermal cycling method yet remain transparent when cross-linked into a hydrogel and swollen at physiological temperature (37 °C), pH, and salt concentration.

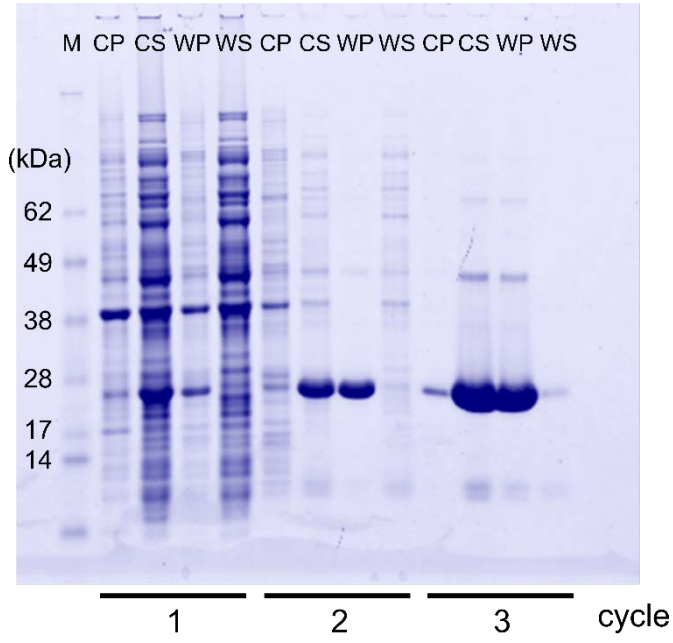

Figure II-2. Temperature cycling purification of ERE. ERE was purified from the *E. coli* lysate by three rounds of temperature cycling above and below the lower critical solution temperature. The target protein is soluble in the cold step (4 °C, 100 mM NaCl) and aggregates into a protein-rich coacervate phase in the warm step (37 °C, 2 M NaCl). The apparent molecular weight of ERE (approx. 25 kDa) is slightly greater than the calculated molecular weight (18.5 kDa), but this is common for elastin-like proteins. The expected molecular weight was confirmed by ESI-MS.

The ERE protein was produced in *Escherichia coli* strain BL21 and purified by three rounds inverse temperature cycling above and below the LCST of the protein. Thermal cycling with hydrophilic ELP sequences has rarely been reported. However, ERE is expressed at high levels in

E. coli and increasing the ionic strength of the lysate by addition of 2 M NaCl was found to be sufficient to shift the LCST to below 37 °C. Raising the temperature above 37 °C and agitating the solution caused the formation of ERE aggregates that could be separated by centrifugation. The ERE proteins were extracted from the pelleted fraction by resuspension in a low ionic strength (100 mM NaCl) buffer at 4 °C. To prevent thiol oxidation, β-mercaptoethanol (βME) was included in the solution throughout the purification. After three cycles, ERE was successfully purified from the *E. coli* lysate proteins (Figure II-2). Tris(hydroxypropyl) phosphine was used to reduce protein disulfides and β-ME/cysteine adducts. The buffer, salts, and reducing agents were removed by gel filtration chromatography and the final product was obtained by lyophilization. The typical yields for ERE were 100 mg per L of culture. The molecular weight of the purified protein was confirmed by intact LC-MS with electrospray ionization ($M_{\text{calcd.}}$ = 18476, $M_{\text{obs.}}$ = 18477).

4.2 Evaluation of Protein Free Thiol Content

The free thiol content of purified ERE was evaluated with Ellman's assay, in which cysteine reacts with (5,5'-dithio-bis-[2-nitrobenzoic acid]) (DTNB) to produce a yellow color corresponding to the 2-nitro-5-thiobenzoate ion (TNB^{2-}) [33]. The absorbance at 412 nm was used to calculate the concentration of TNB^{2-}, which is equal to the concentration of free thiols. For a solution of lyophilized ERE dissolved at 5 mg mL^{-1}, the concentration of free thiols measured by Ellman's assay was found to be 88% of the expected amount based on the protein concentration and the assumption that each ERE protein contains two cysteines (Table II-1). The discrepancy between the observed thiol concentration and the expected thiol concentration is likely due to the formation of higher order protein oligomers linked by intermolecular disulfides, cyclization of ERE by an intramolecular disulfide bond, or other impurities with unknown cysteine contents. To

confirm that the TNB^{2-} detected in Ellman's assay was not due to residual reducing agents (e.g. THP or β-ME) in the ERE preparation that could potentially cleave the disulfide bond in DTNB, the ERE protein solution was filtered through a 10 kDa MWCO column. The column is expected to retain ERE (18.5 kg mol^{-1}) but allow the passage of small molecules such as THP (209 g mol^{-1}) and β-ME (78 g mol^{-1}) into the filtrate. When the filtrate was analyzed by Ellman's assay, the absorbance at 412 nm was too low to be accurately measured (data not shown), confirming that the observed thiol concentration reported in Table II-1 is due to free cysteines on the ERE protein.

Measured [thiol] (μM)	**[ERE] (μM)**	**mol free thiol/ mol protein**
42.6 ± 1.4	24.1	1.76 ± 0.06

Table II-1. Concentraion of free thiols determined by Ellman's assay. The thiol concentration determined from the absorbance of NTB^{2-} was divided by the concetration of protein in the reaction mixture to obtain an estimate of the number of free thiols per protein chain.

The purified ERE protein was also characterized by non-reducing SDS PAGE to determine its oligomerization state (Figure II-3 and Table II-2). Intermolecular disulfide bonds between cysteines on different ERE protein chains lead to chain extension into higher order protein oligomers while intramolecular disulfide formation between the N- and C-terminal cysteines of one protein chain (or an extended chain) leads to cyclization. Samples of ERE were prepared in SDS loading buffer with and without 5% (v/v) β-ME as a disulfide reducing agent. The sample containing β-ME was also boiled for 3 min to improve the reduction. Visualization of the proteins

by Coomassie staining (Figure II-3 a) or Western blotting (Figure II-3 b) after electrophoresis revealed a strong band near the expected molecular weight in both samples. Much weaker bands were also observed in the Coomassie-stained gel at the molecular weight corresponding to an ERE dimer, but higher order oligomers were not observed. The monomeric ERE bands contain a small shoulder at lower apparent molecular weights that is attributed to the cyclized monomer. (The linear and cyclic monomers are not well resolved for the ERE protein, but are for other telechelic proteins that will be considered in next chapters.)

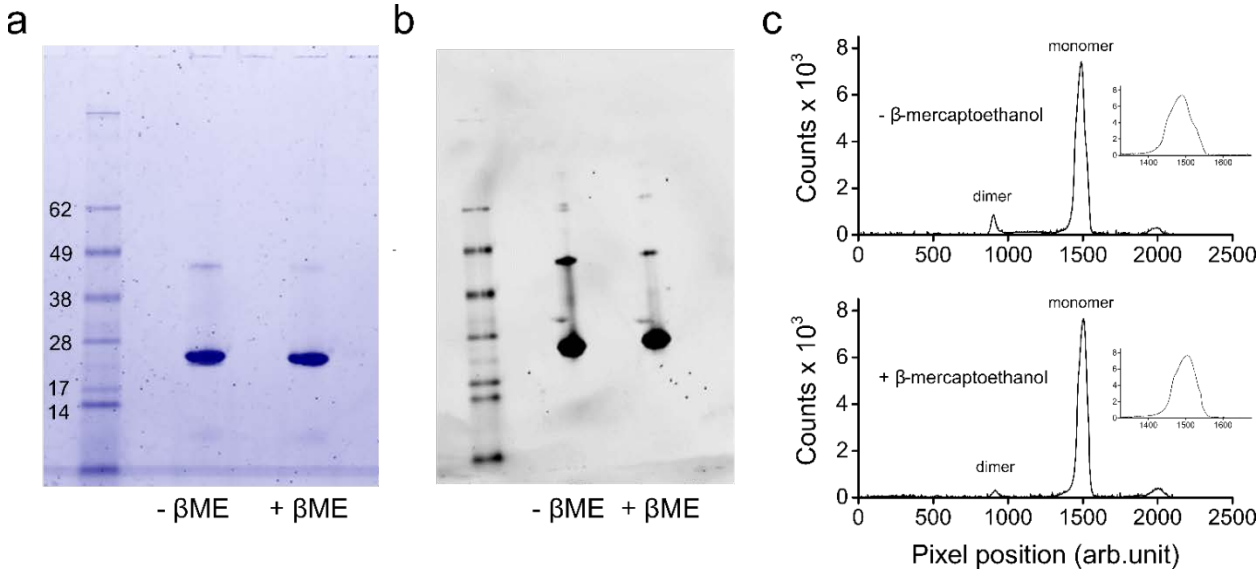

Figure II-3. Assesment of protein purity and oligomerization state by non-reducing SDS-PAGE. (**a**) Purified ERE protein is primarily monomeric by SDS-PAGE in samples prepared with or without β-mercaptoethanol as disulfide reductant, confirming that the protein thiols are reduced following purification. (**b**) The presence of the 6xHis tag at the N-terminus was confirmed by Western blotting using an penta-his antibody. (**c**) The lane profiles of the gel in (a) were quantified by gel densitometry to determine the fraction of monomer, dimer, and higher order species in the ERE preparation.

The average pixel intensity along each lane is plotted in Figure II-3 c. The peak corresponding the dimer is only slightly greater for the ERE sample prepared without β-ME than for the ERE sample prepared with β-ME. Integration of the ERE peaks as well as a small impurity at approximately 10 kDa was used to estimate the free thiol content by assuming that dimers contain one free thiol per protein, linear monomers contain two free thiols per protein, and that cyclic monomers do not contain any free thiols (Table II-2). The unknown impurity accounts for only about 2% of the total peak area and is assumed to not contribute to the sample thiol content. For the ERE sample without β-ME, the estimated free thiol content from the observed distribution of monomers, dimers, and cyclized protein is in excellent agreement with the thiol content measured by Ellman's assay (Table II-1) (1.78 vs. 1.76). From these experiments, it is concluded that ERE can be synthesized in *E. coli* and purified from the lysate by inverse temperature cycling, and that the terminal cysteine residues are in the reduced state and should be available for covalent cross-linking.

SDS-PAGE band	**Fraction total area**	**Thiols per chain**	**mol free thiol/ mol protein**
dimer	0.04	1	0.04
linear monomer	0.87	2	1.74
cyclic monomer	0.07	0	0
impurity (approx. 10 kDa)	0.02	unknown (assume 0)	0
Total	**1**	**-**	**1.78**

Table II-2. Quantiation of the oligomerization state of purified ERE protein by gel densitomtry. The area of the peaks assigned as the linear monomer, cyclic monomer, dimer, and impurity (at approximately 10 kDa) in Figure II-3 (c, *top*) were each divided by the total peak area to obtain the fraction of ERE protein in a particular oligomerization state (column 2). The fractions were multipled by the expected number of thiols per chain (column 3) to obtain an estimate for the number of free thiols per protein (column 4).

4.3 Hydrogel Formation and Characterization

The purified ERE protein was used to prepare hydrogel networks by end-linking with 4-arm PEG tetrakis-vinyl sulfone (PEG-4VS) (Figure II-1 c). The thiol side chains of the cysteine residues at the protein termini react with the vinyl sulfone functional groups at each end of the star PEG through a Michael-type conjugate addition to form a thioether bond (Figure II-1 d). An idealized step-growth network resulting from this reaction is shown in Figure II-1 e. Hydrogels formed upon mixing a solution of ERE protein and a solution of PEG-4VS. In this work, the two macromer solutions were always prepared at equal concentration and mixed at a volumetric ratio that gave the desired functional group stoichiometry (*r*). The ERE solution was prepared by dissolving lyophilized protein in 0.1 M phosphate buffer containing 0.4 M triethanolamine, an organic base that promotes the addition of the thiol nucleophile to the electrophilic alkene, and 6 M guanidinium chloride, a protein denaturant. Guanidinium chloride (GndCl) is not required for cross-linking ERE proteins but is used in subsequent chapters to disrupt the association between artificial proteins containing domains that form intermolecular coiled coils. The cross-linker solution was prepared by dissolving PEG-4VS in 0.4 M triethanolamine. After mixing the protein and cross-linker solutions, the gelation mixture was cured between glass slides separated by rubber spacers. Hydrogel disks formed in this way could be removed from the glass surface and characterized in the as-prepared or unswollen state, or could be swollen in buffer to remove the denaturant as well as the unreacted protein and PEG-4VS.

The typical results of cross-linking 15 wt% ERE and PEG-4VS solutions at a 1:1 vinyl sulfone to thiol ratio are shown in Figure II-4. The gels are tan to light brown in the as-prepared state due the absorbance of the ERE protein (Figure II-4 a), and transparent when swollen in PBS (Figure II-4 b). The gels were characterized by small amplitude oscillatory shear rheology (SAOS)

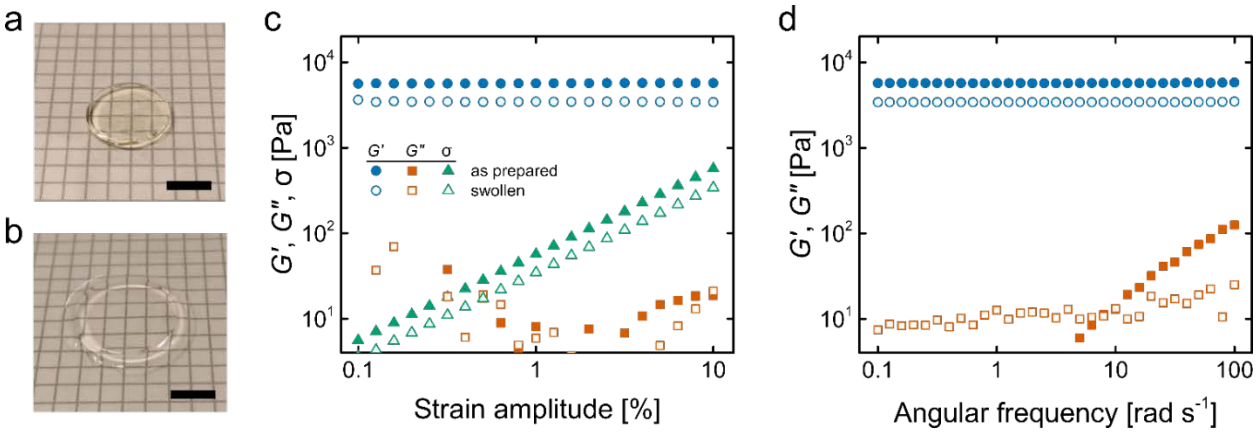

Figure II-4. ERE Hydrogels. Photographs of ERE hydrogels in the (**a**) as-prepared (unswollen) state and (**b**) swollen in PBS, pH 7.4. The gels were cross-linked at 15 wt% total polymer and 1:1 VS:SH stoichiometry. (**c**) Dynamic oscillatory rheology strain sweep of ERE hydrogels in the as-prepared (filled symbols) and swollen (open symbols) states at 10 rad s^{-1}, 25 °C. The storage modulus (*G'*, circles) is much greater than the loss modulus (*G"*, squares), which is difficult to measure accurately. The stress (σ, triangles) increases linearly with the stain amplitude. (**d**) Dynamic oscillatory rheology frequency sweep of ERE hydrogels at 5% strain amplitude, 25 °C. In both (c) and (d), *G'* in the as-prepared state is greater than the swollen state due to the decrease in the density of elastically effective chains upon swelling. The scale bars in (a) and (b) are 1 cm.

in both the as-prepared state and after swelling for 48 hr in phosphate buffered saline (PBS, pH 7.4). The strain sweeps (Figure II-4 c) of these materials demonstrate that the storage modulus (*G'*) is nearly constant over the entire range of strain amplitudes tested (0.1-10%), indicating that the material response is linear in this regime. The frequency sweeps of 15 wt% hydrogels (Figure II-4 d) in both the swollen and as-prepared states are characterized by *G'* that are nearly independent of the oscillation frequency. The storage moduli are also more than two orders of magnitude greater than the loss moduli (*G"*), indicating that the response of the hydrogel to deformation is primarily

elastic. As expected, the swollen gels are softer than the as-prepared gels because the chain density decreases as upon the absorption of additional solvent.

The initial polymer concentration in the cross-linking reaction and the stoichiometry (r) of the vinyl sulfone and thiol functional groups were varied systematically in order to determine their effects on the macroscopic properties of ERE networks: the storage modulus G' and the mass swelling ratio Q_m. Hydrogels were prepared from protein and PEG-4VS solutions at 7.5, 10, 15, 20, and 25 wt% while maintaining a vinyl sulfone to thiol stoichiometry of 1:1 (Figure II-5). In both the as-prepared and swollen states, the hydrogels became stiffer as the initial polymer concentration was increased. The mass swelling ratio Q_m, which is equal to the swollen hydrogel mass divided by the dry polymer mass, decreased as the initial polymer concentration was increased. In this way, the modulus of the ERE-VS hydrogels could be tuned over a range of 0.7 kPa to 12 kPa.

In the course of the experiments to determine the mass swelling ratio, the protein component of the sol fraction, or the fraction of ERE protein that was not connected to the network, was collected and quantified by the bicinchoninic acid (BCA) assay. Following a similar analysis of PEG-*co*-peptide hydrogels by Lutolf and Hubbell [18], the sol fraction was used to estimate the extent of reaction p between the thiol and vinyl sulfone groups as well as the concentration of elastically effective chains (ν) and the cross-link density (μ) by Miller-Macosko theory [34]. These data are summarized in Table II-3. The extent of reaction p increases from 0.78 for networks prepared at 7.5 wt% to 0.88 for networks prepared at 25 wt%, suggesting that a higher concentration of functional groups drives the reaction closer to full conversion. Similar results

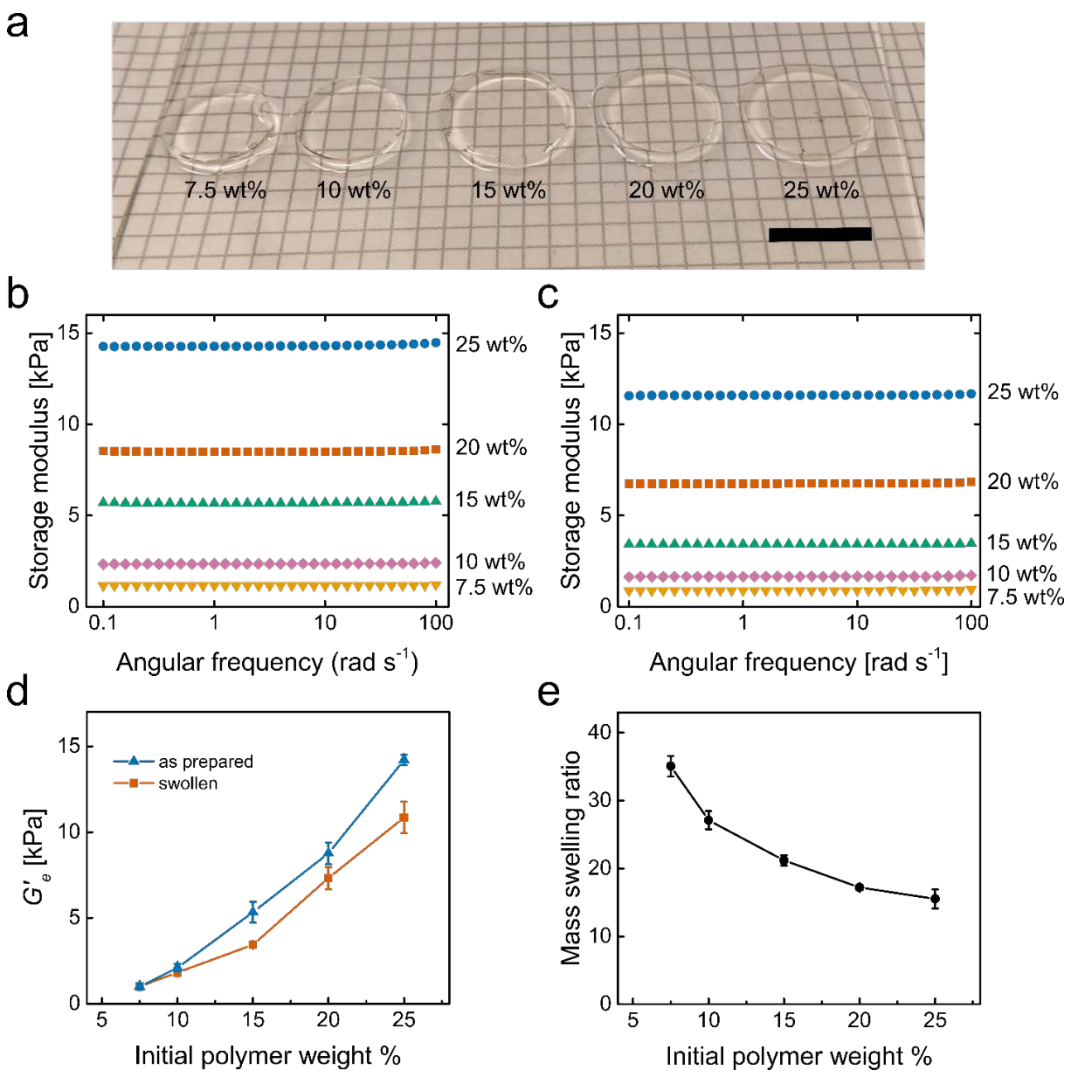

Figure II-5. Variation of the initial polymer concentration between 7.5-25 wt%. (**a**) Photographs of swollen ERE hydrogels. (**b**) Representative frequency sweep experiments show the storage moduli of ERE hydrogels at various initial polymer concentrations in the as-prepared state. (**c**) Representative frequency sweep experiments show the storage moduli of ERE hydrogels at various initial polymer concentrations after swelling to equilibrium in PBS. (**d**) For each initial concentration, the equilibrium modulus G'_e, which is defined here as G' at 1 rad s^{-1}, is plotted for the as-prepared and swollen gels (n = 3, avg. ± s.d.). (**e**) The mass swelling ratio after swelling to equilibrium in PBS decreases as the initial polymer concentration is increased (n = 6 gels, avg. ± s.d.). All frequency sweep experiments were performed at 5% strain amplitude, 25 °C. The scale bar in (a) is 1 cm.

were reported for the reaction of cysteine-containing peptides and PEG-4VS in ref. [18], with p varying from 0.80 for a 5 wt% gelation mixture to 0.88 for a 40 wt% gelation mixture.

The calculated values of ν and μ were then used to compute a theoretical shear modulus by two theories of rubber elasticity: the affine approximation and the phantom network approximation [35]. In the affine approximation, the cross-links are considered fixed in space with no thermal fluctuations. When a cross-linked network is stretched from its original length L_0 to a deformed length $L = \lambda L_0$, the end-to-end vector of a chain segement between cross-link points is assumed to undergo the same deformation. This leads to the following expression for the shear modulus (cross-linked in a θ-solvent):

$$G_{af} = \nu RT\left(\frac{\varphi}{\varphi_0}\right)^{1/3} \qquad \text{(Equation II-1)}$$

where R is the gas constant, T is the temperature, and φ and φ_0 are the polymer volume fractions in the swollen and as-prepared states. The polymer volume fractions were determined from the mass swelling ratio by assuming that the hydrogel density is equal to the density of water (≈ 1 g mL^{-1}) and the dry polymer density is equal the mass average of the density of elastin (1.3 g mL^{-1}) [36] and the density of 10,000 g mol^{-1} PEG (1.2 g mL^{-1}) [37]. The theoretical modulus can also be determined by the phantom network approximation, which allows for the fluctuation of the cross-link points in space. Because these fluctuations increase the entropy and lower the free energy per chain, the phantom network modulus is lower than the affine modulus. The expression for the modulus is:

$$G_{ph} = (\nu - \mu)RT\left(\frac{\varphi}{\varphi_0}\right)^{1/3} \qquad \text{(Equation II-2)}$$

The moduli of ERE gels computed from Eq. II-1 and Eq. II-2 for the as-prepared state ($\varphi = \varphi_0$) and swollen state are listed in Table II-4 along with the experimental values of the equilibrium modulus G'_e (plotted in Figure II-5 d). The experimental values of the modulus fall between the predicted affine and phantom network values, and are typically closer to the phantom network prediction. It should be noted that this analysis does not account for elastically ineffective chains due to loop formation, consumption of thiols by disulfide bond formation, or chain entanglements. The expressions for the moduli also assume ideal behavior of the chain segments between cross-links. Non-idealities are likely present in ERE gels to some extent, and will contribute to the swelling behavior and modulus in different ways. Intramolecular disulfide bonds generate looped ERE chains that cannot react with PEG-4VS and should therefore be part of the sol fraction. Intermolecular disulfide bonds generate extended ERE chains with increased molecular weight between cross-links, and are expected to decrease the modulus and increase the swelling ratio relative to the ideal network. Loops in which the both cysteines on the same ERE chain react with two arms of the same PEG-4VS polymer generate an elastically ineffective chain that does not contribute to the modulus. Finally, entanglements formed during cross-linking are expected to act as virtual cross-links, increasing the modulus and decreasing the swelling ratio.

Next, the stoichiometry of the functional groups (r) was varied from 0.6:1 to 1.4:1 while maintaining the total polymer concentration in the gelation reaction at 15 wt% (Figure II-6). Altering the reactant stoichiometry potentially creates defects in the resulting network that are expected to affect the mechanical properties and swelling behavior of the hydrogels. When ERE is in stoichiometric excess (r = 0.6 or 0.8), ERE networks are more swollen, which suggests that the cross-linking density is lower. When PEG-4VS is added in excess (r = 1.2 or 1.4), there is not a significant difference in the mass swelling ratio compared to gels prepared with r = 1. A similar

Initial polymer concentration	$w_{ERE,sol}$	α	β	p	ν (mM)	μ (mM)
7.5 wt%	0.44%	0.43	0.27	0.79	1.1	0.7
10 wt%	0.42%	0.37	0.23	0.81	1.8	1.1
15 wt%	0.33%	0.29	0.17	0.85	4.9	2.8
20 wt%	0.26%	0.23	0.13	0.88	7.1	3.9
25 wt%	0.34%	0.24	0.13	0.88	8.8	4.9

Table II-3. Estimation of the concentration of elastically effective chains ν and cross-link denisty μ by Miller-Macosko Theory. The weight fraction of protein in the sol phase ($w_{ERE,sol}$) was measured by the BCA protein quantitation assay and used to determine β, the probability that a thiol functional group on ERE is not connected to the infinite network. β was used to calculate α, the probabilty that a vinyl sulfone group on PEG-4VS is not connected to the infinite network, and p, the extent of reaction. α and β were used to calculate ν and μ.

Initial polymer concentration	As-prepared modulus (kPa)			Swollen modulus (kPa)		
	G_{af}	G_{ph}	G'_e	G_{af}	G_{ph}	G'_e
7.5 wt%	2.8	1.1	1.0	2.0	0.7	1.0
10 wt%	4.5	1.8	2.1	3.2	1.3	1.8
15 wt%	12.2	5.3	5.3	8.3	3.6	3.4
20 wt%	17.6	7.9	8.9	11.6	5.2	7.3
25 wt%	21.8	9.8	14.2	13.9	6.2	10.8

Table II-4. Estimation of the modulus by the affine and phantom network approximations. The concentration of elastically effective chains ν and the cross-link density μ reported in Table II-3 and the swelling ratio were used to compute G_{af} and G_{ph} using Eq. II-1 and Eq. II-2, respectively.

effect was also observed for the storage moduli of the swollen gels. The modulus increased from r = 0.6 to 1, but was essentially unchanged from 1 to 1.4. When the vinyl sulfone is present in excess, it may potentially react with other nucleophiles such as the N-terminal amine to generate additional cross-links, minimizing the number of dangling chains. Alternatively, the low molecular weight dangling PEG chains (2.5 kDa per arm) may have a smaller effect on the stiffness and swelling behavior than dangling ERE chains (18.5 kDa). Additional experiments at larger values of r are required to determine if the gels eventually become softer and more swollen when the vinyl sulfone is present in greater excess.

The gelation conditions used to prepare the ERE hydrogels discussed above are not compatible with cell encapsulation due to the high concentration of guanindium chloride protein denaturant as well as the triethanolamine, which is potentially toxic to certain cell types [19]. An alternative cross-linking condition was investigated in which ERE and PEG-4VS were dissolved in HEPES buffered saline, pH 7.4 without triethanolamine. This buffering system was used previously to cross-link PEG-divinyl sulfone and peptides containing three cysteine residues with gelation times of several minutes [38]. Because softer, more swollen gels are expected to be better for 3D cell culture, ERE hydrogels were prepared at initial polymer concentrations of 5, 7.5 and 10 wt% and r = 1. The moduli of the gels in the as-prepared state and after swelling in PBS were similar to gels prepared under denaturing conditions (Figure II-7), confirming that the denaturant and organic base are not required for cross-linking ERE hydrogels.

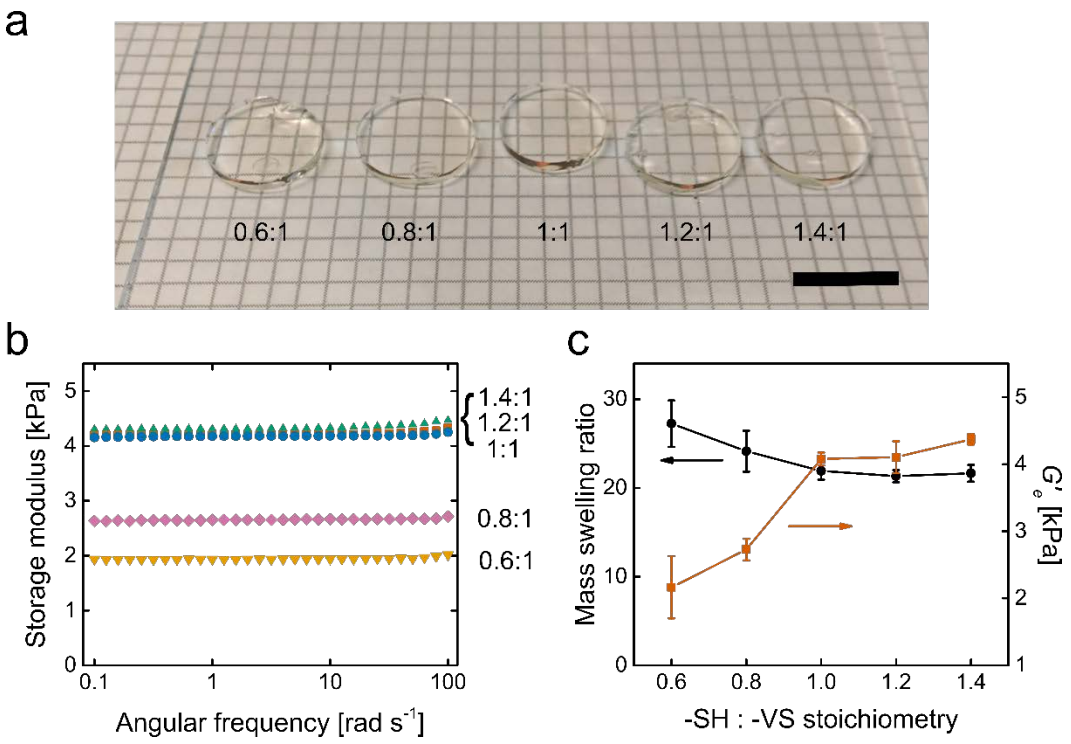

Figure II-6. Variation of the vinyl sulfone to thiol stoichiometry between 0.6-1.4. (**a**) Photographs of swollen ERE hydrogels. (**b**) Representative frequency sweep experiments show the storage moduli of ERE hydrogels prepared at different vinyl sulfone to thiol stoichiometry after swelling to equilibrium in PBS. (**c**) The mass swelling ratio decreases as r is increased from 0.6 to 1, but does not vary from r = 1 to 1.4 (n = 6 gels, avg. ± s.d.). Likewise, the equilibrium modulus G'_e increases as r is increased from 0.6 to 1, but does not vary from r = 1 to 1.4 (n = 3, avg. ± s.d.). The frequency sweep experiments in (b) were performed at 5% strain amplitude, 25 °C. The scale bar in (a) is 1 cm.

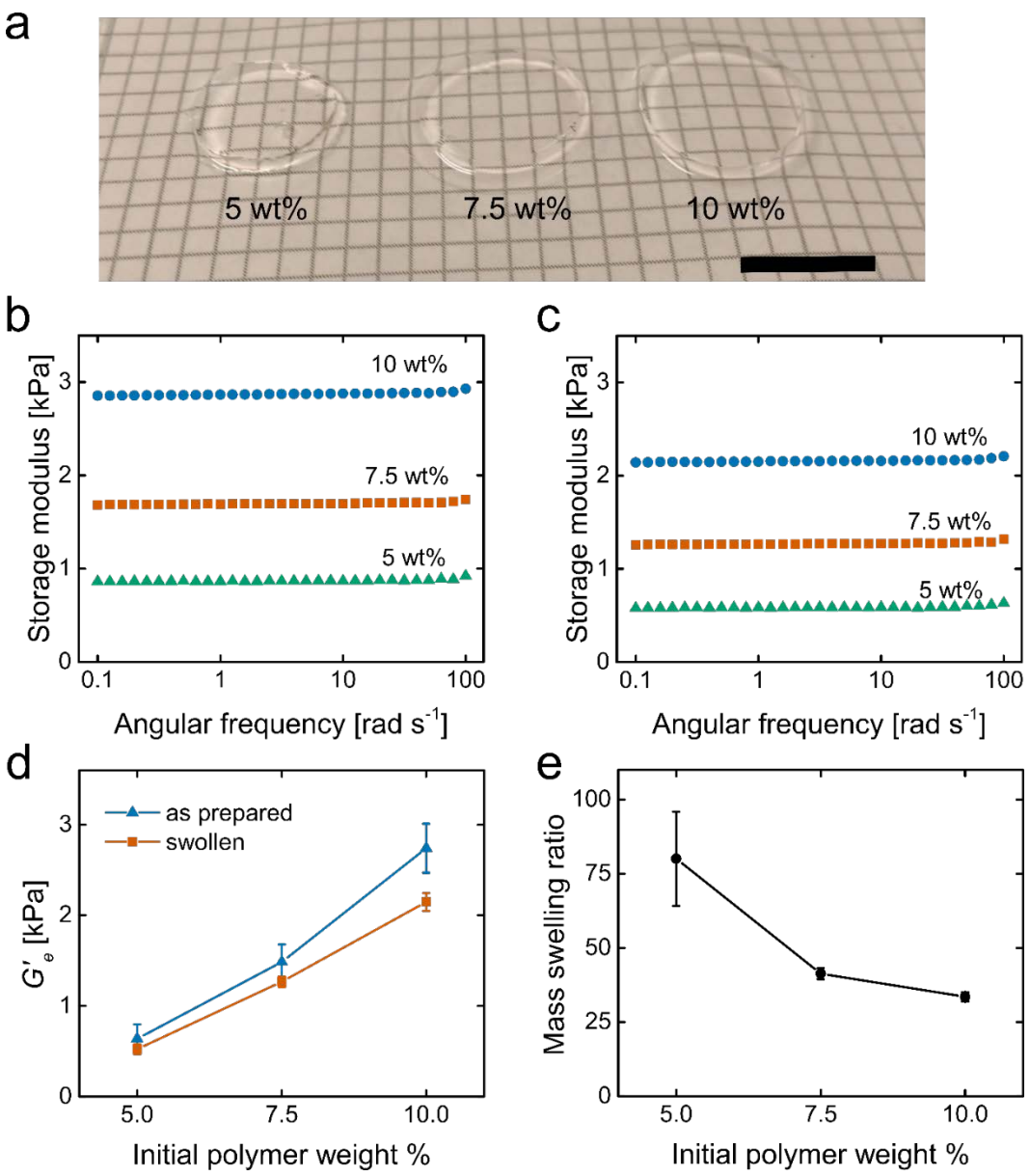

Figure II-7. Cross-linking ERE in HEPES buffered saline. (**a**) Photographs of swollen ERE hydrogels. (**b**) Representative frequency sweep experiments show the storage moduli of ERE hydrogels at initial polymer concentrations of 5, 7.5, and 10 wt% in the as-prepared state. (**c**) Representative frequency sweep experiments show the storage moduli of ERE hydrogels swollen to equilibrium in PBS. (**d**) The equilibrium modulus G'_e increases with increasing polymer concentration in the cross-linking reaction (n = 3, avg. ± s.d.). (**e**) The mass swelling ratio after swelling to equilibrium in PBS decreases as the initial polymer concentration is increased (n = 6 gels, avg. ± s.d.). All frequency sweep experiments were performed at 5% strain amplitude, 25 °C. Scale bar in (a) is 1 cm.

4.4 Gelation Kinetics

The gelation kinetics of 5, 7.5, and 10 wt% hydrogels with 1:1 functional group stoichiometry were determined by a dynamic oscillatory time sweep at 5% strain amplitude and 10 rad s^{-1} at 37 °C (Figure II-8 a). The gel point was determined from the time at which *G'* and *G"* intersect. At short times below the gel point, the mixture is a viscous solution and *G"* is larger than *G'*. After the gel point is reached, energy is stored in the forming network and *G'* is greater than *G"*. The storage modulus continues to increase rapidly before eventually approaching a plateau. The gelation time decreased as the amount of polymer was increased (Figure II-8 b). Gelation of 10 wt% mixtures occured within about 12 min. Gelation of 7.5 wt% and 5 wt% mixtures occur within 20 min and 43 min, respectively. This trend is expected assuming that covalent bond formation between ERE and PEG-4VS is a second order reaction with a rate that is proportional to the product of the reactant concentrations.

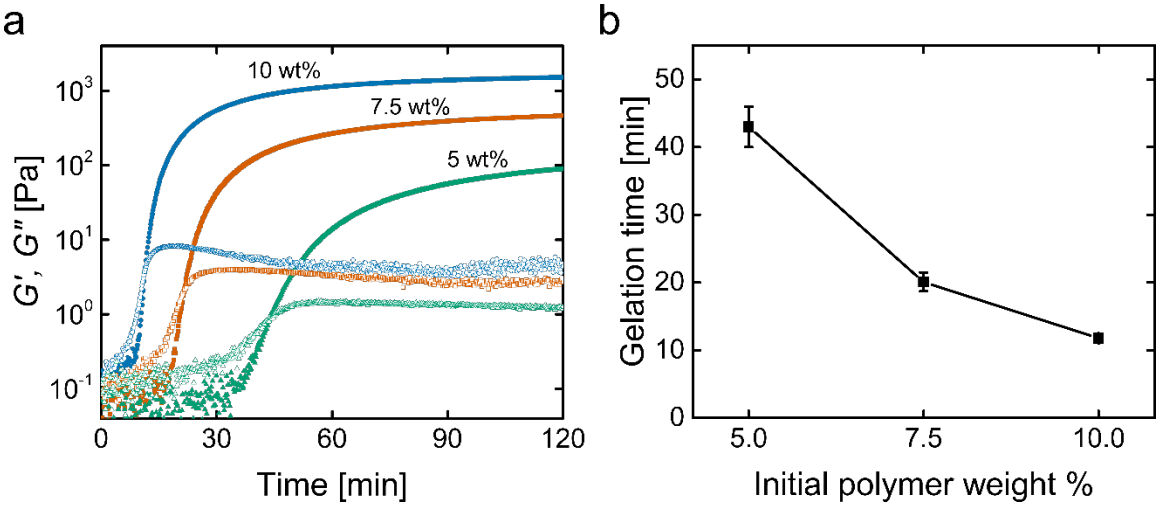

Figure II-8. Kinetics of ERE gelation. (**a**) Dynamic oscillatory time sweep of 5, 7.5, and 10 wt% ERE solutions cross-linked with PEG-4VS (*r* = 1:1) in HEPES buffered saline at 5% strain amplitude, 10 rad s^{-1}, 37 °C. The gel point is taken as the time at which *G'* (filled symbols) and *G"* (open symbols) intersect. (**b**) The gelation time decreases as the polymer concetration is increased (*n* = 3, avg. ± s.d.).

4.5 Preliminary Cell Encapsulation Experiments

The gelation conditions assessed in the previous sections were also evaluated in a cell encapsulation experiment with NIH 3T3 mouse fibroblasts. Cells were added to 5, 7.5, and 10 wt% ERE solutions in HEPES buffered saline at a concentration of 3×10^6 mL^{-1}, followed by cross-linking with PEG-4VS at r = 1:1. The hydrogel was formed as a droplet on a glass-bottom culture dish. After 1-2 hr at 37 °C (depending on the polymer concentration), complete growth medium was added. The gels were stained 3 days later with dyes that label either live or dead cells to evaluate cell viability and morphology. The gelation appeared to proceed normally in the presence of the fibroblasts, although the mechanical properties of the cell-laden hydrogels were not assessed.

Live cells were observed in all three ERE gels; however, they exhibited striking differences in their morphology in the different gel preparations (Figure II-9). In 5 wt% gels, most cells exhibited an elongated, spindle-like morphology. In 7.5 and 10 wt% gels, the cells were mostly round, although some cellular extensions could be observed, particularly in 7.5 wt% gels. The different cellular morphologies suggest that the fibroblasts spread more easily in a softer, more swollen matrix than in a stiffer, denser gel like those prepared at higher polymer concentrations. A similar trend has been reported for myoblast spreading in 4-arm PEG maleimide and 4-arm PEG vinyl sulfone hydrogels [19]. It is also noted that several cells are located in close proximity to one or more other cells, indicating that cells may not only survive in ERE gels but also proliferate.

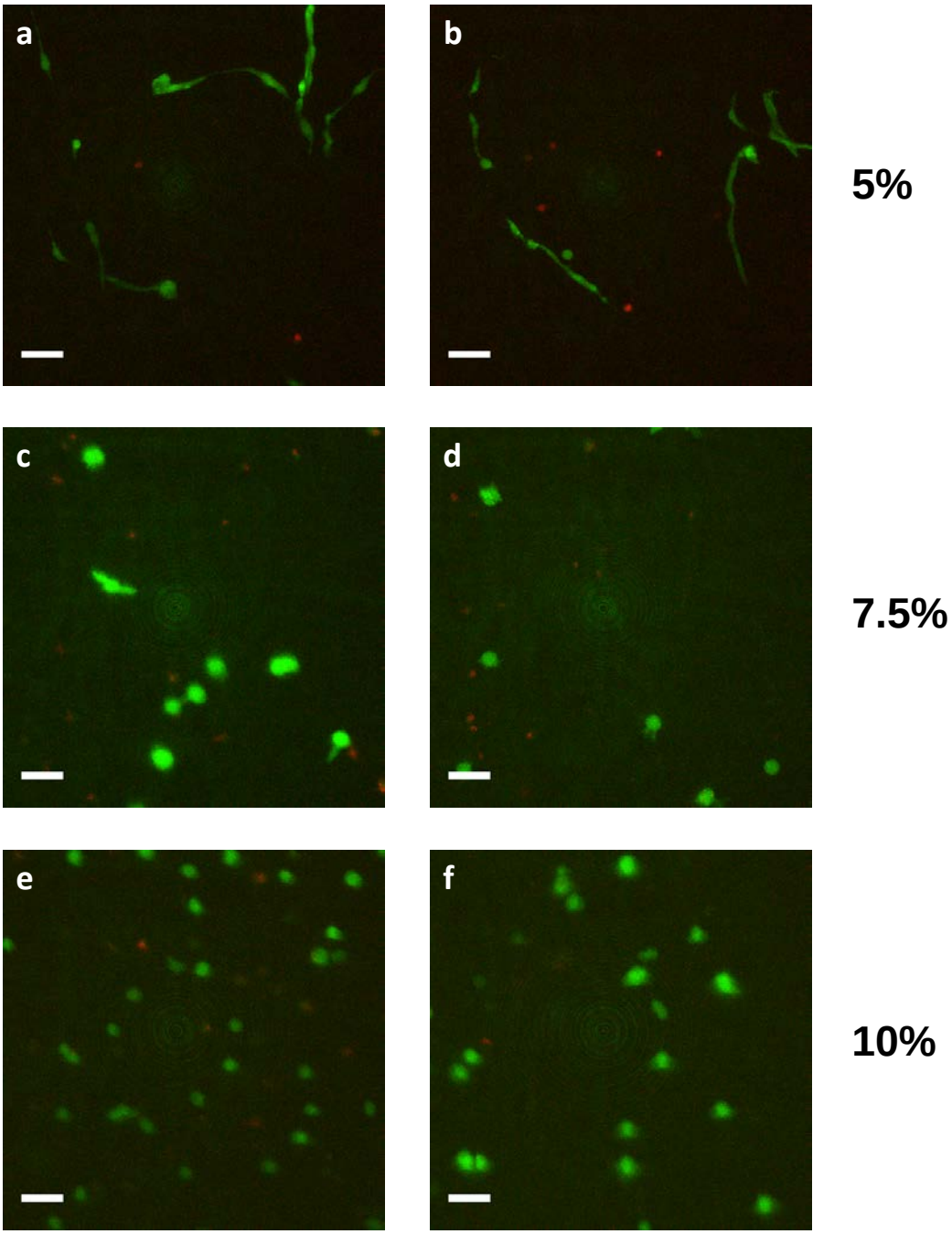

Figure II-9. Encapsulation of NIH 3T3 mouse fibroblasts in ERE gels. Projection of z-stacks acquired every 10 μm over a volume spanning a 200 μm thick section of gel. Live cells are stained with calcein AM (green). Dead cells are stained with ethidium homodimer-1 (red). The left and right panels are z-projections of two different x-y planes of the same gel. (**a**), (**b**) 5% ERE gel. (**c**), (**d**) 7.5 wt% ERE gel. (**e**), (**f**) 10 wt% ERE gel.

5. Conclusions

A new artificial protein ERE was designed and cross-linked into hydrogel networks. ERE was purified from a recombinant host with excellent yields using inverse temperature cycling with a free thiol content of approximately 90% of the expected value. End-linking ERE with PEG-4VS through a Michael-type addition reaction resulted in an optically clear hydrogel network. The mechanical properties of this network were engineered by systematic variation of the protein concentration during cross-linking and the stoichiometry of the protein and PEG cross-linker. In this way, the moduli of ERE networks were varied from 0.5 kPa to greater than 10 kPa. Biological activity was encoded directly within the ERE protein sequence in the form of a cell-binding domain and an MMP-cleavable peptide, potentially providing cues for directing the behavior of encapsulated cells. NIH 3T3 fibroblasts encapsulated in ERE hydrogels survived the cross-linking reaction and exhibited a spindle-like morphology in the softest material. This work demonstrates that end-linking artificial proteins is a promising strategy for engineering hydrogels with well-defined physical and biological properties.

6. Acknowledgements

Preliminary cross-linking and rheology experiments were conceived and performed with Dr. Wen-bin Zhang (W.-B.Z.) and Dr. Tomoyuki Koga. The ERE protein was designed by W.-B.Z. An early draft of a manuscript from which this chapter was adapted was written with W.-B.Z. The rheological experiments were performed in the laboratory of Professor Julia Kornfield. The protein mass spectrometry was performed at the Mass Spectrometry Facility in the Division of Chemistry and Chemical Engineering with assistance from Dr. Mona Shahgholi. The microscopy experiments were performed at the Biological Imaging Facility in the Beckman Institute.

7. References

[1] K.Y. Lee, D.J. Mooney *Chem. Rev.* **2001** *101*, 1869-1880.

[2] A. Panitch, T. Yamaoka, M.J. Fournier, T.L. Mason, and D.A. Tirrell *Macromolecules* **1999** *32*, 1701-1703.

[3] R.A. McMillan, V.P. Conticello *Macromolecules* **2000** *33*, 4809-4821.

[4] K. Di Zio, D.A. Tirrell *Macromolecules* **2003** *36*, 1553-1558.

[5] K. Trabbic-Carlson, L.A. Setton, A. Chilkoti *Biomacromolecules* **2003** *4*, 572-580.

[6] D.W. Lim, D.L. Nettles, L.A. Setton, A. Chilkoti *Biomacromolecules* **2007** *8*, 1463-1470.

[7] J.N. Renner, K.M. Cherry, R.S.C. Su, J.C. Liu *Biomacromolecules* **2012** *13*, 3678-3685.

[8] C. Chung, K.J. Lampe, S.C. Heilshorn *Biomacromolecules* **2012** *13*, 3912-3916.

[9] E.R. Welsh, D.A. Tirrell *Biomacromolecules* **2000** *1*, 23-30.

[10] P.J. Nowatzki, D.A. Tirrell *Biomaterials* **2004** *25*, 1261-1267.

[11] E. Fong, D.A. Tirrell *Adv. Mater.* **2010** *22*, 5271-5275.

[12] N.E. Davis, S. Ding, R.E. Forster, D.M. Pinkas, and A.E. Barron *Biomaterials* **2010** *31*, 7288-7297.

[13] M.K. McHale, L.A. Setton, A. Chilkoti *Tissue Eng.* **2005** *11*, 1768-79.

[14] C.A. DeForest, B.D. Polizzotti, K.S. Anseth *Nat. Mater.* **2009** *8*, 659-664.

[15] A.M. Testera, A. Girotti, I.G. Torre, L. Quintanilla, M. Santos, M. Alonso, and J.C. Rodríguez-Cabello *J. Mater. Sci. Mater. Med.* **2015** *26*, 1-13.

[16] F. Sun, W.-B. Zhang, A. Mahdavi, F.H. Arnold, and D.A. Tirrell *Proc. Natl. Acad. Sci. USA* **2014** *111*, 11269-11274.

[17] S.D. Tilley, N.S. Joshi, M.B. Francis, in *Wiley Encyclopedia of Chemical Biology*, Vol. 4 Wiley, New York **2007**.

[18] M.P. Lutolf, J.A. Hubbell *Biomacromolecules* **2003** *4*, 713-722.

[19] E.A. Phelps, N.O. Enemchukwu, V.F. Fiore, J.C. Sy, N. Murthy, T.A. Sulchek, T.H. Barker, and A.J. García *Adv. Mater.* **2012** *24*, 64-70.

[20] S.C. Rizzi, J.A. Hubbell *Biomacromolecules* **2005** *6*, 1226-1238.

[21] C.L. McGann, R.E. Akins, K.L. Kiick *Biomacromolecules* **2016** *17*, 128-140.

[22] D. Xu, D. Asai, A. Chilkoti, S.L. Craig *Biomacromolecules* **2012** *13*, 2315-2321.

[23] D.T. McPherson, J. Xu, D.W. Urry *Protein Expression Purif.* **1996** *7*, 51-57.

[24] P. Eyer, F. Worek, D. Kiderlen, G. Sinko, A. Stuglin, V. Simeon-Rudolf, and E. Reiner *Anal. Biochem.* **2003** *312*, 224-227.

[25] T.K.L. Meyvis, S.C. De Smedt, J. Demeester, W.E. Hennink *J. Rheol.* **1999** *43*, 933-950.

[26] M.D. Pierschbacher, E. Ruoslahti *Nature* **1984** *309*, 30-33.

[27] A.L. Main, T.S. Harvey, M. Baron, J. Boyd, and I.D. Campbell *Cell* **1992** *71*, 671-678.

[28] U. Hersel, C. Dahmen, H. Kessler *Biomaterials* **2003** *24*, 4385-4415.

[29] H. Nagase, G.B. Fields *Peptide Science* **1996** *40*, 399-416.

[30] M.P. Lutolf, J.L. Lauer-Fields, H.G. Schmoekel, A.T. Metters, F.E. Weber, G.B. Fields, and J.A. Hubbell *Proc. Natl. Acad. Sci. USA* **2003** *100*, 5413-5418.

[31] H. Wang, L. Cai, A. Paul, A. Enejder, and S.C. Heilshorn *Biomacromolecules* **2014** *15*, 3421-3428.

[32] D.W. Urry *J. Phys. Chem. B* **1997** *101*, 11007-11028.

[33] G.L. Ellman *Arch. Biochem. Biophys.* **1959** *82*, 70-77.

[34] D.R. Miller, C.W. Macosko *Macromolecules* **1976** *9*, 206-211.

[35] M. Rubinstein, R.H. Colby, *Polymer Physics* Oxford University Press, Oxford **2003**.

[36] M.A. Lillie, J.M. Gosline *Biopolymers* **2002** *64*, 115-126.

[37] 2012. *Polyethylene glycol [MAK Value Documentation, 1998]*. *The MAK-Collection for Occupational Health and Safety*. 274-270.

[38] A.B. Pratt, F.E. Weber, H.G. Schmoekel, R. Müller, and J.A. Hubbell *Biotechnol. Bioeng.* **2004** *86*, 27-36.

Chapter III

VISCOELASTIC BEHAVIOR OF PROTEIN HYDROGELS CROSS-LINKED BY CHEMICAL AND PHYSICAL NETWORK JUNCTIONS

1. Abstract

The primary sequences of proteins carry information that specifies intermolecular association and higher-order functions such as catalysis, cellular signaling, and the formation of tough, elastic materials. This chapter describes a set of recombinant artificial proteins that can be cross-linked by covalent bonds, by association of helical domains, or by both mechanisms. These proteins were used to construct molecular networks in which the mechanism of cross-linking determines whether the material response to mechanical deformation is elastic or viscoelastic. In viscoelastic networks, stress relaxation and energy dissipation can be tuned by controlling the ratio of physical cross-linking to chemical cross-linking, and the physical cross-links can be disrupted either by protein denaturation or by mutation of the primary sequence. This work demonstrates how protein sequence can be used to engineer the time-dependent responses of macromolecular networks to mechanical deformation.

Content from this chapter was published as: L.J. Dooling, M.E. Buck, W.-B. Zhang, and D.A. Tirrell. “Programming molecular association and viscoelastic behavior in protein networks.” *Advanced Materials*. doi:10.1002/adma.201506216

2. Introduction

Protein-based materials such as fibers, films, and gels derive many of their macroscopic properties from the folded structures and hierarchical assembly specified by the primary amino acid sequence. Despite important recent progress in the chemical synthesis of sequence-controlled polymers, biological synthesis remains the most powerful route to polymers of well-defined sequence and length [1]. Furthermore, although elucidation of the rules governing protein folding remains an important challenge, our understanding of the relationship between primary sequence and higher order structure is more advanced for proteins than for synthetic polymer systems [2]. For these reasons, recombinant artificial proteins constitute a promising class of macromolecules for engineering materials with macroscopic properties that are specified by the sequences of their constituent polymers.

Hydrogels are cross-linked polymeric or supramolecular networks that absorb large amounts of water. They are typically soft and highly swollen, characteristics that make them attractive materials for biomedical engineering applications such as tissue regeneration and cell culture [3, 4]. As discussed in Chapter 1, hydrogel networks can be prepared from artificial proteins by covalent cross-linking of side chain functional groups such as the ε-amine of lysine or the sulfhydryl of cysteine [5, 6]. Alternatively, networks can be cross-linked by noncovalent interactions among folded protein domains that assemble into higher-order structures such as coiled coils and triple helices [7, 8]. These two approaches produce chemical hydrogels and physical hydrogels, respectively. In both cases, the density of cross-linking sites and their location within the hydrogel backbone are specified by the sequence of the artificial protein. Together, the density and type of cross-linking determine the response of the hydrogel to macroscopic deformation. Covalent cross-links formed by irreversible chemical reactions maintain the shape

and elasticity of hydrogels and are essentially permanent. Physical cross-links are often transient, leading to stress relaxation, flow, and material erosion [9]. Encoding desired mechanical properties, material dynamics, and responsiveness to stimuli may require multiple types of cross-linking. The modular nature of genetically encoded artificial proteins is well-suited to this approach. To this end, this chapter describes the viscoelastic behavior of hydrogels prepared from artificial proteins that were designed to form chemical networks, physical networks, and chemical-physical networks.

3. Materials and Methods

3.1 Plasmid Construction

Genes encoding the artificial proteins used in this study were created using a combination of gene synthesis (Genscript, Piscataway, NJ) and standard molecular cloning techniques. The artificial protein PEP was encoded on the pET15b plasmid (pET15b PEP) (Novagen, Madison, WI). All other proteins were encoded on pQE-80L plasmids (pQE-80L EPE, pQE-80L ERE, pQE-80L EPE L44A) (Qiagen, Valencia, CA). The complete amino acid sequence for each protein is given in Appendix A.

3.2 Protein Expression and Purification

Chemically competent BL21 *Escherichia coli* (New England BioLabs, Ipswich, MA) were transformed with plasmids encoding the artificial proteins EPE, ERE, and EPE L44A. Expression was carried out at 37 °C in Terrific broth containing 100 μg mL^{-1} ampicillin (BioPioneer, San Diego, CA). At an optical density at 600 nm (OD_{600}) of 0.9-1, expression was induced with 1 mM isopropyl β-D-1-thiogalactopyranoside (IPTG) (BioPioneer). The cells were harvested 4 hr after

induction by centrifugation at 6000 *g*, 4 °C for 8 min. Cell pellets were subjected to two freeze-thaw cycles, resuspended in TEN buffer (10 mM Tris, 1 mM EDTA, 100 mM NaCl, pH 8.0) at a concentration of 0.5 g mL^{-1}, and subjected to a final freeze-thaw cycle. The lysate was treated with 10 μg mL^{-1} DNase I (Sigma, St. Louis, MO), 5 μg mL^{-1} RNase A (Sigma), 5 mM $MgCl_2$, and 1 mM phenylmethylsulfonyl fluoride (Gold Biotechnology, Olivette, MO) while shaking at 37 °C, 250 rpm for 30 min. Cell lysis was completed by sonication with a probe sonicator (QSonica, Newton, CT).

The artificial proteins were purified based on the inverse temperature transition associated with elastin-like polypeptides (ELPs). To prevent chain extension of the target proteins by disulfide formation, 0.1% (v/v) β-mercaptoethanol (β-ME) (Sigma) was added to the lysate. The lysate was cooled to 4 °C and clarified by centrifugation at 39,000 *g*, 4 °C for 1 hr. To depress the lower critical solution temperature of the hydrophilic ELPs, sodium chloride was added to the supernatant to a final concentration of 2 M. After shaking at 37 °C for 1 hr, aggregated proteins were pelleted by centrifugation at 39,000 *g*, 37 °C for 1 hr. The target proteins were extracted from the pellet with water containing 0.1% (v/v) β-ME overnight at 4 °C. This process was repeated twice but the β-ME was omitted. Instead, after the second and third temperature cycles, the proteins were reduced with 5 mM tris(hydroxypropyl)phosphine (THP) (Santa Cruz Biotechnology, Dallas, TX) at 4 °C. Residual salt and reducing agents were removed by desalting using Zeba 7K MWCO columns (Thermo Fisher Scientific, Waltham, MA) equilibrated with degassed distilled and deionized water (ddH_2O). The proteins were lyophilized and stored under argon at -80 °C. Typical yields of EPE and ERE were 200 mg L^{-1} and 100 mg L^{-1} of culture, respectively.

Expression of PEP from the pET15b plasmid requires the BL21(DE3) *E. coli* strain (Novagen) containing the T7 RNA polymerase. Protein expression was performed in Terrific broth

containing 100 μg mL^{-1} ampicillin. Cells were grown at 37 °C until the OD_{600} reached 0.9-1.0. Protein expression was induced with the addition of 1 mM IPTG and proceeded for 5 hr, after which time the cells were harvested and lysed with 8 M urea. Cells suspended in 8 M urea were subjected to three freeze/thaw cycles followed by sonication. Clarified lysates were obtained by centrifugation and PEP was isolated by affinity chromatography with nickel nitriloacetic acid (NiNTA) resin (Qiagen) under denaturing conditions. The elution fractions containing purified PEP were combined, dialyzed against distilled water for 48 hr at 4 °C using a MWCO 12,000-14,000 membrane (Spectrum Laboratories, Rancho Dominquez, CA), and lyophilized. Yields of PEP were approximately 100 mg per liter of culture.

3.3 MALDI-TOF Mass Spectrometry

Lyophilized proteins (EPE, ERE, EPE L44A, and PEP) were dissolved in ddH_2O at a concentration of 10 mg mL^{-1}. The protein solutions were mixed with sinapinic acid matrix (10 mg mL^{-1} in 6:3:1 water:acetonitrile:1% trifluoroacetic acid) at volumetric ratios varying from 4:1 to 10:1 (matrix to protein). The mixtures were spotted on the MALDI sample plate and allowed to dry. Spectra were acquired on a Voyager DE Pro spectrometer (Applied Biosystems, Carlsbad, CA).

3.4 Measurement of Protein Thiol Content by Ellman's Assay

Ellman's reagent, 5,5'-dithio-bis-(2-nitrobenzoic acid), (Sigma) was used to measure the concentration of free thiols as described in Chapter 2. Briefly, protein was dissolved at a concentration of 5 mg mL^{-1} in reaction buffer (100 mM sodium phosphate, 1 mM EDTA, pH 8.0). In a cuvette, the protein solution (125 μL) and Ellmans' reagent (50 μL, 5 mg mL^{-1} in reaction

buffer) were added to the reaction buffer (2.5 mL). The reaction was incubated for 15 min and the absorbance at 412 nm was measured on a Cary 50 UV/VIS spectrophotometer (Varian, Palo Alto, CA). The thiol concentration was calculated using the molar extinction coefficient 14,150 M^{-1} cm^{-1} [2].

3.5 Hydrogel Preparation

To prepare EPE, ERE, and EPE L44A hydrogels, lyophilized protein was resuspended in degassed 100 mM sodium phosphate, 6 M guanidinium chloride, 400 mM triethanolamine (Sigma) at a concentration of 150 mg mL^{-1}. The 4-arm, 10 kDa PEG vinyl sulfone cross-linker (JenKem Technology USA, Plano, TX) was dissolved in degassed 400 mM triethanolamine at a concentration of 150 mg mL^{-1}. To facilitate dissolution, samples were sonicated in an ultrasonic bath for 1 min and centrifuged at 10,000 *g* for 1 min. The pH of the protein and cross-linker solutions was adjusted to approximately 7.2-7.4 using 6 N HCl. The cross-linker was added to the protein solution at a volumetric ratio that gave a nominal 1:1 thiol to vinyl sulfone stoichiometry. However, based on the thiol quantification using Ellman's assay, the vinyl sulfone was in approximately 1.2-fold excess. After vortexing to mix, a droplet (40 μL) was pipetted onto a glass slide that had been treated with SigmaCote siliconizing fluid (Sigma). The droplet was flattened into a disk by placement of another treated glass slide separated by 0.5 mm silicone spacers (McMaster-Carr, Santa Fe Springs, CA), and the slides were clamped tightly. Gelation occurred within several minutes, but hydrogels were cured overnight (>12 hr) in the dark. The cross-linked hydrogels were swollen in decreasing concentrations of guanidinium chloride (6 M, 3 M, 2 M, 1 M for 3 hr each) in phosphate-buffered saline (PBS) (1.5 mM KH_2PO_4, 4.3 mM Na_2HPO_4, 137 mM NaCl, 2.7 mM KCl, pH 7.4) to remove any unreacted material. The gels were then swollen in

PBS containing 0.02% (w/v) sodium azide (to inhibit microbial growth during swelling) for at least 48 hr.

PEP hydrogels were formed by suspending lyophilized protein in PBS containing 0.02% (w/v) sodium azide. The solutions were placed on ice for 2-4 hr or until a clear solution was formed. The gels were centrifuged briefly to remove all air bubbles. For experiments assessing the denaturing effects of urea on PEP hydrogels, lyophilized protein was suspended in solutions of increasing concentration of urea dissolved in 100 mM sodium phosphate buffer. The pH of each solution was adjusted to 7.4 and the final protein concentration was 7% (w/v).

3.6 Rheological Characterization of Protein Hydrogels

Rheological experiments with ERE, EPE, and mixed composition hydrogels were performed on an ARES-RFS strain-controlled rheometer (TA Instruments, New Castle, DE) equipped with an 8 mm parallel plate test geometry. Swollen hydrogels were cut to this size using an 8 mm biopsy punch (Miltex, York, PA). The gap height was set by lowering the geometry until a plateau in the storage modulus (measured at 5 rad s^{-1} and 1% strain) was reached as described previously [10]. The edge of the gel was surrounded with paraffin oil to minimize evaporation. Strain sweep experiments from 0.01-10% strain amplitude were performed at 5 rad s^{-1} to determine the linear viscoelastic region. Frequency sweep experiments from 100 to 0.001 rad s^{-1} were performed at 1% strain amplitude. The temperature was maintained at 25 °C by a Peltier thermoelectric device. Following frequency sweep experiments, stress relaxation experiments were also performed under 1% strain for 2 hr. For PEP gels, the ARES-RFS was equipped with a 25 mm diameter cone and plate geometry (0.04 rad cone angle). For PEP in 8 M urea, frequency sweep experiments were performed at 10% strain amplitude.

3.7 Swelling Measurements

Swollen hydrogels were blotted with filter paper to remove excess buffer, weighed on an analytical balance (Mettler Toledo, Columbus, OH) to obtain the swollen mass, and placed in ddH_2O for 48 hr with several changes to remove salts. They were then transferred to microcentrifuge tubes, frozen with liquid nitrogen, and lyophilized to obtain the dry mass. The mass swelling ratio, Q_m, is equal to the swollen mass divided by the dry mass. The same procedure was followed for EPE and ERE gels swollen in PBS containing 8 M urea.

4. Results and Discussion

4.1 Protein Design, Synthesis, and Characterization

The artificial proteins EPE and ERE designed for this study feature a triblock architecture in which the endblocks are elastin-like polypeptides (ELPs) containing repeats of the pentapeptide VPGXG (Figure III-1a, see Appendix A for full sequences). The guest position X is occupied by either valine or glutamic acid (at a ratio of 4:1 Val:Glu). This composition was selected to raise the lower critical solution temperature of the elastin-like domains sufficiently that these domains would remain soluble at the temperatures and ionic strengths of interest [11]. Cysteines at the protein termini were included as sites for covalent cross-linking. The midblock domain P of EPE is derived from the N-terminal fragment of the rat cartilage oligomeric matrix protein (COMP). This domain forms homopentameric coiled coils and is responsible for oligomerization of native COMP [12]. ERE also features ELP endblocks and terminal cysteine residues, but in place of the coiled-coil midblock it contains a 17-amino acid sequence (denoted R) derived from the integrin-binding loop of fibronectin [13]. This sequence contains the RGD (Arg-Gly-Asp) tripeptide widely used in cell adhesion studies, but it is not expected to contribute significant interchain interactions.

The EPE and ERE proteins have molar masses of 21.5 and 18.5 kg mol^{-1}, respectively. This difference is expected to have only a small effect on the mechanical properties of materials prepared from these proteins. Much more significant effects are expected to arise from the capacity of the P domain, but not R, to associate and form non-covalent network junctions.

The EPE and ERE proteins were expressed in *Escherichia coli* strain BL21 and purified by inverse temperature cycling [14]. Purity and molecular weight were assessed by SDS-PAGE (sodium dodecyl sulfate polyacrylamide gel electrophoresis) and MALDI-TOF (matrix-assisted laser desorption/ionization time-of-flight) mass spectrometry (Figures III-2 and III-3). After reduction with tris(hydroxypropyl)phosphine, desalting, and lyophilization, the free thiol content of each protein was measured using Ellman's assay (Figure III-4 a). While the proteins are shown to be monomeric by non-reducing SDS-PAGE (Figure III-4 b and c), approximately 15-20% appear to form a cyclic product through an intramolecular disulfide bond between the N- and C-terminal cysteines.

A third protein, denoted PEP, was also designed with a sequence that is similar to ERE but contains P endblocks in place of the terminal cysteine residues (Figure III-1a). PEP was expressed in the BL21(DE3) strain of *E. coli* and purified by immobilized metal affinity chromatography using nickel nitriloacetic acid agarose resin.

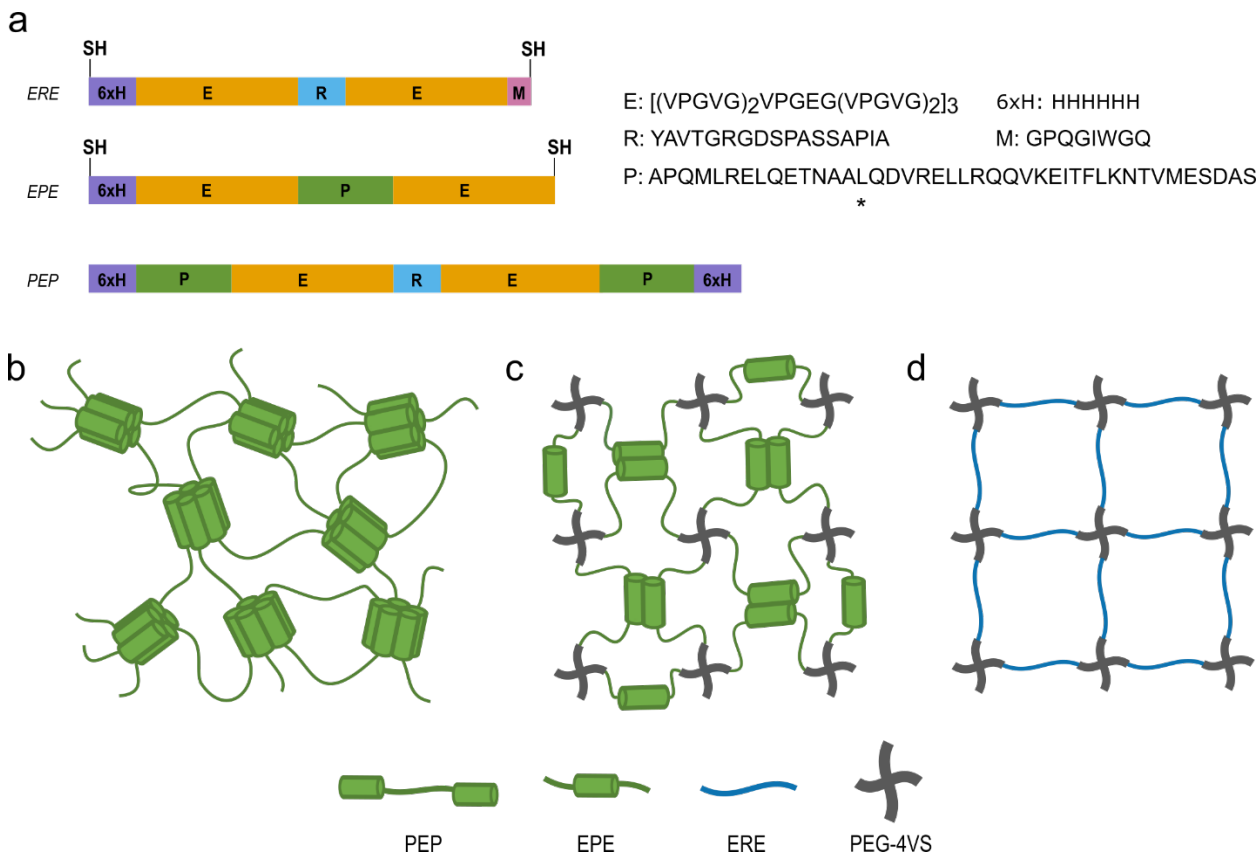

Figure III-1. Artificial protein design and cross-linking scheme. (**a**) Artificial proteins EPE and ERE consist of terminal cysteine residues (-SH), elastin-like endblocks E, and either the P or R midblock domain. ERE also contains an octapeptide recognition sequence M for proteolytic cleavage. The artificial protein PEP contains two P domains near the termini that flank the elastin-RGD-elastin sequence. The * below the sequence of the P domain denotes the position of leucine 44, which was mutated to alanine to create the variant EPE L44A. (**b**) PEP forms physical hydrogels through association of the P endblocks. (**c**) EPE and (**d**) ERE require covalent cross-linking with 4-arm PEG vinyl sulfone to form gels. ERE contains only covalent cross-links while EPE also has the potential to form physical cross-links through association of the midblock domains. Although P assembles in pentameric coiled coils in COMP, the physical cross-links are depicted as dimers in (c) for clarity.

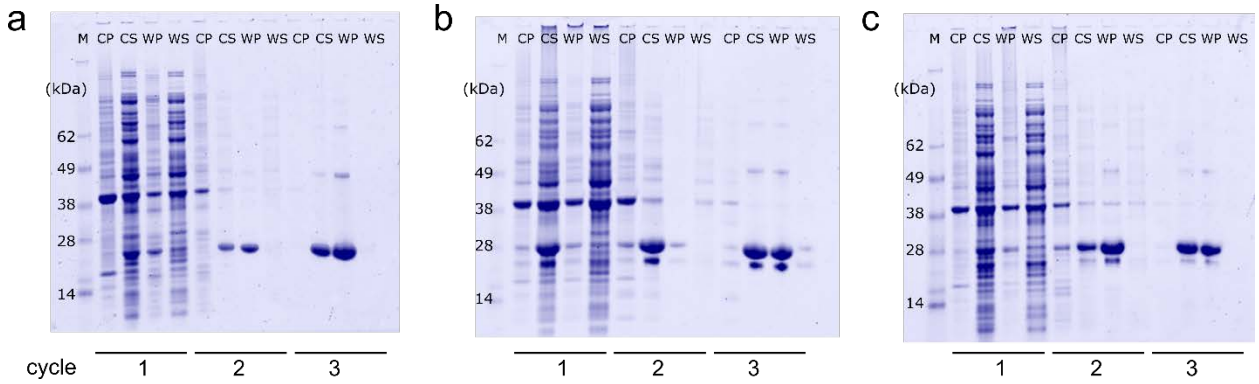

Figure III-2. SDS-PAGE of artificial proteins during inverse temperature cycling. ERE (**a**), EPE (**b**), and EPE L44A (**c**) were purified by three cycles of inverse temperature cycling. After each centrifugation step, samples of the supernatant and pelleted fractions were saved. The target proteins are expected to be soluble in the cold step (4 °C, low ionic strength) and insoluble in the warm step (37 °C, 2 M NaCl). For SDS-PAGE analysis, the proteins in the pelleted fractions were extracted in 8 M urea. The samples were boiled in SDS loading buffer with 2.5% (v/v) β-ME to reduce disulfide bonds. The gel was stained with colloidal blue stain to visualize proteins. After 3 cycles of cold and warm spins, the target proteins were successfully purified from the *E. Coli* lysates. (Abbreviations: CP – cold pellet, CS – cold supernantant, WP – warm pellet, WS – warm supernatant, M – SeeBlue protein marker with molecular weights in kDa).

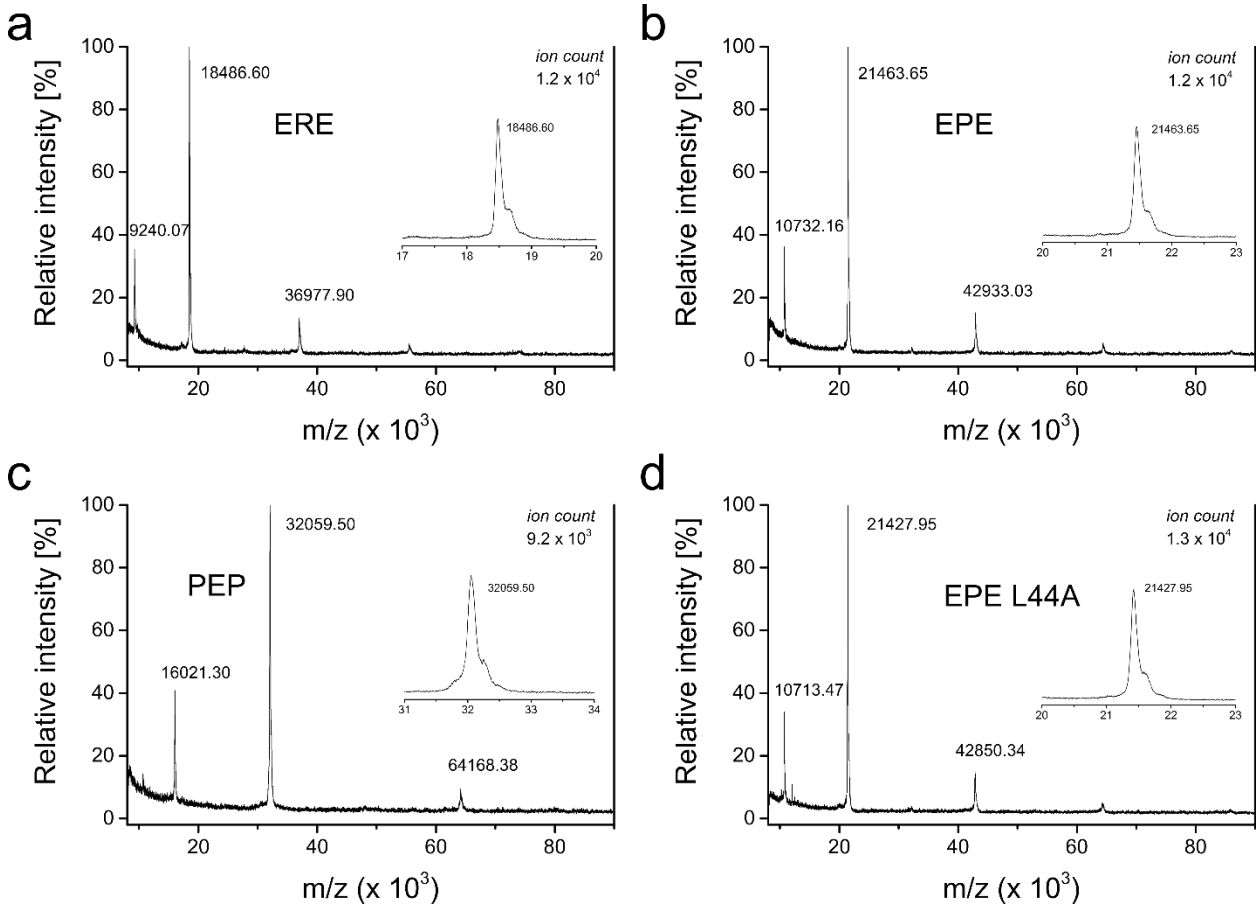

Figure III-3. MALDI-TOF mass spectrometry of purified artificial proteins. (**a**) ERE (calculated 18474, observed 18487), (**b**) EPE (calculated 21465, observed 21464), (**c**) PEP (calculated 32047, observed 32060), and (**d**) EPE L44A (calculated 21422, observed 21428). Peaks assigned to the doubly charged species and dimers are also labeled.

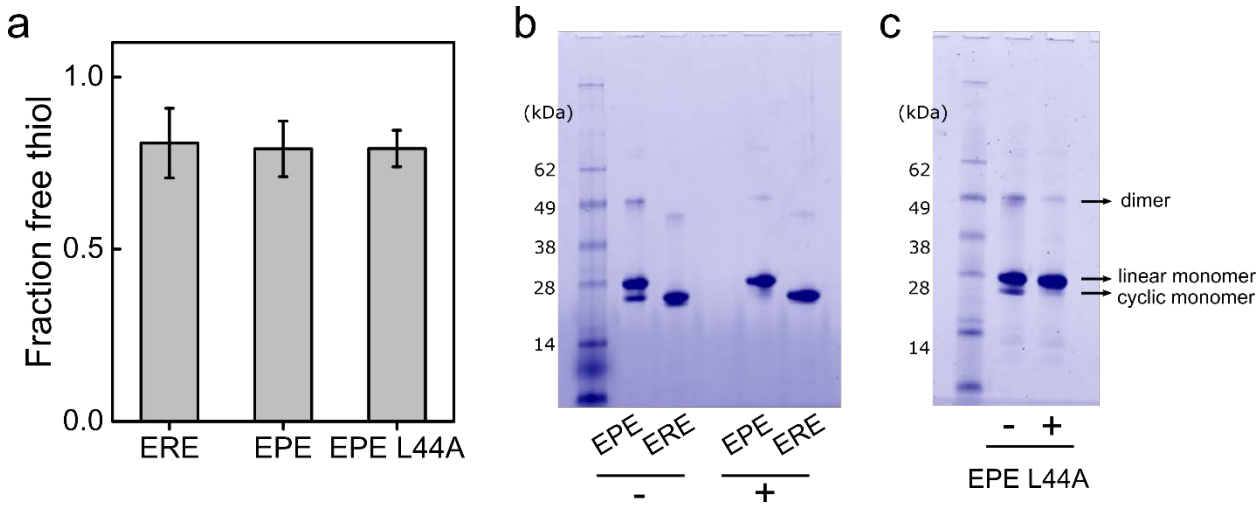

Figure III-4. Ellman's assay and non-reducing SDS-PAGE for purified artificial proteins. (**a**) Ellman's assay measures the concentration of free thiols in the protein preparations (*n* = 3, avg ± sd). The measured thiol concentration for each protein is approximately 80% of the expected concentration based on the amount of protein per reaction and assuming two cysteines per protein. SDS-PAGE performed on samples without reducing agent demonstrates that EPE, ERE (**b**) and EPE L44A (**c**) are primarily monomeric after desalting and lyophilization. However, approximately 20% of the monomeric protein is cyclized, consistent with the results of Ellman's assay in (a). The cyclized proteins run at a lower apparent molecular weight than the linear proteins and are absent in control lanes containing samples that were boiled in loading buffer containing 2.5% (v/v) β-ME as a disulfide reductant.

4.2 Hydrogel Cross-linking

Telechelic artificial proteins such as PEP and others that contain P domains at the N- and C-termini self-assemble into physical hydrogels through association of their endblocks (Figure III-1 b) [9, 15]. Hydrogels were formed from PEP by resuspending lyophilzed protein in PBS at 7 wt% for several hours on ice. Because each EPE protein chain contains only a single P domain, self-assembly of this protein into an extended hydrogel network is not possible, except perhaps under conditions that yield significant chain extension through disulfide bond formation [16]. However, EPE could still be incorporated into covalent hydrogel networks by cross-linking the terminal cysteine residues with 4-arm poly(ethylene glycol) vinyl sulfone (PEG-4VS) [17]. This cross-linking reaction was performed in buffer containing 6 M guanidinium chloride to prevent premature association of the P midblock domains. Swelling the resulting hydrogels in phosphate buffered saline to remove the denaturant allows the P domains within neighboring chains of the chemical network to associate and form physical cross-links (Figure III-1 c). Hydrogels were also prepared from ERE using the same method. Because ERE lacks the associative midblock domain found in EPE, these hydrogels are expected to exhibit only the properties of chemically cross-linked networks (Figure III-1 d). Together, these three artificial proteins demonstrate how a small set of sequences can be combined in different ways to yield chemical gels (ERE), physical gels (PEP), and chemical-physical gels (EPE).

4.3 Viscoelastic Behavior of ERE, EPE, and PEP Hydrogels

The three types of networks depicted in Figure III-1 b, c, and d are expected to exhibit different responses to material deformation. While the covalent cross-links in EPE and ERE gels are expected to be permanent because of the irreversibility of the thioether bond, the association

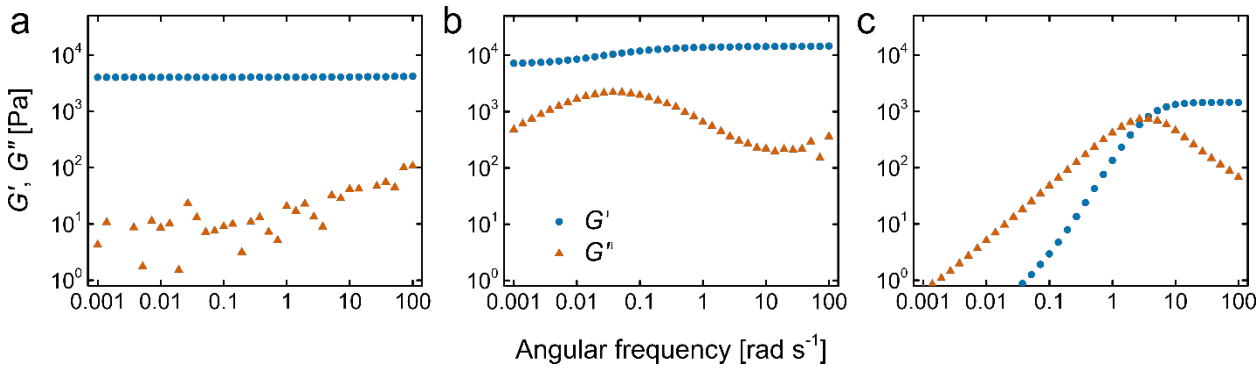

Figure III-5. Linear rheology of protein hydrogels. Small amplitude oscillatory shear rheology frequency sweeps for swollen ERE (**a**) and EPE (**b**) hydrogels at 1% strain amplitude, 25 °C. The mass swelling ratios for ERE and EPE are 19.7 and 13.5, respectively. Hydrogels prepared from EPE demonstrate a transition from a high frequency plateau to a low frequency plateau in *G'* as well as a local maximum in *G"* that coincides with this transition. This is attributed to the combination of permanent chemical cross-links and transient physical cross-links. These features are not observed in hydrogels prepared from ERE, which contain only chemical cross-links. In hydrogels prepared from PEP (**c**), only physical cross-linking is present and *G'* and *G"* exhibit a cross-over point at $\omega = 3.9$ rad s^{-1} (7 wt% protein, 1% strain amplitude, 25 °C).

of P domains in EPE and PEP gels is reversible, and the physical cross-links are expected to be transient. The transient nature of the association should allow stress stored in deformed chains to relax on timescales comparable to the lifetimes of the physical cross-links. To determine whether such relaxation occurs in PEP, EPE, or ERE hydrogels, we performed small amplitude oscillatory shear rheology experiments to measure the storage modulus (*G'*) and loss modulus (*G"*) of each gel over an angular frequency range of 0.001-100 rad s^{-1}. The storage modulus of hydrogels composed entirely of ERE is nearly independent of frequency, as expected for an elastic network connected entirely by covalent cross-links with few network defects (Figure III-5 a). In contrast, hydrogels prepared from EPE are viscoelastic and display a frequency-dependent storage modulus with both high and low frequency plateaus (Figure III-5 b). The high frequency plateau modulus,

denoted $G'(\infty)$, reflects the combined contributions of covalent and physical cross-linking. As the oscillation frequency is decreased, the timescale on which the gel is deformed becomes comparable to the characteristic timescale for exchange or dissociation of the physical cross-linking domains. This results in relaxation of some of the stress stored within the network. At very low frequencies or long times, the physical cross-links are no longer elastically effective but stress is still borne by the deformation of chains connected by covalent cross-links. For this reason, the low frequency storage modulus, $G'(0)$, is associated with the permanent chemical network.

PEP gels also exhibit high frequency plateau storage moduli, $G'(\infty)$, due to physical cross-linking between P domains (Figure III-5 c). Unlike EPE gels, however, PEP hydrogels lack chemical cross-links and exhibit a crossover point ($G' = G''$) corresponding to a transition between regimes of solid-like behavior ($G' > G''$) and liquid-like behavior ($G'' > G'$). This behavior is characteristic of viscoelastic fluids. In EPE hydrogels, which can be characterized as viscoelastic solids, no crossover is observed and $G' > G''$ for all frequencies measured. The loss moduli of EPE and PEP gels are both characterized by local maxima. In PEP, the maximum in G'' occurs near the crossover point. In EPE hydrogels, the maximum in G'' occurs as G' transitions between the high and low frequency plateaus. In contrast, no local maximum in G'' is observed in ERE gels, and accurate measurement of G'' is difficult because of uncertainty in determination of the phase angle in materials that do not dissipate significant amounts of energy. The relaxation time for the physical cross-links, which is determined from the frequency at which the maximum in G'' occurs, differs by nearly two orders of magnitude for PEP and EPE gels. This difference likely represents the effect of constraining the associative domain within a chemical network. A similar effect was observed in physical protein hydrogels cross-linked by P that also contained

entanglements introduced by oxidative chain extension, although the increase in the relaxation time was only 2-3 fold in these materials [16].

4.4 Viscoelastic Behavior of Hydrogels Prepared from Mixtures of EPE and ERE

In order to tune the properties of chemical-physical protein hydrogels, mixtures of EPE and ERE were cross-linked with PEG-4VS. Mixed composition hydrogels were prepared by cross-linking gel precursor solutions containing 75:25, 50:50, or 25:75 ERE:EPE by weight while maintaining the total protein concentration at 15 wt%. The resulting hydrogels behave as viscoelastic solids, but exhibit smaller ratios of $G'(\infty)$ to $G'(0)$ than those observed in EPE gels (Figure III-6 a). For EPE hydrogels, the ratio of $G'(\infty)$ to $G'(0)$ is approximately two as expected from the protein sequence; association of the P domains cuts the average molecular weight between cross-links in half. As the fraction of EPE in the gel is decreased, there are fewer chains that are capable of forming physical cross-links, and the smaller fraction of transient cross-links results in less stress relaxation. This effect is also evident in the behavior of G'', in which the maximum amplitude of the peak associated with stress relaxation diminishes as the fraction of EPE is decreased (Figure III-6 b). Despite ERE and EPE having similar molecular weights and identical covalent cross-linking sites, the storage moduli of the five gel preparations vary slightly even at low frequencies where physical cross-links are not expected to be elastically effective. This observation is consistent with the difference in the swelling ratios (or chain densities) of the networks (Figure III-6 d). Networks that contain more physical cross-linking are less swollen (denser) and therefore remain stiffer even at low frequencies. These results provide further evidence that physical cross-linking through the P domains is responsible for the time-dependent mechanical properties of networks containing EPE, and illustrate the potential for tuning the

viscoelastic and swelling behavior of protein hydrogels by controlling the ratio of physical and chemical cross-links.

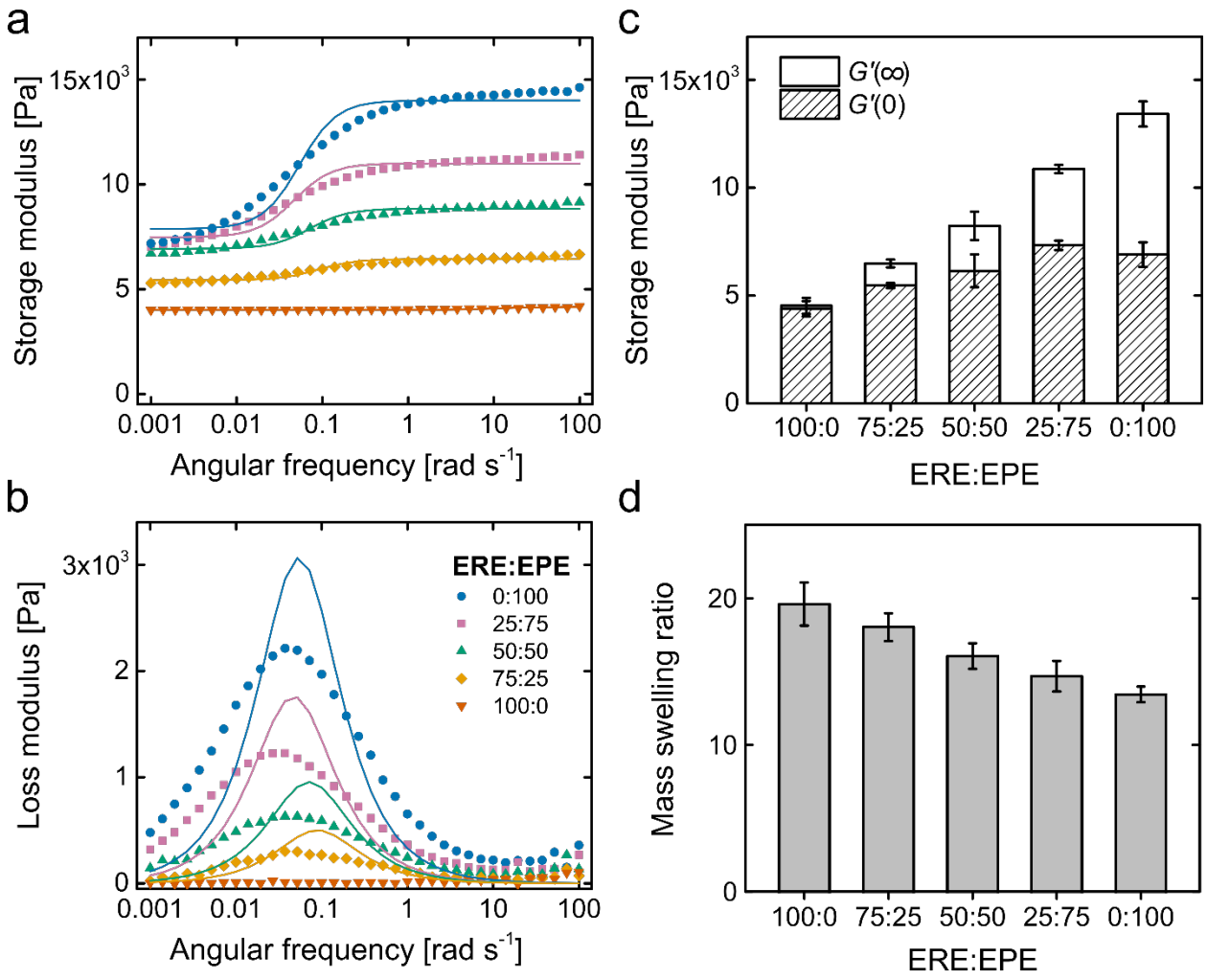

Figure III-6. Rheology and swelling of ERE:EPE chemical-physical hydrogels. Representative frequency sweep rheology showing the storage (**a**) and loss (**b**) moduli at 1% strain amplitude, 25 °C for hydrogels prepared from mixtures of EPE and ERE. The solid lines represent fits of the Maxwell expression for a viscoelastic solid (Equations III-1 and III-2) (**c**) The values of the plateau moduli $G'(\infty)$ and $G'(0)$ were acquired from fits of G' to the Maxwell model for a viscoelastic solid ($n \geq 3$, avg ± sd). The ratio of $G'(\infty)$ to $G'(0)$ and the maximum in G'' increase as the fraction of EPE is increased. (**d**) The mass swelling ratio Q_m of the ERE:EPE hydrogels decreases as the fraction of EPE is increased (n = 5, avg ± sd).

4.5 Rheological Models of Viscoelastic Protein Networks

The Maxwell expression for the storage modulus of a viscoelastic solid (Equations III-1) was used to fit the experimental values of $G'(\omega)$ for each ERE:EPE gel preparation.

$$G'(\omega) = G_0 + G\frac{(\omega\tau)^2}{1+(\omega\tau)^2} \qquad \text{(Equation III-1)}$$

$$G'' = G\frac{(\omega\tau)}{1+(\omega\tau)^2} \qquad \text{(Equation III-2)}$$

In the Maxwell expression, G_0 is the component of the storage modulus that is independent of the oscillation frequency, G describes the component of the storage modulus that varies with the oscillation frequency, and τ is the characteristic relaxation time [18, 19]. The parameters obtained from fitting the experimental $G'(\omega)$ (Table III-1) were used to evaluate the plateau moduli $G'(\infty)$ and $G'(0)$ plotted in Figure III-6 c. In the high frequency limit, the plateau storage modulus $G'(\infty)$ is equal to $G_0 + G$. In the low frequency limit, the plateau storage modulus $G'(0) = G_0$. The values G and τ determined by fitting the storage modulus to Eq. III-1 were also used to evaluate the loss modulus by Eq. III-2. The Maxwell model is only an approximation for the frequency-dependent behavior of ERE:EPE gels. The relaxations observed in the experimental data are broader than those predicted for a single Maxwell mode. Such broad relaxations in physical protein gels were observed by Tang *et al.* and were better fit with a stretched exponential model [16], which is discussed below. However, this analysis still provides a useful method to quantify the plateau values and relaxation times in the dynamic storage moduli.

Composition (ERE:EPE)	G (Pa)	G_0 (Pa)	τ (sec/rad)
100:0	135 ± 16	4391 ± 360	0.11 ± 0.02
75:25	1023 ± 64	5467 ± 120	10.6 ± 1.4
50:50	2087 ± 217	6144 ± 765	15.1 ± 1.0
25:75	3528 ± 25	7334 ± 217	23.8 ± 2.2
0:100	6517 ± 390	6901 ± 572	18.7 ± 0.8

Table III-1. Maxwell model parameters for ERE:EPE hydrogels. The experimental data were fit to Eq. III-1 to obtain the parameters G, G_0, and τ. These parameters were then used to generate the solid curves shown in Figure III-6 a and b and to evaluate the plateau moduli $G'(\infty)$ and $G'(0)$ in Figure III-6 c.

Relaxation in chemical-physical gels was also observed by measuring the stress in gels held at constant 1% strain for 2 hours (Figures III-7 and III-8). For stress relaxation experiments, the relaxation function, $G(t)$, was fit to a single exponential model,

$$G(t) = G\exp\left(-\frac{t}{\tau}\right) + G_e \qquad \text{(Equation III-3)},$$

a double exponential model,

$$G(t) = G_1\exp\left(-\frac{t}{\tau_1}\right) + G_2\exp\left(-\frac{t}{\tau_2}\right) + G_e \qquad \text{(Equation III-4)},$$

and a stretched exponential (or Kohlrausch-Williams-Watts, KWW) model [16],

$$G(t) = G\exp\left(-\left(\frac{t}{\tau_{KWW}}\right)^{\beta}\right) + G_e \qquad \text{(Equation III-5)}.$$

The parameter G_e in Eqs. III-3, III-4, and III-5 is the equilibrium modulus and is analogous to the low frequency modulus in the frequency sweep experiments. In the stretched exponential model, the exponent β reflects heterogeneity in the relaxation process and varies between 0 and 1, with β

= 1 reducing to the single exponential model given by Eq. III-3. The mean relaxation time, $\langle\tau\rangle$, is calculated as

$$\langle\tau\rangle = \frac{\tau_{KWW}}{\beta}\Gamma\left(\beta^{-1}\right) \qquad \text{(Equation III-6)}$$

where $\Gamma(\beta^{-1})$ is the gamma function evaluated at β^{-1}. As in the frequency sweep experiments, a single Maxwell element is not sufficient to fit the broadness of the relaxation. For this reason, the stretched exponential model was used to quantify stress relaxation in EPE and mixed composition hydrogels (Figure III-8 and Table III-2). Potential sources of hetergeneity that may broaden the relaxation include local variation in the chemical cross-linking density and deviation of the physical cross-linking aggreagation number from the expected value of 5.

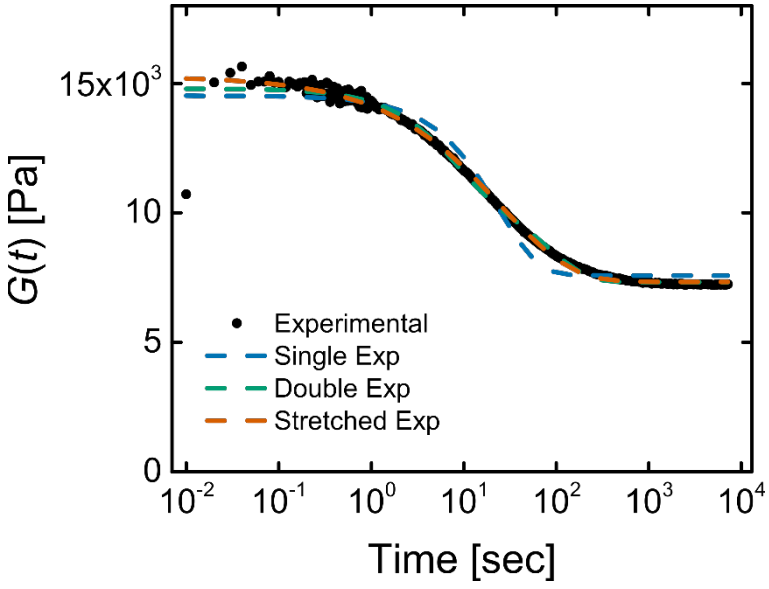

Figure III-7. Relaxation function for an EPE hydrogel fit to single exponential, double exponential, and stretched exponential models. The relaxation function $G(t)$ is plotted against time for a 1% strain over the duration of 2 hours. The dashed lines are fits of the experimental data to a single exponential model (Eq. III-3, blue), a double exponential model (Eq. III-4, green) and a stretched exponential model (Eq. III-5, orange). All of the models capture the short and long time plateau behavior, but the single exponential model does not fit the broadness of the relaxation.

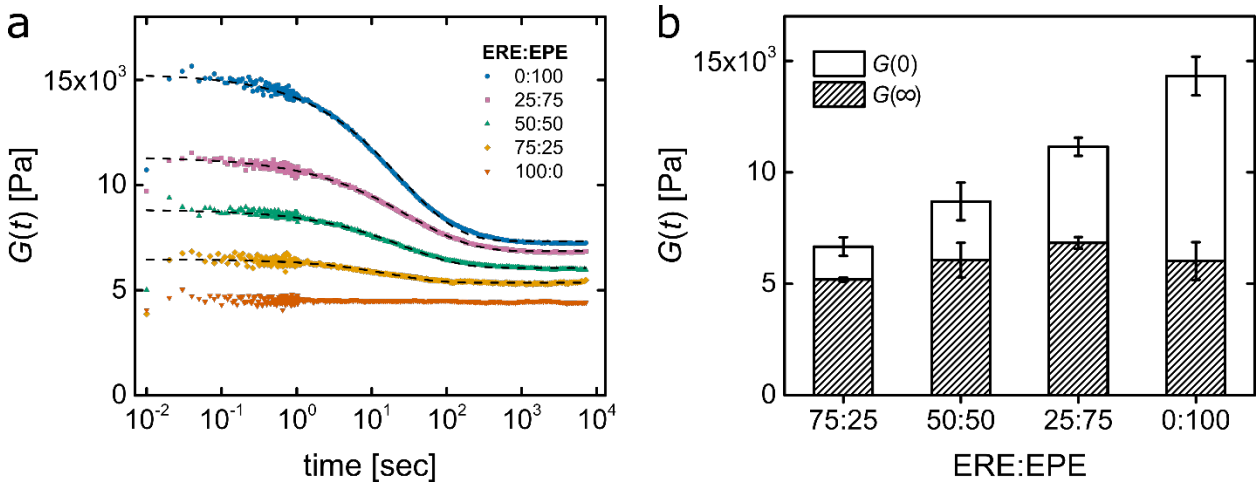

Figure III-8. Stress relaxation in ERE:EPE hydrogels. (**a**) Representative stress relaxation curves are shown for hydrogels prepared from EPE, ERE, and mixtures of the two proteins. The relaxation function $G(t)$ is plotted against time for a 1% strain over the duration of 2 hours. The dashed lines are fits of the experimental data to the stretched exponential model given in Eq. III-5. (**b**) The stretched exponential fit was evaluated at the limits $t = 0$ and $t \rightarrow \infty$ to give $G(0)$ and $G(\infty)$, respectively ($n \geq 3$, avg ± sd). The relaxation function at these limits is in agreement with $G'(\infty)$ and $G'(0)$ from the frequency sweep experiments. The ERE hydrogel does not exhibit significant stress relaxation and was not fit to the stretched exponential model.

Composition (ERE:EPE)	***G* (Pa)**	***G*$_e$ (Pa)**	τ_{KWW} **(s)**	$\langle\tau\rangle$ **(s)**	***β***
75:25	1480 ± 404	5188 ± 192	13.9 ± 3.7	49.3 ± 38.8	0.480 ± 0.179
50:50	2633 ± 291	6056 ± 1105	25.0 ± 2.5	47.8 ± 14.3	0.532 ± 0.074
25:75	4312 ± 155	6840 ± 349	35.3 ± 4.0	63.2 ± 8.3	0.534 ± 0.014
0:100	8171 ± 343	6020 ± 848	27.7 ± 4.4	47.4 ± 7.5	0.551 ± 0.011

Table III-2. Stretched exponential (KWW) parameters for stress relaxation experiments with ERE:EPE hydrogels. The experimental data were fit to Eq. III-5 to obtain the parameters (G_e, G, τ_{KWW}, and β). These parameters were used to generate the dashed curves in Figure III-8 a and to evaluate the plateau values of $G(t)$ shown in Figure III-8 b.

4.6 Calculation of the Average Molecular Weight between Cross-links by Theories of Rubber Elasticity (Affine Approximation and Phantom Network Approximation)

For each gel preparation, an average molecular weight between cross-links (M_c) was computed from the high frequency storage modulus and the swelling ratio using rubber elasticity theory. Assuming affine deformation of chains between chemical and physical cross-links, the shear modulus (G) for a network cross-linked in the presence of solvent is given by Eq. III-7 [17, 20].

$$G_{affine} = RT \frac{C_0}{M_C} \left(\frac{\varphi}{\varphi_0} \right)^{1/3} \qquad \text{(Equation III-7)}$$

where R is the gas constant, T is the temperature, C_0 is the initial (preparation state), and φ_0 and φ are the initial (preparation state) polymer volume fraction and equilibrium swollen polymer volume fraction, respectively. To capture the effect of both the chemical and physical cross-links, the shear modulus is taken as the high frequency plateau in the storage modulus, $G'(\infty)$ 'The swollen polymer volume fractions were determined from the mass swelling ratio, Q_m, assuming a gel density of 1 g cm^{-3} (ie. mostly water) and a dry polymer density weighted by the mass fraction of protein and PEG-4VS (approximately 0.8 and 0.2, respectively). The density of the artificial proteins is taken to be that of elastin, 1.3 g cm^{-3} [21], and the density of 10,000 g mol^{-1} PEG is 1.2 g cm^{-3} [22], giving an estimated dry polymer density of 1.28 g cm^{-3}. The dry polymer mass following lyophilization was divided by the cross-linking volume (40 μL) to estimate the initial polymer volume fraction and the initial concentration of polymer in the network before swelling. The values of M_c computed from Eq. III-7 are given in Table III-3, column 4.

Composition (ERE:EPE)	Q_m	$G'(\infty)$ (kPa)	M_c (kg/mol) (affine)	M_c (kg/mol) (phantom)	M_c (kg/mol) (sequence)
100:0	19.7	4.5	49.6	24.8	23.1
75:25	18.1	6.5	33.8	17.2	20.3
50:50	16.1	8.2	28.4	14.7	17.3
25:75	14.7	10.9	20.9	11.0	14.1
0:100	13.5	13.4	17.3	9.3	10.7

Table III-3. Calculated average molecular weight between cross-links (M_c). The swelling ratios (column 2) and high frequency plateau storage moduli (column 3) were used to compute the average molecular weight between cross-links by the affine approximation (column 4) and the phantom network approximation (column 5). The values are compared to the theoretical molecular weight between cross-links determined from the protein sequences (column 6). With the exception of the covalent ERE network, the theoretical values of M_c fall between the values calculated by the affine and phantom network models.

In the phantom network approximation, the cross-links are not fixed in space as in the affine approximation but instead fluctuate. This decreases the free energy per chain and therefore decreases the modulus. In an ideal network, the phantom network modulus is related to the affine modulus from Eq. III-7 through the cross-linker functionality, f [23].

$$G_{phantom} = \left(1 - \frac{2}{f}\right) G_{affine} \qquad \text{(Equation III-8)}$$

The PEG-4VS cross-linker has a functionality of 4. The physical cross-links have a functionality of 5. The molar ratio of chemical to physical cross-links can be used to calculate an average cross-linker functionality, $\overline{f}$, which varies between $\overline{f}$ = 4.3 for EPE gels and $\overline{f}$ = 4 for ERE gels. In

this case the prefactor in Eq. III-8 becomes 0.53 for EPE gels and 0.5 for ERE gels. Including this adjustment in Eq. III-7 gives M_c based on the phantom network model (Table III-3, column 5), which is approximately one-half of the value from the affine model.

The expected or theoretical molecular weight between cross-links in ideal ERE:EPE gels is based on the protein sequences and the molar ratio of each protein in the gelation mixture. In a fully cross-linked EPE gel, in which all chain ends are linked by PEG-4VS and all P midblocks participate in physical cross-links, the average molecular weight between cross-links is calculated as the average of the molecular weight of the segment N-terminal to the P domain and the segment C-terminal to the P domain. These chains are predominantly elastin-like repeats and PEG. The N- and C-terminal segments of EPE have molecular weights of 8763 Da and 7563 Da, respectively. Each arm of the 4-arm PEG vinyl sulfone has a molecular weight of 10,000/4 = 2500 Da. This gives a theoretical average molecular weight between cross-links of 10,663 Da. In a fully cross-linked ERE gel, the average molecular weight between cross-links is calculated as the molecular weight of the protein between the cysteine residues (18,058 Da) plus two PEG arms (2 x 2500 Da), giving an M_c of 23,058 Da. The theoretical values of M_c for the 75:75, 50:50, and 25:75 ERE:EPE gels, which are calculated from the molar ratio of EPE and ERE in the cross-linking reaction, are listed in Table III-3, column 6.

The calculated values of M_c for the five hydrogel preparations were in reasonable agreement with the theoretical values determined from the protein molar masses. Both the affine and phantom network models have been used previously to describe networks formed by cross-linking PEG macromers [24-26]. In these studies, the experimental data were best modeled by the phantom approximation at lower initial polymer volume fractions and the affine approximation at higher initial polymer volume fractions. With the exception of ERE gels, the theoretical values of

M_c of the gels prepared in this work fall between the values calculated by the affine model and by the phantom network model. In ERE gels, the theoretical value is close to the value calculated by the phantom network model. One possible explanation for this observation is that the covalent cross-links fluctuate as modeled by the phantom approximation whereas the larger physical cross-links do not.

The estimation of M_c described here assumes that a perfect network is formed and that the chains between cross-links behave ideally, which is almost certainly not the case. Non-idealities such as loops, missed cross-links (chemical or physical), dangling chains, and entanglements likely exist in the gels. These effects might explain some of the discrepancies between the theoretical values of M_c and the calculated values of M_c.

4.7 Disrupting Physical Cross-linking by Protein Denaturation

The role of protein folding and protein-protein interactions in mediating physical cross-linking was investigated by characterizing the rheological behavior of PEP and EPE hydrogels in buffer containing the protein denaturant urea. As shown in Figure III-9 a and b, PEP gels prepared in solutions that contain up to 1.5 M urea maintain high frequency elastic behavior. A gel-sol transition occurs at a urea concentration of 1.75 M, as indicated by the arrow in Figure III-9 c where $G' = G''$ at 100 rad s^{-1}. In contrast to PEP, EPE cross-linked with PEG-4VS can be swollen in buffer containing 8 M urea without dissolving the network. Under these conditions, however, the frequency-dependence of G' and the maximum in G'' are abolished (Figure III-9 d), and EPE gels closely resemble ERE gels. This again suggests that P domains in neighboring EPE chains associate noncovalently and that this association can be disrupted under denaturing conditions. By

exploiting these phenomena, one can design protein hydrogels that switch between elastic and viscoelastic behavior in response to environmental cues.

4.8 Disupting Physical Cross-linking by Mutation of the P Domain

To define more fully the role of protein sequence in determining bulk hydrogel properties, the effect of a point mutation in the P domain that is expected to disrupt noncovalent chain association was assessed. Gunasekar *et al*. identified aliphatic residues along the hydrophobic face of the COMP coiled-coil domain that are required for maintaining its structure and oligomerization state [27]. Most notably, a single leucine-to-alanine point mutation at position 44 (Figure III-1 a, denoted by *) results in both decreased helicity (16.6% versus 70.1% for the wild-type P domain) and reduced pentamerization [27]. An EPE variant containing this point mutation (denoted EPE L44A) was prepared (Figures III-2, III-3, and III-4), and hydrogels were formed by covalent cross-linking with PEG-4VS. The modified P domains in EPE L44A are expected to be largely unfolded and incapable of forming physical cross-links. Consistent with this view, hydrogels prepared from EPE L44A do not exhibit the high and low frequency plateau storage moduli characteristic of hydrogels containing EPE (Figure III-10). Instead, *G'* is nearly frequency-independent over the experimental range of 0.001-100 rad s^{-1}, demonstrating that a single mutation is sufficient to abolish physical cross-linking. Because the wild-type and mutant P domains differ by only a single amino acid, the physical cross-linking observed in EPE hydrogels can be attributed to highly specific interactions among folded P domains rather than nonspecific aggregation though hydrophobic or electrostatic interactions, as these interactions would likely also be present between mutant P domains.

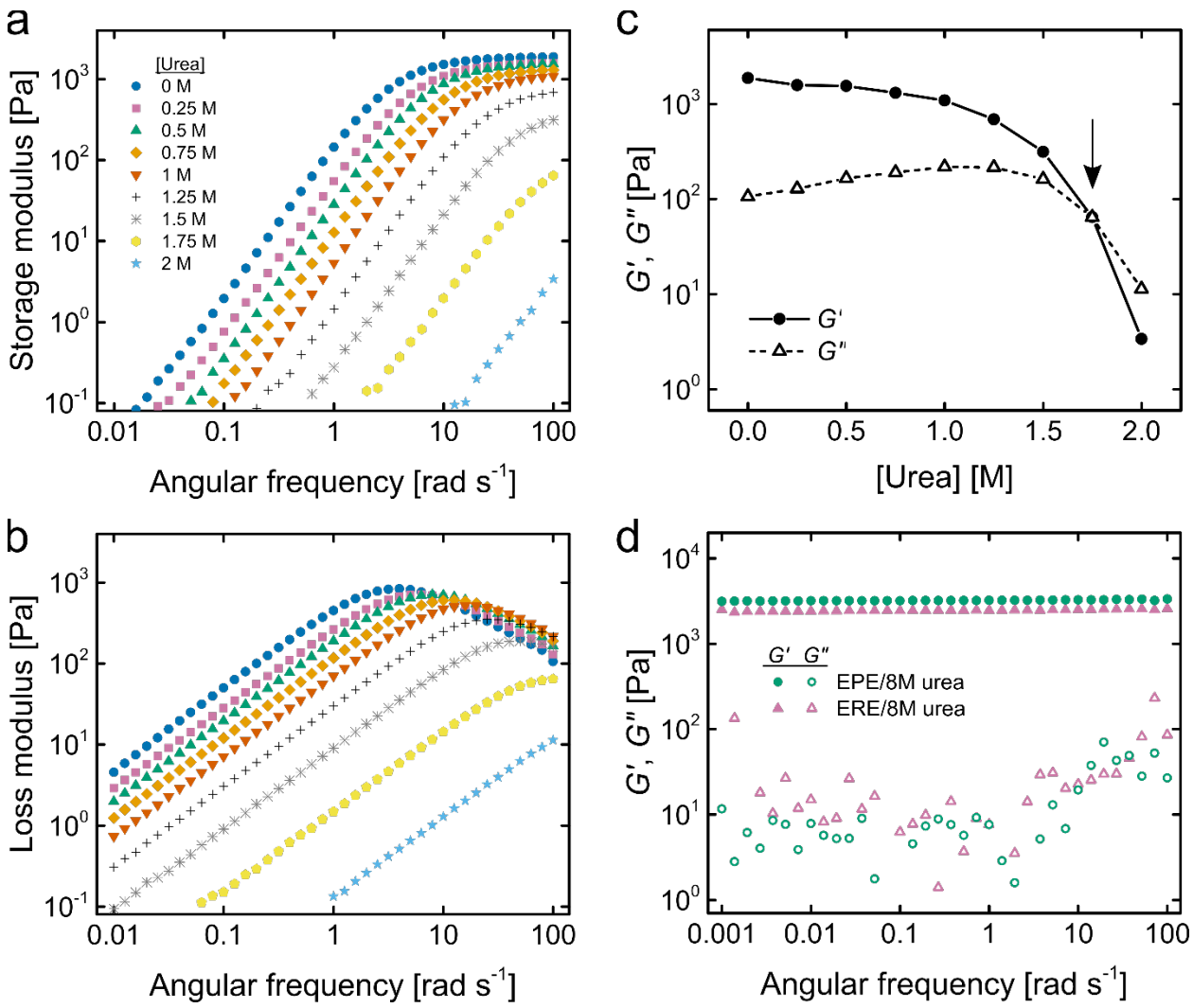

Figure III-9. Disruption of physical cross-linking by denaturant. Storage moduli (**a**) and loss moduli (**b**) of 7 wt% PEP prepared in increasing concentrations of urea at 25 °C, 10% strain amplitude. (**c**) The high frequency values of *G'* and *G"* (at 100 rad s^{-1}) show a decrease in elasticity associated with a loss of physical cross-linking at increasing urea concentrations. An arrow marks the urea concentration of 1.75 M where *G'* and *G"* are equal at 100 rad s^{-1}. (**d**) When EPE and ERE gels are swollen in buffer containing 8 M urea, *G'* is independent of the oscillation frequency and *G"* does not exhibit a maximum (25 °C, 1% strain amplitude). The mass swelling ratios for EPE and ERE swollen in PBS/8 M urea are 32.3 and 34.7, respectively.

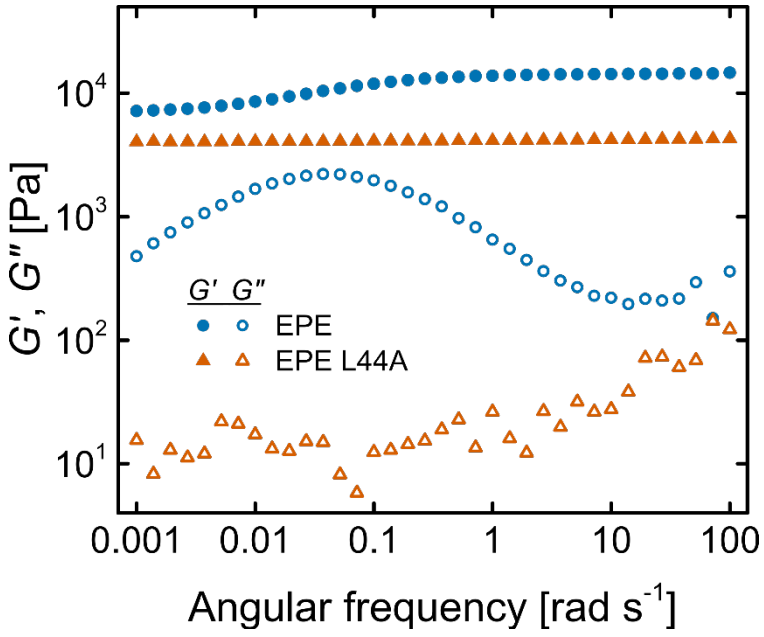

Figure III-10. Disruption of physical cross-linking by a point mutation within the P domain. Hydrogels prepared from the EPE variant EPE L44A (orange triangles) exhibit elastic behavior characterized by a frequency-independent *G'* (filled symbols) and a small loss modulus (open symbols). The frequency sweep of an EPE gel swollen in PBS (blue circles) is shown for comparison. The mass swelling ratio of EPE L44A gels in PBS is 21.7, similar to ERE gels.

5. Conclusions

Previously, chemical cross-links have been introduced into physical gels prepared from zwitterionic polymers, gelatin, and artificial proteins to stabilize these fragile materials against thermal or mechanical disruption [28-31]. Here, dynamic physical cross-links were incorporated into covalent hydrogel networks using engineered protein domains in order to program the time-dependent response to material deformation. Combining covalent and noncovalent cross-linking in gels is emerging as a promising strategy for improving material toughness and resistance to fracture, and mechanical unzipping of coiled-coil domains or analogous processes of programmed

energy dissipation might lead to similar improvements in gel toughness [32-35]. Transient physical cross-linking also has important implications for biological networks, as shown (for example) by the frequency-dependent dynamic moduli of actin networks cross-linked with α-actinin or heavy meromyosin [36, 37]. Stress relaxation and energy dissipation in these networks have been attributed to reversible association of actin cross-links, analogous to the association of the engineered P domains described in this work. In addition to the intracellular cytoskeletal network, the viscoelasticity of the extracellular environment is also an important regulator of cellular behavior on two-dimensional substrates and within three-dimensional matrices [38, 39]. The capacity to program chain sequence at the genetic level opens important new opportunities in the exploration of macromolecular behavior in both biological and engineered systems.

6. References

[1] J.-F. Lutz, M. Ouchi, D.R. Liu, M. Sawamoto *Science* **2013** *341*, 1238149.

[2] K.A. Dill, J.L. MacCallum *Science* **2012** *338*, 1042.

[3] B.V. Slaughter, S.S. Khurshid, O.Z. Fisher, A. Khademhosseini, and N.A. Peppas *Adv. Mater.* **2009** *21*, 3307.

[4] M.W. Tibbitt, K.S. Anseth *Biotechnol. Bioeng.* **2009** *103*, 655.

[5] S.C. Rizzi, J.A. Hubbell *Biomacromolecules* **2005** *6*.

[6] R.A. McMillan, V.P. Conticello *Macromolecules* **2000** *33*.

[7] W.A. Petka, J.L. Harden, K.P. McGrath, D. Wirtz, and D.A. Tirrell *Science* **1998** *281*.

[8] P.J. Skrzeszewska, F.A. de Wolf, M.W.T. Werten, A.P.H.A. Moers, M.A. Cohen Stuart, and J. van der Gucht *Soft Matter* **2009** *5*, 2057.

[9] W. Shen, K. Zhang, J.A. Kornfield, D.A. Tirrell *Nat. Mater.* **2006** *5*.

[10] T.K.L. Meyvis, S.C. De Smedt, J. Demeester, W.E. Hennink *J. Rheol.* **1999** *43*, 933.

[11] D.W. Urry *J. Phys. Chem. B* **1997** *101*, 11007.

[12] V.N. Malashkevich, R.A. Kammerer, V.P. Efimov, T. Schulthess, and J. Engel *Science* **1996** *274*, 761.

[13] A.L. Main, T.S. Harvey, M. Baron, J. Boyd, and I.D. Campbell *Cell* **1992** *71*, 671.

[14] D.T. McPherson, J. Xu, D.W. Urry *Protein Expression Purif.* **1996** *7*, 51.

[15] B.D. Olsen, J.A. Kornfield, D.A. Tirrell *Macromolecules* **2010** *43*.

[16] S. Tang, M.J. Glassman, S. Li, S. Socrate, and B.D. Olsen *Macromolecules* **2014** *47*, 791.

[17] M.P. Lutolf, J.A. Hubbell *Biomacromolecules* **2003** *4*, 713.

[18] J.D. Ferry, *Viscoelastic Properties of Polymers* 3rd ed. Wiley, New York **1980**.

[19] J.W. Goodwin, R.W. Hughes, *Rheology for Chemists: An Introduction* 2nd ed. RSC Publishing, Cambridge **2008**.

[20] N.A. Peppas, E.W. Merrill *J. Appl. Polym. Sci.* **1977** *21*, 1763.

[21] M.A. Lillie, J.M. Gosline *Biopolymers* **2002** *64*, 115.

[22] 2012. *Polyethylene glycol [MAK Value Documentation, 1998]*. *The MAK-Collection for Occupational Health and Safety.* 274-270.

[23] M. Rubinstein, R.H. Colby, *Polymer Physics* Oxford Univ. Press, New York **2003**.

[24] Y. Gnanou, G. Hild, P. Rempp *Macromolecules* **1987** *20*, 1662.

[25] Y. Akagi, J.P. Gong, U.-i. Chung, T. Sakai *Macromolecules* **2013** *46*, 1035.

[26] Y. Akagi, T. Katashima, Y. Katsumoto, K. Fujii, T. Matsunaga, U.-i. Chung, M. Shibayama, and T. Sakai *Macromolecules* **2011** *44*, 5817.

[27] S.K. Gunasekar, M. Asnani, C. Limbad, J.S. Haghpanah, W. Hom, H. Barra, S. Nanda, M. Lu, and J.K. Montclare *Biochemistry* **2009** *48*, 8559.

[28] F. Bode, M.A. da Silva, A.F. Drake, S.B. Ross-Murphy, and C.A. Dreiss *Biomacromolecules* **2011** *12*, 3741.

[29] Z. Zhang, T. Chao, S. Jiang *J. Phys. Chem. B* **2008** *112*, 5327.

[30] R.E. Sallach, W. Cui, J. Wen, A. Martinez, V.P. Conticello, and E.L. Chaikof *Biomaterials* **2009** *30*.

[31] W. Shen, R.G.H. Lammertink, J.K. Sakata, J.A. Kornfield, and D.A. Tirrell *Macromolecules* **2005** *38*.

[32] J.-Y. Sun, X. Zhao, W.R.K. Illeperuma, O. Chaudhuri, K.H. Oh, D.J. Mooney, J.J. Vlassak, and Z. Suo *Nature* **2012** *489*, 133.

[33] Z.S. Kean, J.L. Hawk, S. Lin, X. Zhao, R.P. Sijbesma, and S.L. Craig *Adv. Mater.* **2014** *26*, 6013.

[34] J.A. Neal, D. Mozhdehi, Z. Guan *J. Am. Chem. Soc.* **2015** *137*, 4846.

[35] X. Zhao *Soft Matter* **2014** *10*, 672.

[36] S.M.V. Ward, A. Weins, M.R. Pollak, D.A. Weitz *Biophys. J.* **2008** *95*, 4915.

[37] O. Lieleg, M.M.A.E. Claessens, Y. Luan, A.R. Bausch *Phys. Rev. Lett.* **2008** *101*, 108101.

[38] O. Chaudhuri, L. Gu, M. Darnell, D. Klumpers, S.A. Bencherif, J.C. Weaver, N. Huebsch, and D.J. Mooney *Nat. Commun.* **2015** *6*, 6365.

[39] D.D. McKinnon, D.W. Domaille, T.E. Brown, K.A. Kyburz, E. Kiyotake, J.N. Cha, and K.S. Anseth *Soft Matter* **2014** *10*, 9230.

Chapter IV

ENGINEERING THE DYNAMIC PROPERTIES OF PROTEIN HYDROGEL NETWORKS THROUGH SEQUENCE VARIATION

1. Abstract

Network dynamics control the viscoelasticity and erosion rate of materials and influence biological processes at multiple length scales. In hydrogel networks prepared from recombinant artificial proteins, dynamic behaviors such as stress relaxation and energy dissipation can arise from the transient intermolecular association of protein domains that form physical network junctions. In this chapter, variation of the protein sequence is explored as a strategy to tune the characteristic relaxation timescale of protein networks. Single point mutations to coiled-coil physical cross-linking domains that associate within an end-linked covalent network can alter the characteristic relaxation time over five orders of magnitude as demonstrated by dynamic oscillatory shear rheology experiments and stress relaxation measurements. Using a pair of orthogonal coiled-coil physical cross-linking domains, networks with two distinct relaxation timescales were also engineered. This work demonstrates how the time-dependent response of a polymeric material to mechanical deformation can be encoded within the sequence of a polymer.

2. Introduction

Cellular behaviors such as proliferation [1], spreading and migration [2], and differentiation [3] are regulated in part by the stiffness of the local tissue microenvironment. These observations have led to considerable efforts to design materials with tunable mechanical properties for applications in tissue engineering and for fundamental research of mechanotransduction. The stiffness or compliance of biomaterials is typically characterized by an elastic modulus relating the deformation and stress at small strains. The moduli of materials used in cell culture can vary from less than 1 kPa for soft gels [4] to more than 1 GPa for glass and tissue culture polystyrene [5]. Several recent studies have suggested that in addition to the elasticity of a material, its viscous or dissipative properties may also influence cellular behavior [6-8]. To better understand these phenomena and to potentially harness them for cell and tissue engineering applications, it will be necessary to develop materials with tunable dynamic properties.

Dynamic materials have been engineered from both synthetic polymers and proteins. Examples of dynamic synthetic polymer networks include viscoelastic gels and elastomers cross-linked by hydrophobic interactions [9], hydrogen bonds [10], metal-ligand complexes [11-14], and dynamic covalent bonds [15, 16]. Stress relaxation and energy dissipation in these materials arise from the transient nature of at least some of the network junctions, and the characteristic relaxation timescales can therefore be tuned by modifying the lifetime of the transient cross-links. In protein hydrogel networks, dynamic properties likewise emerge from transient physical cross-links between associating domains on neighboring protein chains. Examples of dynamic physical cross-linking domains in artificial proteins include α-helical coiled coils [17-20] and collagen-like triple helices [21].

Hydrogels cross-linked by coiled-coil domains are the best-studied example of dynamic protein networks, and engineering the sequence the cross-linking domains in these proteins is a potential strategy to program the dynamic viscoelastic behavior of these materials. Using a pH-responsive leucine zipper coiled coil, Shen *et al*. showed that the lifetime of a physical cross-link is related to the characteristic strand exchange time (τ_e), or the exchange rate of a strand between different coils. Although exchange times have only been reported for a small number of coiled coils derived from transcription factors, structural proteins, and designed peptides, these measurements reveal a large dynamic range that may be useful for engineering the relaxation behavior of protein-based materials [18, 22-25]. In these coiled coils, τ_e varied from approximately 1 s to greater than 10^4 s. This large dynamic range might reflect the diverse roles of coiled coils in biological systems. For example, coiled coils that mediate the dimerization of transcription factors such as Fos and Jun may require a very fast exchange rate ($\tau_e < 10$ s) to allow a cell to rapidly alter its transcriptional program [25]. Tropomyosin coiled coils, however, are much more stable ($\tau_e \approx$ 500 to >20,000 s) [22]. Coiled-coil dynamics are also sensitive to pH [18], allosteric regulation by binding partners [25], and mutation of the amino acid sequence [24]. The effects of mutations within coiled coil domains on the characteristic exchange time are particularly intriguing as this might allow the relaxation behavior of protein networks to be encoded within the protein sequence.

In this work, a set of seven artificial proteins was prepared that differ only by the identity of the side chain at one residue within a helical domain (P) that associates to form coiled coils. Association of these domains within an end-linked hydrogel network results in transient physical cross-linking and viscoelastic behavior. These networks were characterized by dynamic oscillatory rheology and stress relaxation experiments in order to measure a characteristic relaxation time for each material. Building on this strategy, hydrogel networks with more complex dynamic behavior

were then prepared from mixtures of two artificial proteins. The results described in this chapter demonstrate that the macroscopic dynamic behavior of a protein network can be encoded at the level of the primary sequence and show that very small changes to a single amino acid reside can have significant effects on the macroscopic length scale.

3. Materials and Methods

3.1 Site-Directed Mutagenesis and Cloning of Artificial Protein Genes

EPE variants were generated by site-directed mutagenesis of the sequence encoding the P domain on a pUC19 plasmid (pUC19 P) using oligonucleotides reported in Appendix A. After sequencing to confirm the correct mutant was obtained, the resulting pUC19 P-*mutant* plasmids (pUC19 P T40A, pUC19 P Q54A, pUC19 P I58A, pUC19 P L37A, pUC19 P L37V, pUC19 P L37I) were digested with *SacI* and *SpeI* (New England BioLabs, Ipswich, MA) to isolate the fragments encoding P-*mutant*. The residue numbering convention is based on the amino acid sequence of rat cartilage oligomeric matrix protein (COMP), from which the P domain is derived [26]. The excised fragments were ligated into the pQE-80L EPE plasmid (described in Chapter 3) that was digested with the same enzymes. This replaces the original P domain with the mutated variant. Site-directed mutagenesis was not carried out directly on pQE-80L EPE due to difficulties created by the highly-repetitive, GC-rich elastin-like domains. Chemically competent BL21 *Escherichia coli* (New England BioLabs) were transformed with the pQE-80L EPE-*mutant* plasmids (pQE-80L EPE T40A, pQE-80L EPE Q54A, and pQE-80L EPE I58A, pQE-80L EPE L37A, pQE-80L EPE L37V, pQE-80L EPE L37I) for protein expression. The gene sequence and amino acid sequence of each protein are listed in Appendix A.

The pQE-80L EAE plasmid was constructed by subcloning the sequence encoding the A domain from pQE-9 PC10A [27] into the pQE-80L EPE plasmid in place of the sequence encoding the P domain. The forward primer (Appendix A) contained a *Sac*I overhang while the reverse primer bound the plasmid downstream of an in-frame *Spe*I site flanking the A domain in pQE-9 PC10A. The amplicon was digested with these enzymes and ligated into the pQE-80L EPE plasmid in place of P. The BL21 strain was also used for expression of EAE.

3.2 Protein Expression and Purification

Recombinant expression and purification of EPE, EAE, and the EPE variants is similar to the protocol described in Chapter 2 and Appendix B. Briefly, 1 L cultures were grown at 37 °C in Terrific broth containing 100 μg mL^{-1} ampicillin (BioPioneer, San Diego, CA) to an optical density at 600 nm (OD_{600}) of 1. Isopropyl β-D-1-thiogalactopyranoside (IPTG) (BioPioneer) was added to a final concentration of 1 mM and the cells were harvested 4 hr later by centrifugation at 6,000 *g* for 8 min at 4 °C. The cells were frozen at a concentration of 0.5 g mL^{-1} in TEN buffer (50 mM Tris, 1 mM EDTA, 100 mM NaCl, pH 8.0) supplemented with 5% (v/v) glycerol, 0.1% (w/v) sodium deoxycholate, and 0.1% (v/v) TritonX-100. After thawing, the lysate was treated with 10 μg mL^{-1} DNase I (Sigma, St. Louis, MO), 5 μg mL^{-1} RNase A (Sigma), 5 mM $MgCl_2$, and 1 mM phenylmethylsulfonyl fluoride (Gold Biotechnology, Olivette, MO) while shaking at 37 °C, 250 rpm for 30 min. The lysate was then sonicated for 5 min (2" on, 2" off, 30% power amplitude) (QSonica, Newton, CT) and allowed to rest for 2 hr on ice. β-mercaptoethanol (βME) (Sigma) was added to the lysate to a final concentration of 1% (v/v) following sonication.

The target proteins were purified from the *E. coli* lysate by three rounds of temperature cycling. The lysate was centrifuged at 39,000 *g* for 1 hr at 4 °C to remove insoluble proteins and cellular debris. Crystalline NaCl was added to the supernatant at a final concentration of 2 M followed by shaking at 250 rpm, 37 °C for 1 hr. The aggregated proteins were collected by centrifugation at 39,000 *g* for 1 hr at 37 °C and solubilized overnight at 4 °C at a concentration of 100 mg mL^{-1} in cold TEN buffer containing 1% (v/v) βME. Two more cycles were completed with 30 min centrifugation spins. The βME was omitted in the final resuspension step. Instead, 5 mM tris(hydroxypropyl)phosphine (THP) (Santa Cruz Biotechnology, Dallas, TX) was added and the protein solution was incubated at 4 °C for 2 hr. The purified protein was desalted into LC-MS grade water (Sigma) using Zeba 7K MWCO columns (Thermo Fisher Scientific, Waltham, MA) and lyophilized for 4 days. The lyophilized protein was stored under argon at -80 °C or used immediately.

3.3 Protein Characterization by SDS-PAGE, ESI-MS, and Ellman's Assay

Fractions were saved from each step in the temperature cycling purification. Proteins were extracted from the pelleted fractions with a volume of 8 M urea equal to the volume of the supernatant from that step. These solutions were then diluted with an equal volume of water to adjust the final urea concentration to 4 M. Samples of the supernatant were diluted with an equal volume of 8 M urea to obtain a final urea concentration of 4 M. All of the fractions were then mixed with 2x SDS loading buffer containing 5% (v/v) βME and boiled for 10 min before loading 2 μL per well in a 15 well, Novex NuPage 4-12% Bis-Tris SDS PAGE gel (Thermo Fisher Scientific). The gel was run in MES/SDS running buffer (Boston BioProducts, Ashland, MA) for

45 min at 180 V, fixed, and stained with colloidal blue protein staining solution (Life Technologies, Carlsbad, CA). Gels were imaged on a Typhoon Trio (GE Healthcare, Pittsburgh, PA).

Protein solutions (0.2 mg mL^{-1} in 0.1% formic acid) were analyzed by LC-MS using a Waters UPLC/LCT Premier XE TOF mass spectrometer (Waters, Milford, MA) by electrospray ionization in the positive ion mode with a MassPREP Micro desalting column. The mass spectrometer was calibrated with NaI using standard procedures and calibration was subsequently verified by running a standard solution of myoglobin. The mass spectrometer settings were: capillary voltage = 2.8 kV, cone voltage = 40, source temperature = 120 °C, and desolvation temperature = 350 °C, desolvation gas = 750 L hr^{-1}, acquisition range = 500 to 2000 in V mode, ion guide = 5. The mobile phase consisted of a gradient of water and acetonitrile with 0.1% formic acid. Electrospray mass spectra were deconvoluted using MaxEnt1 software.

The free thiol content of each protein was measured using Ellman's assay as described in Chapter 2 and Appendix B. Lyophilized proteins were dissolved in reaction buffer (100 mM sodium phosphate, 1 mM EDTA, pH 8) at a concentration of 5 mg mL^{-1}. The protein solution (250 μL) and Ellman's reagent (Sigma) stock solution (50 μL of 5 mg mL^{-1} reagent in reaction buffer) were added to 2.5 mL of reaction buffer. After 15 min incubation, the absorbance at 412 nm was measured on a Cary 50 UV/Vis spectrophotometer. The concentration of thiol groups was calculated from the absorbance value and the extinction coefficient 14,150 M^{-1} cm^{-1}.

The free thiol content was also estimated by non-reducing SDS-PAGE. Samples prepared for thiol quantitation by Ellman's assay were diluted 1:10 in SDS loading buffer, and 2 μL of each solution was loaded in a 15-well, Novex NuPage 4-12% Bis-Tris gel. Control lanes contained samples that were reduced by boiling in the presence of 5% (v/v) βME for 5 min. The gel was run in MES/SDS running buffer at 180 V for 45 min. Proteins were visualized with InstantBlue protein

stain (Expedion, San Diego, CA). The intensity of each band on the protein gel was quantified using ImageQuant software (GE Healthcare).

3.4 Hydrogel Cross-linking and Swelling

Lyophilized artificial proteins were dissolved at a concentration of 150 mg mL^{-1} in degassed cross-linking buffer (0.1 M sodium phosphate, 6 M guanidinium chloride, 0.4 M triethanolamine, pH 7.4) by sonicating for 2 min in an ultrasonic bath. Bubbles were removed by centrifugation at 10,000 *g* for 1 min. The PEG-4VS cross-linker was dissolved at a concentration of 150 mg mL^{-1} in degassed 0.4 M triethanolamine, pH 7.4. Cross-linking was initiated by mixing the two solutions at a volumetric ratio that gave a 1:1 stoichiometry between the thiol and vinyl sulfone functional groups. The solution was vortexed to ensure homogeneous mixing and quickly pipetted onto a glass slide that was treated with SigmaCote (Sigma). A second treated glass slide was placed on top of the droplet separated by spacers cut from a 1 mm rubber sheet (McMaster-Carr, Santa Fe Springs, CA). The slides were clamped together and the gels were allowed to cure in the dark overnight at ambient temperature.

Hydrogels prepared for rheological measurements were transferred to a dish containing 6 mL of PBS (pH 7.4) containing 6 M guanidinium chloride (GndCl). The gels were swollen in this buffer for three hours before switching to PBS with 3 M GndCl for 3 hr, then PBS with 2 M GndCl for 3 hr, PBS with 1 M GndCl for 3 hr, and finally PBS. The gradual decrease in the guanidinium concentration is designed to allow unreacted protein chains to diffuse out of the gel and to promote proper folding of the coiled-coil domains.

For swelling experiments, hydrogels were transferred to 6-well plates containing 3 mL of PBS plus 6 M GndCl per well. The gels were swollen to equilibrium and the swollen mass was measured after 48 hr. The guandinium concentration was gradually decreased from 6 M to 0 M in PBS as described above. Swollen masses were recorded for gels in PBS after 48 hr of swelling followed by washing the gels at least five times with ddH_2O over the course of 72 hr to remove the salts. The dry mass was obtained after lyophilization. The mass swelling ratio Q_m was calculated for PBS with 6 M guanidinium chloride and PBS by dividing the swollen mass for each condition by the dry mass of the network. For extended swelling in PBS longer than 1 day, 0.02% (w/v) sodium azide (Sigma) was added to the buffer to inhibit microbial contamination.

3.5 Rheological Characterization of Protein Hydrogels

Swollen hydrogels prepared from EPE, EAE, and EPE variants were characterized by small amplitude oscillatory shear rheology and shear stress relaxation on an ARES-RFS strain-controlled rheometer (TA Instruments). Gels were cut into disks with an 8 mm biopsy punch (Miltex) and loaded between the 8 mm parallel plate test geometry as described in Chapters 2 and 3 and Appendix B. Frequency sweeps were acquired at 2% strain amplitude, 25 °C. Following the frequency sweep, a stress relaxation experiment was performed with a 2% step strain at 25 °C.

4. Results and Discussion

4.1 Protein Design, Synthesis, and Characterization

To explore the role of protein sequence on the relaxation dynamics of protein networks, six variants of the EPE protein described in Chapter 3 were designed, each containing a single

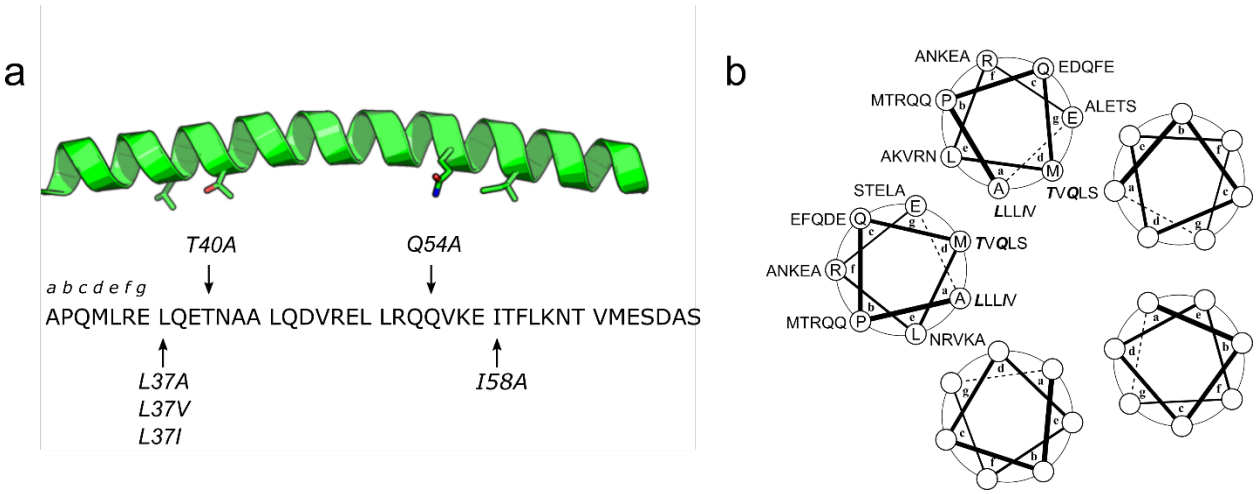

Figure IV-1. Point mutations within the P helical domain. (**a**) The midblock domain P in EPE forms a helical structure when associated in a homopentameric coiled coil (PDB 1VDF from ref. [32]). Below the structure, the amino acid sequence of the P domain is divided into six heptad repeats using the conventional *abcdefg* notation for coiled-coil peptides. The mutated residues leucine 37, threonine 40, glutamine 54, and isoleucine 58 are noted with arrows. (**b**) The pentameric coiled coil can also be represented by a helical wheel diagram. The mutated residues shown in bold, italic type face.

point mutation located within the P midblock domain. The mutated residues were selected based on the work of Gunasekar *et al*., in which alanine scanning mutagenesis was performed on the *a* and *d* positions that comprise the coiled-coil interface [28]. Point mutations to alanine at one of several aliphatic residues in P (Leu37, Leu44, Val47, Leu51, or Ile58) resulted in destabilization of the helical structure while mutations of polar residues (Thr40 or Gln54) to alanine resulted in stabilization [28]. An increase in thermal stability was also observed when Gln54 was mutated to leucine [29] or isoleucine [30]. In Chapter 3, it was shown that hydrogels prepared by cross-linking an EPE variant containing the L44A mutation do not exhibit physical cross-linking, but the effects of other mutations that are stabilizing or less destabilizing than L44A on the behavior of chemical-physical networks are unknown.

The six EPE variants include EPE T40A and EPE Q54A, which are expected to form more stable coiled coils than EPE (referred to as wild-type or WT), and EPE I58A, which is expected to form less stable coiled coils than WT. The remaining three variants, EPE L37A, EPE L37V, and EPE L37I, contain point mutations at residue 37. Replacement of leucine 37 with alanine and valine, which have smaller aliphatic side chains, is expected to decrease coiled-coil stability. The effect of the L37I mutation on the stability of the coiled-coil is difficult to predict because the mutation results in only a small change to the branching structure of the aliphatic side chain. The positions of the point mutations within the P domain are shown in Figure IV-1.

EPE and its variants were expressed in *Escherichia coli* strain BL21 and purified by inverse temperature cycling (Figure IV-2). Typical yields exceeded 100 mg of purified protein per liter of culture. The proteins were reduced, desalted, and stored under inert atmosphere at -80 °C to ensure a high free thiol content, which was measured by Ellman's assay [31] to be between 83-91% for all EPE variants (Figure IV-3 and Table IV-1). The results of Ellman's assay were also consistent with analysis by non-reducing SDS-PAGE, which confirmed that the proteins were monomeric (Figure IV-4 and Table IV-2). The molecular weight of the proteins were confirmed by electrospray ionization mass spectrometry (ESI-MS) (Table IV-3).

4.2 Hydrogel Cross-linking and Swelling

Hydrogels were prepared by end-linking the artificial proteins with 4-arm poly(ethylene glycol) vinyl sulfone (PEG-4VS) as described in the previous chapters. Gels were prepared from each EPE variant in an identical manner, although slight variations may arise due to differences in the protein thiol content or purity. For all gels, the total polymer (protein and PEG-4VS)

concentration was 15 wt% during cross-linking and the stoichiometry of protein thiols to vinyl sulfone groups on PEG-4VS was nominally 1:1. After cross-linking, the gels were swollen in decreasing concentrations of guanidinium chloride (6M, 3M, 2M, 1M, 0M) in PBS to remove unreacted polymer and to promote refolding of the helical midblocks into coiled-coil cross-links. Hydrogels were swollen in PBS for at least 48 hr prior to either measurement of the swollen mass or rheological characterization. The mass swelling ratio (Q_m) for each hydrogel is plotted in Figure IV-5.

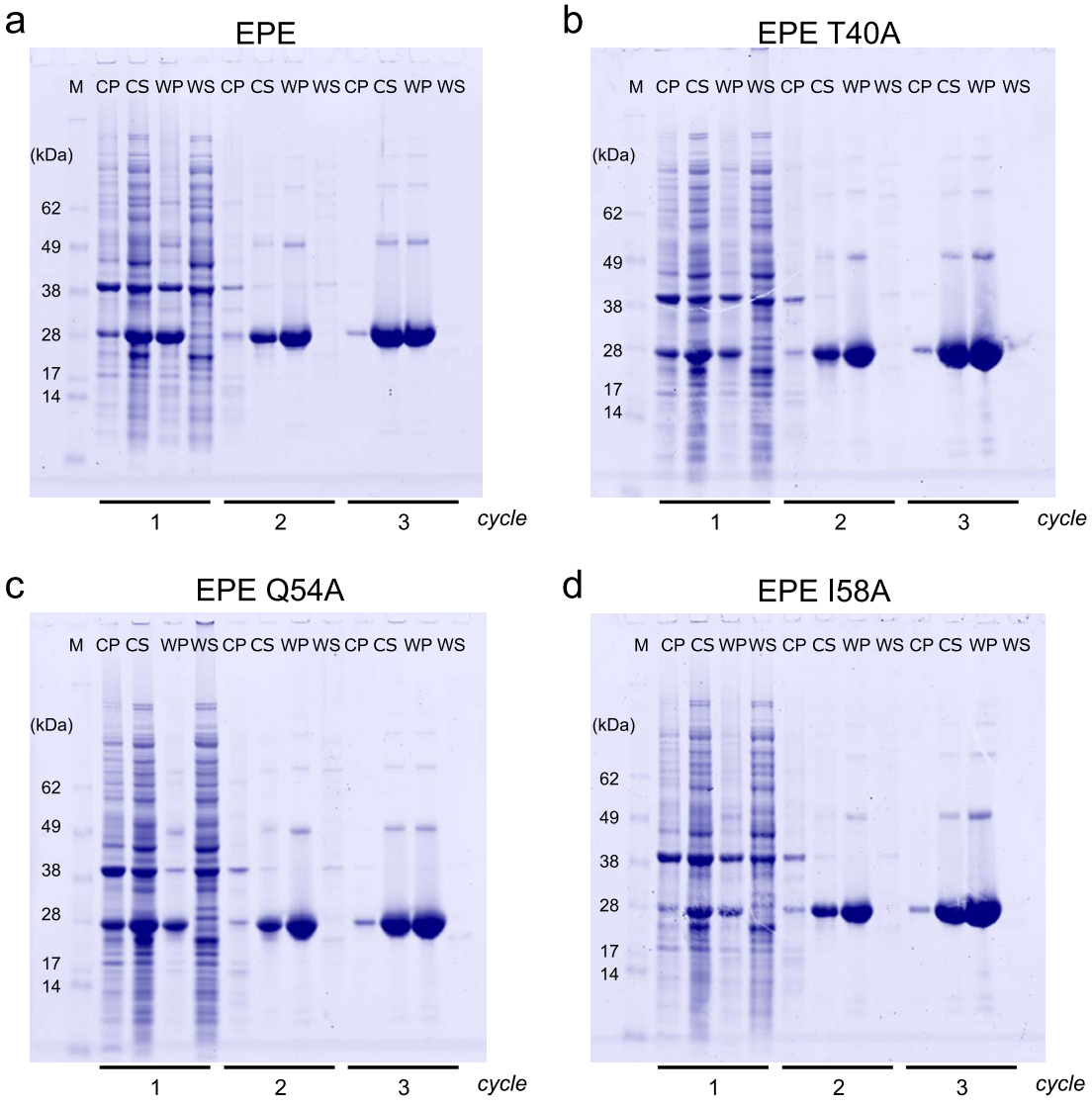

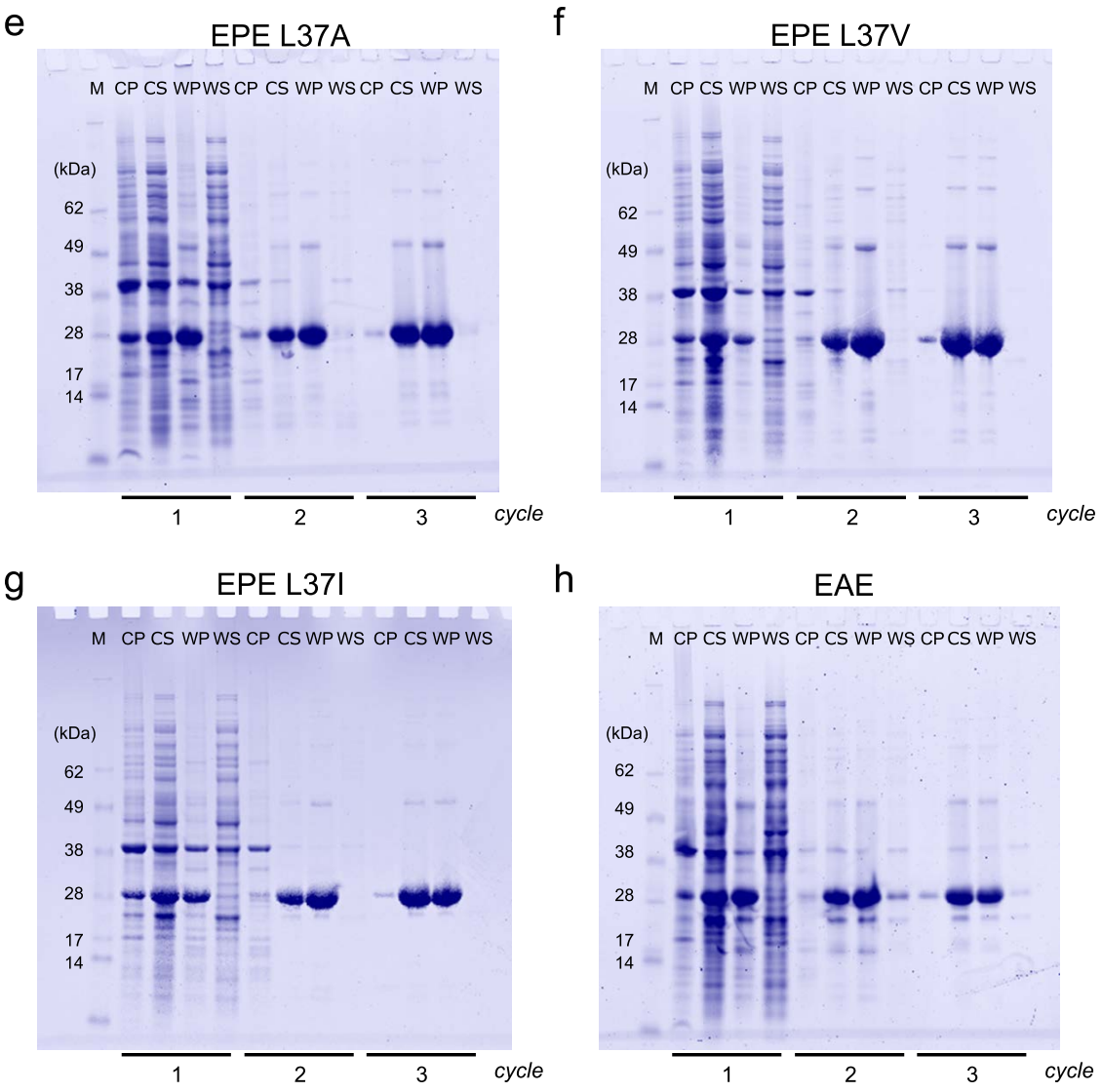

Figure IV-2 (begins on previous page). SDS PAGE analysis of inverse temperature cycling. Samples of each fraction were saved throughout the inverse temperature cycling purification. (**a-h)** EPE, EPE T40A, EPE Q54A, EPE I58A, EPE L37A, EPE L37V, EPE L37I, and EAE. Elastin-like proteins are soluble in the cold step of each cycle (4 °C, low ionic strength) and insoluble in the warm step of each cycle (37 °C, 2 M NaCl). Pure proteins were obtained after three cycles. The molar masses of the nine artificial proteins are nearly identical. Only EAE can be distinguished from the EPE variants on the basis of electrophoretic mobility. (Abbreviations: CP – cold pellet, CS – cold supernantant, WP – warm pellet, WS – warm supernatant, M – SeeBlue protein marker with molecular weights in kDa).

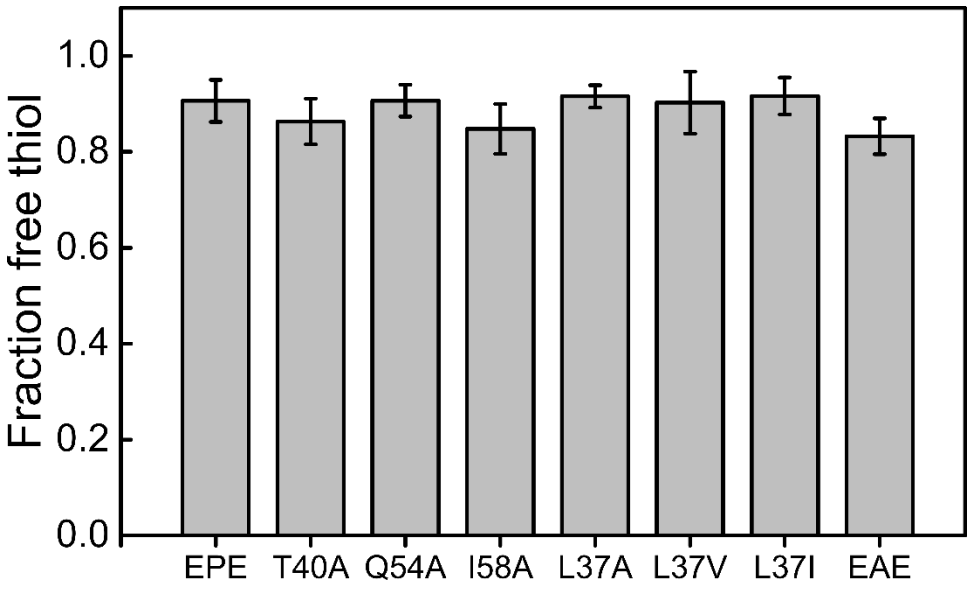

Figure IV-3. Ellman's assay quantitation of the free thiol content in artificial proteins. The fraction of free thiol groups was calculated by dividing the concentration of thiols measured by Ellman's assay by the expected concentration of thiols assuming that each protein chain contains two cysteine residues. The values all fall between 83% and 91%. Analysis of the proteins by non-reducing SDS-PAGE (Figure IV-4 and Table IV-1) suggest that deviations from the expected concentration of free thiols arise from the formation of intermolecular disulfides (dimers, trimers, etc.) and intramolecular disulfides (cyclized monomers and higher order species).

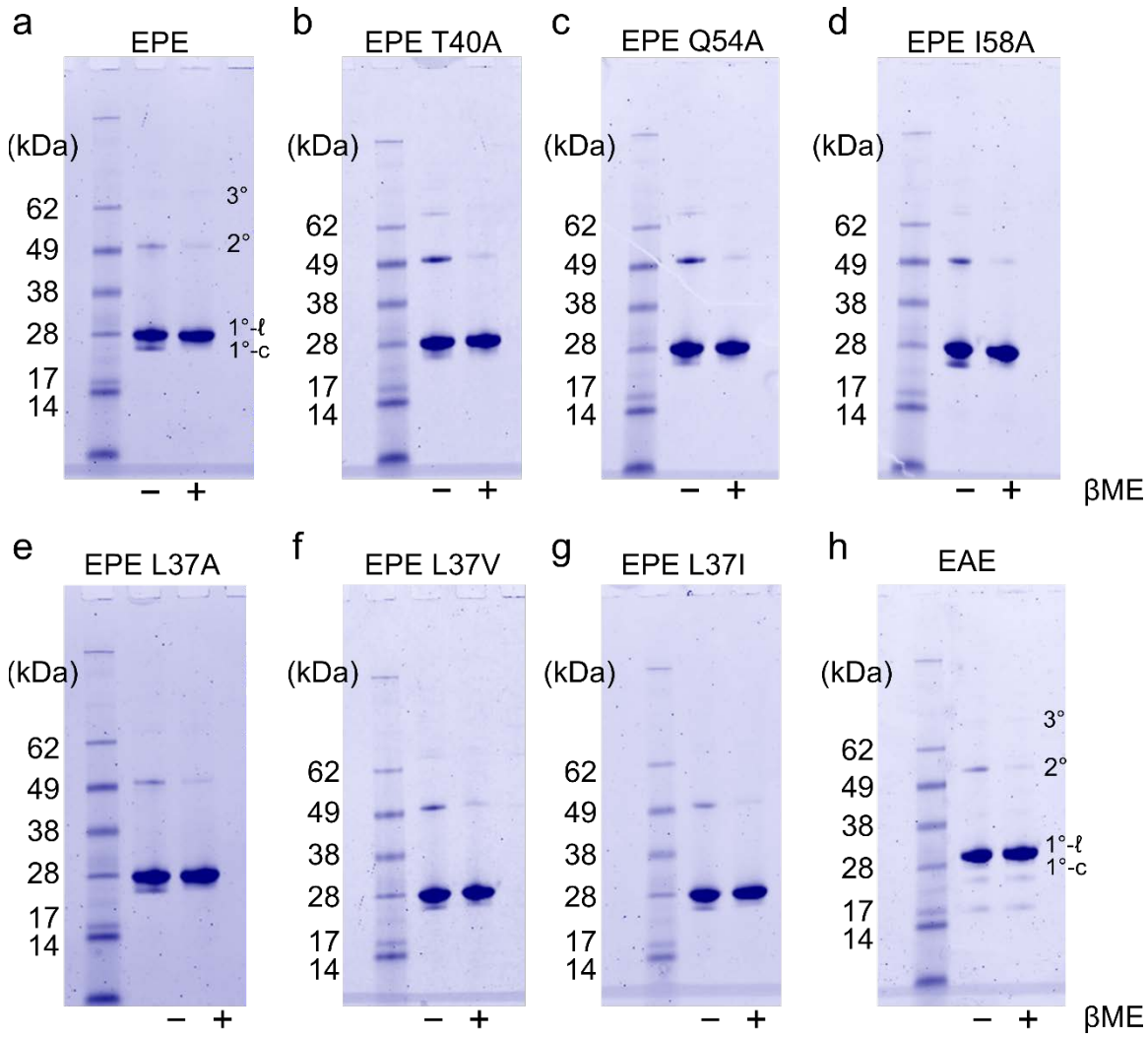

Figure IV-4. Analysis of protein oligomerization state by non-reducing SDS-PAGE. Each gel image contains three lanes. Lane 1: SeeBlue protein molecular weight marker with molecular weights (in kDa) of select bands labeled. Lane 2: artificial protein prepared in non-reducing buffer, denoted as "–" βME. Lane 3: artificial protein prepared in reducing buffer (with 5% (v/v) βME), denoted as "+" βME. In (**a**) and (**h**), the bands assigned as protein trimers (3°), dimers (2°), linear monomers (1°-ℓ), and cyclized monomers (1°-c) are labeled on the right-hand side of the gel. All artificial proteins are predominately monomeric and linear, although in general slightly more oligomers and cyclized monomers are present under non-reducing conditions (−) than in the reduced control lanes (+).

Protein	EPE	EPE L37A	EPE L37V	EPE L37I	EPE T40A	EPE Q54A	EPE I58A	EAE[a]
Trimer	<1	< 1	1	< 1	2	2	1	< 1
Dimer	6	5	9	7	15	14	11	7
Monomer (linear)	83	87	85	86	81	80	75	84
Monomer (cyclic)	9	8	5	7	2	5	12	4

[a] The EAE protein preparation has two small impurities that are likely degradation products. The integrated intensities of these bands on the SDS-PAGE gel were 3% and 2% of the total.

Table IV-1. Gel densitometry of protein bands in non-reducing SDS-PAGE. Lane profiles were created for the non-reducing sample lanes of the gel images in Figure IV-4. The intensities of bands assigned as linear monomers, cyclic monomers, dimers, and trimers in each lane were quantified by integrating the peak corresponding to each species. The data are reported as the percentage of the total area of all peaks detected in the lane.

Protein	EPE	EPE L37A	EPE L37V	EPE L37I	EPE T40A	EPE Q54A	EPE I58A	EAE
Ellman's assay	91	92	90	92	86	91	85	83
SDS-PAGE	86	90	90	90	89	87	81	88

Table IV-2. Percent free thiol by Ellman's assay and by non-reducing SDS-PAGE. The percentage of free thiol groups measured by Ellman's assay is compared to the percentage of free thiols calculated from the relative amount of each oligomer in the non-reducing SDS-PAGE gels (Figure IV-4 and Table IV-1). The data in Table IV-1 were multiplied by the expected number of free thiols per protein chain for each species (2 for linear monomers, 0 for cyclized monomers, 1 for dimers, and 2/3 for trimers). This value is then divided by 2, the expected number of thiols per chain if all proteins were in the reduced form.

EPE variant	Calculated mass	Observed mass
EPE	21,464	21,462
EPE T40A	21,434	21,434
EPE Q54A	21,407	21,406
EPE I58A	21,422	21,421
EPE L37A	21,422	21,423
EPE L37V	21,450	21,449
EPE L37I	21,464	21,462
EAE	21,908	21,909

Table IV-3. Protein mass determination by ESI-MS. Proteins were analyzed by LC-MS with electrospray ionization. The deconvoluted masses were all within 0.02% of the masses calculated from the protein sequences.

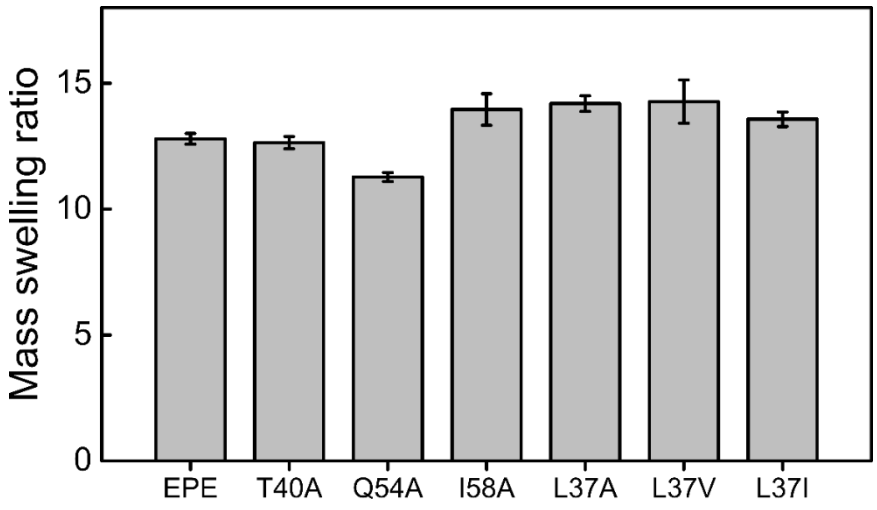

Figure IV-5. Equilibrium mass swelling ratio of hydrogels prepared from EPE and EPE variants. Hydrogels were swollen for 48 hr in PBS, pH 7.4 containing 0.02% (w/v) NaN_3 at ambient temperature.

4.3 Viscoelastic Behavior of EPE T40A, EPE Q54A, and EPE I58A Hydrogels

The rheological behavior of chemical-physical hydrogels prepared from EPE T40A, EPE Q54A, or EPE I58A was assessed by dynamic oscillatory rheology. In small amplitude oscillatory shear (SAOS) frequency sweep experiments (Figure IV-6 a), EPE T40A and EPE Q54A gels exhibit high frequency plateaus in *G'* that are similar in magnitude to the high frequency plateau observed with EPE gels. In these variants, however, the plateau behavior extends to lower frequencies than in EPE gels. Likewise, the maximum in *G"* also occurs at a lower frequency (0.003 rad s^{-1}) in EPE T40A gels. For hydrogels prepared from EPE Q54A, the maximum in *G"* was not observed in the experimental frequency range but likely occurs between 10^{-4} and 10^{-3} rad s^{-1}. In other words, the storage and loss modulus both appear to be shifted to lower frequencies compared to EPE. These observations are consistent with slower relaxation timescales for the coiled-coiled cross-linkers containing either the T40A mutation or the Q54A mutation. In hydrogels prepared from EPE I58A, the opposite behavior is observed. Both the transition zone between the plateaus in *G'* and the maximum in *G"* occur at higher values of ω, meaning that the relaxation of the physical cross-linking is faster in these materials. These experiments reveal a trend in the relaxation timescales of these materials (EPE Q54A > EPE T40A > EPE > EPE I58A) that is similar to the trend in the thermal stability measured by Gunaseker *et al* [28].

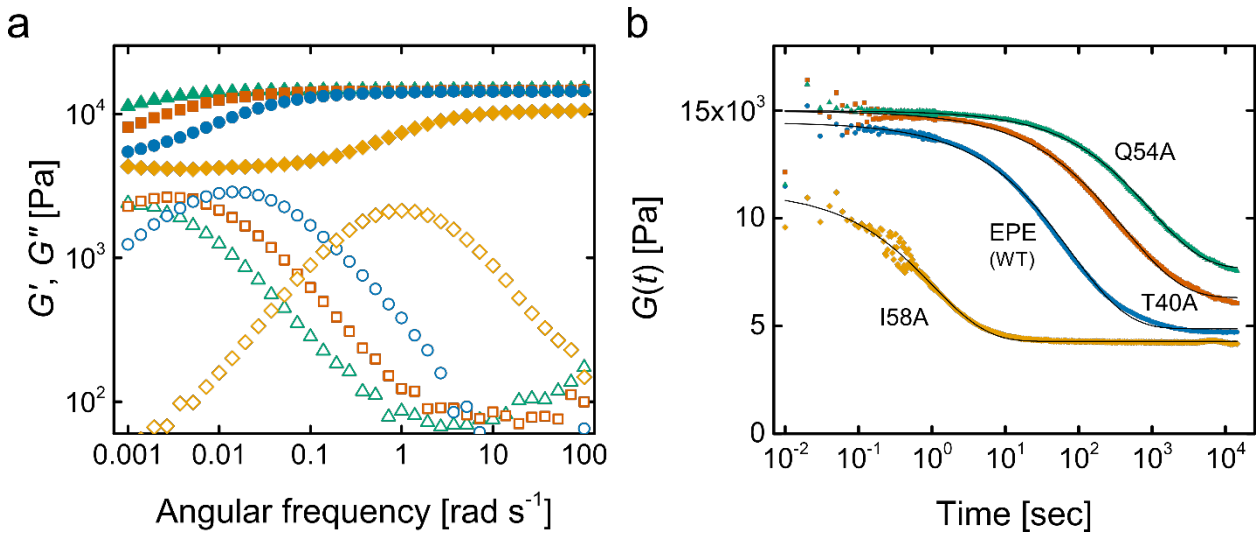

Figure IV-6. Rheology of EPE and variants EPE Q54A, EPE T40A, and EPE I58A. (**a**) Dynamic oscillatory frequency sweeps showing the storage modulus, (*G'*, filled symbols) and loss modulus (*G"*, open symbols) at 2% strain amplitude, 25 °C. In gels prepared from the EPE Q54A (triangles) and EPE T40A (squares) variants, the *G'* and *G"* curves are shifted to lower frequencies relative to EPE gels (circles). In gels prepared from the EPE I58A (diamonds) variant, the *G'* and *G"* curves are shifted to higher frequencies relative to EPE gels. (**b**) The same trend is observed in stress relaxation experiments in which gels were subjected to a 2% step strain at 25 °C. The characteristic relaxation times determined from the fitting the stretched exponential model (solid black lines) follow the trend $\tau_{Q54A} > \tau_{T40A} > \tau_{WT} > \tau_{I58A}$.

Because the dynamics of networks cross-linked by coiled-coil domains containing the T40A and Q54A mutations are too slow to observe the low frequency plateau behavior associated with the covalent network in the frequency sweep experiments, stress relaxation experiments were performed in which the gels were subjected to at a constant 2% strain for 4 hours (Figure IV-6 b). The relaxation function $G(t)$ was fit with the stretched exponential, or KWW, model previously used for physical protein hydrogels [19] and modified here with the parameter G_e to account for the presence of the permanent covalent network.

$$G(t) = G\exp\left(-\left(\frac{t}{\tau_{KWW}}\right)^{\beta}\right) + G_e \qquad \text{(Equation IV-1)}$$

The physical cross-linking is described by the parameter G as well as the relaxation timescale τ_{KWW} and the exponent β, which varies between 0 and 1. Calculation of a mean relaxation time, $\langle\tau\rangle$, for each material by Equation IV-2 confirmed the trend observed in the SAOS frequency sweeps.

$$\langle\tau\rangle = \frac{\tau_{KWW}}{\beta}\Gamma\left(\frac{1}{\beta}\right) \qquad \text{(Equation IV-2)}$$

($\Gamma\left(\frac{1}{\beta}\right)$ is the gamma function evaluated at β^{-1}.)

The mean relaxation time varied from approximately 1 second for EPE I58A gels to over 1500 seconds for EPE Q54A (Table IV-4). While this range is quite large considering the four materials differ by only a single amino acid side chain, the results are consistent with the strand exchange times measured for various coiled-coil systems. The more stable variants EPE Q54A and EPE T40A are slightly stiffer than EPE I58A and also slightly less swollen (Figure IV-5). Both observations can be explained by a greater fraction of folded P domains in the more stable variants, although differences in the amount of covalent cross-linking in each material arising from variations in the free thiol content or from the efficiency of the cross-linking reaction are also possible.

Protein	Mean Relaxation Time (s)
EPE L37A[a]	0.22 ± 0.13
EPE L37V	1.02 ± 0.14
EPE I58A	1.70 ± 0.15
EPE L37I	9.83 ± 1.19
EPE	134 ± 8
EPE T40A	762 ± 62
EPE Q54A	1608 ± 135

[a] EPE L37A was fit with a single exponential model

Table IV-4. **Characteristic relaxation times for EPE and the six single mutant variants.** The mean relaxation times were determined by fitting the stress relaxation data to the stretched exponential model in Eq. IV-1 and using the fitted parameters to evaluate Eq. IV-2.

The crystal structure of the P coiled-coil domain reported by Malashkevich *et al.* may provide some insight into the importance of the Thr40 and Gln54 positions [32]. The folded structure contains a pore along the entire coiled-coil axis. Although the buried residues are primarily hydrophobic, bound water molecules were observed near the hydroxyl side chain of Thr40 while a chloride ion is bound in an ion trap formed by the five Gln54 side chains (Figure IV-7). MacFarlane *et al*. suggested that water molecules in the hydrophobic pore allow the P domain to undergo dynamic opening or "breathing" motions in order to allow the entry of hydrophobic ligands such as all-*trans* retinol, vitamin D, and fatty acids [33-35]. In the native cartilage oligomeric matrix protein from which the P domain is derived, the coiled coil is stabilized by a C-terminal cysteine knot involving two cysteine residues from each chain [32]. The cysteine knot is not present in EPE or its variants as the cysteines were mutated to serine [27]. Therefore, the breathing motions that lead to channel opening in the knotted structure could lead to complete

dissociation of the physical cross-links in EPE hydrogels. The T40A and Q54A mutations may alter this process to produce less dynamic physical cross-linking, particularly if water or ion binding are altered in the mutant coils.

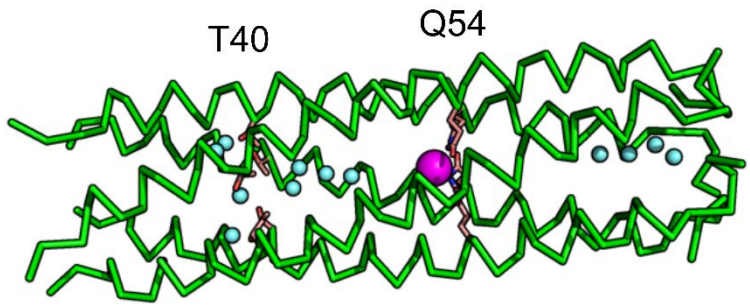

Figure IV-7. Structure of the P coiled coil pentamer. The five P strands are shown as green ribbons. Only the side chains of Thr40 and Gln54 are shown. Water molecules as depicted as light blue spheres, several of which are bound near Thr40. The chloride ion is depicted as a magenta sphere and is bound in the ion trap formed by side chains of the Gln54 residues. The structure was rendered in PyMol from PDB 1VDF in ref. [32].

4.4 Viscoelastic Behavior of EPE L37A, EPE L37V, and EPE L37I Hydrogels

Sequence variation in the coiled-coil domain was further explored using EPE variants containing point mutations at leucine 37. Mutation of this residue to alanine by Gunasekar *et al*. resulted in a decrease in the helicity of the P domain from 70% in the wild-type to 22% in the mutant [28]. In hydrogels prepared by cross-linking EPE L37A with PEG-4VS, *G'* is independent of the oscillation frequency below approximately 5 rad s^{-1} but increases with increasing frequency beyond this value (Figure IV-8 a). A high frequency plateau is not observed in the experimental frequency range, which extends to 100 rad s^{-1}. The increase in *G'* is also accompanied by a local maximum in *G"*. As with the EPE variant containing the I58A mutation, the shift of the *G'* and

G" curves to higher frequencies relative to EPE suggests that transient physical cross-linking is still present, but significantly more dynamic. The relaxation time of the EPE L37A network, which is estimated as 0.06 s from the frequency at which the maximum in *G"* occurs and 0.02 s from the stress relaxation experiment (Figure IV-8 b and Table IV-4), is approximately three orders of magnitude less than the relaxation time in the EPE network. This effect is similar to the difference in the strand exchange time measured for leucine zipper peptides when single leucine to alanine substitutions were made (~1800 s to ~1) [24].

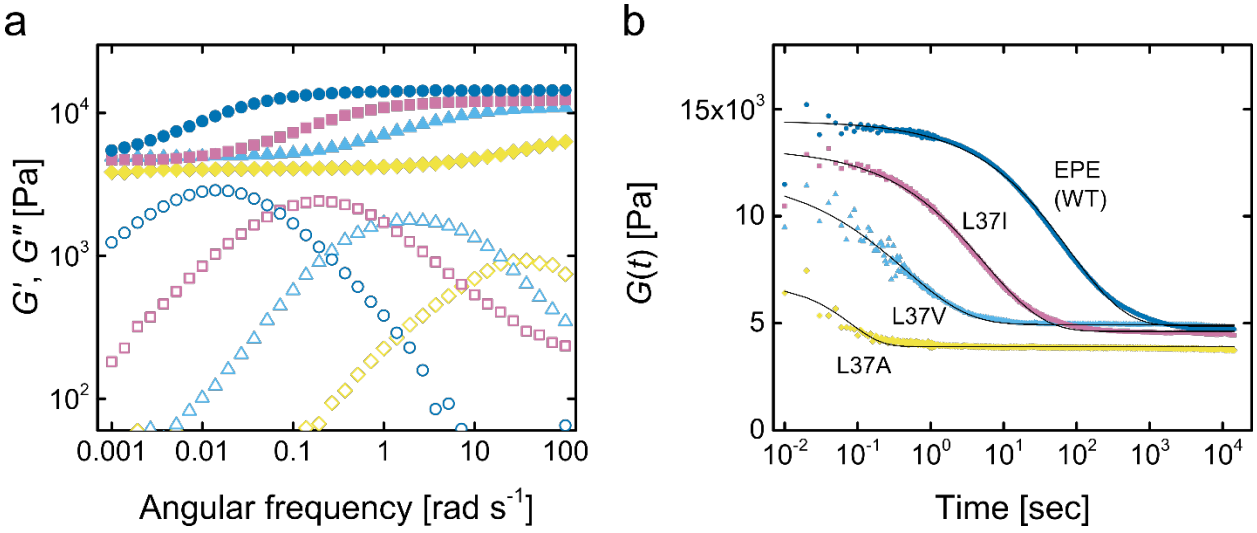

Figure IV-8. Rheology of EPE variants with point mutations at position 37 (EPE L37I, EPE L37V, and EPE L37A). (**a**) Dynamic oscillatory frequency sweeps showing the storage modulus, (*G'*, filled symbols) and loss modulus (*G"*, open symbols) at 2% strain amplitude, 25 °C. In gels prepared from the EPE L37I (squares), EPE L37V (triangles), and EPE L37A (diamonds) variants, the *G'* and *G"* curves are shifted to higher frequencies relative to EPE gels (circles). (**b**) The same trend is observed in stress relaxation experiments in which gels were subjected to a 2% step strain at 25 °C. The characteristic relaxation times were determined from the fitting the stretched exponential model for WT, L37I, and L37V (solid black lines). The relaxation function for EPE L37A was not well fit by the stretched exponential model, so the single exponential fit is shown instead. The trend in the characteristic relaxation time is $\tau_{WT} > \tau_{L37I} > \tau_{L37V} > \tau_{L37A}$.

The accessible surface area of the alanine side chain is approximately one-half that of the leucine side chain (67 $Å^2$ versus 137 $Å^2$) [36], and the loss of hydrophobic contacts at this position likely destabilizes the coiled-coil cross-linking and leads to faster network relaxation. Based on this hypothesis, EPE variants containing either the L37V or L37I mutation were also prepared. The accessible surface area of valine (117 $Å^2$) is between leucine and alanine. Isoleucine has an accessible surface area (140 $Å^2$) that is similar to leucine but its carbon atoms are arranged in a different branching structure [36]. In both EPE L37V and EPE L37I gels, the curves for *G'* and *G"* are shifted to higher frequencies relative to EPE gels, but the shift is not as large as observed in EPE L37A gels (Figure IV-8 a). The characteristic relaxation timescales for EPE L37V and EPE L37I networks are on the order of 1 s and 10 s, respectively (Figure IV-8 b and Table IV-4). These results establish a trend in the network relaxation time for EPE variants that differ by the identity of the side chain at position 37 (EPE L37 > EPE L37I > EPE L37V > EPE L37A), and demonstrate how rational design of the coiled-coil cross-linking domains can be used to program the relaxation behavior of chemical-physical hydrogels.

4.5 Disruption of Physical Cross-linking Under Denaturing Conditions

When hydrogels prepared from EPE and its variants are swollen in buffer containing 6 M guanidinium chloride as protein denaturant, the physical cross-links between the midblock domains are disrupted but the gels remain intact due to the covalent cross-links. The storage modulus of gels swollen in denaturing buffers is nearly independent of the oscillation frequency (Figure IV-9 a). This behavior is characteristic of covalent elastic networks. Hydrogels swollen in PBS with 6 M guanidinium chloride are also more swollen than hydrogels swollen in PBS (Figure IV-9 b), which is likely due to a combination of the loss of physical cross-linking and a more

extended conformation of protein chains. Because the association between the coils is absent under denaturing conditions, the proteins are nearly indistinguishable and the sequence variation no longer determines the macroscopic properties of the hydrogel.

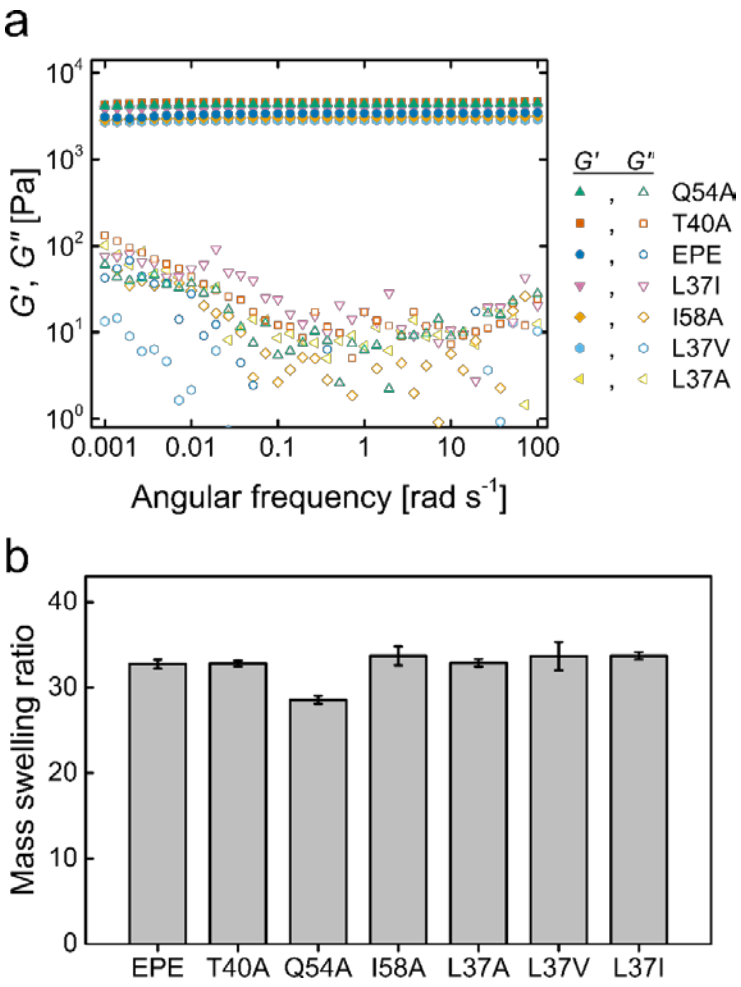

Figure IV-9. Rheology and swelling of EPE and EPE variants under denaturing conditions. (**a**) Hydrogels were swollen in PBS, pH 7.4 with 6 M guanidinium chloride. In frequency sweeps at 2% strain amplitude, 25 °C, the storage moduli are nearly independent of the oscillation frequency and the loss moduli do not exhibit local maxima. The rise in *G"* at low frequency (0.001-0.01 rad s^{-1}) may be due to slip. (**b**) Hydrogels swollen in PBS containing 6 M guanidinium chloride exhibit similar mass swelling ratios, with the exception of EPE Q54A, which is slightly less swollen than the other gels.

4.6 Chemical-Physical Protein Hydrogels with Multiple Relaxation Timescales

The approach developed here can be extended to design materials with more complex relaxation dynamics. In Chapter 3, hydrogels were prepared by cross-linking mixtures of EPE and a second artificial protein, ERE, that contains a non-associative midblock R in place of P. In these materials the amount of stress relaxation decreased as the amount of ERE was increased relative to EPE. The same approach was used to design a material that would exhibit two distinct relaxation timescales that are encoded by orthogonal coiled-coil cross-linkers. Shen *et al.* developed physical hydrogels from telechelic artificial proteins with two different helical endblocks that do not associate with one another [27]. The N-terminal block was the P domain used in this study, and the C-terminal block was a leucine zipper domain A that associates to form homotetrameric coiled coils (Figure IV-10 a). This topology successfully decreased the erosion rate by suppressing the formation of loops, but the individual relaxation times of the two coiled coils were not observed. One explanation is that the relaxation timescales for P coiled coils and A coiled coils in these gels are too similar to observe in SAOS frequency sweep experiments. More likely, however, is that once the faster relaxing domain dissociates, the proteins are no longer connected to the network and behave instead as 8- or 10-arm star polymers until the second relaxation time is reached.

It should be possible to observe two distinct relaxation timescales in chemical-physical networks by cross-linking a mixture of proteins that meet two criteria. First, the proteins must have orthogonal physical cross-linking domains, and second, the relaxation timescales for these domains must be sufficiently separated. In a SAOS frequency sweep experiment, these materials would be expected to exhibit three plateaus in the storage modulus and two local maxima in the loss modulus. The first plateau would correspond to high frequencies or timescales that are shorter than the dissociation times of both physical cross-linkers. A second plateau at intermediate

frequencies or timescales would occur once the chain segments cross-linked by the fast dissociating cross-linker relax. Finally, the low frequency plateau would correspond to the stress stored between the chemical cross-links at timescales greater than the dissociation times of both physical cross-linkers.

To construct such a network, an artificial protein EAE was designed in which the P domain was replaced with the A leucince zipper. Hydrogels prepared from EAE exhibit relaxation behavior (Figure IV-10 c and d) that is similar to one of more stable EPE variants, EPE Q54A. The mean relaxation time for the EAE network is approximately 1200 s, consistent with measurements of the strand exchange time for A measured by Shen *et al*. [18]. This suggests that physical cross-links formed by the A domain have a longer average lifetime than physical cross-links formed by the P domain. To enhance this difference and meet the two criteria for observing multiple relaxation timescales, EAE was paired with EPE L37V within the same covalent network (Figure IV-10 b, iv). The single leucine to valine point mutation in P is not expected to affect its orthogonality with A, and the relaxation times of the individual EAE and EPE L37V networks are separated by approximately three orders of magnitude. Hydrogels were prepared by cross-linking a mixture containing equal amounts of EAE and EPE L37V under denaturing conditions followed by swelling to equilibrium in PBS, pH 7.4. In both SAOS frequency sweep experiments and stress relaxation experiments (Figure IV-10 c and d and Figure IV-12 a), two relaxation timescales are present that correspond to the relaxation timescales observed in EPE L37V and EAE single protein networks. These relaxations represent the transition from a high frequency/short time plateau to an intermediate frequency/intermediate time plateau, and from the intermediate frequency/intermediate time plateau to the low frequency/long time plateau, respectively. As expected, the frequencies at which the transitions between these plateaus occur correspond to the

frequencies at which local maxima in *G"* occur. Notably, a local minimum in *G"* in the EPE L37V:EAE gel occurs near the intersection of the *G"* curves of the individual EPE L37V and EAE gels.

The stress relaxation function, $G(t)$, was fit by a double stretched exponential model,

$$G(t) = G_1 \exp\left(-\left(\frac{t}{\tau_{L37V}}\right)^{\beta_{L37V}}\right) + G_2 \exp\left(-\left(\frac{t}{\tau_{EAE}}\right)^{\beta_{EAE}}\right) + G_e \qquad \text{(Equation IV-3)}$$

which contains two exponential terms identical to those observed in Eq. IV-1 and an equilibrium modulus G_e representing the chemical cross-linking. To fit the experimental $G(t)$ data for the EPE L37V:EAE network, the characteristic relaxation timescales (τ_{L37V} and τ_{EAE}) and the stretching exponents (β_{L37V} and β_{EAE}) were fixed at the values determined from the EPE L37V and EAE single protein networks, leaving G_1, G_2, and G_e as adjustable parameters. This assumes that the exchange rate of P L37V and A coiled coils in the EPE L37V:EAE mixed protein network is the same as the exchange rate in the single protein networks, which appears to be the case based on the frequency sweep experiments (Figure IV-10 e and d). As shown in Figure IV-12 a, the double stretched exponential model provides a good fit of the experimental data.

The same material design was employed to prepare chemical-physical hydrogel networks from a mixture of proteins that are not expected to exhibit orthogonal physical cross-linking (Figure IV-10 b, v). While the relaxation timescales in single protein networks prepared from EPE L37V and EPE Q54A are separated by several orders of magnitude, mixed species physical cross-linkers are expected to form in a network prepared from an equimolar mixture of the two proteins. In this network, six combinations of strands are possible assuming pentameric association of the midblock domains. While these six combinations are expected to have six different relaxation

times that lie between the fastest combination (all strands from EPE L37V) and the slowest combination (all strands from EPE Q54A), the equilibrium distribution of these combinations is not known *a priori*. Frequency sweep and stress relaxation experiments of EPE L37V:EPE Q54A gels reveal a much broader relaxation than was observed with EAE:EPE L37V gels, consistent with several relaxation timescales (Figure IV-10 e and f and Figure IV-12 b). Unlike the EPE L37V:EAE network, the EPE L37V:EPE Q54A network is not well fit by the double stretched exponential model, suggesting that several relaxation timescales are present and that additional terms are needed to adequately model the experimental data.

It is also noted that a decrease in *G'* and an increase in *G"* are observed near an angular frequency of 0.001 rad s^{-1} in EPE Q54A:EPE L37V gels. These features occur near the characteristic relaxation timescale expected for P Q54A physical cross-links. This suggests that a significant number of homotypic P Q54A cross-links are present in this gel, which is not surprising given that EPE Q54A is expected to have a higher fraction of folded midblock domains than EPE L37V. These experiments demonstrate that multiple relaxation timescales can be programmed in chemical-physical protein networks, and that the use of orthogonal coiled-coil domains as physical cross-linkers allows two distinct relaxation timescales to be observed.

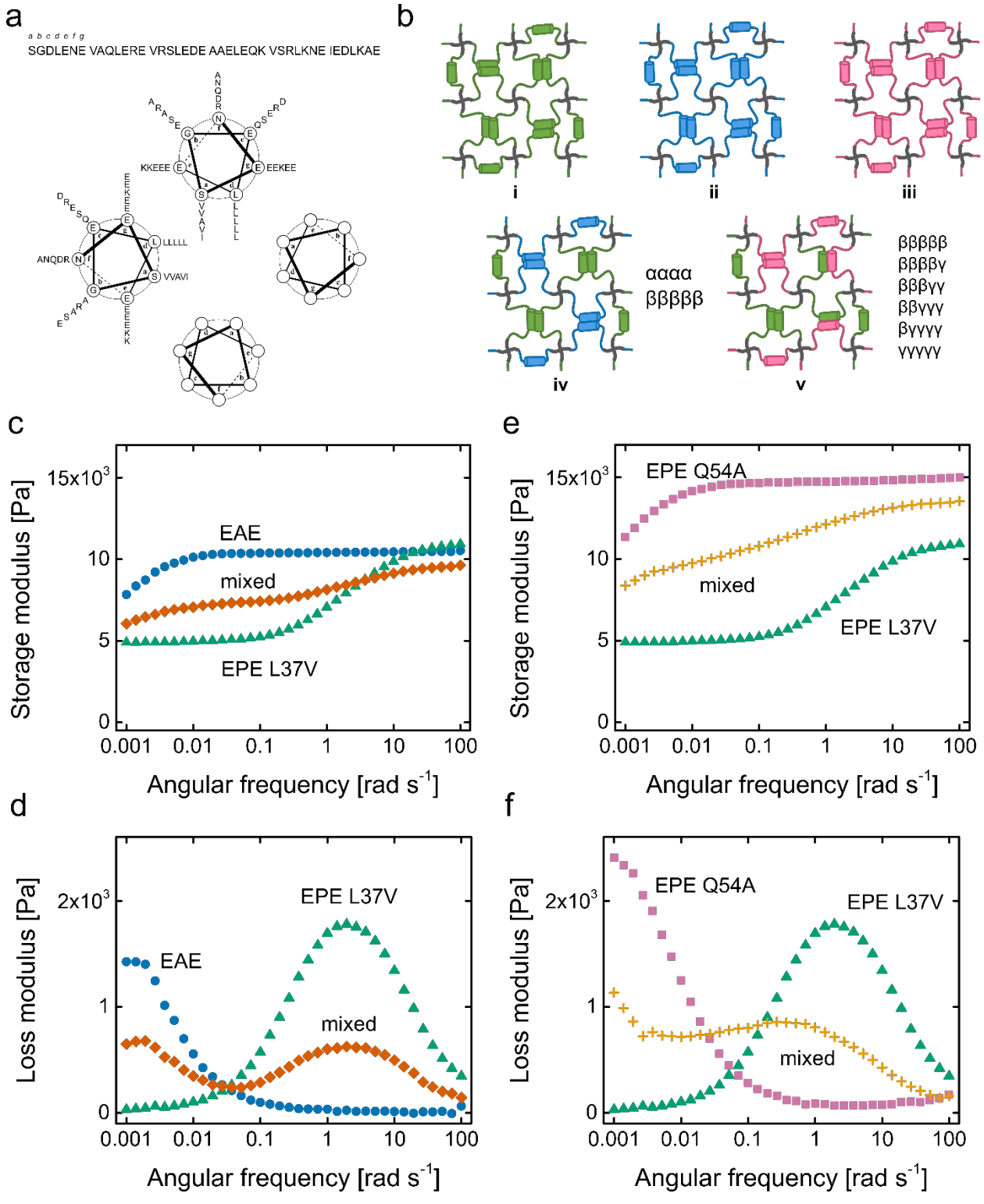
a
b
i
ii
iii
iv
v
αααα
ββββββ
βββββ
ββββγ
βββγγ
ββγγγ
βγγγγ
γγγγγ
c
e
d
f
Storage modulus [Pa]
Loss modulus [Pa]
Angular frequency [rad s-1]
EAE
mixed
EPE L37V
EPE Q54A
15x10^3
2x10^3
0.001
0.01
0.1
1
10
100

Figure IV-10 (previous page). Chemical-physical protein networks with multiple relaxation timescales. (**a**) Sequence of the A leucine zipper protein domain and helical wheel representation of a parallel A homotetramer (antiparallel orientations are also possible). (**b**) Schematic representation of chemical-physical protein networks prepared from a single artificial protein (i. EPE L37V, ii. EAE, iii. EPE Q54A) or two artificial proteins with different associative midblocks (iv. EPE L37V:EAE, v. EPE L37V:EPE Q54A). In network iv, the coiled coils are orthogonal to one another and two types of physical cross-links are present, tetramers composed of α and pentamers composed of β. In network v, mixed species cross-linking is possible, leading to six different pentamers of β and γ. (**c**) Storage modulus and (**d**) loss modulus of EAE gels (circles), EPE L37V gels (triangles), and gels prepared by cross-linking an equimolar mixture of EAE and EPE L37V (diamonds). (**e**) Storage modulus and (**f**) loss modulus of EPE Q54A gels (squares), EPE L37V gels (up triangles), and gels prepared by cross-linking an equimolar mixture of EPE Q54A and EPE L37V (crosses).

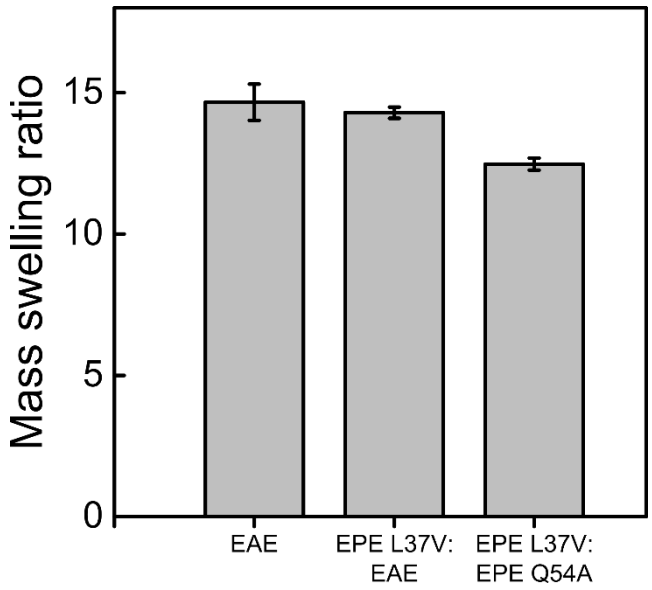

Figure IV-11. Equilibrium mass swelling ratio of EAE gels and mixed protein networks. The mass swelling ratios of the EAE single protein network and EPE L37V:EAE and EPE L37V:EPE Q54A mixed protein networks swollen in PBS, pH 7.4, room temperature.

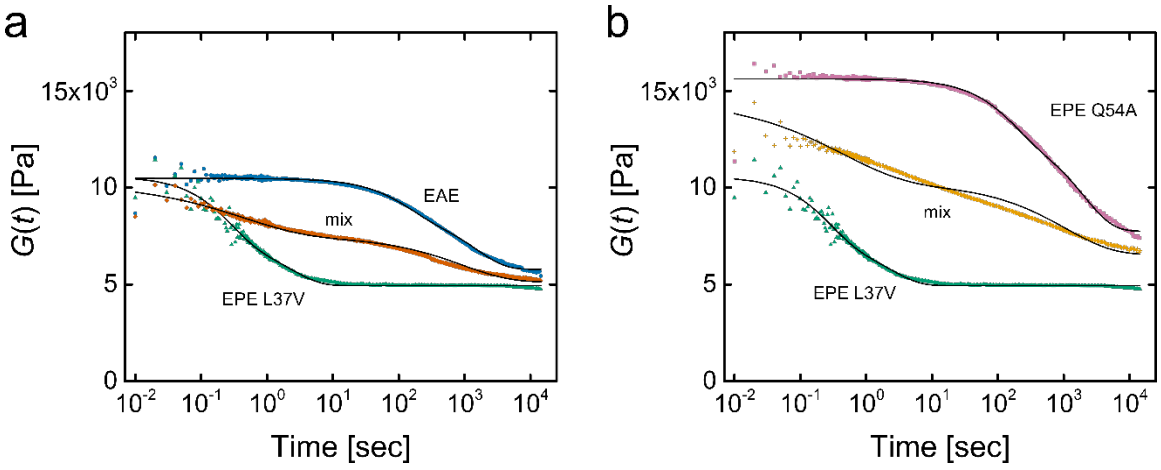

Figure IV-12. Stress relaxation of EPE L37V:EAE and EPE L37V:EPE Q54A mixed composition gels. (**a**) The relaxation function $G(t)$ is plotted for single protein networks EPE L37V and EAE and the mixed protein network EPE L37V:EAE. (**b**) $G(t)$ was also plotted for the EPE Q54A single protein network and the EPE L37V:EPE Q54A mixed protein network. The solid lines are fits of the stretched exponential model (Eq. IV-1) for single protein networks and a double stretched exponential model (Eq. IV-3) for mixed protein networks. The double stretched exponential model is well fit by the EPE L37V:EAE network, which contains an orthogonal pair of physical cross-linking domains, but not EPE L37V:EPE Q54A.

5. Conclusions

The sequence-structure-function paradigm has guided our understanding of how protein structure and function are encoded in an amino acid sequence as well as efforts to predict protein function and to design new proteins. The same paradigm can be applied to designing sequences of artificial proteins in order to encode the macroscopic behavior of protein-based materials. Here, sequence variation within the physical cross-linking domain of an artificial protein was used to engineer the dynamic behavior of protein networks. Single point mutations within a helical domain that forms coiled-coil cross-links resulted in variations of the characteristic relaxation timescale over five orders of magnitude. Networks prepared from mixtures of artificial proteins containing two different physical cross-linking domains exhibited more complex dynamic behavior and are capable of stress relaxation and energy dissipation on multiple timescales. Dynamic materials might play important roles in regulating or directing cell and tissue behavior [6-8, 37-39]. They also exhibit enhancements in toughness and extensibility that is related to their ability to dissipate energy when deformed [40]. The ability to program relaxation behavior in networks consisting of a single artificial protein or multiple artificial proteins will have important applications in these areas and others.

6. References

[1] H.-B. Wang, M. Dembo, Y.-L. Wang *Am. J. Physiol. - Cell Ph.* **2000** *279*, C1345-C1350.

[2] R.J. Pelham, Y.-l. Wang *Proc. Natl. Acad. Sci. USA* **1997** *94*, 13661-13665.

[3] A.J. Engler, S. Sen, H.L. Sweeney, D.E. Discher *Cell* **2006** *126*, 677-689.

[4] S.S. Soofi, J.A. Last, S.J. Liliensiek, P.F. Nealey, and C.J. Murphy *J. Struct. Biol.* **2009** *167*, 216-219.

[5] M.F. Ashby, *Materials Selection in Mechanical Design* Elsevier Butterworth-Heinemann, Amsterdam **2005**.

[6] A.R. Cameron, J.E. Frith, J.J. Cooper-White *Biomaterials* **2011** *32*, 5979-5993.

[7] O. Chaudhuri, L. Gu, M. Darnell, D. Klumpers, S.A. Bencherif, J.C. Weaver, N. Huebsch, and D.J. Mooney *Nat. Commun.* **2015** *6*.

[8] M. Murrell, R. Kamm, P. Matsudaira *Biophys J.* **2011** *101*, 297-306.

[9] T. Annable, R. Buscall, R. Ettelaie, D. Whittlestone *J. Rheol.* **1993** *37*, 695-726.

[10] R.P. Sijbesma, F.H. Beijer, L. Brunsveld, B.J.B. Folmer, J.H.K.K. Hirschberg, R.F.M. Lange, J.K.L. Lowe, and E.W. Meijer *Science* **1997** *278*, 1601-1604.

[11] D.E. Fullenkamp, L. He, D.G. Barrett, W.R. Burghardt, and P.B. Messersmith *Macromolecules* **2013** *46*, 1167-1174.

[12] M.S. Menyo, C.J. Hawker, J.H. Waite *ACS Macro Lett.* **2015** *4*, 1200-1204.

[13] S.C. Grindy, R. Learsch, D. Mozhdehi, J. Cheng, D.G. Barrett, Z. Guan, P.B. Messersmith, and N. Holten-Andersen *Nat. Mater.* **2015** *14*, 1210-1216.

[14] D.M. Loveless, S.L. Jeon, S.L. Craig *Macromolecules* **2005** *38*, 10171-10177.

[15] D.D. McKinnon, D.W. Domaille, J.N. Cha, K.S. Anseth *Adv. Mater.* **2014** *26*, 865-872.

[16] H. Ying, Y. Zhang, J. Cheng *Nat. Commun.* **2014** *5*.

[17] W.A. Petka, J.L. Harden, K.P. McGrath, D. Wirtz, and D.A. Tirrell *Science* **1998** *281*, 389-392.

[18] W. Shen, J.A. Kornfield, D.A. Tirrell *Macromolecules* **2007** *40*, 689-692.

[19] S. Tang, M. Wang, B.D. Olsen *J. Am. Chem. Soc.* **2015** *137*, 3946-3957.

[20] C. Xu, V. Breedveld, J. Kopeček *Biomacromolecules* **2005** *6*, 1739-1749.

[21] P.J. Skrzeszewska, F.A. de Wolf, M.W.T. Werten, A.P.H.A. Moers, M.A. Cohen Stuart, and J. van der Gucht *Soft Matter* **2009** *5*, 2057-2062.

[22] S. Ozeki, T. Kato, M.E. Holtzer, A. Holtzer *Biopolymers* **1991** *31*, 957-966.

[23] S.-Y. Park, C.M. Quezada, A.M. Bilwes, B.R. Crane *Biochemistry* **2004** *43*, 2228-2240.

[24] H. Wendt, C. Berger, A. Baici, R.M. Thomas, and H.R. Bosshard *Biochemistry* **1995** *34*, 4097-4107.

[25] L.R. Patel, T. Curran, T.K. Kerppola *Proc. Natl. Acad. Sci. USA* **1994** *91*, 7360-7364.

[26] V.P. Efimov, A. Lustig, J. Engel *FEBS Lett.* **1994** *341*, 54-58.

[27] W. Shen, K. Zhang, J.A. Kornfield, D.A. Tirrell *Nat. Mater.* **2006** *5*, 153-158.

[28] S.K. Gunasekar, M. Asnani, C. Limbad, J.S. Haghpanah, W. Hom, H. Barra, S. Nanda, M. Lu, and J.K. Montclare *Biochemistry* **2009** *48*, 8559-8567.

[29] A.V. Terskikh, S.A. Potekhin, T.N. Melnik, A.V. Kajava *Lett. Pept. Sci.* **1997** *4*, 297-304.

[30] Y. Guo, R.A. Kammerer, J. Engel *Biophys. Chem.* **2000** *85*, 179-186.

[31] G.L. Ellman *Arch. Biochem. Biophys.* **1959** *82*, 70-77.

[32] V.N. Malashkevich, R.A. Kammerer, V.P. Efimov, T. Schulthess, and J. Engel *Science* **1996** *274*, 761-765.

[33] Y. Guo, D. Bozic, V.N. Malashkevich, R.A. Kammerer, T. Schulthess, and J. Engel *EMBO J.* **1998** *17*, 5265-5272.

[34] A.A. MacFarlane, G. Orriss, N. Okun, M. Meier, T. Klonisch, M. Khajehpour, and J. Stetefeld *PLOS One* **2012** *7*, e48130.

[35] S. Özbek, J. Engel, J. Stetefeld *EMBO J.* **2002** *21*, 5960-5968.

[36] S. Miller, J. Janin, A.M. Lesk, C. Chothia *J. Mol. Biol.* **1987** *196*, 641-656.

[37] Y. Liu, B. Liu, J.J. Riesberg, W. Shen *Macromol. Biosci.* **2011** *11*, 1325-1330.

[38] D.D. McKinnon, D.W. Domaille, T.E. Brown, K.A. Kyburz, E. Kiyotake, J.N. Cha, and K.S. Anseth *Soft Matter* **2014** *10*, 9230-9236.

[39] H. Wang, S.C. Heilshorn *Adv. Mater.* **2015** *27*, 3717-3736.

[40] X. Zhao *Soft Matter* **2014** *10*, 672-687.

Chapter V

CONTROL OF HYDROGEL VISCOELASTICITY BY SMALL MOLECULE PROTEIN LIGANDS

1. Abstract

The transient association of physical cross-linking domains such as coiled coils in protein hydrogels results in a viscoelastic response to applied stresses. In this chapter, the timescale for the viscoelastic stress relaxation in chemical-physical protein hydrogels was modulated by the addition of small, hydrophobic molecules including vitamin D3 and medium- and long-chain fatty acids. Addition of fatty acids of varying chain lengths increased the characteristic relaxation time of the protein network by 10- to 1000-fold. The relationship between the length of the fatty acid chain and the network relaxation time was shown to be biphasic or bell-shaped, with the 12-carbon ligand lauric acid having the largest effect. The proposed mechanism for the increase in the relaxation time involves binding of the ligands within the hydrophobic pore or channel created by a coiled-coil physical cross-link. Binding of hydrophobic ligands is known to stabilize coiled coils, which would increase the average lifetime of the physical cross-links and result in a slower network relaxation. Exploiting natural and designed protein-ligand interactions represents a new approach to developing hydrogel “formulations” in which the viscoelastic properties of the material can be engineered to meet specific design criteria.

2. Introduction

Protein hydrogels can be regulated by external stimuli including temperature, pH, and ionic strength. External stimuli are often used to trigger a gel-sol transition by causing protein domains to fold or unfold, or by promoting the assembly or disassembly of cross-links between protein chains. This behavior is exploited for the encapsulation and release of cells and biomolecules. Examples include temperature- and pH-induced unfolding of coiled-coiled cross-linkers [1] and temperature-induced aggregation of elastin-like polypeptide domains [2]. External stimuli can also have more subtle effects on network properties such as viscoelastic behavior. In physical gels cross-linked by leucine zipper coiled coils, viscoelastic behavior arises from the transient association of the coiled-coil network junctions. By varying the pH over a narrow range from 7-8, the characteristic relaxation time of the network could be tuned from approximately 100 s to 1000 s [3]. This pH sensitivity arises from changes to the protonation state of glutamic acids at the *e* and *g* positions of the helical heptad repeat, which influences that rate of strand exchange between coils. The relaxation dynamics of a protein hydrogel containing nucleoporin-like polypeptide (NLP) repeats were also tunable by an external stimulus, specifically the addition of 1,6-hexanediol, which disrupts the association of Phe-Gly dipeptides in the NLP domains [4]. Developing new strategies for regulating the viscoelastic behavior of protein hydrogels has important implications for engineering tough elastic materials, tuning the material erosion rate, and controlling the behavior of cells cultured on or within the material.

Protein binding to ions, metals, and organic ligands is crucial for a variety of functions including catalysis, signaling, regulation of protein function, storage, and transport. Several hydrogel designs have exploited these interactions to regulate material properties. Among the most common are hydrogels that respond to environmental calcium ions behavior or cross-linking.

Calcium sensitivity in these materials is mediated by the reversible folding or conformational changes of *β*-roll domains [5, 6] and calmodulin domains [7, 8], respectively. Other protein-ligand interactions that have been exploited in hydrogel networks include the enzyme-substrate binding exhibited by a polymer-grafted adenylate kinase and ATP [9], antibody-antigen binding [10], and binding of a small molecule inhibitor of the *Escherichia coli* DNA gyrase enzyme [11].

The N-terminal fragment (residues 20-83) of the rat cartilage oligomeric matrix protein (COMP) forms a homopentameric coiled coil that has been used extensively to cross-link physical protein hydrogels [12, 13]. In the crystal structure of the pentameric coiled coil [14], the pore or channel is lined primarily by hydrophobic residues with two exceptions: glutamine at position 54 and threonine at position 40. The amide side chains of Gln54 form a hydrogen-bonded ring that binds a chloride ion in the crystal structure. The channel is also occupied by several water molecules, particularly near Thr40. Due to the apolar nature of the other side chains buried within the channel, it was hypothesized that small hydrophobic molecules, rather than water, would bind preferentially and that COMP might play some role in the storage of these molecules *in vivo*. Subsequently, crystal structures were obtained of the COMP coiled coil in complex with several small hydrophobic molecules including vitamin D3 [15], all-*trans*-retinol [16], and several long-chain fatty acids (myristic acid, palmitic acid, stearic acid, and oleic acid) [17]. In the presence of vitamin D3, the folded coiled-coil structure displays a modest increase in thermal stability; a shift of +8 °C in the melting temperature was measured by circular dichroism spectroscopy [16]. Fluorescence spectroscopy studies have also indicated that all-*trans*-retinol and long-chain fatty acids bind within the COMP coiled coil, with dissociation constants varying between 0.4-0.9 μM [16, 17].

In Chapter 3, chemical-physical protein hydrogels were described consisting of a triblock artificial protein (EPE) end-linked with a tetrafunctional cross-linker to form a covalent network. The midblock sequence of EPE contains the COMP coiled-coil domain (denoted P), which forms transient noncovalent cross-links within the covalent network. In Chapter 4, several single mutant variants of the P domain were described with respect to their effects on the dynamic properties of protein hydrogels. Networks prepared from EPE variants containing the T40A or Q54A mutation in P exhibited longer characteristic relaxation times than networks prepared from proteins containing the wild-type P domain. This was attributed to an increase in the lifetime of the coiled-coil physical cross-links, and was consistent with the increased thermal stability of these mutant P domains as reported by Gunasekar *et al*. [18]. Given that the binding of small hydrophobic molecules within the channel or pore of P also results in increased thermal stability of the coiled-coil structure, it was reasoned that these ligands might likewise affect the relaxation behavior of protein networks. The data presented in this chapter represent preliminary experiments assessing the effects of vitamin D3 on chemical-physical hydrogels prepared from EPE as well as the effects of various fatty acids containing six to eighteen carbon atoms on chemical-physical hydrogels prepared from EPE L37V.

3. Materials and Methods

3.1 Small Molecule Ligands

Lauric (dodecanoic) acid, myristic (tetradecanoic) acid, palmitic (hexadecanoic) acid, and stearic (octadecanoic) acid were obtained from Fluka. Caproic (hexanoic) acid, capryilic (octanoic) acid, capric (decanoic) acid, and vitamin D3 (cholecalciferol) were obtained from Sigma.

3.2 Protein Synthesis and Characterization

The expression and purification of EPE L37V were performed as described in Chapter 4 and Appendix B. Following reduction with tris(hydroxypropyl) phosphine, the protein solution was desalted with several PD10 columns (GE Healthcare Life Sciences), lyophilized, and stored under argon at -80 °C. The thiol content and protein oligomerization state were characterized by Ellman's assay and non-reducing SDS-PAGE.

3.3 Hydrogel Swelling with Small Molecule Ligands

Hydrogel cross-linking was also performed as described in Chapter 4 and Appendix B. A single large hydrogel was formed by cross-linking 1 mL of 15 wt% EPE L37V with 231 μL of 15 wt% PEG-4VS between glass slides separated by a 1 mm spacer. The cross-linked EPE L37V hydrogel was swollen in decreasing concentrations of guanidinium chloride (6M, 3M, 2M, 1M) in PBS for 3 hr each. The gel was then swollen in PBS containing 0.02% (w/v) sodium azide. For rheological experiments, disks 8 mm in diameter were cut from the larger hydrogel and transferred to a 35 mm dish with 4 mL of PBS containing 0.02% (w/v) NaN_3. To these dishes, the hydrophobic ligands were added as solids (or as liquids in the case of caprylic acid and caproic acid) to a final concentration of approximately 5 mM. Most of the ligands were not soluble at this concentration, so solid particulates and oil-like liquid droplets remained suspended in the buffer. Addition of the fatty acid ligands required the pH of the buffer to be adjusted back to 7.4 with NaOH. EPE gels were prepared in a similar manner and swollen with vitamin D3 (100 μg mL^{-1}, diluted 1:100 from a 10 mg mL^{-1} stock solution in ethanol).

3.4 Rheological Characterization

The EPE L37V gels were swollen in buffer containing a fatty acid ligand for 3 days, rinsed briefly in PBS to remove solids sticking to the surface of the gel, and loaded on the ARES-RFS rheometer as described in the previous chapters and Appendix B. Strain sweep (at 10 rad s^{-1}), frequency sweep (at 1% strain amplitude), and stress relaxation (at 2% strain) experiments were performed at 25 °C. EPE gels were swollen for 7 days with vitamin D3 prior to rheological measurements.

4. Results and Discussion

4.1 Vitamin D3 Increases the Characteristic Relaxation Time of EPE Hydrogels

Motivated in part by the increase in the thermal stability reported by Özbek *et al*. for P coiled coils incubated with vitamin D3 [16], EPE hydrogels cross-linked by PEG-4VS were treated in a similar way. A large excess of vitamin D3 (100 μg mL^{-1}) (Figure V-1 a) was added to PBS buffer containing an EPE hydrogel. Vitamin D3 is not soluble at this concentration, but it was assumed that the solid vitamin D3 was in equilibrium with a saturated solution, and that the vitamin D3 in solution could diffuse into the hydrogel and bind within the coiled-coil cross-linkers (Figure V-1 b). Hydrogels treated in this way were characterized by dynamic oscillatory shear rheology (Figure V-1 c) and stress relaxation experiments (Figure V-1 d). In EPE gels swollen with vitamin D3 solutions, the storage and loss moduli (*G'* and *G"*) curves are shifted to lower frequencies relative to the EPE control without vitamin D3. Likewise, the relaxation function $G(t)$ measured in the stress relaxation experiment is shifted to longer times by two orders of magnitude. This behavior is similar to that of hydrogels prepared from the EPE variants EPE T40A and EPE Q54A described in Chapter 4. The mean relaxation times determined by fitting $G(t)$ with a stretched

exponential model (Equation IV-1 and IV-2) were 107 s for EPE and 10,700 s for EPE with vitamin D3. These results indicate that vitamin D3 binding slows the relaxation of the stress stored in chain segments cross-linked by transient coiled-coil cross-linkers and demonstrate that protein hydrogels can be formulated with small molecule ligands in order to tune their viscoelastic behavior.

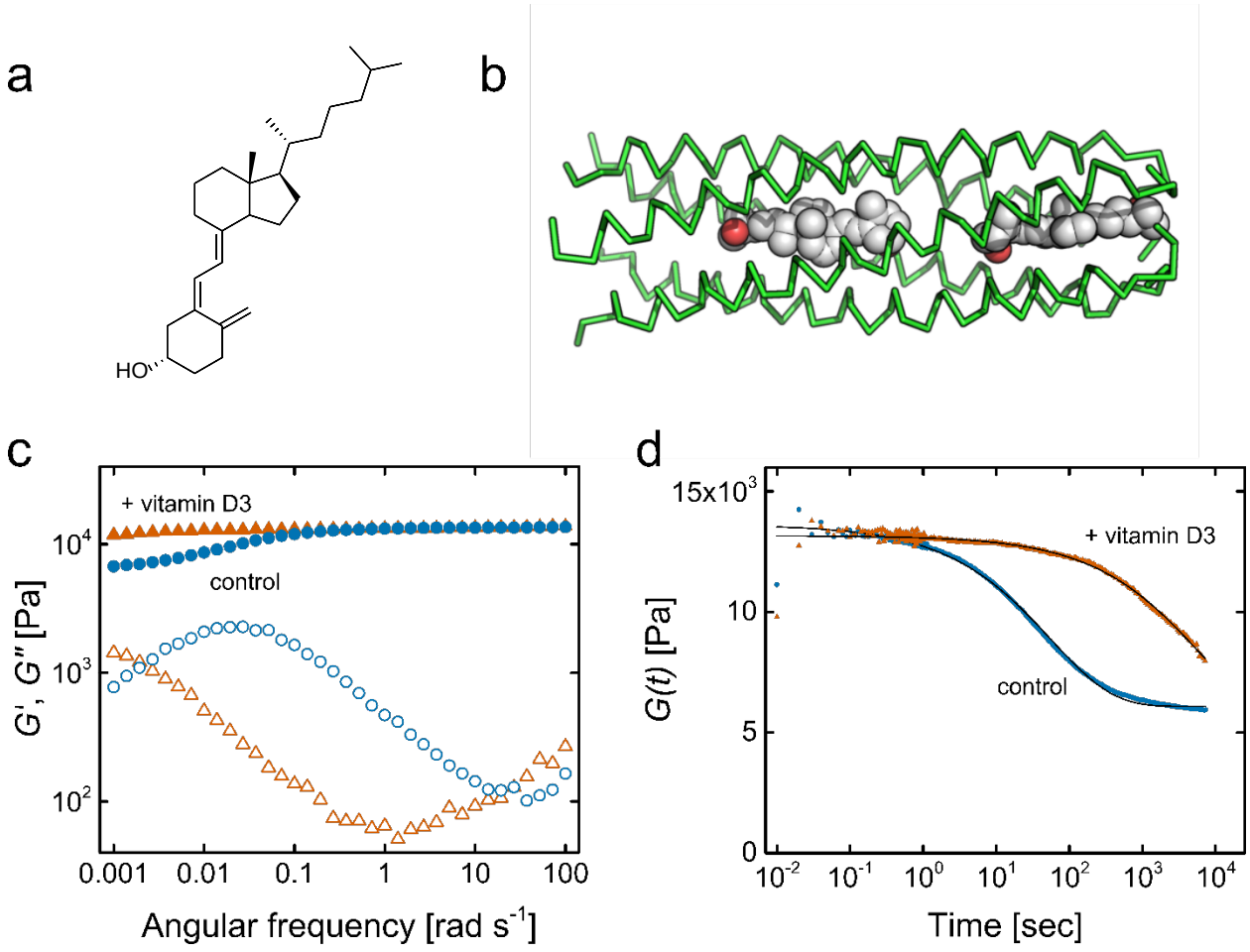

Figure V-1. Effect of vitamin D3 on the viscoelastic behavior of EPE hydrogels. (**a**) Chemical structure of vitamin D3. (**b**) Structure of P coiled coil (green ribbons) with two bound vitamin D3 molecules (white and red spheres). Rendered in PyMol from PDB 1MZ9. (**c**) Frequency sweeps (1% strain amplitude, 25 °C) showing the storage modulus (filled symbols) and loss modulus (open symbols) for EPE gels with vitamin D3 (triangles) and control gels (circles). (**d**) Stress relaxation experiments at 2% strain, 25 °C with and without vitamin D3.

4.2 Rheology of EPE L37V Hydrogels Swollen in the Presence of Medium- and Long-Chain Fatty Acids

Because other ligands were also anticipated to stabilize physical cross-links in protein hydrogels, subsequent experiments were performed with a faster relaxing EPE variant so that the effects of these ligands could be observed more easily. As shown in Chapter 4, hydrogels prepared by cross-linking an EPE variant containing a single leucine to valine point mutation at position 37 exhibit a faster relaxation time than hydrogels prepared from EPE. The relaxation times differ by approximately two orders of magnitude (ca. 1 s for EPE L37V versus ca. 100 s for EPE). In frequency sweep experiments with EPE L37V gels, the transition zone between the high and low frequency plateaus in *G'* and the local maximum in *G"* are centered at an angular frequency of approximately 3 rad s^{-1}. Below 0.1 rad s^{-1}, *G'* is nearly constant, indicating that the stress stored between chain segments cross-linked by P L37V has relaxed, and only chain segments between the covalent cross-links remain elastically effective. These observations suggest that the longer relaxation timescales anticipated for hydrogels treated with various hydrophobic ligands should be observable in the dynamic range accessible in frequency sweep experiments (0.001-100 rad s^{-1}). Furthermore, the crystal structures of P in complex with vitamin D3 [15], all-*trans*-retinol [16], and myristic acid, palmitic acid, and stearic acid [17] indicate that the side chain of leucine 37 does not make direct contact with these ligands, with the possible exception of the longest ligand, stearic acid.

The straight chain fatty acids are an attractive set of ligands for engineering the viscoelastic behavior of chemical-physical hydrogels cross-linked by P coiled coils. They are non-toxic and readily available in many different chain lengths. It was anticipated that systematic variation of the fatty acid chain length would be a useful way to investigate the effects of hydrophobic ligands on

EPE L37V hydrogels. While only the long-chain fatty acids (14 to 20 carbon atoms) have been reported previously to bind within P coiled coils, medium-chain fatty acids (6 to 12 carbon atoms) were also considered here. The fatty acids used in this chapter are summarized in Table V-1, which includes the common name, systematic name, structure, and log P value (water-octanol partition coefficient) [19-25].

Common Name/ Systematic Name	**Length (# of carbon atoms)**	**Structure**	**Log P**
Caproic acid/ Hexanoic acid	6	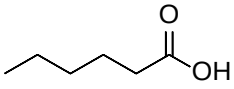	1.92
Caprylic acid/ Octanoic acid	8	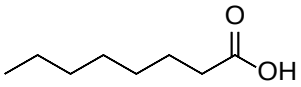	3.05
Capric acid/ Decanoic acid	10	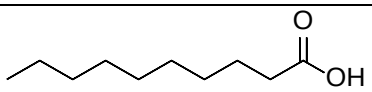	4.09
Lauric acid/ Dodecanoic acid	12	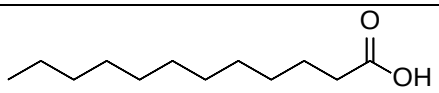	4.60
Myristic acid/ Tetradecanoic acid	14	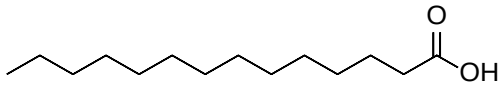	6.11
Palmitic acid/ Hexadecanoic acid	16	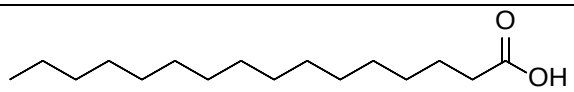	7.17
Stearic acid/ Octadecanoic acid	18	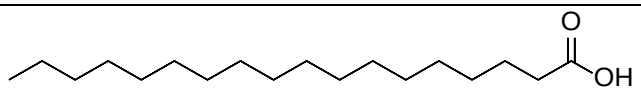	8.23

Table V-1. Medium- and long-chain fatty acids. The values of log P are from the PubChem Compound Database in refs. [19-25].

EPE L37V hydrogels were swollen in PBS containing 5 mM of the different fatty acids. Similar to vitamin D3, most ligands were not soluble at this concentration and instead formed a suspension of solid particles or oil-like droplets dispersed in the buffer. Binding within the coiled-coil cross-links therefore required a partitioning from the solid or oil phase into solution, diffusion into the hydrogel, and partitioning into the coiled coil. The viscoelastic behavior of the EPE L37V hydrogels was assessed by dynamic oscillatory shear rheology and stress relaxation experiments after 3 days of swelling in the presence of a particular ligand. The frequency sweep experiments are shown in Figure V-2 and the stress relaxation experiments are shown in Figure V-3. For clarity, the data are divided into two plots, one showing fatty acids 6 to 12 carbon atoms in length and the other showing fatty acids 12 to 18 carbon atoms in length. The stress relaxation function, $G(t)$, was fit with a stretched exponential model to determine a mean relaxation time, $\langle\tau\rangle$, as described in Chapters 3 and 4.

A clear trend emerged in the relaxation behavior of EPE L37V hydrogels swollen with fatty acids of different chain lengths. Lauric acid, which is 12 carbon atoms long, had the largest effect on the network relaxation time, increasing τ more than 1000-fold compared to the control EPE L37V gel without fatty acid. When the fatty acid length was increased or decreased by 2 carbon atoms (myristic acid and capric acid, respectively), the effect was smaller than lauric acid but both gels still exhibited relaxation times 100-fold greater than the control gel. The effect was smaller yet for the 8-carbon and 16-carbon fatty acids (caprylic acid and palmitic acid). These gels also appear to have two relaxation timescales; one timescale is approximately 10-fold greater than EPE L37V gels and the other is approximately the same as EPE L37V gels. This is evident in the loss moduli of the two gels, which exhibit a shoulder at the same frequency as the maximum in

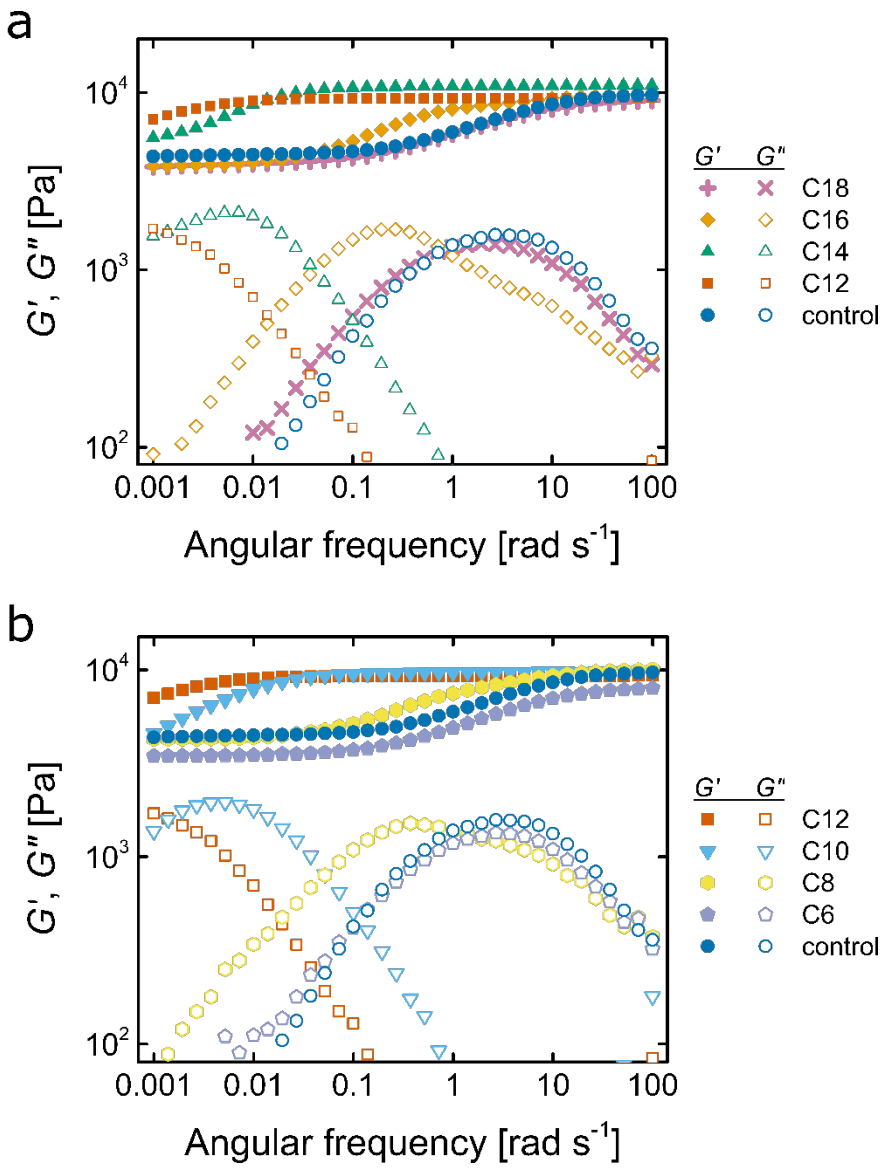

Figure V-2. Frequency sweeps of EPE L37V hydrogels swollen with various fatty acid ligands. (a) Fatty acids 6 to 12 carbon atoms in length. (b) Fatty acids 12 to 18 carbons atoms in length.

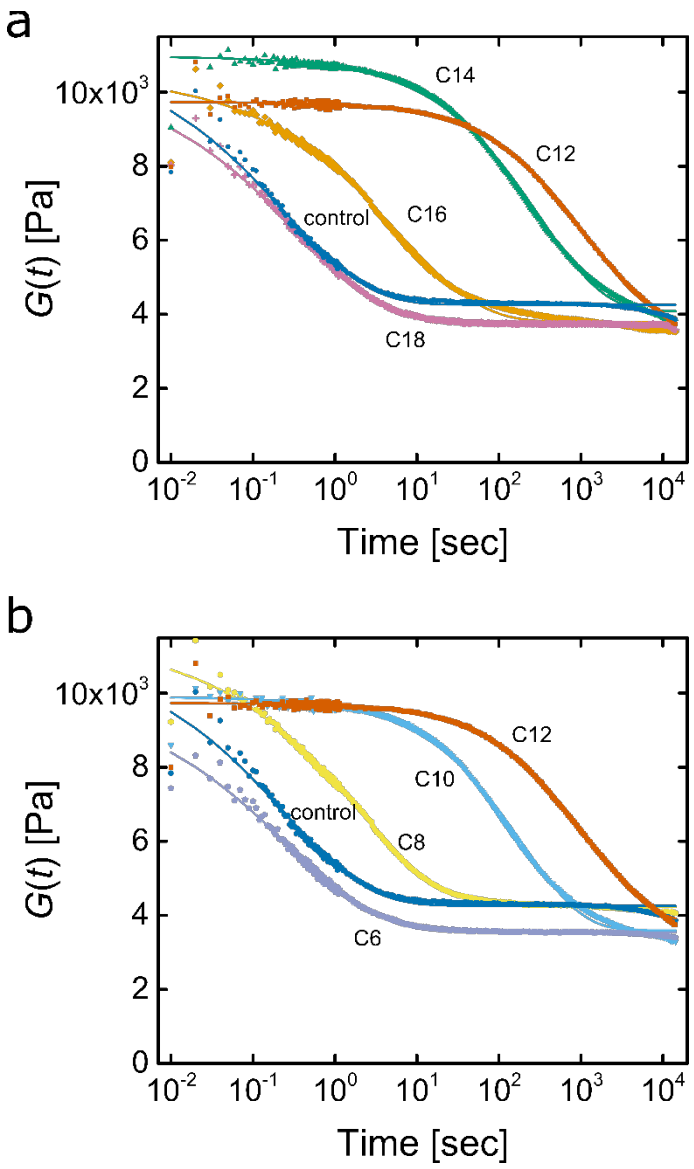

Figure V-3. Stress relaxation of EPE L37V hydrogels swollen with various fatty acid ligands. (a) Fatty acids 6 to 12 carbon atoms in length. (b) Fatty acids 12 to 18 carbons atoms in length. Stretched exponential fits are shown as solid lines.

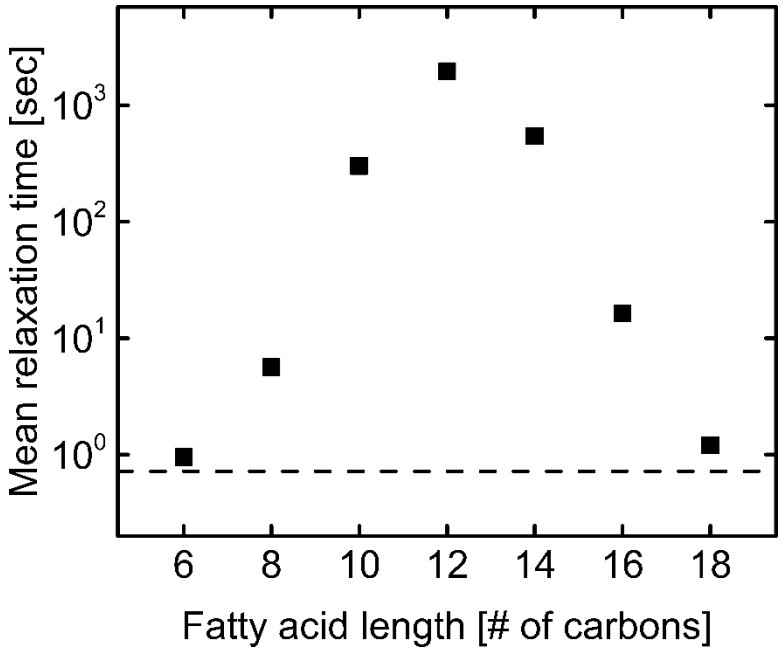

Figure V-4. Plot of mean relaxation time versus fatty acid length. The parameters from the stretched exponential fits in Figure V-3 were used to evaluate the mean relaxation time for each gel. The mean relaxation time of the control EPE L37V gel is shown by the dashed horizontal line.

G" in the control gel. The most likely explanation for this behavior is partial occupancy of the coiled-coil cross-links by these ligands. Finally, hydrogels swollen with 6- and 18-carbon fatty acids (caproic acid and stearic acid) have characteristic relaxation timescales that are similar to the control gels, demonstrating that these compounds do not affect the viscoelastic behavior of EPE L37V gels. Together, these results produce a biphasic or bell-shaped curve describing the relationship between the fatty acid chain length and the characteristic network relaxation time (Figure V-4). The shape of this curve suggests that the lauric acid represents an optimal chain length for binding within the P channel, at least with respect to its effect on the lifetime of the coiled-coil association.

4.3 Proposed Rationale for the Effects of Fatty Acids on EPE L37V Hydrogels

One possible molecular explanation for lauric acid as the optimal ligand length for the P channel involves its length relative to the distance between the polar side chains of Thr40 and Gln54. The crystal structures of P in complex with myristic acid, palmitic acid, and stearic acid indicate that polar carboxylate head groups of these fatty acids interact with the amide side chains of the Gln54 residues [17], which together form a pentameric ring that has been described as an ion trap [14]. Binding of a hydrophobic ligand also appears to displace the water molecules that line the portion of the channel between Gln54 and Thr40 in the *apo*-crystal structure [14]. However, the aliphatic tails of the 14- to 18-carbon fatty acids also extend outside of this region toward the N-terminus and create potentially unfavorable interactions with the Thr40 side chains (Figure V-5). Although the crystal structure of P in complex with lauric acid is not available, it is reasoned that removal of two carbon atoms from the bound myristic acid ligand can provide an estimation of its binding (Figure V-5, top). In this structure, lauric acid is short enough that is does not interact with Thr40. Thus, lauric acid might represent an optimal fatty acid because it maximizes favorable interactions with the apolar side chains of Leu44, Val47, and Leu51 and displaces water from this portion of the channel, but does not have significant interactions with the polar side chain of Thr40. This hypothesis could be tested by mutating Thr40 to an apolar amino acid to determine whether the bell-shaped curve in Figure V-4 shifts toward longer fatty acid chain lengths.

The differences in the solubility of the various fatty acids in aqueous buffer are also likely to influence how they affect the viscoelastic behavior of EPE L37V networks. As shown in Table V-1, the log P values of the fatty acids range from 1.9 for hexanoic acid to 8.2 for stearic acid. The shorter chain fatty acids may be too water soluble and lack the driving force to enter the

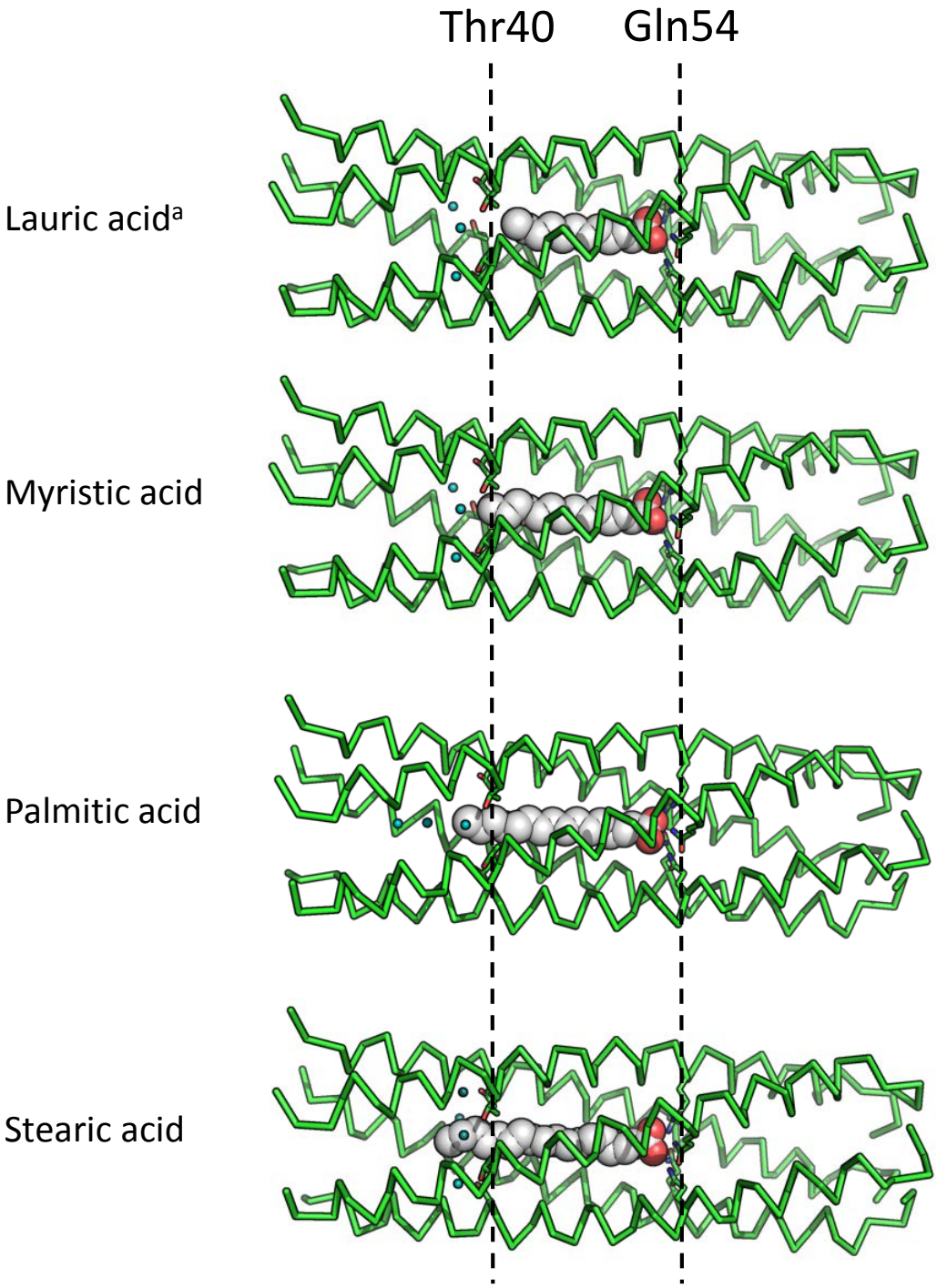

Figure V-5. Fatty acid binding in P coiled coils. The protein chains are shown in green. The fatty acids are shown as spheres (carbon – white, oxygen – red). Water molecules are shown as small teal spheres. The position of Thr40 and Gln54 are denoted by the dashed vertical lines. The structures were rendered in PyMol from PDB 3V2N (myristic acid), 3V2Q (palmitic acid), and 3V2P (stearic acid) reported in ref. [17]. [a]The structure for P with lauric acid was generated by removing 2 carbon atoms from myristic acid in PDB 3V2N.

hydrophobic channel. Conversely, the longer chain fatty acids are poorly soluble in water and may not be capable of dissolving sufficiently and diffusing into the hydrogel. This would explain the apparent lack of an effect of stearic acid on the relaxation time of the EPE L37V network. Lauric acid, myristic acid, and capric acid might represent an ideal balance between dissolution of the ligand in the aqueous media and partitioning into the hydrophobic channel of the coiled-coil. However, differences in solubility alone cannot explain the biphasic relationship between fatty acid chain length and the relaxation time. For example, it does not provide an adequate explanation for why networks swollen in the presence of myristic acid and palmitic acid have shorter relaxation times than networks swollen in the presence of lauric acid. If water solubility the fatty acids was the only determinant of their effect on the network relaxation time, then it is likely that once the longer fatty acids were bound within the channel, the coils would be much more difficult to dissociate and these networks would exhibit longer relaxation times.

MacFarlane *et al*. also reported a biphasic relationship between the fatty acid chain length and the equilibrium dissociation constant (K_d) for the binding of various fatty acids and the P coiled coil [17]. In their experiment, however, stearic acid had the lowest value of K_d (0.44 μM), indicating it was bound most tightly. The dissociation constant increased as the fatty acid length was decreased to 14 or 16 carbon atoms or increased to 20 carbon atoms, indicating weaker affinity. This is somewhat surprising given that stearic acid does not seem to affect the viscoelastic behavior of EPE L37V hydrogels, and it is unclear whether it is even bound within the physical cross-linking domains of the gels. It is possible that stearic acid is bound in the hydrogels, but that tight ligand binding is not necessarily correlated with the network relaxation time. Alternatively, the discrepancy may arise from other differences between the experiment described here and that by MacFarlane *et al*., including differences in the protein concentration and the protein sequence.

The measurements of K_d were obtained at a much lower protein concentration (100 nM) than the typical protein concentration in a hydrogel (approximately 2 mM), which could be important given the poor solubility of stearic acid. Constraining the P domain within a covalent network is almost certain to affect the association energy and dynamics of P coiled coils, and may influence the energetics of ligand binding as well. Finally, although the COMP coiled coil investigated by MacFarlane *et al*. did not contain the L37V mutation used in this chapter, this is likely not the source of the discrepancy because the same trend in the relaxation time was observed for wild-type EPE gels swollen with fatty acids (data not shown).

5. Future Experiments

Experiments are underway to determine whether the various ligands described in this chapter are actually bound within the coiled-coil cross-linkers in EPE and EPE L37V hydrogels. Several hydrophobic compounds including all-*trans*-retinol [16], *cis*-parinaric acid [17], and curcumin [18] have been reported to undergo an increase in fluorescence when bound within the hydrophobic channel of P. This allows for the spectroscopic detection of binding, either by direct detection of one of these fluorescent ligands or by a competition assay between a fluorescent ligand and a non-fluorescent ligand. Extraction of the hydrophobic ligands into organic solvent and detection by high-performance liquid chromatography can also be performed to measure their concentration within the hydrogel.

The kinetics of ligand diffusion into the hydrogels will also be evaluated. The experiments with fatty acids were conducted at a single time point after 3 days of swelling, which is clearly sufficient to observe the effect for some of the ligands. However, the larger, less soluble ligands

such as stearic acid or palmitic acid may require longer swelling times to diffuse into the hydrogel and partition into the coiled coils.

6. Conclusions

Small hydrophobic molecules including vitamin D3 and medium- and long-chain fatty acids were used to engineer the relaxation timescales of protein networks cross-linked by the association of helical domains derived from cartilage oligomeric matrix protein. Using saturated, straight-chain fatty acids varying in length from six to eighteen carbon atoms, the relaxation time of chemical-physical hydrogel networks could be increased 10- to 1000-fold. While the mechanism is still not clear, it is proposed to involve the binding of these ligands within the hydrophobic channel of the P coiled coil, which has been demonstrated previously by crystallization of protein-ligand complexes and by fluorescence spectroscopy. Binding of ligands within the channel stabilizes the coiled coil and is expected to increase the lifetime of the physical cross-links within the hydrogel network. The optimal fatty acid ligand for increasing the network relaxation time was lauric acid, with networks swollen in the presence of shorter and longer fatty acids exhibiting smaller increases in the relaxation time. Further fine-tuning of the relaxation time would likely be possible with odd-numbered saturated fatty acids, unsaturated fatty acids, branched fatty acids, and fatty acids containing heteroatoms. In addition to engineering the viscoelasticity of protein-based materials, the capacity of P coiled coils to bind hydrophobic compounds could also be exploited for drug delivery applications. Incorporating these domains within a hydrogel would provide a method for the local, sustained delivery of therapeutics. This work represents the initial steps toward a new approach to materials design in which different

“formulations” of protein hydrogels and small molecule ligands can be used to engineer material properties for specific applications.

7. References

[1] W.A. Petka, J.L. Harden, K.P. McGrath, D. Wirtz, and D.A. Tirrell *Science* **1998** *281*, 389-392.

[2] E.R. Wright, R.A. McMillan, A. Cooper, R.P. Apkarian, and V.P. Conticello *Adv. Func. Mater.* **2002** *12*, 149-154.

[3] W. Shen, J.A. Kornfield, D.A. Tirrell *Macromolecules* **2007** *40*, 689-692.

[4] M. Kim, W.G. Chen, J.W. Kang, M.J. Glassman, K. Ribbeck, and B.D. Olsen *Adv. Mater.* **2015** *27*, 4207-4212.

[5] K. Dooley, B. Bulutoglu, S. Banta *Biomacromolecules* **2014** *15*, 3617-3624.

[6] K. Dooley, Y.H. Kim, H.D. Lu, R. Tu, and S. Banta *Biomacromolecules* **2012** *13*, 1758-1764.

[7] J.D. Ehrick, S.K. Deo, T.W. Browning, L.G. Bachas, M.J. Madou, and S. Daunert *Nat. Mater.* **2005** *4*, 298-302.

[8] S. Topp, V. Prasad, G.C. Cianci, E.R. Weeks, and J.P. Gallivan *J. Am. Chem. Soc.* **2006** *128*, 13994-13995.

[9] W. Yuan, J. Yang, P. Kopečková, J. Kopeček *J. Am. Chem. Soc.* **2008** *130*, 15760-15761.

[10] T. Miyata, N. Asami, T. Uragami *Nature* **1999** *399*, 766-769.

[11] M. Ehrbar, R. Schoenmakers, E.H. Christen, M. Fussenegger, and W. Weber *Nat. Mater.* **2008** *7*, 800-804.

[12] B.D. Olsen, J.A. Kornfield, D.A. Tirrell *Macromolecules* **2010** *43*, 9094-9099.

[13] W. Shen, K. Zhang, J.A. Kornfield, D.A. Tirrell *Nat. Mater.* **2006** *5*, 153-158.

[14] V.N. Malashkevich, R.A. Kammerer, V.P. Efimov, T. Schulthess, and J. Engel *Science* **1996** *274*, 761-765.

[15] S. Özbek, J. Engel, J. Stetefeld *EMBO J.* **2002** *21*, 5960-5968.

[16] Y. Guo, D. Bozic, V.N. Malashkevich, R.A. Kammerer, T. Schulthess, and J. Engel *EMBO J.* **1998** *17*, 5265-5272.

[17] A.A. MacFarlane, G. Orriss, N. Okun, M. Meier, T. Klonisch, M. Khajehpour, and J. Stetefeld *PLOS One* **2012** *7*, e48130.

[18] S.K. Gunasekar, M. Asnani, C. Limbad, J.S. Haghpanah, W. Hom, H. Barra, S. Nanda, M. Lu, and J.K. Montclare *Biochemistry* **2009** *48*, 8559-8567.

[19] National Center for Biotechnology Information. PubChem Compound Database; CID=985, https://pubchem.ncbi.nlm.nih.gov/compound/985 (accessed 2016 May 8).

[20] National Center for Biotechnology Information. PubChem Compound Database; CID=5281, https://pubchem.ncbi.nlm.nih.gov/compound/5281 (accessed 2016 May 8).

[21] National Center for Biotechnology Information. PubChem Compound Database; CID=11005, https://pubchem.ncbi.nlm.nih.gov/compound/11005 (accessed 2016 May 8).

[22] National Center for Biotechnology Information. PubChem Compound Database; CID=3893, https://pubchem.ncbi.nlm.nih.gov/compound/3893 (accessed 2016 May 8).

[23] National Center for Biotechnology Information. PubChem Compound Database; CID=2969, https://pubchem.ncbi.nlm.nih.gov/compound/2969 (accessed 2016 May 8).

[24] National Center for Biotechnology Information. PubChem Compound Database; CID=379, https://pubchem.ncbi.nlm.nih.gov/compound/379 (accessed 2016 May 8).

[25] National Center for Biotechnology Information. PubChem Compound Database; CID=8892, https://pubchem.ncbi.nlm.nih.gov/compound/8892 (accessed May 8, 2016). (accessed 2016 May 8).

Chapter VI

PROGRESS TOWARD TOUGHER PROTEIN HYDROGELS BY COMBINING CHEMICAL AND PHYSICAL CROSS-LINKING

1. Abstract

The combination of permanent covalent cross-links and reversible physical cross-links in polymeric hydrogels has been demonstrated to enhance the toughness and extensibility of these materials. These two types of interactions are present in chemical-physical hydrogels prepared by end-linking the triblock artificial protein EPE, which is capable of forming noncovalent, coiled-coil cross-links through the association of midblock domains within a covalent network. In this chapter, cross-linked EPE networks were tested in uniaxial tension to determine the stress and strain required to fracture the hydrogels. Two chemical networks were also prepared from the artificial proteins ERE and ER_CE, which differ in the number of cysteine residues available for covalent cross-linking. Hydrogels prepared from EPE could be extended further than both covalent hydrogels and also exhibited a greater work of extension, which is considered a measure of material toughness. These results demonstrate some progress toward engineering tougher, more extensible protein hydrogels by the incorporation of physical cross-linking by coiled-coil domains.

2. Introduction

Hydrogels are used widely in biomedical applications and consumer products due to their favorable elastic properties and their ability to absorb large amounts of water by swelling. However, the tendency for soft, highly swollen hydrogels to fracture easily imposes significant limitations on these applications. Absorption of solvent by swollen hydrogel networks decreases the polymer volume fraction, which in turn decreases the number of chains per unit area across a fracture surface. This results in the rupture of covalent bonds and the propagation of the fracture surface until the material fails. A number of strategies have been developed to overcome the weak, brittle nature of hydrogels and other polymeric materials. Many of these strategies have been reviewed recently [1, 2], and those that are most relevant to protein-based materials are discussed here.

A relatively simple approach to tough hydrogels is one that uses highly efficient covalent reactions to cross-link macromer precursors. This approach stands in contrast to what are termed conventional hydrogels that are polymerized from mixtures of small molecule monomers and cross-linkers. Conventional hydrogels are often characterized by heterogeneous network structures in which dense, tightly cross-linked regions are loosely connected by long polymer chains [1]. This can lead to very high amounts of stress per chain in the loosely cross-linked regions, which can contribute to fracture. An example of a more homogeneous hydrogel prepared by end-linking poly(ethylene) glycol (PEG) chains with a click reaction was reported by Hawker and coworkers [3]. In this work, bifunctional PEG alkyne chains and tetrafunctional PEG azide chains were linked together by the copper catalyzed azide-alkyne cycloaddition. The resulting hydrogel networks could be extended over 1500% and sustained true stresses of up to 2 MPa. In comparison, PEG hydrogels polymerized by conventional photochemical methods were significantly weaker and

less extensible. Similar homogeneous networks have been prepared by end-linking PEG macromers by Michael-type addition of thiols and vinyl sulfones [4] and by amide bond formation [5, 6]. This approach was also used in Chapter 2 to end-link ERE artificial protein chains with 4-arm PEG vinyl sulfone. Because proteins are monodisperse polymers, they are especially well-suited to forming homogeneous networks that may be tougher than conventional hydrogels.

Many recent strategies for developing tough hydrogels are based on the concept of dissipating energy by the incorporation of reversible or sacrificial cross-links. This strategy is perhaps best demonstrated by hydrogel networks containing polyacrylamide and alginate cross-linked within the same covalent network [7]. While polyacrylamide networks would normally be considered brittle conventional hydrogels, they were reinforced by ionic Ca^{2+} cross-links between the alginate chains. In this material design, the permanent covalent cross-links are proposed to maintain the shape and elasticity of the material while the ionic cross-links unzip reversibly to prevent the rupture of covalent bonds. Similar polymeric networks that have been described as tough include synthetic polyampholyte gels cross-linked by a pair of weak and strong ionic bonds [8], polyacrylamide-*co*-polyacrylic acid hydrogels containing Fe^{3+} ionic cross-links [9], triblock copolymers with poly(methylmethacrylate) endblocks and ionically cross-linked poly(methacrylic acid) midblocks [10], and poly(vinylpyridine) organogels with organometallic physical cross-links [11].

Coiled coils are candidates for the reversible or sacrificial cross-linking component in protein networks based on this toughening strategy. Compared to other protein structures including β-sheets, α-helical domains are considered mechanically weak with typical unfolding forces of tens of piconewtons as measured by single molecule force spectroscopy [12-14]. In protein hydrogels, the association of coiled coils as physical cross-linking domains is sufficiently weak

that these domains dissociate reversibly under thermal forces, resulting in viscoelastic behavior [15]. This suggests that they may be capable of dissipating energy during hydrogel deformation. Despite the potential of artificial proteins to participate in several different toughening mechanism, to date there have been only a few research efforts in this area [16-19].

The initial motivation for preparing EPE chemical-physical hydrogels was to assess whether toughness and extensibility could be encoded within a polymeric material by programming the molecular association between artificial protein domains. In Chapter 3, it was shown that EPE could be used to prepare covalent hydrogel networks that also contained physical cross-links formed by the association of the helical domains on different protein chains. This behavior was clearly demonstrated in small angle oscillatory shear rheology experiments in which the transient physical cross-links resulted in a viscoelastic response to small strains. In this chapter, EPE hydrogels were stretched in uniaxial tension to determine the strain and stress at which these networks fracture. It was anticipated that the combination of the permanent covalent cross-linking and reversible physical cross-linking in EPE gels might result in toughening behavior that is analogous to the polyacrylamide-*co*-alginate network described by Sun *et al*. [7]. For comparison, two different chemical protein networks were also prepared with different cross-linking densities. The results described here demonstrate that the EPE network can be stretched further than either chemical network, but further experiments are required to conclude whether EPE chemical-physical networks can be classified as truly tough hydrogels.

3. Methods and Materials

3.1 Protein Synthesis

The EPE and ERE proteins were expressed and purified as described in the previous chapters and in Appendix B. The gene encoding the ER_CE protein was prepared by site-directed mutagenesis of the pQE-80L ERE plasmid using oligonucleotides reported in Appendix A. The resulting plasmid, pQE-80L ER_CE, was transformed into the BL21 strain of *Escherichia coli* and expressed and purified in the same way as ERE. The complete DNA and amino acid sequence of ER_CE is reported in Appendix A.

3.2 Preparation of Cross-linked Hydrogel Test Specimens

All hydrogels were prepared at 15 wt% total polymer and a 1:1 stoichiometry of vinyl sulfone and thiol functional groups. For tensile experiments, the proteins were cross-linked in a custom-designed, dumbbell-shaped mold with a narrow rectangular test region and wider tabs for improved gripping of the gel in the test fixture. The dimensions of the test region of the mold were 15 mm x 3 mm x 1 mm (L x W x H). Approximately 500 μL of the cross-linking mixture was required to fill each mold. In a typical cross-linking experiment with EPE, 75 mg of protein was dissolved in 500 μL of degassed cross-linking buffer (0.1 M sodium phosphate, 6 M guanidinium chloride, and 0.4 M triethanolamine, pH 7.4) by sonication for 1 min in an ultrasonic bath and centrifugation for 1 min at 10,000 *g*. The protein solution was combined with 115 μL of PEG-4VS solution (150 mg mL^{-1} in degassed 0.4 M triethanolamine, pH 7.4) and mixed quickly by vortexing. Approximately 500 μL was pipetted into the dumbbell-shaped mold. The mixture was spread evenly and cured overnight at room temperature in a humidified chamber.

Cross-linked gels were removed from the mold and swollen in decreasing concentrations (6 M, 3 M, 2 M, 1 M) of guanidinium chloride in PBS (phosphate buffered saline, 1.5 mM KH_2PO_4,

4.3 mM Na_2HPO_4, 137 mM NaCl, 2.7 mM KCl, pH 7.4) over the course of approximately 30 hrs. The gels were then swollen in PBS containing 0.02% (w/v) sodium azide for 24-48 hr before uniaxial tensile testing or rheological testing.

3.3 Rheological Testing of As-Prepared and Swollen Hydrogels

Hydrogels were characterized by dynamic oscillatory shear rheology in the as-prepared and swollen states. The tests were performed on an ARES-RFS strain-controlled rheometer (TA Instruments). Hydrogel disks were loaded between 8 mm parallel plates as described in the previous chapters and in Appendix B. Frequency sweep experiments were performed from 100-0.1 rad s^{-1} at 1% strain amplitude and 25 °C. Three replicates were performed for each gel.

3.4 Uniaxial Tensile Testing

Uniaxial tensile tests were performed on an Instron 5422 testing machine with a 5 N load cell. The instrument was controlled with the Bluehill3 software package (Instron). All tests were performed in an environmental chamber filled with buffer and maintained at 25 °C by a water jacket. The width of the swollen dumbbell hydrogels was measured with a digital caliper (Mitutoyo) and the thickness was measured with a digital micrometer (Mitutoyo). The gauge length was calculated by multiplying the measured width by 5 under the assumption that the gels swell isotropically. Hydrogels were prevented from slipping out of the grips by coarse sand paper. The tests were performed at a strain rate of 2 min^{-1} (200% of gauge length per minute). To correct for the change in the buoyant force as the test fixture was raised out of the bath, the change in the volume of displaced buffer was calculated from the diameter of the cylindrical portion of the

fixture (3.13 mm). EPE, ERE, and ER_CE hydrogels were tested with the environmental chamber filled with PBS. Five replicates were performed for each protein gel. EPE and ERE gels were also tested under denaturing conditions. The gels were swollen in PBS containing 6 M guanidinium chloride for 24-48 hr and tested with the environmental chamber filled with the same buffer. Four EPE gels were tested and three ERE gels were tested (the fourth ERE gel broke during sample loading).

4. Results and Discussion

4.1 Protein Design and Synthesis

Three artificial proteins were designed to investigate the influence of coiled-coil physical cross-linking on the strength and extensibility of protein hydrogels. As described in Chapters 2 and 3, the artificial proteins ERE and EPE are triblock sequences containing elastin-like endblocks and terminal cysteine residues. Covalent hydrogels are formed from these proteins by end-linking with 4-arm poly(ethylene glycol) vinyl sulfone (PEG-4VS). EPE also contains a helical midblock domain P that forms homopentameric coiled coils with midblock domains on nearby chains. This association forms transient physical cross-links within the end-linked EPE network resulting in a chemical-physical hydrogel. In contrast, ERE contains a non-associative midblock domain R, and end-linking with PEG-4VS results in a chemical or covalent hydrogel. The viscoelastic properties and swelling behavior of ERE and EPE hydrogels are reported in Chapter 3. While ERE chemical networks store stress elastically, EPE hydrogels are viscoelastic due to the transient association of the physical cross-linking domains. When deformed, EPE hydrogels exhibit stress relaxation with a characteristic timescale of approximately 100 seconds. At shorter times (t << 100 s), energy or stress is stored within chain segments between both the chemical and physical cross-links. At

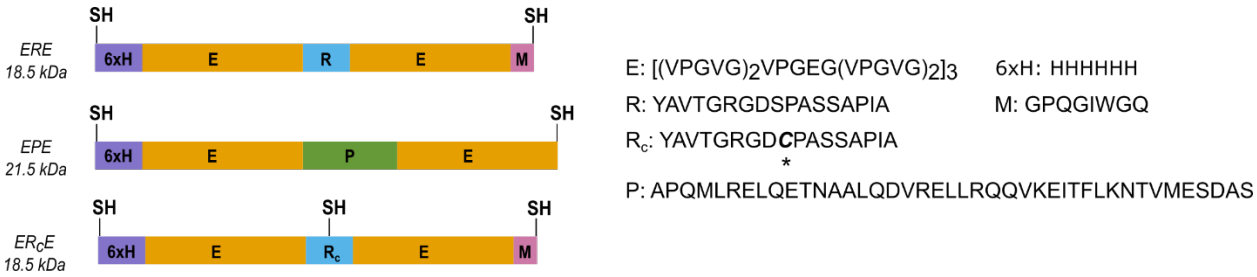

Figure VI-1. Sequences of artificial proteins EPE, ERE, and ER$_C$E. The multiblock structure is shown along with the sequences of each domain. The position of the serine to cysteine mutation in ER$_C$E is denoted by the * below the sequence.

longer times (t >> 100 s), energy or stress is stored only within chain segments between the chemical cross-links. Because the physical cross-links occur within the middle of each end-linked EPE chain, the modulus at short times is approximately twice the modulus at long times. In other words, when a constant strain is applied, the amount of stress stored at short times is approximately twice the amount of stress stored at long times. As the stress relaxes, energy is dissipated as heat. In contrast, the stress stored in ERE hydrogels is nearly independent of time and little energy dissipation occurs.

EPE hydrogels are stiffer and more swollen than ERE hydrogels due to their increased cross-linking density. To understand how this might affect the tensile properties of protein networks, a second chemical hydrogel network was designed with the capacity to form an additional covalent cross-link at an internal cysteine residue located within the midblock domain R. This was accomplished by synthesizing a new artificial protein sequence by site-directed mutagenesis of the ERE gene to replace a serine residue within the R domain with a cysteine residue. The resulting protein, denoted ER$_C$E (Figure VI-1), differs from the ERE protein by a single atom; the oxygen of the Ser side chain is replaced by sulfur in the Cys side chain. However,

the introduction of an internal cross-linking site within the protein chain is expected to have a significant effect on the mechanical properties of materials prepared from this protein. It is anticipated that the increased covalent cross-linking density of ER_CE hydrogels will result in a modulus and polymer volume fraction that closely match the properties of EPE hydrogels. The capacity to precisely define covalent cross-linking sites in a polymer chain is a unique feature of genetically encoded artificial proteins.

4.2 Comparison of As-Prepared and Swollen EPE, ERE, and ER_CE Hydrogels

The three artificial proteins were cross-linked with PEG-4VS at an initial total polymer concentration of 15 wt% and a 1:1 vinyl sulfone to thiol stoichiometry. As in the previous chapters, cross-linking was performed under denaturing conditions in phosphate buffer containing 6 M guanidinium chloride. Because ER_CE contains three cysteine residues per chain, the fraction of PEG-4VS in the cross-linking reaction is higher than the fraction in the ERE and EPE reactions (28.6% for ERcE, 21.3% for ERE, and 18.8% for EPE). The cross-linked gels were characterized in the as-prepared or unswollen state by dynamic oscillatory shear rheology. The storage moduli of the three gels are shown in Figure VI-2 a. EPE and ERE gels have nearly identical storage moduli (approximately 6 kPa) in the as-prepared state. This is expected because the two proteins have a similar molecular weight and identical sites for covalent cross-linking. The physical cross-linking domains in EPE gels are not expected to be associated in the as-prepared state because the cross-linking buffer contains protein denaturant. ER_CE gels are approximately twice as stiff as ERE and EPE gels in the as-prepared state. This is also expected because the additional cysteine cross-linking site in ER_CE occurs in the middle of the protein chain, cutting the average molecular weight between cross-links in half and doubling the modulus.

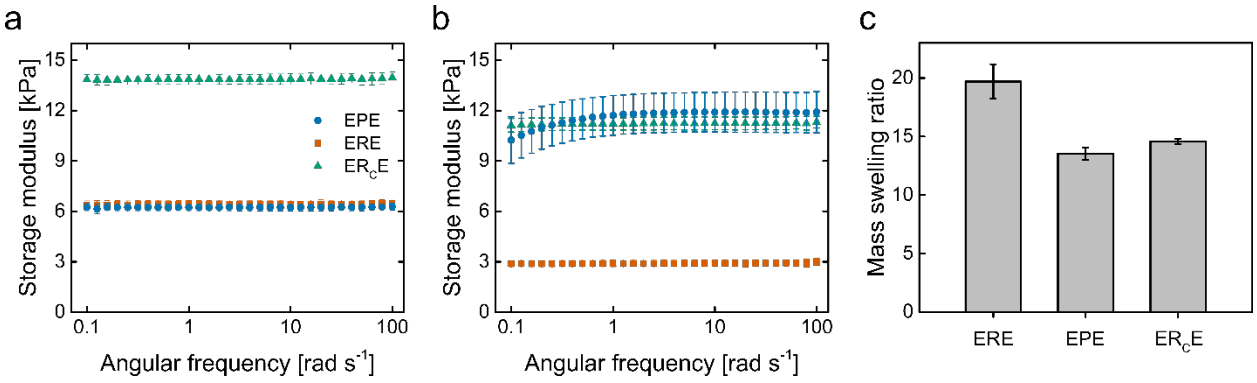

Figure VI-2. Rheology and swelling of EPE, ERE, and ER$_C$E hydrogels. Storage moduli (n = 3) in the as-prepared state (**a**) and after swelling to equilibrium in PBS (**b**) at 1% strain amplitude, 25 °C. (**c**) Mass swelling of the three protein hydrogels in PBS (n = 6).

The moduli of the hydrogels after swelling to equilibrium in phosphate buffered saline are quite different than in the as-prepared state (Figure VI-2 a and b). After removing the denaturant that was present during cross-linking, the midblock domains of EPE can associate with one another to form physical cross-links within the covalent network. As a result, the storage modulus of EPE in the swollen state is greater than the storage modulus in the as-prepared state despite a decrease in the polymer volume fraction. The viscoelastic behavior of the EPE hydrogels is also evident from the decrease in the storage modulus at lower frequencies. The frequency sweep experiments in Figure VI-2 were performed over an angular frequency range of 0.1-100 rad s^{-1}, so the long time or low frequency behavior described in Chapter 3 is not observed here. Unlike EPE gels, ERE and ER$_C$E hydrogels are softer in the swollen state than in the as-prepared state because the chain density decreases upon swelling and no additional cross-links are formed. The storage moduli of the ERE and ER$_C$E gels are approximately 3 kPa and 11 kPa, respectively. In contrast to the as-prepared state, the high frequency modulus of EPE gels in the swollen state is similar to the modulus of ER$_C$E gels rather than ERE gels. From these experiments, it is concluded that the rheological behavior of the three networks is consistent with the protein design and that these gels

can be used to compare the behavior of cross-linked protein networks with (1) no association between midblock domains, (2) physical or noncovalent association between midblock domains, and (3) chemically cross-linked midblock domains.

4.3 Uniaxial Tensile Testing of EPE, ERE, and ER$_C$E Hydrogels

Hydrogel specimens for tensile testing were prepared by cross-linking the three artificial proteins in dumbbell-shaped molds followed by swelling in decreasing concentrations of guanidinium chloride in PBS until the denaturant was removed. The swollen hydrogels (Figure VI-3) were clamped at the ends in the test fixture and extended in uniaxial tension at a strain rate of 2 min^{-1} until failure. The tests were performed in a chamber filled with PBS and maintained at 25 °C. As the gels were stretched, the load was measured as a function of the hydrogel extension in order to calculate the engineering stress (force per initial cross-sectional area) and the engineering strain (the change in length divided by the initial length). Representative stress-strain curves for EPE, ERE, and ER$_C$E hydrogels are plotted in Figure VI-4. The hydrogels generally fractured away from the test fixture grips, with the exception of two ER$_C$E gels that broke very close to the bottom grip (Figure VI-5).

The stress to break (σ_b) and strain to break (ε_b) for five replicates of each gel are plotted in Figure VI-6 a and b. EPE hydrogels can be extended further than ERE or ER$_C$E gels before fracture. The stress required to fracture the EPE and ER$_C$E gels is similar, and is approximately 2-2.5 times greater than the stress required to fracture ERE gels. The work of extension (W_e), which is calculated by integrating the area under the stress-strain curve, is a measure of energy input as

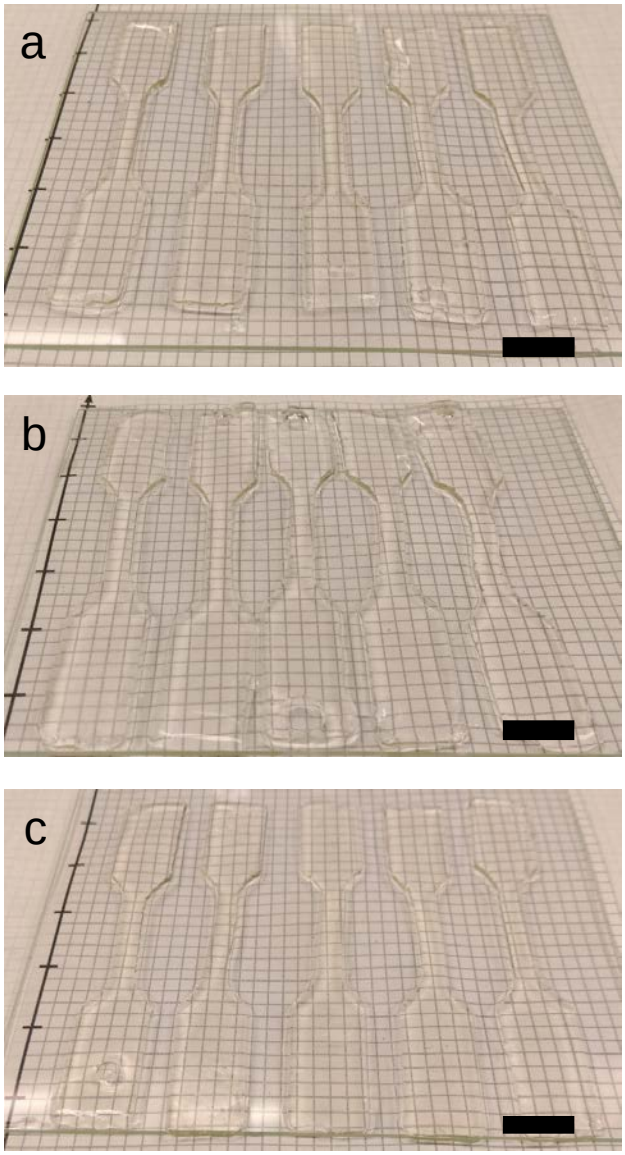

Figure VI-3. Swollen dumbbell-shaped hydrogels prior to tensile testing. (**a**) EPE (**b**) ERE (**c**) ER_CE. Scale bar 1 cm.

gel is stretched. As shown in Figure VI-6 c, EPE gels have a greater W_e than ERE or ER_CE gels. This difference may be related to the energy dissipated by the reversible physical cross-links. Finally, the Young's moduli of EPE and ER_CE are also similar (Figure VI-6 d), as expected based on the rheological experiments and swelling behavior indicating a similar cross-linking density. In contrast, ERE gels are softer and have a lower Young's modulus than EPE and ER_CE.

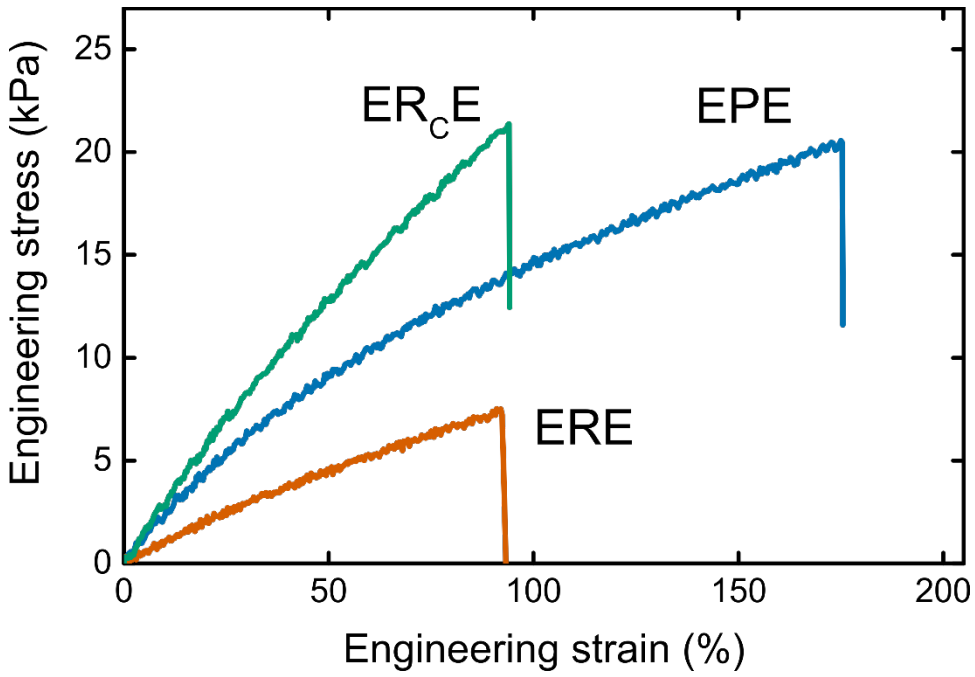

Figure VI-4. Representative stress-strain curves for EPE, ERE, and ER$_C$E hydrogels.

Concerning the toughness and extensibility of protein hydrogels, the most interesting feature to emerge from the tensile experiments is the increased strain to break for EPE chemical-physical networks relative to the ERE and ER$_C$E chemical networks. While EPE and ER$_C$E gels have similar fracture stresses, the stress-strain curves take different trajectories to reach this level of stress. For EPE gels, the slope of the stress-strain curve decreases at high strains, allowing the gel to be stretched further before rupturing. This effect is most likely due to either the viscoelasticity of the chemical-physical network or the forced mechanical unfolding of the physical cross-links at higher stress. Olsen *et al.* reported yielding behavior at a shear stress of 1.4 kPa in large amplitude oscillatory shear rheological experiments with physical protein hydrogels cross-linked by P coiled coils [20]. A similar phenomena may occur in EPE gels, with the unfolding of the physical cross-links between midblock domains preceding rupture of covalent bonds and material failure.

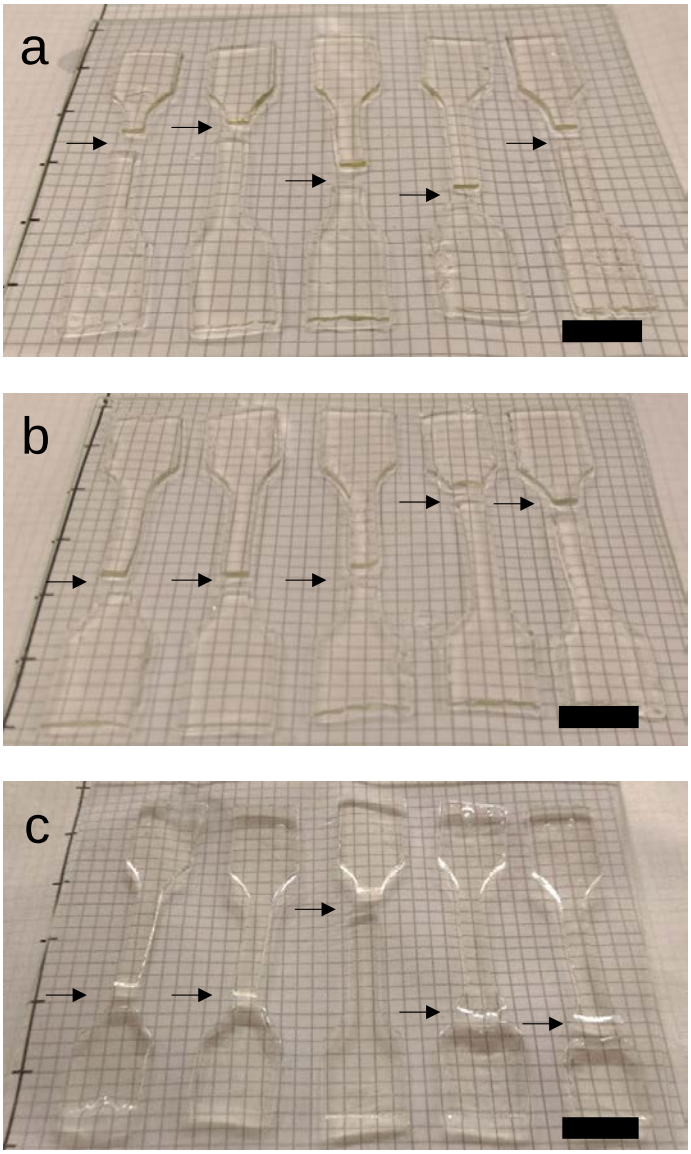

Figure VI-5. Swollen dumbbell-shaped hydrogels after tensile testing. (**a**) EPE (**b**) ERE (**c**) ER_CE. Arrows indicate the failure point in each gel. Scale bar 1 cm.

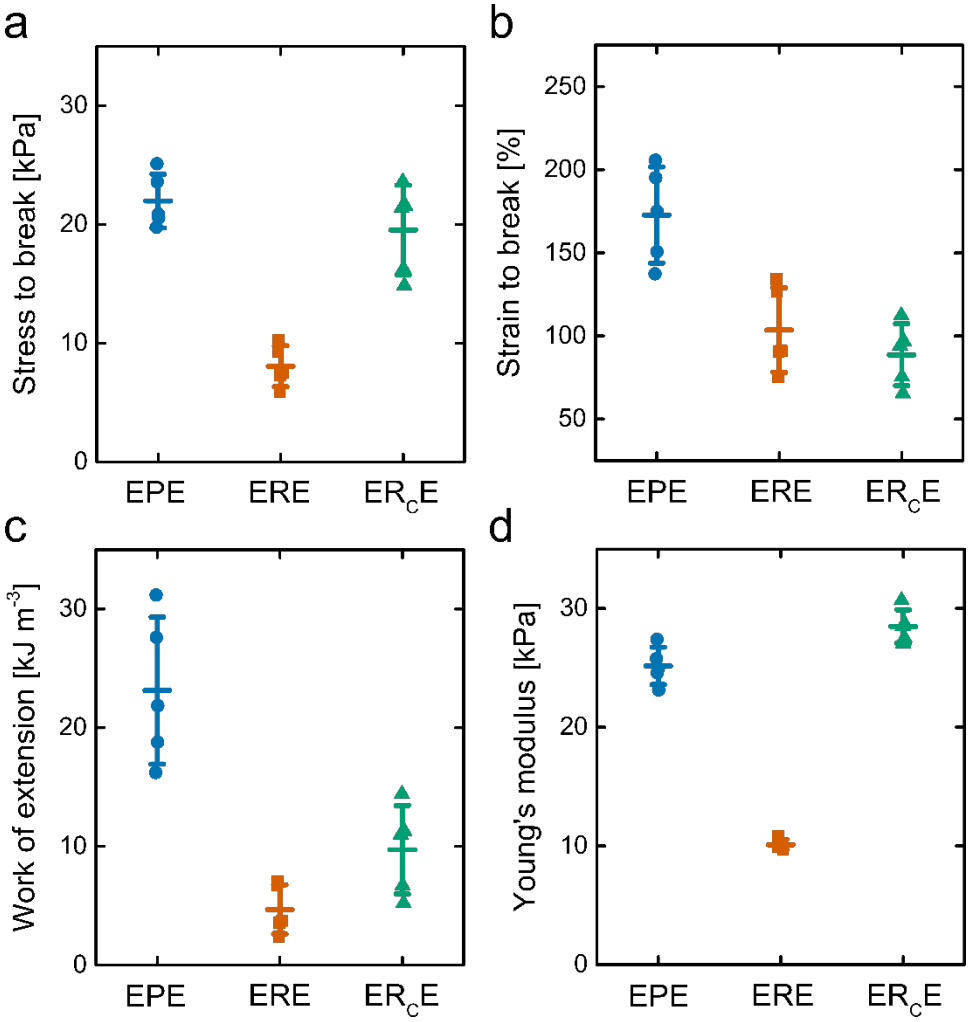

Figure VI-6. Tensile testing results for EPE, ERE, and ER$_C$E hydrogels. (**a**) Stress to break. (**b**) Strain to break. (**c**) Work of extension. (**d**) Young's modulus. The average values are shown by the dashes and error bars represent one standard deviation (n = 5 gels).

4.4 Tensile Testing of EPE and ERE Hydrogels under Denaturing Conditions

Rheological characterization and tensile testing were also conducted on EPE and ERE hydrogels swollen in denaturing buffer (6 M guanidinium chloride in PBS). Under these conditions, EPE and ERE gels have nearly identical storage moduli in the dynamic oscillatory frequency sweep experiments (2.7 and 2.9 kPa, respectively) (Figure VI-7). Like in the as-prepared state, EPE gels swollen in denaturant are not expected to exhibit physical cross-linking and should have a network structure that is similar to ERE gels. However, both EPE and ERE gels in denaturing buffer are softer than in the as-prepared state due to the decrease in the polymer volume fraction upon swelling.

The tensile tests for EPE and ERE gels swollen in denaturing buffer were performed with the environmental chamber filled with PBS containing 6 M guanidinium chloride. Stress-strain curves that are somewhat representative of the average behavior of EPE and ERE gels are shown in Figure VI-8. The average values of the stress to break, strain to break, work of extension, and the Young's modulus for EPE and ERE gels under denaturing conditions were not significantly different (Figure VI-9), suggesting that the tensile behavior of EPE gels in PBS may be attributable to the presence of physical cross-linking within the EPE network. However, it should be noted that there was considerable variability in the ERE gels, which together with the small sample sizes (n = 4 gels for EPE and 3 gels for ERE) makes it difficult to draw meaningful conclusions from this experiment. More replicates of each gel are required.

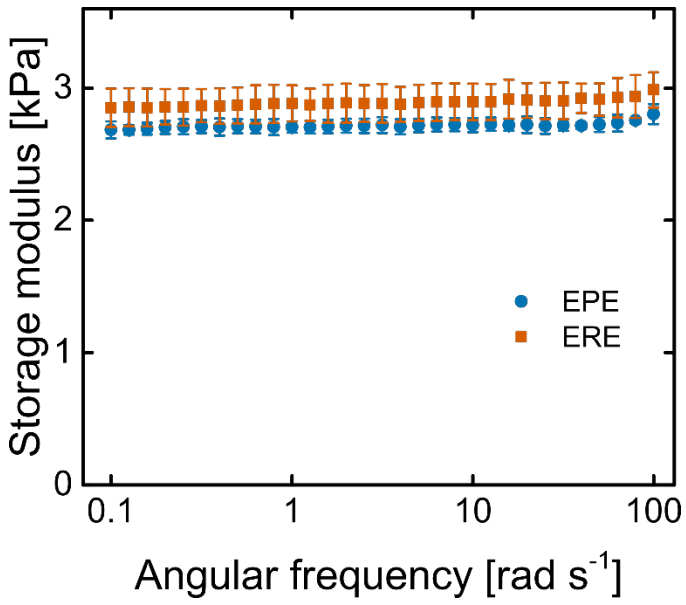

Figure VI-7. Rheology of EPE and ERE hydrogels under denaturing conditions (PBS with 6 M guanidinium chloride). 1% strain amplitude, 25 °C.

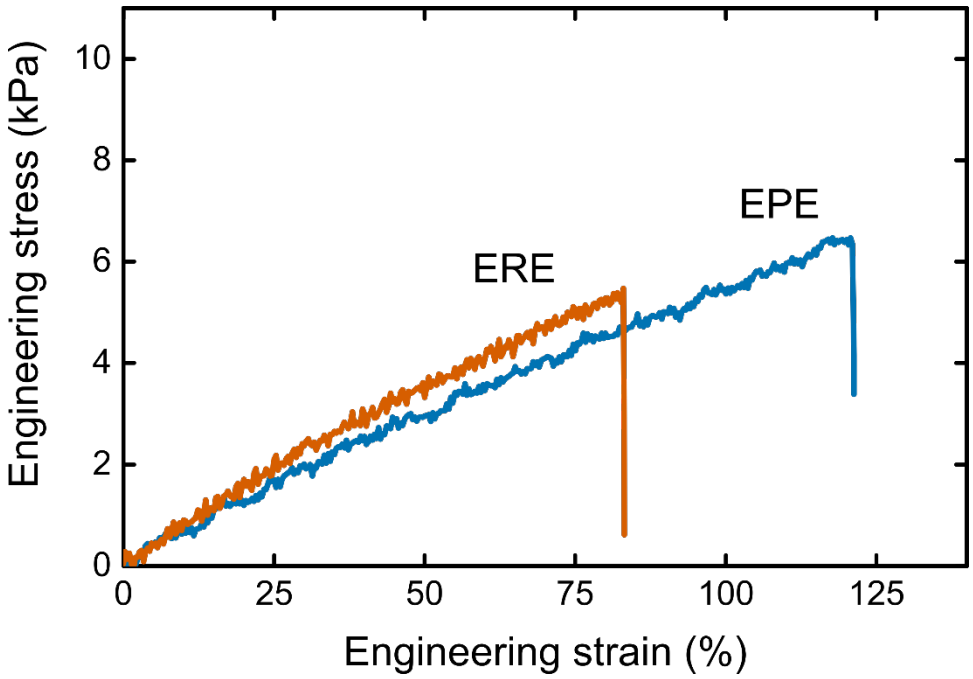

Figure VI-8. Representative stress-strain curves for EPE and ERE hydrogels under denaturing conditions (PBS with 6 M guanidinium chloride).

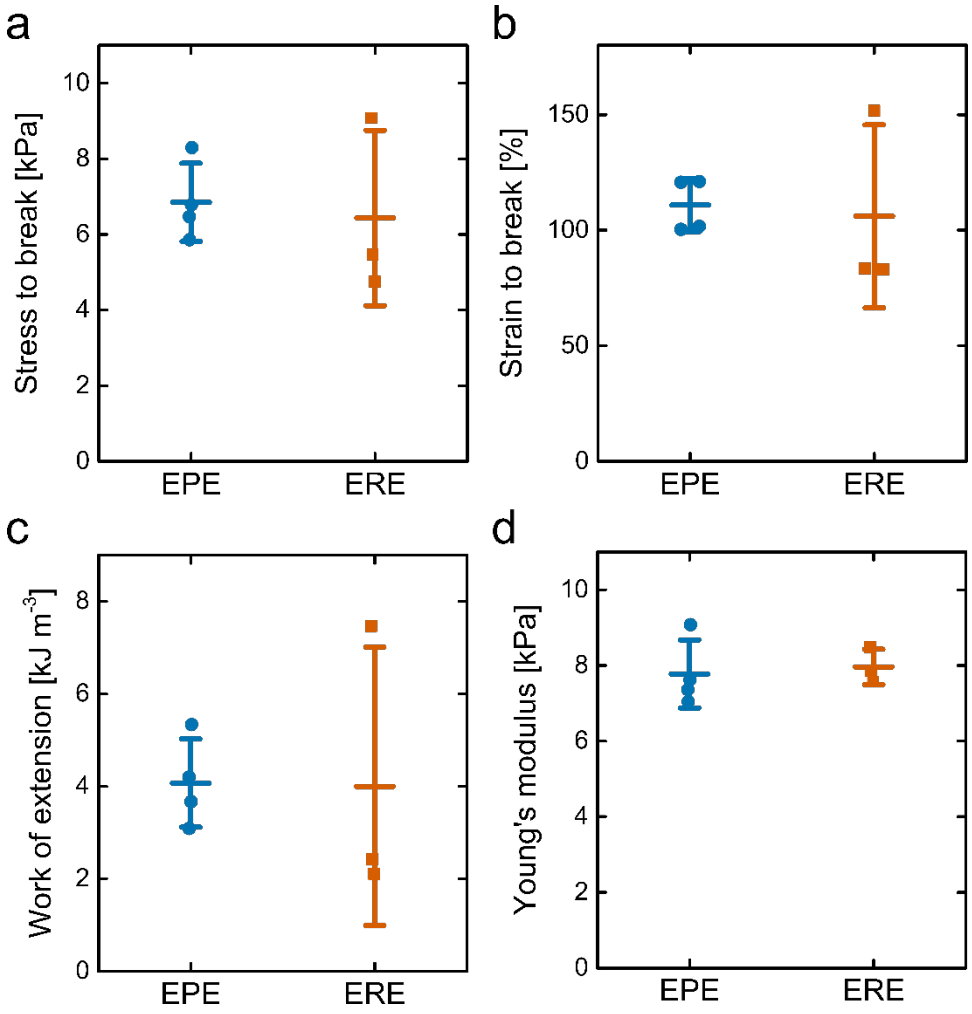

Figure VI-9. Tensile testing results for EPE and ERE hydrogels under denaturing conditions (PBS with 6 M guanidinium chloride). (**a**) Stress to break. (**b**) Strain to break. (**c**) Work of extension. (**d**) Young's modulus. The average values are shown by the dashes and error bars represent one standard deviation (n = 4 gels for EPE and 3 gels for ERE).

5. Future Experiments

Three further experiments are required to assess the toughness of the protein networks described in this chapter. First, loading-unloading cycles would provide a measure of the amount of energy that is recoverable after deformation and the amount of energy that is dissipated as heat. Based on rheological measurements, the viscoelastic EPE chemical-physical network is anticipated to dissipate more energy than the elastic ERE and ER_CE chemical networks. Preliminary measurements of EPE hydrogels indicate that up to 40% of the energy absorbed during loading is dissipated in a hysteresis loop. Cyclic strain experiments also provide a measurement of the fatigue of hydrogels after repeated loading and unloading. Many current hydrogel toughening strategies suffer from poor recovery after large strains because their sacrificial noncovalent cross-links are slow to reform after breaking. The fast recovery of physical protein hydrogels after large oscillatory strain and the short network relaxation timescales of hydrogels prepared from several EPE variants may prove useful for this purpose.

The effects of the network viscoelasticity on hydrogel toughness will be evaluated by performing tensile elongation to break experiments at different strain rates. Recent studies have suggested that deforming polymeric networks at strain rates that are much slower than the characteristic exchange time of transient physical cross-links results in enhancements to the fracture strain and fracture stress relative to faster strain rate experiments [11]. It may also be possible to address this issue by comparing the performance of hydrogels with different characteristic relaxation timescales prepared by the strategies described in Chapters 4 and 5.

Finally, tear tests including the trouser test and the pure shear test are regarded as better methods for evaluating the toughness of materials. These tests are used to determine the amount of energy required to generate a new surface by propagation of a defect or tear in the initial,

undeformed sample. Tough hydrogels typically have mechanisms for dissipating energy and preventing the propagation of defects so that the materials can be stretched further prior to failure. Whether these mechanisms exist in EPE hydrogels remains unclear. Preliminary trouser tear testing of an EPE hydrogel suggests that the fracture energy G_c is on the order of 10 J m^{-2}. While this value is greater than some conventional synthetic polymer hydrogels [1], it is still significantly lower than the values reported for double network hydrogels [21] and the polyacrylamide-*co*-alginate hydrogel [7].

6. Conclusions

Chemical-physical hydrogels prepared from the artificial protein EPE and chemical hydrogels prepared from the artificial proteins ERE and ER_CE were tested in uniaxial tension to determine their ultimate strength and elongation at break. Hydrogels prepared from EPE were the most extensible, with an average elongation of nearly 200%. They were also more extensible than ER_CE hydrogels despite having a similar stress to break. This may be due to either viscoelasticity of EPE hydrogels or to the mechanical unfolding or unzipping of the coiled-coil physical cross-links that has been described for several other tough hydrogels. EPE and ER_CE hydrogels also have similar moduli and swelling ratios, suggesting that the extensibility of protein networks can be tuned independently of other physical properties. Additional experiments have been proposed to determine whether EPE networks should be considered tough hydrogels and what the mechanism of toughening in these materials might be.

7. References

[1] S. Naficy, H.R. Brown, J.M. Razal, G.M. Spinks, and P.G. Whitten *Aust. J. Chem.* **2011** *64*, 1007-1025.

[2] X. Zhao *Soft Matter* **2014** *10*, 672-687.

[3] M. Malkoch, R. Vestberg, N. Gupta, L. Mespouille, P. Dubois, A.F. Mason, J.L. Hedrick, Q. Liao, C.W. Frank, K. Kingsbury, and C.J. Hawker *Chem. Commun.* **2006** 2774-2776.

[4] M.W. Tibbitt, A.M. Kloxin, L.A. Sawicki, K.S. Anseth *Macromolecules* **2013** *46*, 2785-2792.

[5] Y. Akagi, J.P. Gong, U.-i. Chung, T. Sakai *Macromolecules* **2013** *46*, 1035-1040.

[6] Y. Akagi, T. Katashima, Y. Katsumoto, K. Fujii, T. Matsunaga, U.-i. Chung, M. Shibayama, and T. Sakai *Macromolecules* **2011** *44*, 5817-5821.

[7] J.-Y. Sun, X. Zhao, W.R.K. Illeperuma, O. Chaudhuri, K.H. Oh, D.J. Mooney, J.J. Vlassak, and Z. Suo *Nature* **2012** *489*, 133-136.

[8] T.L. Sun, T. Kurokawa, S. Kuroda, A.B. Ihsan, T. Akasaki, K. Sato, M.A. Haque, T. Nakajima, and J.P. Gong *Nat. Mater.* **2013** *12*, 932-937.

[9] P. Lin, S. Ma, X. Wang, F. Zhou *Adv. Mater.* **2015** *27*, 2054-2059.

[10] K.J. Henderson, T.C. Zhou, K.J. Otim, K.R. Shull *Macromolecules* **2010** *43*, 6193-6201.

[11] Z.S. Kean, J.L. Hawk, S. Lin, X. Zhao, R.P. Sijbesma, and S.L. Craig *Adv. Mater.* **2014** *26*, 6013-6018.

[12] T. Bornschlögl, J.C.M. Gebhardt, M. Rief *ChemPhysChem* **2009** *10*, 2800-2804.

[13] T. Bornschlögl, M. Rief *Phys. Rev. Lett.* **2006** *96*, 118102.

[14] M.M. Stevens, S. Allen, J.K. Sakata, M.C. Davies, C.J. Roberts, S.J.B. Tendler, D.A. Tirrell, and P.M. Williams *Langmuir* **2004** *20*, 7747-7752.

[15] W. Shen, J.A. Kornfield, D.A. Tirrell *Macromolecules* **2007** *40*, 689-692.

[16] J. Fang, A. Mehlich, N. Koga, J. Huang, R. Koga, X. Gao, C. Hu, C. Jin, M. Rief, J. Kast, D. Baker, and H. Li *Nat. Commun.* **2013** *4*.

[17] M.J. Glassman, R.K. Avery, A. Khademhosseini, B.D. Olsen *Biomacromolecules* **2016** *17*, 415-426.

[18] S. Lv, D.M. Dudek, Y. Cao, M.M. Balamurali, J. Gosline, and H. Li *Nature* **2010** *465*, 69-73.

[19] S. Tang, M.J. Glassman, S. Li, S. Socrate, and B.D. Olsen *Macromolecules* **2014** *47*, 791-799.

[20] B.D. Olsen, J.A. Kornfield, D.A. Tirrell *Macromolecules* **2010** *43*, 9094-9099.

[21] J.P. Gong *Soft Matter* **2010** *6*, 2583-2590.

Appendix A

LIST OF STRAINS, VECTORS, AND PLASMIDS

TABLE OF CONTENTS

A.1 Strains for Cloning and Protein Expression

DH10B

Genotype: F- *mcrA* Δ*(mrr-hsdRMS-mcrBC)* φ80d*lacZ*ΔM15 *lac*X74 *rec*A1 *end*A1 *ara*D139 Δ(*ara, leu*)7697 *gal*U *gal*K λ- *rps*L *nup*G *ton*A

Source: Invitrogen Max Efficiency DH10B-$T1^R$ (from Kai Yuet)

Use(s): Cloning strain. Plasmid storage and propagation. Preparation of chemically competent bacteria using the Mix & Go *E. coli* Transformation kit (Zymo Research).

Notes: Resistant to phage T1 and T5 infection (*ton*A)

Availability: (1) 25 v/v % glycerol stock

(2) Invitrogen Cat. No. 12331-013

BL21

Genotype: F- *fhuA2 [lon] ompT gal [dcm]* Δ*hsdS*

Source: New England BioLabs

Use(s): Protein expression strain. Preparation of chemically competent bacteria using the Mix & Go *E. coli* Transformation kit (Zymo Research).

Notes: Resistant to phage T1 and T5 infection (*fhuA2*, synonym for *tonA*). This strain does not contain the DE3 lysogen and cannot be used to express proteins from the T7 promoter.

Availability: (1) 25 v/v % glycerol stock

(2) NEB Cat. No. C2530H

A.2 Vectors for Cloning and Protein Expression

pUC19

Strain(s)/Plasmid: DH10B/pUC19

Antibiotic Resistance: Ampicillin

Size 2686 bp

Description: Standard cloning strain developed by Messing and coworkers (*Gene*. 33, 103-119). Site-directed mutagenesis of the P coding region to generate P variants was carried out in pUC19 due to its small size as well as the lack of elastin domains present in pQE-80L EPE, which were found to complicate the mutagenesis protocol.

The multiple cloning site of pUC19 contains numerous restriction enzymes. *EcoRI* and *XbaI* were used to subclone P.

Sequencing primers: M13F, M13R available from most sequencing facilities.

Available Sources: (1) miniprep DNA (-20°C)

(2) 25 v/v % glycerol stock in (a) DH10B

(3) Addgene plasmid #50005

pQE-80L

Strain(s)/Plasmid: None

Antibiotic Resistance: Ampicillin

Size 4751 bp

Description: Qiagen vector for protein expression in *E coli*. T5 promoter recruits endogenous RNA polymerase (ie. DE3 lysogen is not required for T7 RNAP mediated transcription). Contains two copies of lac operator (lacO) in promoter region to regulate transcription. Contains a copy of lac repressor gene (lacI) (ie. pREP4 plasmid is not required as it is for other *trans*-repressed pQE vectors). The ribosomal binding site (RBS) is located several bp upstream of the start codon. The vector contains a sequence encoding an N-terminal 6xHis tag for IMAC purification. This can be removed by cloning at the *EcoRI* restriction enzyme site, however this site is upstream of the RBS and start codon so these elements must be included in the sequence subcloned into this site.

Note: The pQE-80L vectors used in this work were all modified to remove the XhoI restriction site at position 1.

Sequencing primers: pQEfor 5' CCC GAA AAG TGC CAC CTG
pQErev 5' GTT CTG AGG TCA TTA CTG G

Available Sources: (1) Qiagen Cat. No. 32943

A.3 Plasmids Encoding Artificial Protein Genes

pUC19 P

Submitted by: Larry Dooling

Strain(s)/Plasmid: DH10B/pUC19 P

Vector: pUC19

Insert: P

Antibiotic Resistance: Ampicillin

Description: P coiled coil domain in the pUC19 vector for mutagenesis. Does not contain start/stop codons. This plasmid is not for protein expression.

Construction: The P domain was amplified from pQE-80L EPE with *EcoRI* and *XbaI* overhangs, digested and subcloned into pUC19 at the same sites.

Available Sources: (1) miniprep DNA (-20°C)

(2) 25 v/v % glycerol stock in DH10B (-80°C)

Plasmid Map:

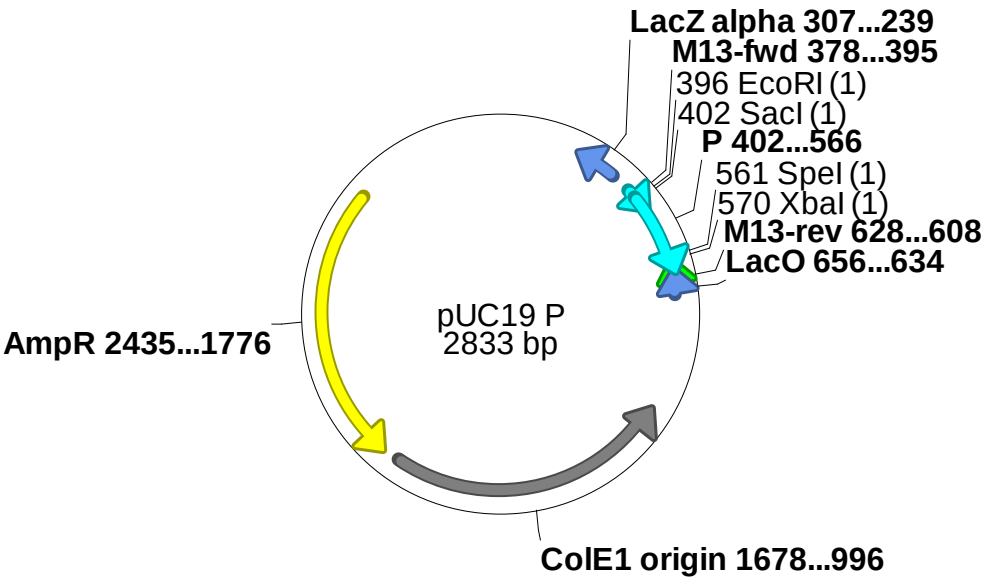

Coding sequence *(EcoRI to XbaI)*:

GAATTCGAGCTCGGATCAGGACTTGGATCCGCGCCGCAAATGCTGCGTGAACTGCA
GGAAACCAATGCCGCGCTTCAGGATGTGCGGGAATTGCTTCGTCAACAGGTCAAGG
AGATAACGTTCTTGAAGAACACCGTCATGGAGTCGGATGCGTCCAAGCTTAATACTA
GTGTGTCTAGA

Translation *(EcoRI to XbaI)*:

EFELGSGLGSAPQMLRELQETNAALQDVRELLRQQVKEITFLKNTVMESDASKLNTSVS
R

pUC19 A

Submitted by: Larry Dooling

Strain(s)/Plasmid: DH10B/pUC19 A

Vector: pUC19

Insert: A

Antibiotic Resistance: Ampicillin

Description: A coiled coil domain in the pUC19 vector. Does not contain start/stop codons.

Construction: The A domain was amplified by PCR from pQE-9 PC10A with *SacI* and *SpeI* overhangs, digested and subcloned into pUC19 at the same sites.

Available Sources: (1) miniprep DNA (-20°C)

(2) 25 v/v % glycerol stock in DH10B (-80°C)

Plasmid Map:

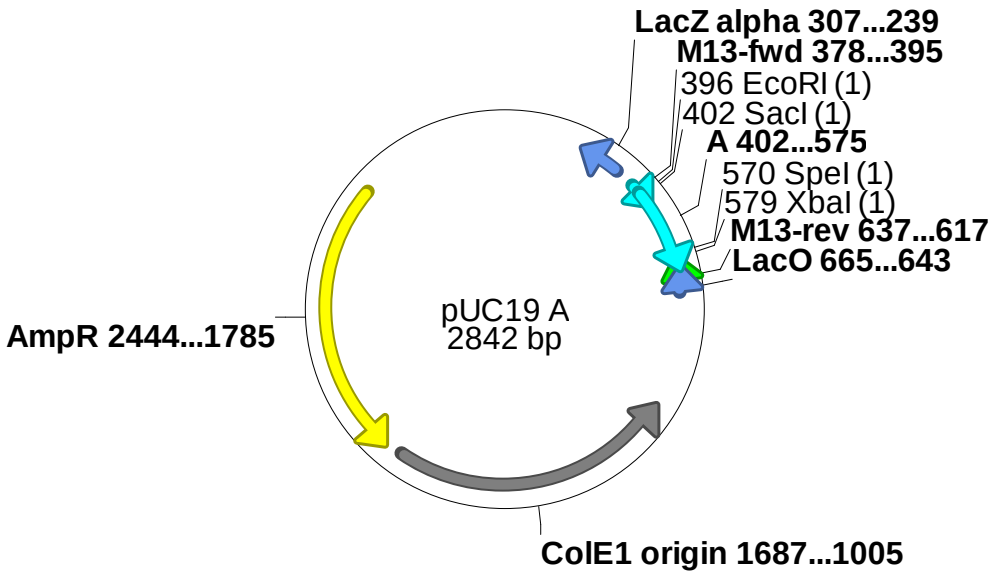

Coding sequence *(EcoRI to XbaI)*:

GAATTCGAGCTCATGCCGACTAGCGGTGACCTGGAAAACGAAGTGGCCCAGCTGGA
AAGGGAAGTTAGATCTCTGGAAGATGAAGCGGCTGAACTGGAACAAAAAGTCTCGA
GACTGAAAAATGAAATCGAAGACCTGAAAGCCGAAATTGGTGACCATGTGGCGCCT
CGAGACACTAGTGTGTCTAGA

Translation *(EcoRI to XbaI)*:

EFELMPTSGDLENEVAQLEREVRSLEDEAAELEQKVSRLKNEIEDLKAEIGDHVAPRDTS
VSR

pUC19 P L37A

Submitted by: Larry Dooling

Strain(s)/Plasmid: DH10B/pUC19 P L37A

Vector: pUC19

Insert: P L37A

Antibiotic Resistance: Ampicillin

Description: P coiled coil domain with L37A mutation based on Gunasekar *et al.*, *Biochemistry* 2009.

Construction: The P domain in pUC19 P was mutated by Quick Change with the following primers:

(+) CAA ATG CTG CGT GAA **GCG** CAG GAA ACC AAT GCC
(-) GGC ATT GGT TTC CTG **CGC** TTC ACG CAG CAT TTG

Available Sources: (1) miniprep DNA (-20°C)

(2) 25 v/v % glycerol stock in DH10B (-80°C)

Plasmid Map:

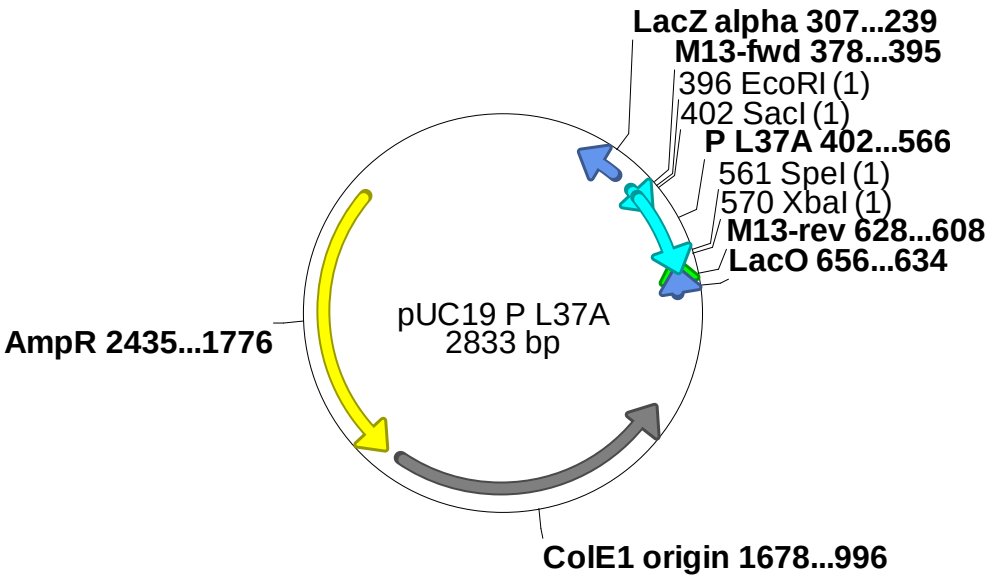

Coding sequence *(EcoRI to XbaI)*:

GAATTCGAGCTCGGATCAGGACTTGGATCCGCGCCGCAAATGCTGCGTGAAGCGCA
GGAAACCAATGCCGCGCTTCAGGATGTGCGGGAATTGCTTCGTCAACAGGTCAAGG
AGATAACGTTCTTGAAGAACACCGTCATGGAGTCGGATGCGTCCAAGCTTAATACTA
GTGTGTCTAGA

Translation *(EcoRI to XbaI)*:

EFELGSGLGSAPQMLREAQETNAALQDVRELLRQQVKEITFLKNTVMESDASKLNTSVS
R

pUC19 P L37V

Submitted by: Larry Dooling

Strain(s)/Plasmid: DH10B/pUC19 P L37V

Vector: pUC19

Insert: P L37V

Antibiotic Resistance: Ampicillin

Description: P coiled coil domain with L37V mutation. This mutation was not made in Gunasekar *et al.*, *Biochemistry* 2009, but is at the same position as the L37A mutation in that work.

Construction: The P domain in pUC19 P was mutated by Quick Change with the following primers:

(+) CAA ATG CTG CGT GAA **GTG** CAG GAA ACC AAT GCC
(-) GGC ATT GGT TTC CTG **CAC** TTC ACG CAG CAT TTG

Available Sources: (1) miniprep DNA (-20°C)

(2) 25 v/v % glycerol stock in DH10B (-80°C)

Plasmid Map:

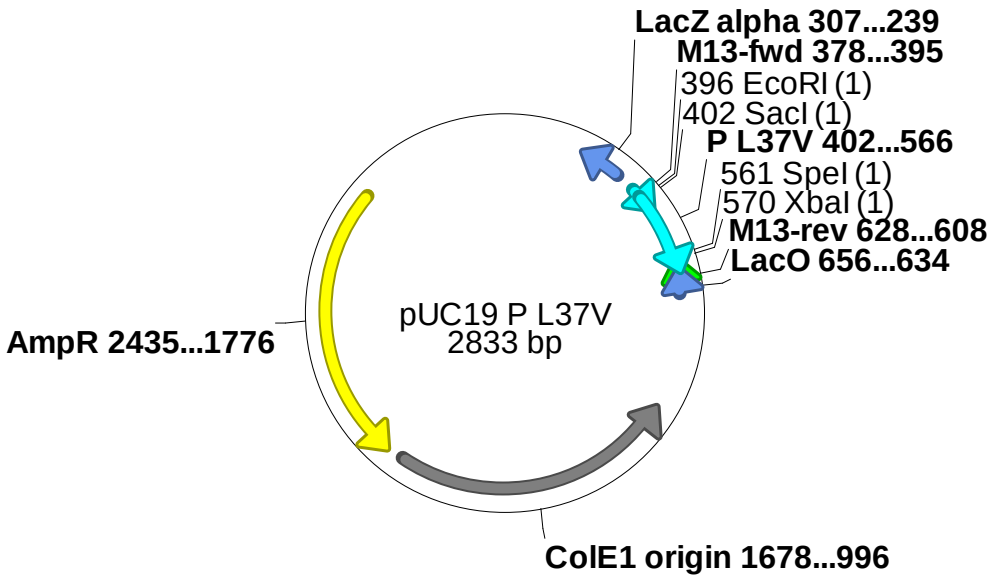

Coding sequence *(EcoRI to XbaI)*:

GAATTCGAGCTCGGATCAGGACTTGGATCCGCGCCGCAAATGCTGCGTGAAGTGCA
GGAAACCAATGCCGCGCTTCAGGATGTGCGGGAATTGCTTCGTCAACAGGTCAAGG
AGATAACGTTCTTGAAGAACACCGTCATGGAGTCGGATGCGTCCAAGCTTAATACTA
GTGTGTCTAGA

Translation *(EcoRI to XbaI)*:

EFELGSGLGSAPQMLREVQETNAALQDVRELLRQQVKEITFLKNTVMESDASKLNTSVS
R

pUC19 P L37I

Submitted by: Larry Dooling

Strain(s)/Plasmid: DH10B/pUC19 P L37I

Vector: pUC19

Insert: P L37I

Antibiotic Resistance: Ampicillin

Description: P coiled coil domain with L37I mutation. This mutation was not made in Gunasekar *et al.*, *Biochemistry* 2009, but is at the same position as the L37A mutation in that work.

Construction: The P domain in pUC19 P was mutated by Quick Change with the following primers:

(+) CAA ATG CTG CGT GAA **ATT** CAG GAA ACC AAT GCC
(-) GGC ATT GGT TTC CTG **CAC** TTC ACG CAG CAT TTG

Available Sources: (1) miniprep DNA (-20°C)

(2) 25 v/v % glycerol stock in DH10B (-80°C)

Plasmid Map:

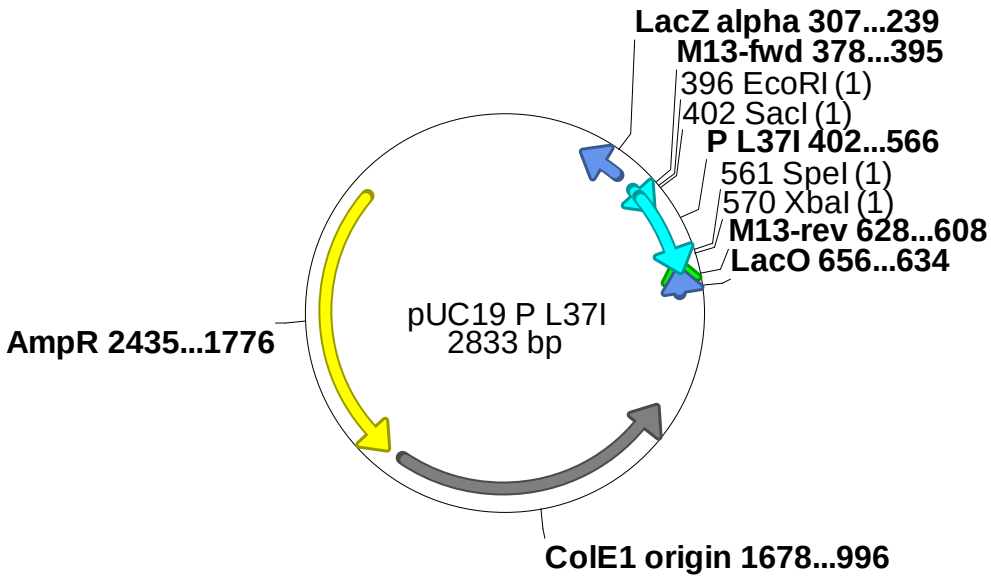

Coding sequence *(EcoRI to XbaI)*:

GAATTCGAGCTCGGATCAGGACTTGGATCCGCGCCGCAAATGCTGCGTGAAATTCA
GGAAACCAATGCCGCGCTTCAGGATGTGCGGGAATTGCTTCGTCAACAGGTCAAGG
AGATAACGTTCTTGAAGAACACCGTCATGGAGTCGGATGCGTCCAAGCTTAATACTA
GTGTGTCTAGA

Translation *(EcoRI to XbaI)*:

EFELGSGLGSAPQMLREIQETNAALQDVRELLRQQVKEITFLKNTVMESDASKLNTSVS
R

pUC19 P L44A

Submitted by: Larry Dooling

Strain(s)/Plasmid: DH10B /pUC19 P L44A

Vector: pUC19

Insert: P L44A

Antibiotic Resistance: Ampicillin

Description: P coiled coil domain with L44A mutation based on Gunasekar *et al.*, *Biochemistry* 2009.

Construction: The P domain in pUC19 P was mutated by Quick Change with the following primers:

(+) CAG GAA ACC AAT GCC GCG **GCT** CAG GAT GTG CGG GAA TTG C
(-) GCA ATT CCC GCA CAT CCT GA**G** **C**CG CGG CAT TGG TTT CCT G

Available Sources: (1) miniprep DNA (-20°C)

(2) 25 v/v % glycerol stock in DH10B (-80°C)

Plasmid Map:

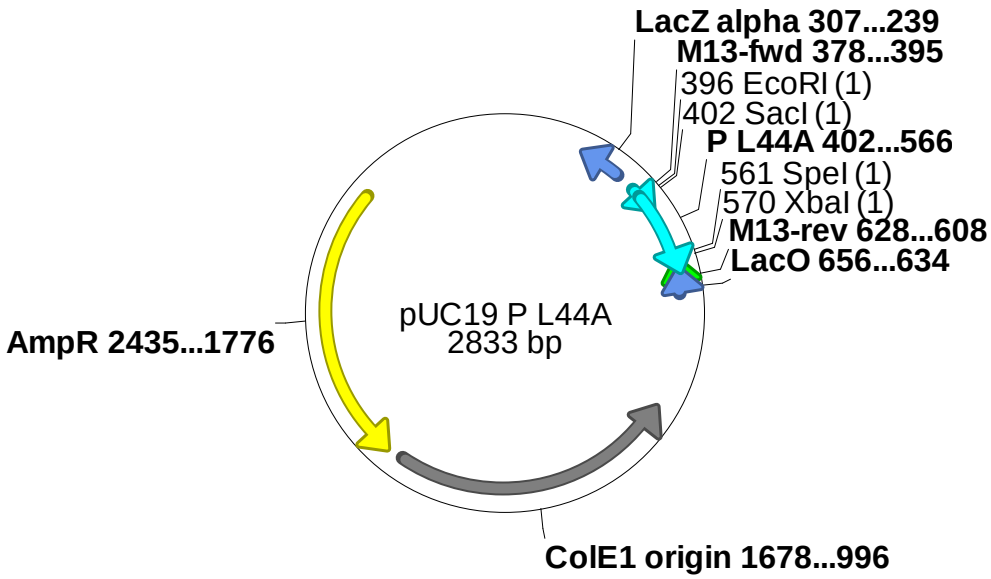

Coding sequence *(EcoRI to XbaI)*:

GAATTCGAGCTCGGATCAGGACTTGGATCCGCGCCGCAAATGCTGCGTGAACTGCA
GGAAACCAATGCCGCGGCTCAGGATGTGCGGGAATTGCTTCGTCAACAGGTCAAGG
AGATAACGTTCTTGAAGAACACCGTCATGGAGTCGGATGCGTCCAAGCTTAATACTA
GTGTGTCTAGA

Translation *(EcoRI to XbaI)*:

EFELGSGLGSAPQMLRELQETNAAAQDVRELLRQQVKEITFLKNTVMESDASKLNTSVS
R

pUC19 P T40A

Submitted by: Larry Dooling

Strain(s)/Plasmid: DH10B/pUC19 P T40A

Vector: pUC19

Insert: P T40A

Antibiotic Resistance: Ampicillin

Description: P coiled coil domain with T40A mutation based on Gunasekar *et al.*, *Biochemistry* 2009.

Construction: The P domain in pUC19 P was mutated by Quick Change with the following primers:

(+) GAA CTG CAG GAA **GCC** AAT GCC GCG C
(-) G CGC GGC ATT **GGC** TTC CTG CAG TTC

Available Sources: (1) miniprep DNA (-20°C)

(2) 25 v/v % glycerol stock in DH10B (-80°C)

Plasmid Map:

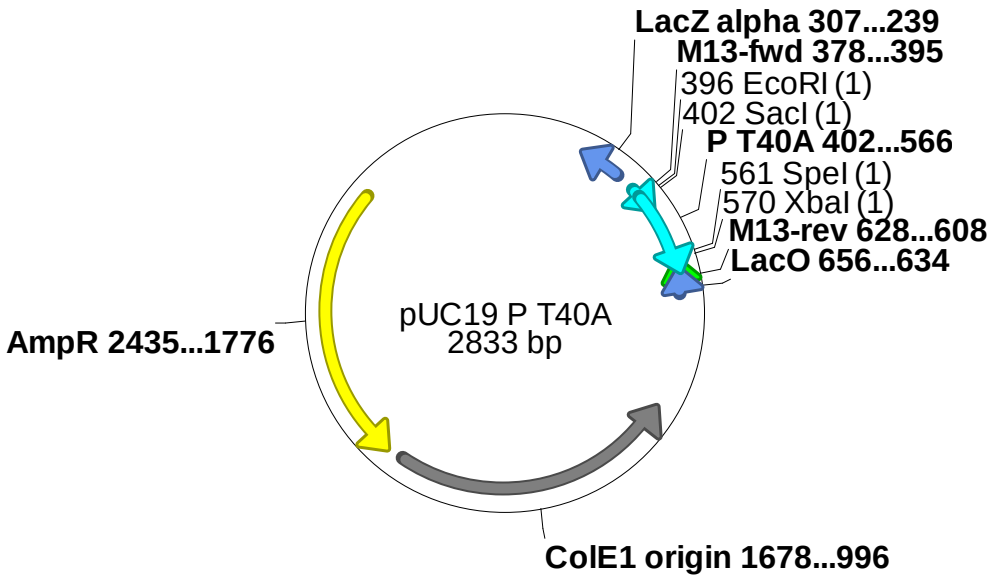

Coding sequence *(EcoRI to XbaI)*:

GAATTCGAGCTCGGATCAGGACTTGGATCCGCGCCGCAAATGCTGCGTGAACTGCA
GGAAGCCAATGCCGCGCTTCAGGATGTGCGGGAATTGCTTCGTCAACAGGTCAAGG
AGATAACGTTCTTGAAGAACACCGTCATGGAGTCGGATGCGTCCAAGCTTAATACTA
GTGTGTCTAGA

Translation *(EcoRI to XbaI)*:

EFELGSGLGSAPQMLRELQEANAALQDVRELLRQQVKEITFLKNTVMESDASKLNTSVS
R

pUC19 P Q54A

Submitted by: Larry Dooling

Strain(s)/Plasmid: DH10B/pUC19 P Q54A

Vector: pUC19

Insert: P Q54A

Antibiotic Resistance: Ampicillin

Description: P coiled coil domain with Q54A mutation based on Gunasekar *et al., Biochemistry* 2009.

Construction: The P domain in pUC19 P was mutated by Quick Change with the following primers:

(+) GAA TTG CTT CGT CAA **GCG** GTC AAG GAG ATA AC
(-) GT TAT CTC CTT GAC **CGC** TTG ACG AAG CAA TTC

Available Sources: (1) miniprep DNA (-20°C)

(2) 25 v/v % glycerol stock in DH10B (-80°C)

Plasmid Map:

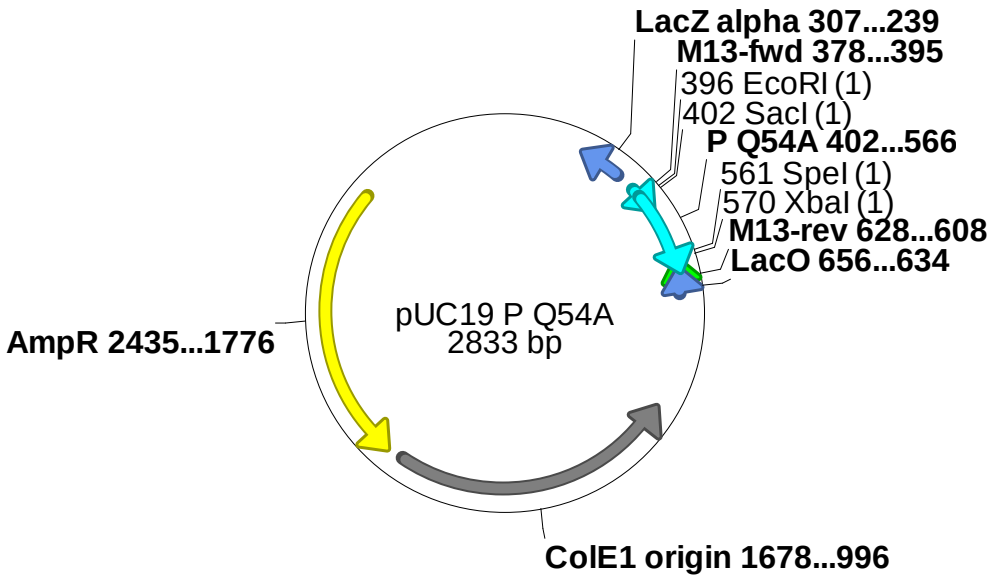

Coding sequence *(EcoRI to XbaI)*:

GAATTCGAGCTCGGATCAGGACTTGGATCCGCGCCGCAAATGCTGCGTGAACTGCA
GGAAACCAATGCCGCGCTTCAGGATGTGCGGGAATTGCTTCGTCAAGCGGTCAAGG
AGATAACGTTCTTGAAGAACACCGTCATGGAGTCGGATGCGTCCAAGCTTAATACTA
GTGTGTCTAGA

Translation *(EcoRI to XbaI)*:

EFELGSGLGSAPQMLRELQETNAALQDVRELLRQAVKEITFLKNTVMESDASKLNTSVS
R

pUC19 P I58A

Submitted by: Larry Dooling

Strain(s)/Plasmid: DH10B/pUC19 P I58A

Vector: pUC19

Insert: P I58A

Antibiotic Resistance: Ampicillin

Description: P coiled coil domain with I58A mutation based on Gunasekar *et al.*, *Biochemistry* 2009.

Construction: The P domain in pUC19 P was mutated by Quick Change with the following primers:

(+) CAG GTC AAG GAG **GCA** ACG TTC TTG AAG
(-) CTT CAA GAA CGT **TGC** CTC CTT GAC CTG

Available Sources: (1) miniprep DNA (-20°C)

(2) 25 v/v % glycerol stock in DH10B (-80°C)

Plasmid Map:

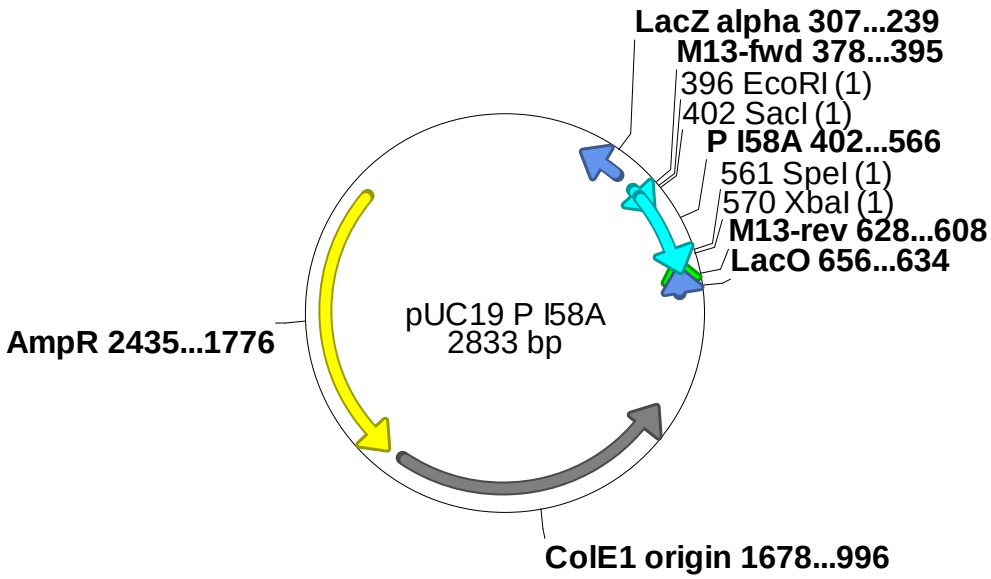

Coding sequence *(EcoRI to XbaI)*:

GAATTCGAGCTCGGATCAGGACTTGGATCCGCGCCGCAAATGCTGCGTGAACTGCA
GGAAACCAATGCCGCGCTTCAGGATGTGCGGGAATTGCTTCGTCAACAGGTCAAGG
AGGCAACGTTCTTGAAGAACACCGTCATGGAGTCGGATGCGTCCAAGCTTAATACTA
GTGTGTCTAGA

Translation *(EcoRI to XbaI)*:

EFELGSGLGSAPQMLRELQETNAALQDVRELLRQQVKEATFLKNTVMESDASKLNTSV
SR

pQE-80L EPE

Submitted by: Wen-Bin Zhang/Larry Dooling

Strain(s)/Plasmid: DH10B/pQE-80L EPE
BL21/pQE-80L EPE

Vector: pQE-80L

Insert: EPE

Antibiotic Resistance: Ampicillin

Description: Hydrophilic elastin-like repeats $[(VPGVG)_2VPGEG(VPGVG)_2]_3$ flanking a P coiled coil motif. N- and C-terminal Cys residues facilitate cross-linking with 4-arm PEG maleimide, vinyl sulfone, etc.

Construction: Prepared by Wen-Bin Zhang.

Available Sources: (1) miniprep DNA (-20°C)

(2) 25 v/v % glycerol stock in DH10B (-80°C)

(3) 25 v/v % glycerol stock in BL21 (-80°C)

Plasmid Map:

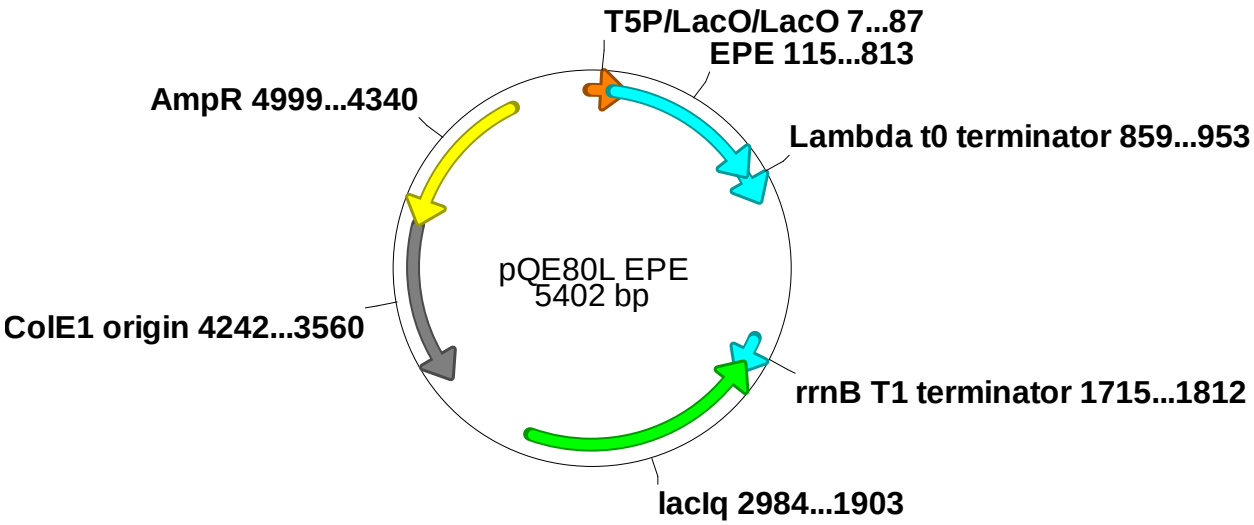

Coding sequence:

ATGAGATGCAGCAGCCATCATCATCATCATCACGTCGACGGCCACGGCGTGGGTGTT
CCGGGCGTCGGTGTGCCGGGTGTGGGTGTGCCGGGCGAAGGTGTGCCGGGCGTCGG
TGTGCCGGGTGTTGGTGTTCCGGGCGTTGGTGTGCCGGGCGTTGGCGTGCCGGGCGA
GGGTGTGCCGGGCGTTGGTGTTCCGGGCGTGGGTGTGCCGGGCGTGGGCGTGCCGG
GCGTCGGTGTTCCGGGCGAGGGTGTGCCGGGCGTAGGTGTGCCGGGCGTTGGTGAG
CTCGGATCAGGACTTGGATCCGCGCCGCAAATGCTGCGTGAACTGCAGGAAACCAA
TGCCGCGCTTCAGGATGTGCGGGAATTGCTTCGTCAACAGGTCAAGGAGATAACGTT
CTTGAAGAACACCGTCATGGAGTCGGATGCGTCCAAGCTTAATACTAGTGTGCCGGG
CGTCGGCGTGCCGGGCGTAGGTGTTCCGGGCGAGGGTGTTCCGGGCGTTGGTGTGCC
GGGCGTCGGCGTGCCGGGCGTGGGTGTTCCGGGCGTAGGTGTGCCGGGCGAGGGTG
TGCCGGGCGTGGGCGTGCCGGGCGTAGGTGTTCCGGGCGTAGGTGTTCCGGGCGTA
GGTGTTCCGGGTGAAGGCGTGCCGGGCGTTGGTGTGCCGGGTGTGGGCGTGCCGGG
CGGGCTGCTCGAGTGCATGTAA

Translation:

MRCSSHHHHHHVDGHGVGVPGVGVPGVGVPGEGVPGVGVPGVGVPGVGVPGVGVPG
EGVPGVGVPGVGVPGVGVPGVGVPGEGVPGVGVPGVGELGSGLGSAPQMLRELQETN
AALQDVRELLRQQVKEITFLKNTVMESDASKLNTSVPGVGVPGVGVPGEGVPGVGVPG
VGVPGVGVPGVGVPGEGVPGVGVPGVGVPGVGVPGVGVPGEGVPGVGVPGVGVPGG
LLECM*

pQE-80L ERE

Submitted by: Wen-Bin Zhang/Larry Dooling

Strain(s)/Plasmid: DH10B/pQE-80L ERE
BL21/pQE-80L ERE

Vector: pQE-80L

Insert: ERE

Antibiotic Resistance: Ampicillin

Description: Hydrophilic elastin-like repeats $[(VPGVG)_2VPGEG(VPGVG)_2]_3$ flanking a 17mer RGD motif. N- and C-terminal Cys residues facilitate cross-linking with 4-arm PEG maleimide, vinyl sulfone, etc. The MMP1 recognition sequence (GPQGIWGQ) is included before the C-terminal Cys. Also originally denoted as CEC for Cysteine-Elastin-Cysteine.

Construction: Prepared by Wen-Bin Zhang.

Available Sources: (1) miniprep DNA (-20°C)

(2) 25 v/v % glycerol stock in DH10B (-80°C)

(3) 25 v/v % glycerol stock in BL21 (-80°C)

Plasmid Map:

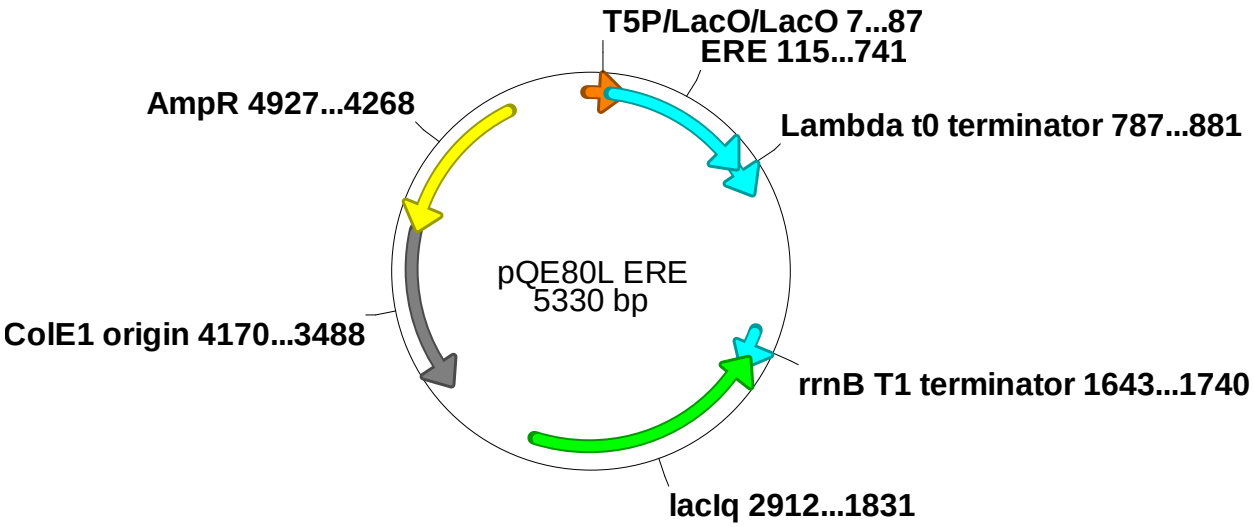

Coding sequence:

ATGAGATGCAGCAGCCATCATCATCATCATCACGTCGACGGCCACGGCGTGGGTGTT
CCGGGGCGTCGGTGTGCCGGGTGTGGGTGTGCCGGGCGAAGGTGTGCCGGGCGTCGG
TGTGCCGGGTGTTGGTGTTCCGGGCGTTGGTGTGCCGGGCGTTGGCGTGCCGGGCGA
GGGTGTGCCGGGCGTTGGTGTTCCGGGCGTGGGTGTGCCGGGCGTGGGCGTGCCGG
GCGTCGGTGTTCCGGGCGAGGGTGTGCCGGGCGTAGGTGTGCCGGGCGTTGGTGAG
CTCTATGCGGTTACCGGCCGTGGTGATAGTCCGGCCAGCTCTGCCCCGATCGCCACT
AGTGTGCCGGGCGTCGGCGTGCCGGGCGTAGGTGTTCCGGGCGAGGGTGTTCCGGG
CGTTGGTGTGCCGGGCGTCGGCGTGCCGGGCGTGGGTGTTCCGGGCGTAGGTGTGCC
GGGCGAGGGTGTGCCGGGCGTGGGCGTGCCGGGCGTAGGTGTTCCGGGCGTAGGTG
TTCCGGGCGTAGGTGTTCCGGGTGAAGGCGTGCCGGGCGTTGGTGTGCCGGGTGTGG
GCGTGCCGGGCGGGCTGCTCGACGGTCCGCAAGGTATTTGGGGTCAGCTCGAGTGC
ATGTAA

Translation:

MRCSSHHHHHHVDGHGVGVPGVGVPGVGVPGEGVPGVGVPGVGVPGVGVPGVGVPG
EGVPGVGVPGVGVPGVGVPGVGVPGEGVPGVGVPGVGELYAVTGRGDSPASSAPIATS
VPGVGVPGVGVPGEGVPGVGVPGVGVPGVGVPGVGVPGEGVPGVGVPGVGVPGVGVP
GVGVPGEGVPGVGVPGVGVPGGLLDGPQGIWGQLECM*

pQE-80L ER_CE

Submitted by: Larry Dooling

Strain(s)/Plasmid: DH10B/pQE-80L ER_CE
BL21/pQE-80L ER_CE

Vector: pQE-80L

Insert: ER_CE or ERE S104C

Antibiotic Resistance: Ampicillin

Description: Hydrophilic elastin-like repeats $[(VPGVG)_2VPGEG(VPGVG)_2]_3$ flanking a 17mer RGD motif. N- and C-terminal Cys residues facilitate cross-linking with 4-arm PEG maleimide, vinyl sulfone, etc. The MMP1 recognition sequence (GPQGIWGQ) is included before the C-terminal Cys. The RGD domains contains a Ser to Cys mutation (RGDS → RGDC) to introduce a cross-linking site in the middle of the protein. This new RGD domain is abbreviated R_C.

Construction: Serine 104 was mutated to cysteine by Quick Change of pQE-80L ERE with the following primers:

(+) GTT ACC GGC CGT GGT GAT **TGT** CCG GCC AGC TCT GCC
(-) GGC AGA GCT GGC CGG **ACA** ATC ACC ACG GCC GGT AAC

This resulted in the correct mutation but was accompanied by the deletion of the C-terminal E domain. To generate the correct construct, the *EcoRI-SpeI* fragment of this plasmid was isolated by restriction enzyme digestion and subcloned into pQE-80L ERE digested with the same enzymes (replacing ER with ER_C).

Available Sources: (1) miniprep DNA (-20°C)

(2) 25 v/v % glycerol stock in DH10B (-80°C)

(3) 25 v/v % glycerol stock in BL21 (-80°C)

Plasmid Map:

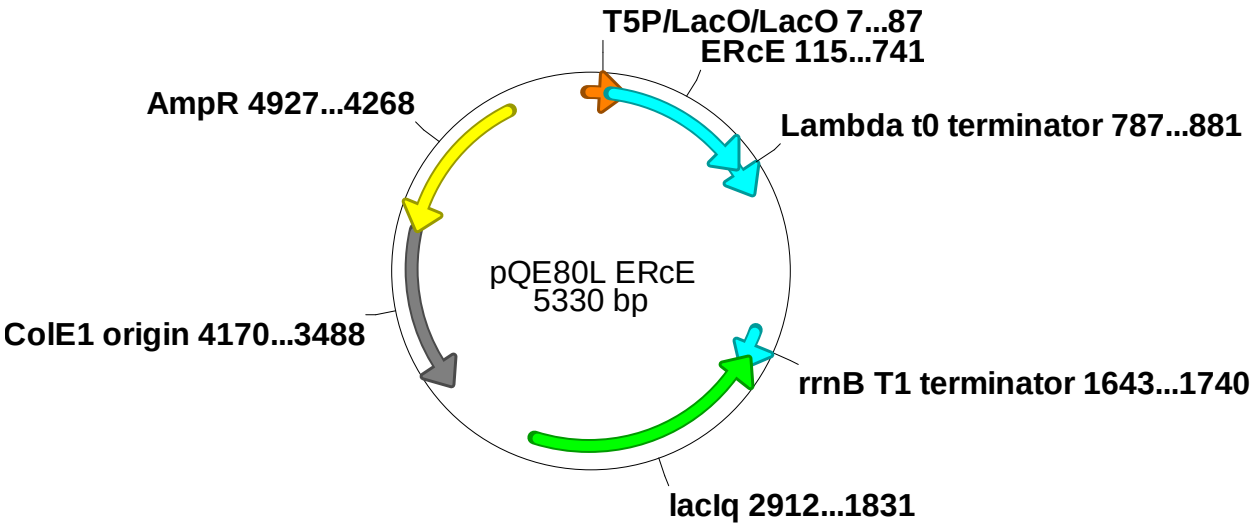

Coding sequence:

ATGAGATGCAGCAGCCATCATCATCATCATCACGTCGACGGCCACGGCGTGGGTGTT
CCGGGCGTCGGTGTGCCGGGTGTGGGTGTGCCGGGCGAAGGTGTGCCGGGCGTCGG
TGTGCCGGGTGTTGGTGTTCCGGGCGTTGGTGTGCCGGGCGTTGGCGTGCCGGGCGA
GGGTGTGCCGGGCGTTGGTGTTCCGGGCGTGGGTGTGCCGGGCGTGGGCGTGCCGG
GCGTCGGTGTTCCGGGCGAGGGTGTGCCGGGCGTAGGTGTGCCGGGCGTTGGTGAG
CTCTATGCGGTTACCGGCCGTGGTGATTGTCCGGCCAGCTCTGCCCCGATCGCCACT
AGTGTGCCGGGCGTCGGCGTGCCGGGCGTAGGTGTTCCGGGCGAGGGTGTTCCGGG
CGTTGGTGTGCCGGGCGTCGGCGTGCCGGGCGTGGGTGTTCCGGGCGTAGGTGTGCC
GGGCGAGGGTGTGCCGGGCGTGGGCGTGCCGGGCGTAGGTGTTCCGGGCGTAGGTG
TTCCGGGCGTAGGTGTTCCGGGTGAAGGCGTGCCGGGCGTTGGTGTGCCGGGTGTGG
GCGTGCCGGGCGGGCTGCTCGACGGTCCGCAAGGTATTTGGGGTCAGCTCGAGTGC
ATGTAA

Translation:

MRCSSHHHHHHVDGHGVGVPGVGVPGVGVPGEGVPGVGVPGVGVPGVGVPGVGVPG
EGVPGVGVPGVGVPGVGVPGVGVPGEGVPGVGVPGVGELYAVTGRGDCPASSAPIATS
VPGVGVPGVGVPGEGVPGVGVPGVGVPGVGVPGVGVPGEGVPGVGVPGVGVPGVGVP
GVGVPGEGVPGVGVPGVGVPGGLLDGPQGIWGQLECM*

pQE-80L EAE

Submitted by: Larry Dooling

Strain(s)/Plasmid: DH10B/pQE-80L EAE
BL21/pQE-80L EAE

Vector: pQE-80L

Insert: EAE

Antibiotic Resistance: Ampicillin

Description: Hydrophilic elastin-like repeats $[(VPGVG)_2VPGEG(VPGVG)_2]_3$ flanking a A coiled coil/leucine zipper motif.

Construction: The A domain was amplified by PCR from pQE-9 PC10A with *SacI* and *SpeI* overhangs, digested and subcloned into the similarly-digested pQE-80L EPE plasmid.

Available Sources: (1) miniprep DNA (-20°C)

(2) 25 v/v % glycerol stock in DH10B (-80°C)

(3) 25 v/v % glycerol stock in BL21 (-80°C)

Plasmid Map:

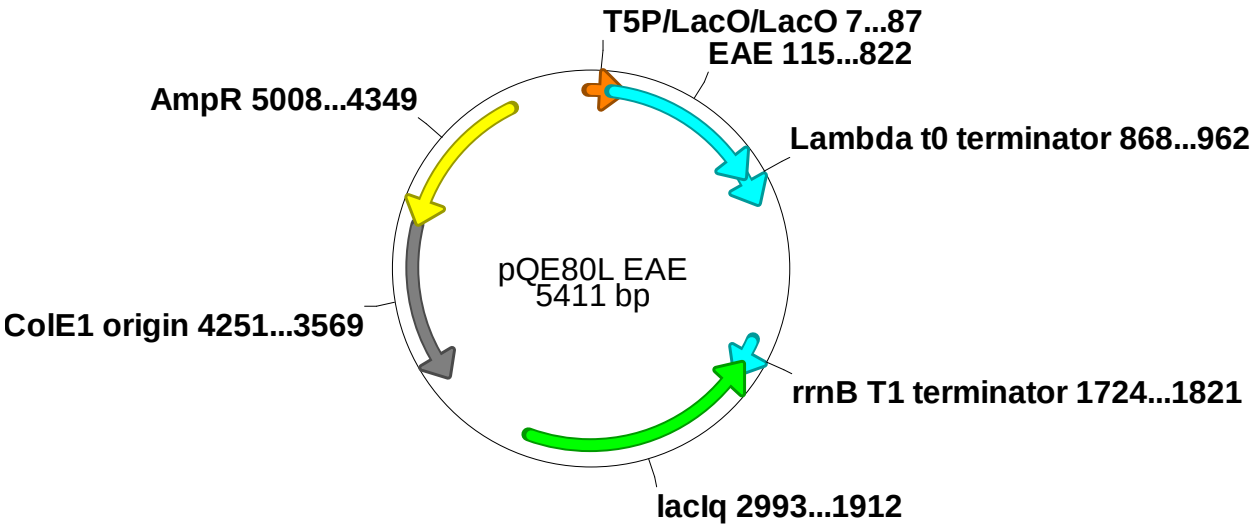

Coding sequence:

ATGAGATGCAGCAGCCATCATCATCATCACGTCGACGGCCACGGCGTGGGTGTT
CCGGGCGTCGGTGTGCCGGGTGTGGGTGTGCCGGGCGAAGGTGTGCCGGGCGTCGG
TGTGCCGGGTGTTGGTGTTCCGGGCGTTGGTGTGCCGGGCGTTGGCGTGCCGGGCGA
GGGTGTGCCGGGCGTTGGTGTTCCGGGCGTGGGTGTGCCGGGCGTGGGCGTGCCGG
GCGTCGGTGTTCCGGGCGAGGGTGTGCCGGGCGTAGGTGTGCCGGGCGTTGGTGAG
CTCATGCCGACTAGCGGTGACCTGGAAAACGAAGTGGCCCAGCTGGAAAGGGAAGT
TAGATCTCTGGAAGATGAAGCGGCTGAACTGGAACAAAAAGTCTCGAGACTGAAAA
ATGAAATCGAAGACCTGAAAGCCGAAATTGGTGACCATGTGGCGCCTCGAGACACT
AGTGTGCCGGGCGTCGGCGTGCCGGGCGTAGGTGTTCCGGGCGAGGGTGTTCCGGG
CGTTGGTGTGCCGGGCGTCGGCGTGCCGGGCGTGGGTGTTCCGGGCGTAGGTGTGCC
GGGCGAGGGTGTGCCGGGCGTGGGCGTGCCGGGCGTAGGTGTTCCGGGCGTAGGTG
TTCCGGGCGTAGGTGTTCCGGGTGAAGGCGTGCCGGGCGTTGGTGTGCCGGGTGTGG
GCGTGCCGGGCGGGCTGCTCGAGTGCATGTAA

Translation:

MRCSSHHHHHHVDGHGVGVPGVGVPGVGVPGEGVPGVGVPGVGVPGVGVPGVGVPG
EGVPGVGVPGVGVPGVGVPGVGVPGEGVPGVGVPGVGELMPTSGDLENEVAQLEREV
RSLEDEAAELEQKVSRLKNEIEDLKAEIGDHVAPRDTSVPGVGVPGVGVPGEGVPGVGV
PGVGVPGVGVPGVGVPGEGVPGVGVPGVGVPGVGVPGVGVPGEGVPGVGVPGVGVPG
GLLECM*

pQE-80L EPE L37A

Submitted by: Larry Dooling

Strain(s)/Plasmid: DH10B1/pQE-80L EPE L37A
BL21/pQE-80L EPE L37A

Vector: pQE-80L

Insert: EPE L37A

Antibiotic Resistance: Ampicillin

Description: Hydrophilic elastin-like repeats $[(VPGVG)_2VPGEG(VPGVG)_2]_3$ flanking a P coiled coil motif containing the L37A mutation.

Construction: The P domain was isolated from pUC19 P L37A by digestion with *SacI* and *SpeI* and subcloned into pQE-80L EPE digested with the same enzymes.

Available Sources: (1) miniprep DNA (-20°C)

(2) 25 v/v % glycerol stock in DH10B (-80°C)

(3) 25 v/v % glycerol stock in BL21 (-80°C)

Plasmid Map:

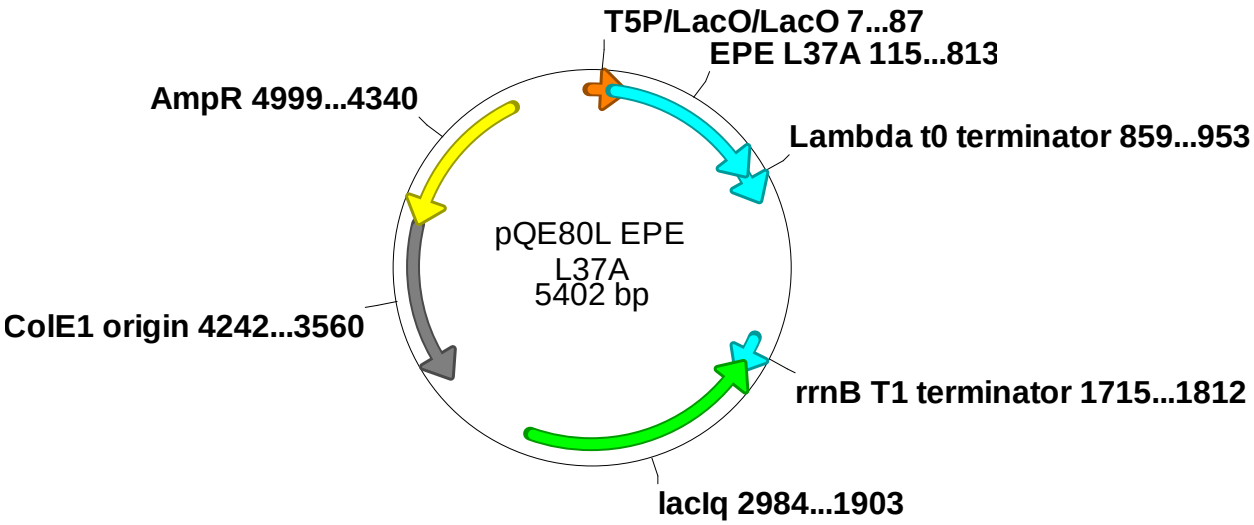

Coding sequence:

ATGAGATGCAGCAGCCATCATCATCATCATCACGTCGACGGCCACGGCGTGGGTGTT
CCGGGCGTCGGTGTGCCGGGTGTGGGTGTGCCGGGCGAAGGTGTGCCGGGCGTCGG
TGTGCCGGGTGTTGGTGTTCCGGGCGTTGGTGTGCCGGGCGTTGGCGTGCCGGGCGA
GGGTGTGCCGGGCGTTGGTGTTCCGGGCGTGGGTGTGCCGGGCGTGGGCGTGCCGG
GCGTCGGTGTTCCGGGCGAGGGTGTGCCGGGCGTAGGTGTGCCGGGCGTTGGTGAG
CTCGGATCAGGACTTGGATCCGCGCCGCAAATGCTGCGTGAAGCGCAGGAAACCAA
TGCCGCGCTTCAGGATGTGCGGGAATTGCTTCGTCAACAGGTCAAGGAGATAACGTT
CTTGAAGAACACCGTCATGGAGTCGGATGCGTCCAAGCTTAATACTAGTGTGCCGGG
CGTCGGCGTGCCGGGCGTAGGTGTTCCGGGCGAGGGTGTTCCGGGCGTTGGTGTGCC
GGGCGTCGGCGTGCCGGGCGTGGGTGTTCCGGGCGTAGGTGTGCCGGGCGAGGGTG
TGCCGGGCGTGGGCGTGCCGGGCGTAGGTGTTCCGGGCGTAGGTGTTCCGGGCGTA
GGTGTTCCGGGTGAAGGCGTGCCGGGCGTTGGTGTGCCGGGTGTGGGCGTGCCGGG
CGGGCTGCTCGAGTGCATGTAA

Translation:

MRCSSHHHHHHVDGHGVGVPGVGVPGVGVPGEGVPGVGVPGVGVPGVGVPGVGVPG
EGVPGVGVPGVGVPGVGVPGVGVPGEGVPGVGVPGVGELGSGLGSAPQMLREAQETN
AALQDVRELLRQQVKEITFLKNTVMESDASKLNTSVPGVGVPGVGVPGEGVPGVGVPG
VGVPGVGVPGVGVPGEGVPGVGVPGVGVPGVGVPGVGVPGEGVPGVGVPGVGVPGG
LLECM*

pQE-80L EPE L37V

Submitted by: Larry Dooling

Strain(s)/Plasmid: DH10B/pQE-80L EPE L37V
BL21/pQE-80L EPE L37V

Vector: pQE-80L

Insert: EPE L37V

Antibiotic Resistance: Ampicillin

Description: Hydrophilic elastin-like repeats $[(VPGVG)_2VPGEG(VPGVG)_2]_3$ flanking a P coiled coil motif containing the L37V mutation.

Construction: The P domain was isolated from pUC19 P L37V by digestion with *SacI* and *SpeI* and subcloned into pQE-80L EPE digested with the same enzymes.

Available Sources: (1) miniprep DNA (-20°C)

(2) 25 v/v % glycerol stock in DH10B (-80°C)

(3) 25 v/v % glycerol stock in BL21 (-80°C)

Plasmid Map:

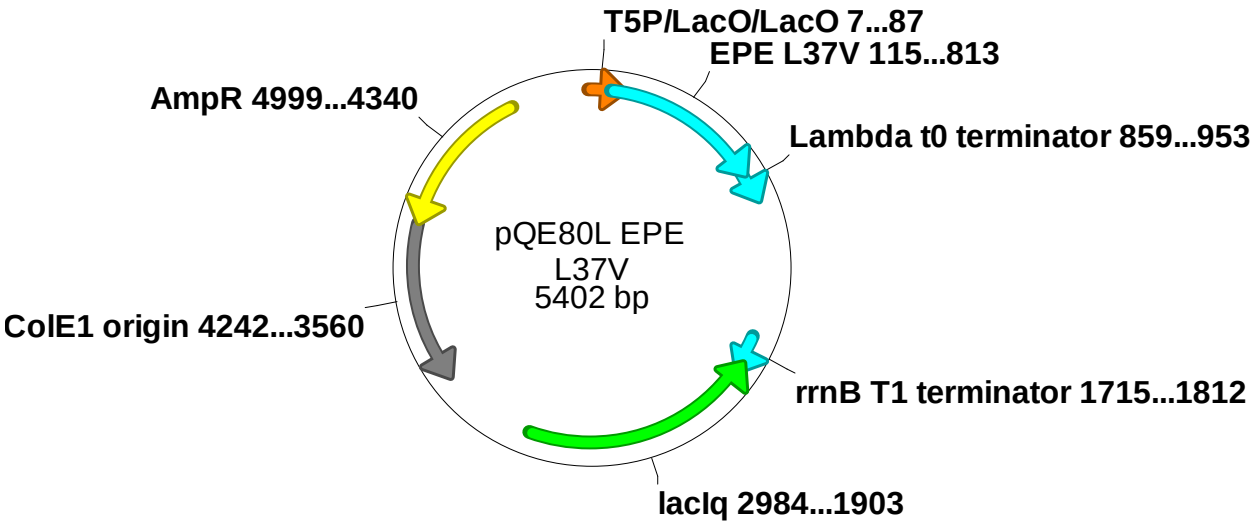

Coding sequence:

ATGAGATGCAGCAGCCATCATCATCATCATCACGTCGACGGCCACGGCGTGGGTGTT
CCGGGCGTCGGTGTGCCGGGTGTGGGTGTGCCGGGCGAAGGTGTGCCGGGCGTCGG
TGTGCCGGGTGTTGGTGTTCCGGGCGTTGGTGTGCCGGGCGTTGGCGTGCCGGGCGA
GGGTGTGCCGGGCGTTGGTGTTCCGGGCGTGGGTGTGCCGGGCGTGGGCGTGCCGG
GCGTCGGTGTTCCGGGCGAGGGTGTGCCGGGCGTAGGTGTGCCGGGCGTTGGTGAG
CTCGGATCAGGACTTGGATCCGCGCCGCAAATGCTGCGTGAAGTGCAGGAAACCAA
TGCCGCGCTTCAGGATGTGCGGGAATTGCTTCGTCAACAGGTCAAGGAGATAACGTT
CTTGAAGAACACCGTCATGGAGTCGGATGCGTCCAAGCTTAATACTAGTGTGCCGGG
CGTCGGCGTGCCGGGCGTAGGTGTTCCGGGCGAGGGTGTTCCGGGCGTTGGTGTGCC
GGGCGTCGGCGTGCCGGGCGTGGGTGTTCCGGGCGTAGGTGTGCCGGGCGAGGGTG
TGCCGGGCGTGGGCGTGCCGGGCGTAGGTGTTCCGGGCGTAGGTGTTCCGGGCGTA
GGTGTTCCGGGTGAAGGCGTGCCGGGCGTTGGTGTGCCGGGTGTGGGCGTGCCGGG
CGGGCTGCTCGAGTGCATGTAA

Translation:

MRCSSHHHHHHVDGHGVGVPGVGVPGVGVPGEGVPGVGVPGVGVPGVGVPGVGVPG
EGVPGVGVPGVGVPGVGVPGVGVPGEGVPGVGVPGVGELGSGLGSAPQMLREVQETN
AALQDVRELLRQQVKEITFLKNTVMESDASKLNTSVPGVGVPGVGVPGEGVPGVGVPG
VGVPGVGVPGVGVPGEGVPGVGVPGVGVPGVGVPGVGVPGEGVPGVGVPGVGVPGG
LLECM*

pQE-80L EPE L37I

Submitted by: Larry Dooling

Strain(s)/Plasmid: DH10B/pQE-80L EPE L37I
BL21/pQE-80L EPE L37I

Vector: pQE-80L

Insert: EPE L37I

Antibiotic Resistance: Ampicillin

Description: Hydrophilic elastin-like repeats $[(VPGVG)_2VPGEG(VPGVG)_2]_3$ flanking a P coiled coil motif containing the L37I mutation.

Construction: The P domain was isolated from pUC19 P L37I by digestion with *SacI* and *SpeI* and subcloned into pQE-80L EPE digested with the same enzymes.

Available Sources: (1) miniprep DNA (-20°C)

(2) 25 v/v % glycerol stock in DH10B (-80°C)

(3) 25 v/v % glycerol stock in BL21 (-80°C)

Plasmid Map:

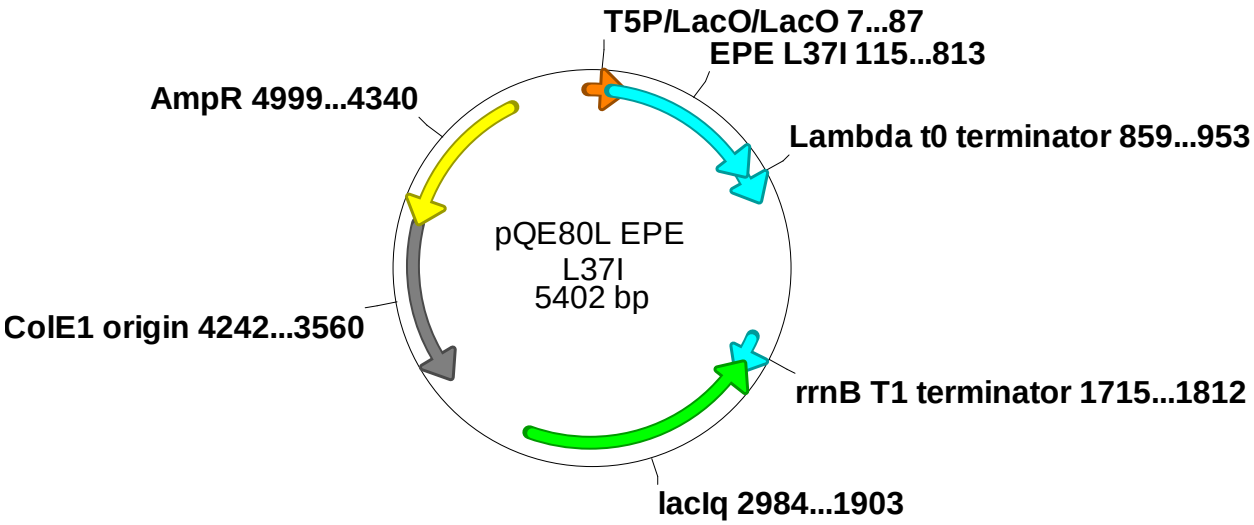

Coding sequence:

ATGAGATGCAGCAGCCATCATCATCATCATCACGTCGACGGCCACGGCGTGGGTGTT
CCGGGCGTCGGTGTGCCGGGTGTGGGTGTGCCGGGCGAAGGTGTGCCGGGCGTCGG
TGTGCCGGGTGTTGGTGTTCCGGGCGTTGGTGTGCCGGGCGTTGGCGTGCCGGGCGA
GGGTGTGCCGGGCGTTGGTGTTCCGGGCGTGGGTGTGCCGGGCGTGGGCGTGCCGG
GCGTCGGTGTTCCGGGCGAGGGTGTGCCGGGCGTAGGTGTGCCGGGCGTTGGTGAG
CTCGGATCAGGACTTGGATCCGCGCCGCAAATGCTGCGTGAAATTCAGGAAACCAA
TGCCGCGCTTCAGGATGTGCGGGAATTGCTTCGTCAACAGGTCAAGGAGATAACGTT
CTTGAAGAACACCGTCATGGAGTCGGATGCGTCCAAGCTTAATACTAGTGTGCCGGG
CGTCGGCGTGCCGGGCGTAGGTGTTCCGGGCGAGGGTGTTCCGGGCGTTGGTGTGCC
GGGCGTCGGCGTGCCGGGCGTGGGTGTTCCGGGCGTAGGTGTGCCGGGCGAGGGTG
TGCCGGGCGTGGGCGTGCCGGGCGTAGGTGTTCCGGGCGTAGGTGTTCCGGGCGTA
GGTGTTCCGGGTGAAGGCGTGCCGGGCGTTGGTGTGCCGGGTGTGGGCGTGCCGGG
CGGGCTGCTCGAGTGCATGTAA

Translation:

MRCSSHHHHHHVDGHGVGVPGVGVPGVGVPGEGVPGVGVPGVGVPGVGVPGVGVPG
EGVPGVGVPGVGVPGVGVPGVGVPGEGVPGVGVPGVGELGSGLGSAPQMLREIQETNA
ALQDVRELLRQQVKEITFLKNTVMESDASKLNTSVPGVGVPGVGVPGEGVPGVGVPGV
GVPGVGVPGVGVPGEGVPGVGVPGVGVPGVGVPGVGVPGEGVPGVGVPGVGVPGGLL
ECM*

pQE-80L EPE L44A

Submitted by: Larry Dooling

Strain(s)/Plasmid: DH10B/pQE-80L EPE L44A
BL21/pQE-80L EPE L44A

Vector: pQE-80L

Insert: EPE L44A

Antibiotic Resistance: Ampicillin

Description: Hydrophilic elastin-like repeats $[(VPGVG)_2VPGEG(VPGVG)_2]_3$ flanking a P coiled coil motif containing the L44A mutation.

Construction: The P domain was isolated from pUC19 P L44A by digestion with *SacI* and *SpeI* and subcloned into pQE-80L EPE digested with the same enzymes.

Available Sources: (1) miniprep DNA (-20°C)

(2) 25 v/v % glycerol stock in DH10B (-80°C)

(3) 25 v/v % glycerol stock in BL21 (-80°C)

Plasmid Map:

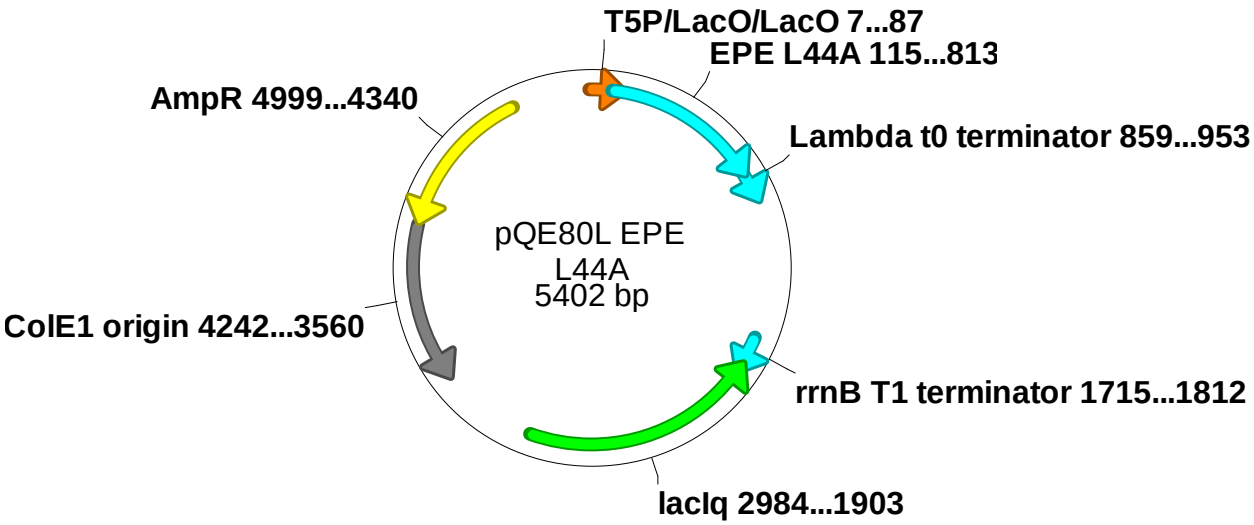

Coding sequence:

ATGAGATGCAGCAGCCATCATCATCATCATCACGTCGACGGCCACGGCGTGGGTGTT
CCGGGCGTCGGTGTGCCGGGTGTGGGTGTGCCGGGCGAAGGTGTGCCGGGCGTCGG
TGTGCCGGGTGTTGGTGTTCCGGGCGTTGGTGTGCCGGGCGTTGGCGTGCCGGGCGA
GGGTGTGCCGGGCGTTGGTGTTCCGGGCGTGGGTGTGCCGGGCGTGGGCGTGCCGG
GCGTCGGTGTTCCGGGCGAGGGTGTGCCGGGCGTAGGTGTGCCGGGCGTTGGTGAG
CTCGGATCAGGACTTGGATCCGCGCCGCAAATGCTGCGTGAACTGCAGGAAACCAA
TGCCGCGGCTCAGGATGTGCGGGAATTGCTTCGTCAACAGGTCAAGGAGATAACGT
TCTTGAAGAACACCGTCATGGAGTCGGATGCGTCCAAGCTTAATACTAGTGTGCCGG
GCGTCGGCGTGCCGGGCGTAGGTGTTCCGGGCGAGGGTGTTCCGGGCGTTGGTGTGC
CGGGCGTCGGCGTGCCGGGCGTGGGTGTTCCGGGCGTAGGTGTGCCGGGCGAGGGT
GTGCCGGGCGTGGGCGTGCCGGGCGTAGGTGTTCCGGGCGTAGGTGTTCCGGGCGT
AGGTGTTCCGGGTGAAGGCGTGCCGGGCGTTGGTGTGCCGGGTGTGGGCGTGCCGG
GCGGGCTGCTCGAGTGCATGTAA

Translation:

MRCSSHHHHHHVDGHGVGVPGVGVPGVGVPGEGVPGVGVPGVGVPGVGVPGVGVPG
EGVPGVGVPGVGVPGVGVPGVGVPGEGVPGVGVPGVGELGSGLGSAPQMLRELQETN
AAAQDVRELLRQQVKEITFLKNTVMESDASKLNTSVPGVGVPGVGVPGEGVPGVGVPG
VGVPGVGVPGVGVPGEGVPGVGVPGVGVPGVGVPGVGVPGEGVPGVGVPGVGVPGG
LLECM*

pQE-80L EPE T40A

Submitted by: Larry Dooling

Strain(s)/Plasmid: DH10B/pQE-80L EPE T40A
BL21/pQE-80L EPE T40A

Vector: pQE-80L

Insert: EPE T40A

Antibiotic Resistance: Ampicillin

Description: Hydrophilic elastin-like repeats $[(VPGVG)_2VPGEG(VPGVG)_2]_3$ flanking a P coiled coil motif containing the T40A mutation.

Construction: The P domain was isolated from pUC19 P T40A by digestion with *SacI* and *SpeI* and subcloned into pQE-80L EPE digested with the same enzymes.

Available Sources: (1) miniprep DNA (-20°C)

(2) 25 v/v % glycerol stock in DH10B (-80°C)

(3) 25 v/v % glycerol stock in BL21 (-80°C)

Plasmid Map:

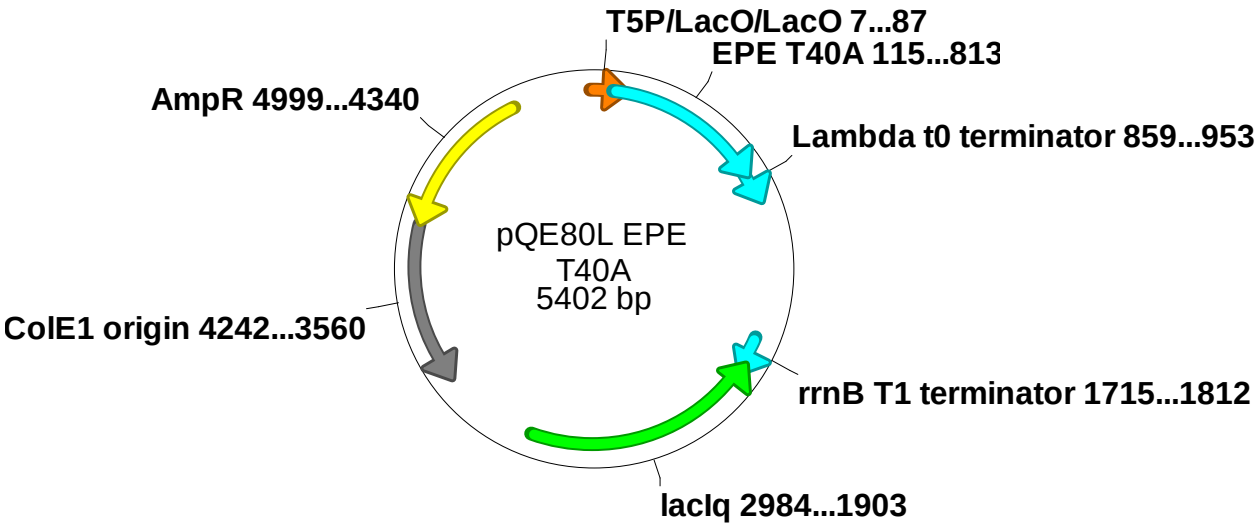

Coding sequence:

ATGAGATGCAGCAGCCATCATCATCATCATCACGTCGACGGCCACGGCGTGGGTGTT
CCGGGCGTCGGTGTGCCGGGTGTGGGTGTGCCGGGCGAAGGTGTGCCGGGCGTCGG
TGTGCCGGGTGTTGGTGTTCCGGGCGTTGGTGTGCCGGGCGTTGGCGTGCCGGGCGA
GGGTGTGCCGGGCGTTGGTGTTCCGGGCGTGGGTGTGCCGGGCGTGGGCGTGCCGG
GCGTCGGTGTTCCGGGCGAGGGTGTGCCGGGCGTAGGTGTGCCGGGCGTTGGTGAG
CTCGGATCAGGACTTGGATCCGCGCCGCAAATGCTGCGTGAACTGCAGGAAGCCAA
TGCCGCGCTTCAGGATGTGCGGGAATTGCTTCGTCAACAGGTCAAGGAGATAACGTT
CTTGAAGAACACCGTCATGGAGTCGGATGCGTCCAAGCTTAATACTAGTGTGCCGGG
CGTCGGCGTGCCGGGCGTAGGTGTTCCGGGCGAGGGTGTTCCGGGCGTTGGTGTGCC
GGGCGTCGGCGTGCCGGGCGTGGGTGTTCCGGGCGTAGGTGTGCCGGGCGAGGGTG
TGCCGGGCGTGGGCGTGCCGGGCGTAGGTGTTCCGGGCGTAGGTGTTCCGGGCGTA
GGTGTTCCGGGTGAAGGCGTGCCGGGCGTTGGTGTGCCGGGTGTGGGCGTGCCGGG
CGGGCTGCTCGAGTGCATGTAA

Translation:

MRCSSHHHHHHVDGHGVGVPGVGVPGVGVPGEGVPGVGVPGVGVPGVGVPGVGVPG
EGVPGVGVPGVGVPGVGVPGVGVPGEGVPGVGVPGVGELGSGLGSAPQMLRELQEAN
AALQDVRELLRQQVKEITFLKNTVMESDASKLNTSVPGVGVPGVGVPGEGVPGVGVPG
VGVPGVGVPGVGVPGEGVPGVGVPGVGVPGVGVPGVGVPGEGVPGVGVPGVGVPGG
LLECM*

pQE-80L EPE Q54A

Submitted by: Larry Dooling

Strain(s)/Plasmid: DH10B/pQE-80L EPE Q54A
BL21/pQE-80L EPE Q54A

Vector: pQE-80L

Insert: EPE Q54A

Antibiotic Resistance: Ampicillin

Description: Hydrophilic elastin-like repeats $[(VPGVG)_2VPGEG(VPGVG)_2]_3$ flanking a P coiled coil motif containing the Q54A mutation.

Construction: The P domain was isolated from pUC19 P Q54A by digestion with *SacI* and *SpeI* and subcloned into pQE-80L EPE digested with the same enzymes.

Available Sources: (1) miniprep DNA (-20°C)

(2) 25 v/v % glycerol stock in DH10B (-80°C)

(3) 25 v/v % glycerol stock in BL21 (-80°C)

Plasmid Map:

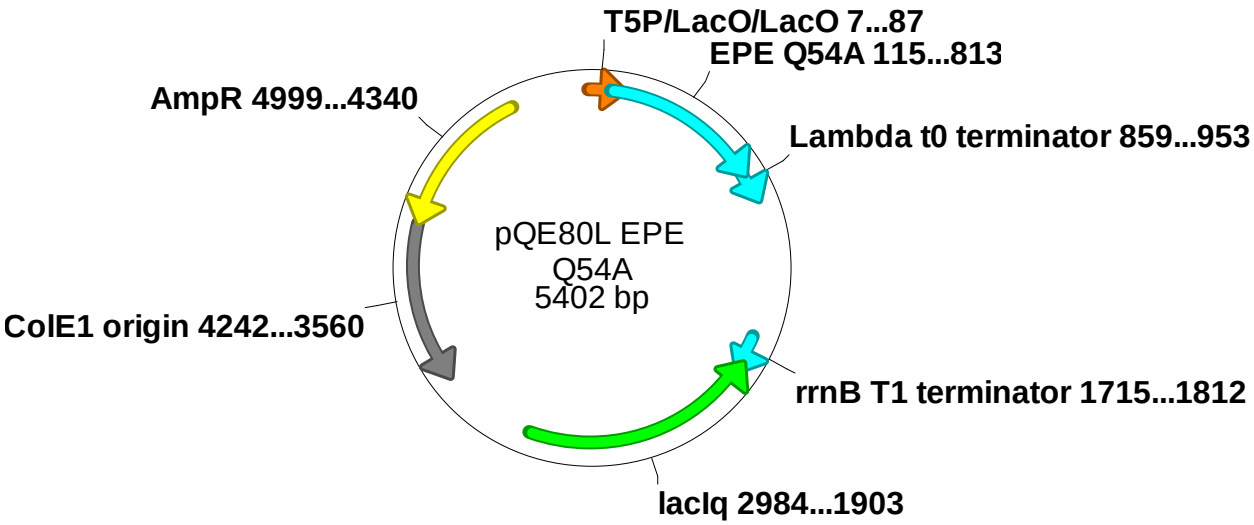

Coding sequence:

ATGAGATGCAGCAGCCATCATCATCATCATCACGTCGACGGCCACGGCGTGGGTGTT
CCGGGCGTCGGTGTGCCGGGTGTGGGTGTGCCGGGCGAAGGTGTGCCGGGCGTCGG
TGTGCCGGGTGTTGGTGTTCCGGGCGTTGGTGTGCCGGGCGTTGGCGTGCCGGGCGA
GGGTGTGCCGGGCGTTGGTGTTCCGGGCGTGGGTGTGCCGGGCGTGGGCGTGCCGG
GCGTCGGTGTTCCGGGCGAGGGTGTGCCGGGCGTAGGTGTGCCGGGCGTTGGTGAG
CTCGGATCAGGACTTGGATCCGCGCCGCAAATGCTGCGTGAACTGCAGGAAACCAA
TGCCGCGCTTCAGGATGTGCGGGAATTGCTTCGTCAAGCGGTCAAGGAGATAACGTT
CTTGAAGAACACCGTCATGGAGTCGGATGCGTCCAAGCTTAATACTAGTGTGCCGGG
CGTCGGCGTGCCGGGCGTAGGTGTTCCGGGCGAGGGTGTTCCGGGCGTTGGTGTGCC
GGGCGTCGGCGTGCCGGGCGTGGGTGTTCCGGGCGTAGGTGTGCCGGGCGAGGGTG
TGCCGGGCGTGGGCGTGCCGGGCGTAGGTGTTCCGGGCGTAGGTGTTCCGGGCGTA
GGTGTTCCGGGTGAAGGCGTGCCGGGCGTTGGTGTGCCGGGTGTGGGCGTGCCGGG
CGGGCTGCTCGAGTGCATGTAA

Translation:

MRCSSHHHHHHVDGHGVGVPGVGVPGVGVPGEGVPGVGVPGVGVPGVGVPGVGVPG
EGVPGVGVPGVGVPGVGVPGVGVPGEGVPGVGVPGVGELGSGLGSAPQMLRELQETN
AALQDVRELLRQAVKEITFLKNTVMESDASKLNTSVPGVGVPGVGVPGEGVPGVGVPG
VGVPGVGVPGVGVPGEGVPGVGVPGVGVPGVGVPGVGVPGEGVPGVGVPGVGVPGG
LLECM*

pQE-80L EPE I58A

Submitted by: Larry Dooling

Strain(s)/Plasmid: DH10B/pQE-80L EPE I58A
BL21/pQE-80L EPE I58A

Vector: pQE-80L

Insert: EPE I58A

Antibiotic Resistance: Ampicillin

Description: Hydrophilic elastin-like repeats $[(VPGVG)_2VPGEG(VPGVG)_2]_3$ flanking a P coiled coil motif containing the I58A mutation.

Construction: The P domain was isolated from pUC19 P I58A by digestion with *SacI* and *SpeI* and subcloned into pQE-80L EPE digested with the same enzymes.

Available Sources: (1) miniprep DNA (-20°C)

(2) 25 v/v % glycerol stock in DH10B (-80°C)

(3) 25 v/v % glycerol stock in BL21 (-80°C)

Plasmid Map:

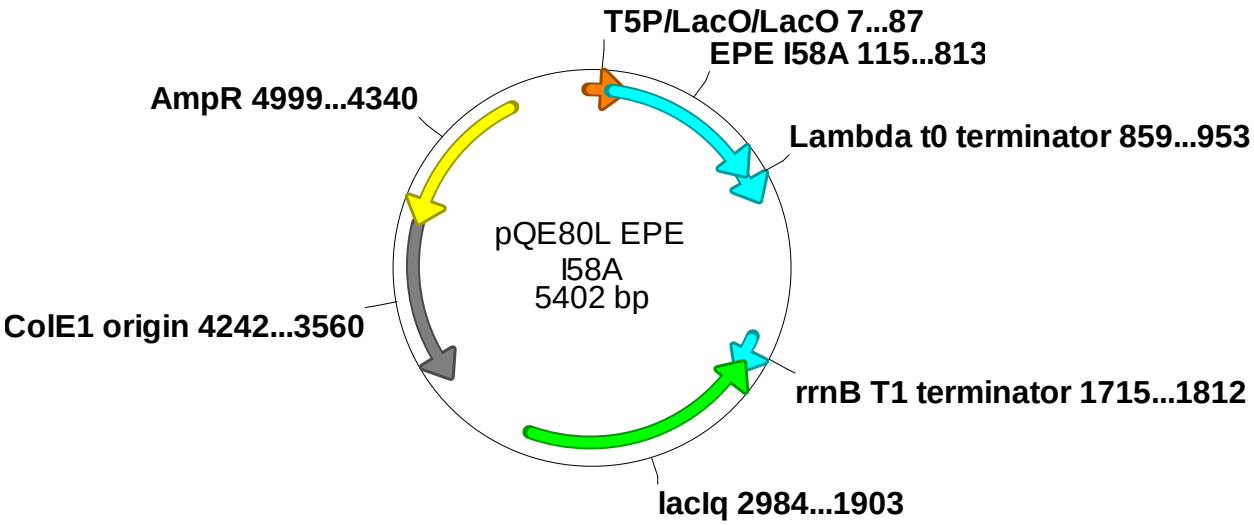

Coding sequence:

ATGAGATGCAGCAGCCATCATCATCATCATCACGTCGACGGCCACGGCGTGGGTGTT
CCGGGCGTCGGTGTGCCGGGTGTGGGTGTGCCGGGCGAAGGTGTGCCGGGCGTCGG
TGTGCCGGGTGTTGGTGTTCCGGGCGTTGGTGTGCCGGGCGTTGGCGTGCCGGGCGA
GGGTGTGCCGGGCGTTGGTGTTCCGGGCGTGGGTGTGCCGGGCGTGGGCGTGCCGG
GCGTCGGTGTTCCGGGCGAGGGTGTGCCGGGCGTAGGTGTGCCGGGCGTTGGTGAG
CTCGGATCAGGACTTGGATCCGCGCCGCAAATGCTGCGTGAACTGCAGGAAACCAA
TGCCGCGCTTCAGGATGTGCGGGAATTGCTTCGTCAACAGGTCAAGGAGGCAACGTT
CTTGAAGAACACCGTCATGGAGTCGGATGCGTCCAAGCTTAATACTAGTGTGCCGGG
CGTCGGCGTGCCGGGCGTAGGTGTTCCGGGCGAGGGTGTTCCGGGCGTTGGTGTGCC
GGGCGTCGGCGTGCCGGGCGTGGGTGTTCCGGGCGTAGGTGTGCCGGGCGAGGGTG
TGCCGGGCGTGGGCGTGCCGGGCGTAGGTGTTCCGGGCGTAGGTGTTCCGGGCGTA
GGTGTTCCGGGTGAAGGCGTGCCGGGCGTTGGTGTGCCGGGTGTGGGCGTGCCGGG
CGGGCTGCTCGAGTGCATGTAA

Translation:

MRCSSHHHHHHVDGHGVGVPGVGVPGVGVPGEGVPGVGVPGVGVPGVGVPGVGVPG
EGVPGVGVPGVGVPGVGVPGVGVPGEGVPGVGVPGVGELGSGLGSAPQMLRELQETN
AALQDVRELLRQQVKEATFLKNTVMESDASKLNTSVPGVGVPGVGVPGEGVPGVGVP
GVGVPGVGVPGVGVPGEGVPGVGVPGVGVPGVGVPGVGVPGEGVPGVGVPGVGVPG
GLLECM*

Appendix B

DETAILED EXPERIMENTAL PROTOCOLS

TABLE OF CONTENTS

B.1 Expression of artificial proteins

Overview: This protocol describes the expression of artificial proteins that are encoded by genes on a pQE-80L plasmid harbored within the BL21 strain of *E. coli*. This includes ERE, EPE, EAE, and their variants.

Materials:

LB (Luria-Bertani) liquid medium supplemented with 100 μg mL^{-1} ampicillin

Per liter:

-10 g tryptone/casein hydrolysate (Affymetrix 12855**)**

-5 g yeast extract (Affymetrix 23547**)**

-10 g NaCl

LB/ampicillin agar plate supplemented with 100 μg mL^{-1} ampicillin

-LB liquid medium

-15 g Bacto agar (BD 214010)

2xYT liquid medium supplemented with 100 μg mL^{-1} ampicillin

Per liter:

-16 g tryptone

-10 g yeast extract

-5 g NaCl

Terrific broth supplemented with 100 μg mL^{-1} ampicillin

Per liter:

-12 g tryptone

-24 g yeast extract

-100 mL 10x buffering salts (2.31 g KH_2PO_4, 16.4 g $K2HPO_4 \cdot 3H_2O$) (Note: autoclaved separately from medium)

-8 mL 50% (v/v) glycerol (Note: autoclaved separately for convenience)

IPTG (Biopioneer, C0012-100): 1000x stock at 1 M stock in ddH_2O, sterilized by 0.2 micron filter

Ampicillin (BioPioneer C0029): 1000x stock at 100 mg mL^{-1} in ddH_2O, sterilized by 0.2 micron filter

15 mL culture tube

125 mL Erlenmeyer flask

2.8 L Fernbach baffled shake flask

Lysis buffer: 10 mM Tris, 1 mM EDTA, 100 mM NaCl, 5% (v/v) glycerol, 0.1% (v/v) Triton X-100, 0.1% (w/v) sodium deoxycholate, pH 8

Per liter:

-1.2 g Tris base (Sigma-Aldrich T1503)

-2 mL 0.5 M EDTA (Ethylenediaminetetraacetic acid) (Sigma-Aldrich ED2SS)

-5.8 g NaCl

-5 mL glycerol

-1 mL Triton X-100 (Sigma-Aldrich X-100)

-1 g sodium deoxycholate (Sigma-Aldrich D6750)

(Note: The additives glycerol, Triton X-100, and sodium deoxycholate were included to improve the protein stability, but are not strictly required.)

Equipment:

37 °C incubator: VWR Model 1525 (Spalding 332A)

37 °C shaking incubator(s): VWR Signature benchtop (Spalding 332A) and Thermo Forma orbital (Spalding 312)

Beckman-Coulter Avati J-25 centrifuge with JA-10 rotor (Spalding 332A)

Nalgene 500 mL centrifuge bottles (Thermo Scientific 3141-0500)

Day 1: Streak an LB/ampicillin agar plate with an inoculation loop containing cells from the appropriate glycerol stock in order to obtain single colonies. Incubate the plate overnight (12-18 hr) at 37 °C.

Day 2: Inoculate 3 mL LB/ampillin with a single colony from plate. Incubate the culture at 37 °C, 250 rpm for 8-10 hr.

Prepare an overnight starter culture by inoculating 25 mL 2xYT/ampicillin with 0.25 mL of growing culture in an autoclaved Erlenmeyer flask. Incubate at 37 °C, 250 rpm for 10-12 hr.

Prepare the Terrific broth by adding 12 g tryptone and 24 g yeast extract to 900 mL ddH_2O in the Fernbach baffled shake flask. Autoclave to sterilize.

Day 3: Add 8 mL sterile 50% (v/v) glycerol and 100 mL sterilized 10x buffering salts to the Terrific broth. Supplement with 1 mL 1000x ampicillin stock. Save several mL of the culture to use as a blank for optical density measurements.

Inoculate the Terrific broth with 20 mL (1:50) of the overnight starter culture. Grow the culture at 37 °C, 160 rpm (in Thermo Forma shaker) until the OD_{600} reaches approximately 0.8-1.0. This typically takes 2-2.5 hr.

Induce protein expression by the addition of 1 mL of 1000x IPTG solution (final concentration 1 mM).

After 4-5 hr, harvest the *E. coli* by centrifugation at 6,000 *g*, 4 °C for 8 min.

Weigh the cell pellets to determine the wet cell mass and resuspend in 25 mL of lysis buffer. Freeze at -20 °C.

Expected results: The final OD_{600} after 4-5 hr of expression varies from 4-8. It is typically higher during the expression of EPE and its variants than for ERE. The typical wet cell mass likewise varies from 7 g per L of culture to 15 g per L of culture.

B.2 Inverse thermal cycling purification of artificial proteins with elastin-like polypeptide domains

Overview: This protocol describes the purification of artificial proteins from *E. coli* lysate by inverse temperature cycling above and below the lower crucial solution temperature of the elastin-like domain. Three cycles are typically sufficient to obtain pure protein. This protocol also describes the reduction and desalting of proteins to obtain monomeric artificial proteins with high free thiol content.

Materials:

Phenylmethylsulfonyl fluoride, PMSF (Gold Biotechnology P-470-10)

DNase I (Sigma-Aldrich DN25)

RNase A (Sigma-Aldrich R4875)

$MgCl_2$

β-mercaptoethanol (Sigma-Aldrich M6250)

NaCl

TEN buffer (10 mM Tris, 1 mM EDTA, 100 mM NaCl, pH 8)

Tris(hydroxypropyl)phospine (THP) (Santa Cruz Biotechonolgy, sc-204915)

Zeba™ 7K MWCO spin desalting columns, 10 mL (Thermo Fisher Scientific 89894)

50 mL conical tubes (Corning 430829 or BD Falcon 352098)

water, LCMS Chromasolv® (Sigma-Aldrich/Fluka 39253)

liquid nitrogen (Spalding 312)

Equipment:

QSonica probe sonicator (Spalding 316)

Beckman-Coulter Avati J-25 centrifuge with JA-17 or JA-25.50 rotor (Spalding 332A)

50 mL Nalgene Oakridge centrifuge tubes (Thermo Scientific 3139-0050)

Beckman-Coulter Allegra 25R centrifuge with TS 5.1-500 spinning bucket rotor (Spalding 332A)

Labconco Freezone 4.5 L lyophillzer (Spalding 312)

Day 1: Thaw the resuspended cell pellets in a cold water bath. Add crystalline PMSF to approximately 1 mM.

(Note: PMSF is poorly soluble in aqueous solutions.)

To the thawed cell solution, add 10 μg mL^{-1} DNase I, 10 μg mL^{-1} RNase A, and 5 mM $MgCl_2$. Incubate at 37 °C, 250 rpm for 30 min. (Note: I typically do not weigh PMSF or nucleases. Instead I just add a small spatula tip worth of solid into thawing lysate.)

Sonicate the cell solution. For 25 mL in a 50 mL conical tube, typical sonication conditions are 5 min processing time with 2 sec "on" pulse at 30% power amplitude, and 2 second "off" rest between pulses. For larger volumes (i.e. pooled cells from several liters of culture), increase the processing time.

Add 1% (v/v) β-mercaptoethanol and incubate on ice for 1-2 hr.

(Note: βME is crucial for telechelic artificial proteins with cysteine residues at the termini. Omitting βME or using too little results in chain extension through disulfide formation. For EPE and variants that form physical cross-links, this can cause the pelleted protein fractions in subsequent thermal cycling steps to form physical gels that are difficult to resuspend. Add βME in a fume hood and in subsequent steps only open tubes in the hood.)

Centrifuge at 39,000 *g*, 4 °C for 1 hr. (Note: This is the maximum speed of the JA-17 rotor. The JA-25.50 can spin at higher speeds.) Carefully decant the supernatant into a new centrifuge tube and discard the pellet. The supernatant should be tan and mostly clear.

(Note: When purifying a new artificial protein or when it is necessary to assess the purification by SDS-PAGE, save all fractions. The protein in the pelleted fractions can be extracted with 8 M urea, typically using the same volume as the supernatant that was removed.)

Add crystalline NaCl to a final concertation of 2 M. Incubate at 37 °C, 250 rpm for 1 hr. The solution should become cloudy.

Meanwhile, spin the rotor at 39,000 *g*, 37 °C for 1 hr without any tubes. This allows the centrifuge and rotor to warm up more quickly. The centrifuge does not have a method of heating the rotor, only refrigerating the system. Therefore, it relies of heat or friction generated during a spin to warm above room temperature.

Centrifuge at 39,000 *g*, 37 °C for 1 hr. Discard the supernatant and resuspend the pellet in TEN buffer at a concentration of 100 mg mL^{-1}. Break up the pellet using a spatula. Add 1% (v/v) βME and incubate overnight on the tube rotator in the cold room.

Day 2: Centrifuge at 39,000 *g*, 4 °C for 30 min. Carefully decant the supernatant into a new centrifuge tube and discard the pellet.

Add crystalline NaCl to a final concertation of 2 M. Incubate at 37 °C, 250 rpm for 30 min-1 hr while warming the centrifuge and rotor to 37 °C. The solution should become cloudy again and the proteins may begin to flocculate.

Centrifuge at 39,000 *g*, 37 °C for 1 hr. Discard the supernatant and resuspend the pellet in TEN buffer at a concentration of 100 mg mL^{-1}. If properly reduced, the pelleted fraction will be runny and will resuspend easily. If not properly reduced, the pelleted fraction will be rubbery and difficult to resuspend. Add 1% (v/v) βME and incubate overnight on the tube rotator in the cold room.

Day 3: Centrifuge at 39,000 *g*, 4 °C for 30 min. Carefully decant the supernatant into a new centrifuge tube and discard the pellet.

Add crystalline NaCl to a final concertation of 2 M. Incubate at 37 °C, 250 rpm for 30 min-1 hr while warming the centrifuge and rotor to 37 °C. The solution should become cloudy again and the proteins should begin to flocculate.

Centrifuge at 39,000 *g*, 37 °C for 1 hr. Discard the supernatant and resuspend the pellet in TEN buffer at a concentration of 100 mg mL^{-1}. If this is the final cycle, do not add βME. It is best to round to the nearest multiple of 4 mL at this step.

Once the pelleted fraction is well resuspended (typically 30 min-2 hr), add THP to a final concentration of 5 mM and reduce for 1-3 hr at 4 °C.

To check the reduction, take a 2 μL sample and dilute 1:10 in water. Dilute this 1:10 in SDS loading buffer. As a control, prepare a second sample in the same way but add βME to a final concentration of 5% (v/v). Boil only the control sample containing βME for 2-3 min. Load 5 μL of each solution on a 10-well gel. Run for 45 minutes at 180 V. Stain with InstantBlue to determine whether the protein is monomeric (vs. dimeric or greater) and linear (vs. cyclic, which will have a slightly lower apparent molecular weight). More details are given in B.6.

(Note: Fresh 1x MES/SDS running buffer is critical. Do not reuse buffer. Either a degradation product from the buffer or metals leaching from the electrode cause rapid oxidation of the proteins and can produce false negatives.)

Desalt the protein to remove the TEN buffer and THP according to the Zeba desalting column manufacturers protocol. Remove the storage buffer by centrifugation at 1000 *g*, 4 °C for 2 min. Equilibrate three times with degassed 5 mL LCMS grade water. The first two equilibration steps are done at 1000 *g*, 4 °C for 2 min. The final equilibration should be done at 1000 *g*, 4 °C for 6 min. Apply 4 mL of the protein solution each column and centrifuge 1000 *g*, 4 °C for 4 min, eluting into 50 mL conical tubes.

(Note: LCMS grade water is likely not strictly required, but was used due to potential concerns over the consistency of water from the still. This was likely not an issue.)

Combine the elution from each column into a tared conical tube, freeze in liquid nitrogen, and lyophilize for 3-4 days or until all water is removed.

Expected results: Typical yields vary from 80 mg per L of culture for ERE to >300 mg per L of culture for EPE. The proteins are quite pure, but occasionally have small amounts of lower molecular weight impurities (estimated at <6%). Lower molecular weight impurities are most common in ERE and EAE protein preparations.

B.3 Ellman's assay and non-reducing SDS-PAGE

Overview: This protocol describes the measurement of the free thiol content in purified artificial proteins containing cysteine residues and SDS-PAGE under non-reducing conditions to determine the fraction of protein in the monomeric state.

Materials:

5,5'-dithiobis-(2-nitrobenzoic acid), Ellman's reagent (Sigma D8130)

Reaction buffer:

100 mM sodium phosphate

1 mM EDTA

pH to 8.0

Disposable cuvettes

2x SDS sample loading buffer

β-mercaptoethanol (Sigma-Aldrich M6250)

10- or 15-well Novex NuPAGE Bis-Tris 4-12% SDS PAGE gels (Thermo Fisher NP0322)

20x MES/SDS Running buffer (Boston Bioproducts BP-177)

InstantBlue protein stain (Expedion ISBL1)

Equipment

Cary50 UV/Vis spectrophotometer (Spalding 312)

Heating block set to 95 °C (Spalding 332A)

Gel electrophoresis cell and power source (Spalding 332A)

Typhoon Trio (Spalding 312)

Protocol

Prepare 5 mg mL^{-1} Ellman's reagent in reaction buffer. Reagent must be prepared fresh.

(Note: Weigh Ellman's reagent and protein with a Teflon-coated spatula and forceps, respectively. Metal surfaces could oxidize thiols.)

Pipette 2.5 mL reaction buffer into a cuvette.

Dissolve protein in reaction buffer at a concentration of 5 mg mL^{-1}. (Note: I typically weigh a minimum of 2 mg per sample.) Vortex or sonicate briefly as needed.

Add 50 µL Ellman's reagent solution and 250 µL protein solution to the cuvette containing the reaction buffer. Pipette up and down several times to mix. The solution should turn yellow instantly. At the same time, prepare a blank containing 50 µL of Ellman's reagent solution and 250 µL of reaction buffer without protein. Incubate all samples on benchtop for 15 min. Turn spectrophotometer on.

(Note: The concentration of protein has been optimized in this protocol to detect two thiols per protein. The concentration may require adjustment for proteins with additional thiols.)

Meanwhile, prepare samples for non-reducing SDS-PAGE from the protein solutions prepared above. Add 2 µL protein solution to a microcentrifuge tube containing 10 µL 2x SDS sample loading buffer and 8 µL water. Prepare a second sample in the same way, but also add 1 µL βME as a positive control for reduced protein. Boil only the control sample for 2-5 min on heating block.

Load 5 µL of each sample in a 10-well gel (or 2.5 µL in a 15-well gel). Load 5 µL of the SeeBlue protein marker. Run for 35-45 min at 180V with MES running buffer.

(Note: Fresh 1x MES running buffer is critical. Do not reuse buffer. Either a degradation product from the buffer or metals leaching from the electrode cause rapid oxidation of the proteins and can produce false negatives.)

While gel is running, measure the absorbance of the protein solution with Ellman's reagent. Set the measurement wavelength to 412 nm. From the absorbance values, determine the concentration of free thiols using the extinction coefficient of 2-nitro-5-thiobenzoate, which is 14,150 M^{-1} cm^{-1} under the conditions of this assay. It is assumed that each free thiol reacts with 5,5'-dithiobis-(2-nitrobenzoic acid) to produce one molecule of 2-nitro-5-thiobenzoate.

(Note: A standard curve can be constructed with known concentrations of cysteine reacted with Ellman's reagent. This is useful for determining the linear region of the assay, but somewhat tedious as the standards must be prepared fresh each time.)

When the gel has finished running, rinse with water and stain with InstantBlue protein stain for 15-60 min. Destain with water.

Image the gel on the Typhoon with the red laser, no filter and a PMT of 500 V. If desired, quantify the density of each band using the ImageQuant software.

Expected results: After optimization of the purification protocol, artificial proteins can typically be prepared with 85-95% free thiol content relative to the expected free thiol content. Otherwise the discrepancy between the observed and expected thiol content can arise due to disulfide formation in dimers, trimers, etc. and intramolecular cyclization reactions.

By non-reducing SDS PAGE, the proteins are primarily monomeric. A small amount of dimeric and trimeric protein run are present. A band corresponding to the cyclized monomer occurs at a slightly lower apparent molecular weight than the predominate linear monomer protein band.

B.4 End-linking artificial proteins with 4-arm PEG vinyl sulfone

Overview: This protocol describes the procedure used to form covalent networks by end-linking artificial proteins that contain terminal cysteine residues with 4-arm PEG vinyl sulfone. The same procedure can be applied to end-linking with 4-arm PEG maleimide and 4-arm PEG acrylate, although these reactions occur much faster and slower, respectively, than the reaction with 4-arm PEG vinyl sulfone.

Materials:

Purified artificial protein with high free thiol content (see Protocols 1-3)

4-arm PEG vinyl sulfone (Jenkem USA 4ARM-VS), maleimide (4ARM-MAL), or acrylate (4ARM-ACLT)

Cross-linking buffer:

100 mM sodium phosphate

400 mM triethanolamine (Sigma 90279)

6 M guanidinium chloride (Sigma G4505)

Adjust pH to approximately 7.4 using 6 N HCl.

(Note: Triethanolamine should be omitted or reduced to 4 mM for cross-linking with 4-arm PEG maleimide.)

Sigmacote® siliconizing fluid (Sigma SL2)

Glass slides 75 x 50 mm

Silicone rubber, 1 mm thick (McMaster-Carr 3788T22)

95% ethanol

Binder clips

Protocol

In advance, prepare clean glass slides by treating with 0.5-1 mL SigmaCote® for 1 min. Remove excess liquid, rinse with water, and allow to dry. Clean with 95% ethanol and Kimwipe. Test hydrophobicity by pipetting a droplet of water onto the slide. It should not spread. Cut a rectangle slightly smaller than the slide from the rubber sheet, and then cut a

smaller rectangle out of the middle of this piece to obtain a frame that will serve as a 1 mm spacer between two slides.

(Note: Treated glass slides can be reused for many gels. Clean with 95% ethanol and test hydrophobicity.)

Degas 0.1 M sodium phosphate/6 M guanidinium chloride in a 25 mL side arm flask by pulling under vacuum while sonicating. Repeat with ddH_2O.

(Note: This step is optional and does not appear to be vital. Because dissolving the protein and mixing the gelation reaction requires vortexing, oxygen is likely to be reintroduced into the solution.)

Add triethanolamine to the degassed 0.1 M sodium phosphate/6 M guanidinium chloride to a final concentration of 400 mM. Do the same with the degassed ddH_2O. Adjust the pH of each solution to the desired value, typically 7.2-7.4, with 6 N HCl.

Dissolve protein solution (50 to 250 mg per 1 mL) in cross-linking buffer (0.1 M sodium phosphate/6 M guanidinium chloride/0.4 M triethanolamine). Dissolve the 4-arm PEG vinyl sulfone (50 to 250 mg per 1 mL) in 0.4 M triethanolamine.

(Note: Weigh protein and PEG-4VS with Teflon-coated forceps and spatulas.)

(Note: The 4-arm PEG vinyl sulfone can also be dissolved in cross-linking buffer rather than 0.4 M triethanolamine.)

Sonicate (about 2 min) in ultrasonic bath. Vortex to mix. Centrifuge at 10,000 *g* for 1 min at room temperature or 4 °C. This removes bubbles or foam. Vortex to mix again and repeat centrifugation if necessary.

(Note: After centrifugation, a very viscous, protein-rich phase can form at the bottom of the tube. This may be protein aggregation. It can be resuspended by vortexing.)

Mix the protein solution and PEG-4VS solution at the desired volumetric ratio, vortex, and pipette a droplet onto a treated glass within the rectangular spacer. Place another glass slide on top with the treated side facing the droplet. Carefully clamp the slides together with binder clips, being careful not to introduce bubbles.

(Note: PEG-4MAL cross-linking occurs much too quickly to process in this way. Instead, a droplet of the protein solution can be formed on a treated glass slide. The cross-linker solution should be pipetted directly into this droplet, mixing as best as possible by pipetting up and down in a swirling motion.)

Example: In a typical formulation of hydrogels in this thesis, 160 mg of protein was dissolved in 1.07 mL of degassed cross-linking buffer in a microcentrifuge tube. In a separate tube, 45 mg of PEG-4VS was dissolved in 300 mL degassed 400 mM triethanolamine. The tubes were both sonicated for 2 min, vortexed, centrifuged, and vortexed again. The volumes of the protein solution increased slightly (≈10%) due to the dissolved solids. A similar increase is observed with PEG-4VS. After dissolving completely, 1 mL of the protein solution was transferred to a new tube. To this solution, 231 μL of the PEG-4VS solution was added. This volumetric ratio gives a 1:1 ratio of thiols to vinyl sulfones while maintaining a constant polymer concentration of approximately 15 wt% (actually slightly less when accounting for the volume increases). The gelation mixture was vortexed and pipetted onto a treated glass slide. For swelling experiments, 50 μL droplets were formed. For rheology experiments, 70 μL droplets were formed. For tensile tests, 1 mL droplets were formed. A second glass slide was placed on top, separated by rubber spacers, taking care not to introduce bubbles.

Expected results: Gelation with PEG-4VS at the concentration ranges explored (7.5-25 wt%) occurs within 10-30 minutes; however, longer times are required to completely cross-link the materials. If the slide is treated with SigmaCote and cross-linking reaction proceeds as expected, gels can be easily removed from the slide with a spatula. A small amount of PBS buffer for also helps in removing the gels. Poorly cross-linked gels are sticky and difficult to remove from the slides.

Alternative cross-linking Cross-linking can be performed without guanidinium chloride and without triethanolamine. For cell encapsulation experiments in Chapter 2, protein and PEG-4VS were both dissolved in HEPES-buffered saline (25 mM HEPES, 150 mM NaCl, pH 7.4). The kinetics of the gelation reaction are only slightly slower under these conditions.

B.5. Hydrogel swelling experiments

Overview: Hydrogels swell in the presence of water. According to classical theories, swelling results from a balance of the free energy of mixing polymer chains and solvent and elastic free energy. Electrostatic effects also contribute. The swelling experiments in this thesis are simple measurements of the swollen mass in a specified buffer divided by the dry mass of the cross-linked polymer network. This specific protocol describes the mass swelling measurements of EPE gels swollen in denaturing buffer for 48 hr, followed by swelling in PBS buffer for 48 hr. The first step can be omitted if desired.

Materials:

Hydrogels prepared according to Protocol 4.

Phosphate buffered saline, PBS

1.5 mM KH_2PO_4

4.3 mM Na_2HPO_4

137 mM NaCl

2.7 mM KCl

Guanidinium chloride

Sodium azide (Sigma S2002)

1.7 mL microcentrifuge tubes

Sterile destilled and deionized water, ddH_2O (Spalding 332A)

Liquid nitrogen (Spalding 312)

Equipment

Mettler AE50 balance (Spalding 332A)

Mettler AT201 balance (Arnold lab)

Biorocker (Spalding 332)

Lyophilizer (Spalding 312)

Protocol

Day 1: Remove hydrogels from glass slide cross-linking apparatus and transfer to PBS with 6 M guanidinium chloride, pH 7.4. Typically I have 6 gels per condition and transfer them to 6 mL of buffer in a 35 mm dish. Swell on rocker for desired length of time. Measurements were typically taken at 24 hr and 48 hr. If the swollen mass is unchanged, proceed to the next step. Otherwise wait until equilibrium is reached.

(Note: In poorly cross-linked gels, erosion is often observed and an equilibrium will not be reached.)

Day 2: Measure swollen mass at 24 hr on Mettler AE50 balance. Transfer gels to individual wells of a 6-well plate with 3 mL PBS containing 6 M GndCl.

Day 3: Measure swollen mass at 48 hr.

Dilute buffer with an equal volume of PBS to obtain a final concentration of 3 M GndCl in PBS. Swell for 3 hr, then change to 2 M GndCl in PBS for 3 hr, 1 M GndCl in PBS for 3 hr, and finally PBS buffer overnight.

Day 4: Change PBS buffer to remove final traces of GndCl. Swell in PBS containing 0.02% (w/v) sodium azide to inhibit microbial growth.

(Note: NaN_3 is only required for longer term experiments or if there is concern about contamination. However, I almost always include it out of precaution.)

After 24 hr in PBS, measure the swollen mass.

Day 5: After 48 hr in PBS, measure the swollen mass.

Remove PBS buffer and replace with 5 mL sterile ddH_2O.

(Note: Follow safe disposal of buffer with sodium azide.)

Day 6-7: Replace water to ensure salts are removed. Gels will swell due to charged residues and then begin to shrink (likely due to self-buffering by the charged residues to near the pI).

Day 8: Make a final change of the water in morning. In the evening, transfer to tared microcentrifuge tubes, freeze in liquid nitrogen, and dry on the lyophiziler.

Day 9: Gels are typically completely dried after several hours. Measure the mass of the dry gel and vial, then subtract the vial tare. Masses were measured on the Mettler AT201 balance for higher precision.

Calculate the mass swelling ratio. $Q_m = \frac{swollen\ mass}{dry\ mass}$

Expected results

Hydrogels prepared from EPE and its variants have a typical mass swelling ratio, Q_m, of 11-15 in PBS. ERE hydrogels have a Q_m of 19-21 in PBS. In PBS with 6 M GndCl, the swelling ratios of all gels are typically 29-35.

B.6 Rheological measurements with swollen hydrogels

Overview: This protocol describes sample loading and rheological tests for swollen protein gels as prepared above. The method for loading swollen hydrogels on the rheometer was adapted from T.K.L. Meyvis, S.C. De Smedt, J. Demeester, W.E. Hennink *J. Rheol.* **1999** *43*, 933-950.

Materials:

Protein hydrogels prepared according to Protocol 4.

Biopsy punch, 8 mm diameter (Miltex)

Paraffin oil

Equipment

ARES-RFS strain-controlled rheometer (Kornfield lab)

8 mm parallel plate test geometry

Protocol

Setting the gap height Due to variation in the height of swollen gels, the gap height must be set for each gel. The following protocol was adapted from Meyvis *et al.*

Swell hydrogels in desired buffer. Typically, gels are swollen in decreasing concentrations of guanidinium chloride in PBS, then swollen for 48 hr in PBS with 0.02% (w/v) sodium azide.

Set ARES-RFS temperature control (25 °C) and turn motor on.

Cut gels to 8 mm with biopsy punch. Place gel on bottom plate and lower test geometry until it contacts the gel, noting the normal force. When the normal force exceeds 10 gf, pipette a thin layer of paraffin oil around the gel to prevent evaporation.

Perform an oscillatory single point measurement at 1% strain amplitude, 5 or 10 rad s^{-1}. Record the storage modulus *G'* and normal force at the beginning of the measurement.

Lower the gap 10 microns, repeating the single point measurement at the new gap height. Continue repeating this process until a *G'* is unchanged (see figure below). This is the gap

height at which data will be collected. Samples were typically compressed 10-30% from the height at which a normal force was first detected.

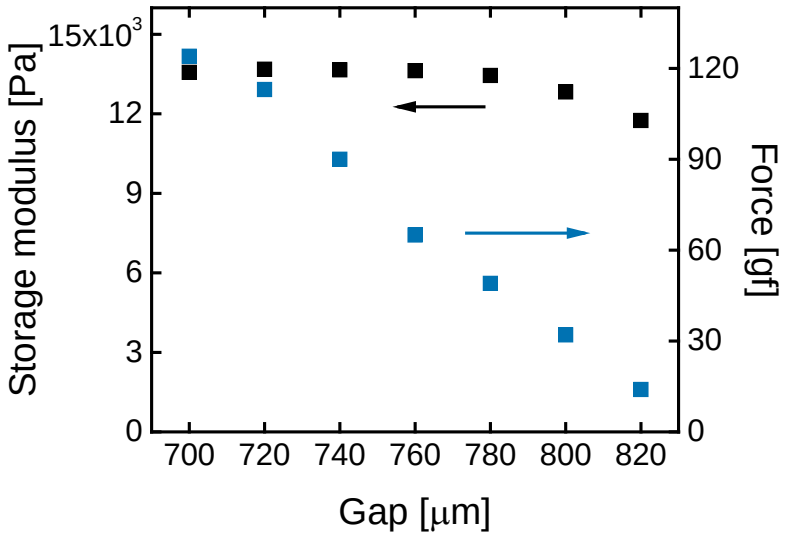

Strain sweep test Perform a strain sweep experiment from 0.01-20% strain at 10 rad s^{-1}, 25 °C to determine the linear viscoelastic regime. In this regime *G'* or |*G**| is constant. In cross-linked gels, the loss modulus *G"* and the phase angle δ are small.

Non-linear behavior may be a property of the material at higher strains, or may be due to slip between the gel and the plate.

Frequency sweep test Select a strain amplitude in the linear viscoelastic regime. Typical strain amplitudes were 1-5%.

Frequency sweeps were performed from 100 rad s^{-1} to 0.001 rad s^{-1}, starting at high frequency since these measurements are fast. Three decade (100-0.1 rad s^{-1}) tests take 5-10 min. Four decade (100-0.01 rad s^{-1}) tests take 1.5-2.5 hr. Five decade (100-0.001 rad s^{-1}) tests take 12-18 hr. Data were collected at 7 points per decade.

(Note: The loss modulus, *G"*, is difficult to measure accurately for covalent hydrogels. For an elastic solid (steel), the ARES-RFS has an expected phase angle δ of ±0.25 or a tan(δ) = ±0.004. In my experience, the loss moduli become very noisy at tan(δ) < 0.01.)